APPENDIX A

KINETICS AND PHOTOCHEMISTRY

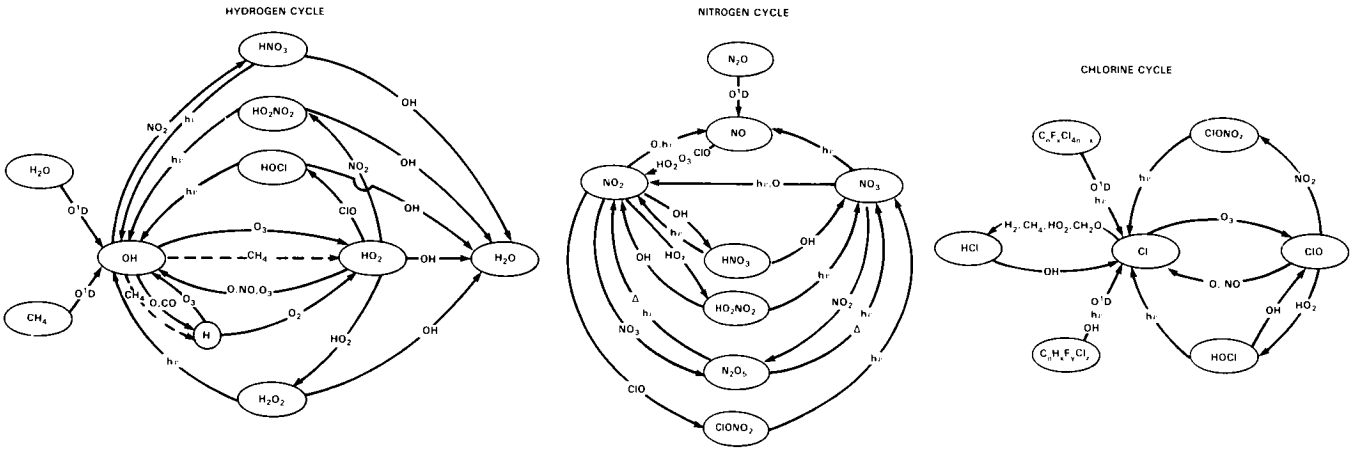

Panel Members

W.B. DeMore, Chairman

D.M. Golden
R.F. Hampson
C.J. Howard
M.J. Kurylo
J.J. Margitan
M.J. Molina
A.R. Ravishankara
R.T. Watson

APPENDIX A

KINETICS AND PHOTOCHEMICAL DATA BASE

The data for chemical kinetics rate constants and photochemical cross sections used in the present assessment were taken from a compilation prepared in early 1985 by the NASA Panel for Data Evaluation. That compilation is entitled "Chemical Kinetics and Photochemical Data for Use in Stratospheric Modeling", and is published by the Jet Propulsion Laboratory as JPL Publication 85-37.*

The NASA Data Evaluation Panel was established in 1977 by the NASA Upper Atmosphere Research Program for the purpose of providing a standardized, critical tabulation of the latest kinetics and photochemical data for use by modelers in computer simulations of stratospheric chemistry. The 1985 edition represents the seventh evaluation prepared by the panel. In earlier years the evaluations were updated annually; however, with the steadily increasing completeness and reliability of the data, future reevaluations are expected to be held approximately biennially.

Chapter 2 of the present assessment is an independent appraisal of the overall quality of the chemistry data base, along with discussions of other topics such as the best methods for testing the completeness of the chemical model and the question of error appraisal in data evaluation. Chapter 13 presents the results of model calculations using the data base, and also provides calculations which show the sensitivities of model predictions to uncertainties in the chemical data.

The following tables of data for chemical rate constants and equilibrium constants are excerpted from JPL 85-37, and are included for convenience to the reader who may not have immediate access to the complete publication.

*A copy of JPL Publication 85-37 may be obtained from the Documentation Section, Bldg. 111-116B, Jet Propulsion Laboratory, Pasadena CA 91109.

Table 1. Rate Constants for Second Order Reactions

Reaction	A-Factor	E/R±Δ(E/R)	k(298K)	Uncertainty Factor/298K
	O_x Reactions			
$O + O_2 \xrightarrow{M} O_3$	(See Table 2)			
$O + O_3 \rightarrow O_2 + O_2$	8.0×10^{-12}	2060±250	8.0×10^{-15}	1.15
	$O(^1D)$ Reactions			
$O(^1D) + N_2O \rightarrow N_2 + O_2$	4.9×10^{-11}	0±100	4.9×10^{-11}	1.3
$\rightarrow NO + NO$	6.7×10^{-11}	0±100	6.7×10^{-11}	1.3
$O(^1D) + H_2O \rightarrow OH + OH$	2.2×10^{-10}	0±100	2.2×10^{-10}	1.2
$O(^1D) + CH_4 \rightarrow OH + CH_3$	1.4×10^{-10}	0±100	1.4×10^{-10}	1.2
$\rightarrow H_2 + CH_2O$	1.4×10^{-11}	0±100	1.4×10^{-11}	1.2
$O(^1D) + H_2 \rightarrow OH + H$	1.0×10^{-10}	0±100	1.0×10^{-10}	1.2
$O(^1D) + N_2 \rightarrow O + N_2$	1.8×10^{-11}	-(107±100)	2.6×10^{-11}	1.2
$O(^1D) + N_2 \xrightarrow{M} N_2O$	(See Table 2)			
$O(^1D) + O_2 \rightarrow O + O_2$	3.2×10^{-11}	-(67±100)	4.0×10^{-11}	1.2
$O(^1D) + O_3 \rightarrow O_2 + O_2$	1.2×10^{-10}	0±100	1.2×10^{-10}	1.3
$\rightarrow O_2 + O + O$	1.2×10^{-10}	0±100	1.2×10^{-10}	1.3
*$O(^1D) + HCl \rightarrow$ products	1.5×10^{-10}	0±100	1.5×10^{-10}	1.2
$O(^1D) + CCl_4 \rightarrow$ products	3.3×10^{-10}	0±100	3.3×10^{-10}	1.2
$O(^1D) + CFCl_3 \rightarrow$ products	2.3×10^{-10}	0±100	2.3×10^{-10}	1.2
$O(^1D) + CF_2Cl_2 \rightarrow$ products	1.4×10^{-10}	0±100	1.4×10^{-10}	1.3
$O(^1D) + CF_4 \rightarrow CF_4 + O$	1.8×10^{-13}	0±100	1.8×10^{-13}	2.0
$O(^1D) + CCl_2O \rightarrow$ products	3.6×10^{-10}	0±100	3.6×10^{-10}	2.0
$O(^1D) + CFClO \rightarrow$ products	1.9×10^{-10}	0±100	1.9×10^{-10}	2.0
$O(^1D) + CF_2O \rightarrow$ products	7.4×10^{-11}	0±100	7.4×10^{-11}	2.0
$O(^1D) + NH_3 \rightarrow OH + NH_2$	2.5×10^{-10}	0±100	2.5×10^{-10}	1.3

*Indicates a change from the previous Panel evaluation (JPL 83-62).
#Indicates a new entry that was not in the previous evaluation.

Table 1. (Continued)

Reaction	A-Factor	E/R±Δ(E/R)	k(298K)	Uncertainty Factor/298K
$O(^1D) + CO_2 \rightarrow O + CO_2$	7.4×10^{-11}	-(117±100)	1.1×10^{-10}	1.2
*$O(^1D) + HF \rightarrow OH + F$	1.4×10^{-10}	0±100	1.4×10^{-10}	2.0
		HO_x Reactions		
$H + O_2 \xrightarrow{M} HO_2$	(See Table 2)			
$H + O_3 \rightarrow OH + O_2$	1.4×10^{-10}	470±200	2.9×10^{-11}	1.25
$H + HO_2 \rightarrow$ products	7.4×10^{-11}	0±400	7.4×10^{-11}	1.6
$O + OH \rightarrow O_2 + H$	2.2×10^{-11}	-(117±100)	3.3×10^{-11}	1.2
$O + HO_2 \rightarrow OH + O_2$	3.0×10^{-11}	-(200±200)	5.9×10^{-11}	1.2
$O + H_2O_2 \rightarrow OH + HO_2$	1.4×10^{-12}	2000±1000	1.7×10^{-15}	2.0
*$OH + HO_2 \rightarrow H_2O + O_2$	1.7×10^{-11}	-(416±200)	7.0×10^{-11}	1.3
$\xrightarrow{M} H_2O + O_2$	$3.0\times10^{-31}[M]$	-(500±500)	$1.6\times10^{-30}[M]$	2.0
$OH + O_3 \rightarrow HO_2 + O_2$	1.6×10^{-12}	940±300	6.8×10^{-14}	1.3
$OH + OH \rightarrow H_2O + O$	4.2×10^{-12}	242±242	1.9×10^{-12}	1.4
$\xrightarrow{M} H_2O_2$	(See Table 2)			
*$OH + H_2O_2 \rightarrow H_2O + HO_2$	3.1×10^{-12}	187^{+100}_{-300}	1.7×10^{-12}	1.3
$OH + H_2 \rightarrow H_2O + H$	6.1×10^{-12}	2030±400	6.7×10^{-15}	1.2
$HO_2 + HO_2 \rightarrow H_2O_2 + O_2$	2.3×10^{-13}	-(590±200)	1.7×10^{-12}	1.3
$\xrightarrow{M} H_2O_2 + O_2$	$1.7\times10^{-33}[M]$	-(1000±400)	$4.9\times10^{-32}[M]$	1.3
$HO_2 + O_3 \rightarrow OH + 2O_2$	1.4×10^{-14}	580^{+500}_{-100}	2.0×10^{-15}	1.5
		NO_x Reactions		
$N + O_2 \rightarrow NO + O$	4.4×10^{-12}	3220±340	8.9×10^{-17}	1.25
$N + O_3 \rightarrow NO + O_2$	-	-	$<1.0\times10^{-15}$	-
$N + NO \rightarrow N_2 + O$	3.4×10^{-11}	0±100	3.4×10^{-11}	1.3
$N + NO_2 \rightarrow N_2O + O$	-	-	3.0×10^{-12}	3

*Indicates a change from the previous Panel evaluation (JPL 83-62).
#Indicates a new entry that was not in the previous evaluation.

Table 1. (Continued)

Reaction	A-Factor	E/R±Δ(E/R)	k(298K)	Uncertainty Factor/298K
$O + NO \xrightarrow{M} NO_2$	(See Table 2)			
$O + NO_2 \rightarrow NO + O_2$	9.3×10^{-12}	0^{+0}_{-150}	9.3×10^{-12}	1.1
$O + NO_2 \xrightarrow{M} NO_3$	(See Table 2)			
$O + NO_3 \rightarrow O_2 + NO_2$	1.0×10^{-11}	0±150	1.0×10^{-11}	1.5
$O + N_2O_5 \rightarrow$ products	-	-	$<3.0\times10^{-16}$	-
$O + HNO_3 \rightarrow OH + NO_3$	-	-	$<3.0\times10^{-17}$	-
$O + HO_2NO_2 \rightarrow$ products	7.0×10^{-11}	3370±750	8.6×10^{-16}	3.0
$O_3 + NO \rightarrow NO_2 + O_2$	1.8×10^{-12}	1370±200	1.8×10^{-14}	1.2
$NO + HO_2 \rightarrow NO_2 + OH$	3.7×10^{-12}	-(240±80)	8.3×10^{-12}	1.2
$*NO + NO_3 \rightarrow 2NO_2$	1.3×10^{-11}	-(250±250)	3.0×10^{-11}	1.3
$OH + NO \xrightarrow{M} HONO$	(See Table 2)			
$OH + NO_2 \xrightarrow{M} HNO_3$	(See Table 2)			
$*OH + HNO_3 \rightarrow H_2O + NO_3$	(See ≠ below)			1.3
$OH + HO_2NO_2 \rightarrow$ products	1.3×10^{-12}	$-(380^{+270}_{-500})$	4.6×10^{-12}	1.5
$HO_2 + NO_2 \xrightarrow{M} HO_2NO_2$	(See Table 2)			
$O_3 + NO_2 \rightarrow NO_3 + O_2$	1.2×10^{-13}	2450±140	3.2×10^{-17}	1.15
$O_3 + HNO_2 \rightarrow O_2 + HNO_3$	-	-	$<5.0\times10^{-19}$	-
$NO_2 + NO_3 \xrightarrow{M} N_2O_5$	(See Table 2)			
$\#N_2O_5 + H_2O \rightarrow 2HNO_3$	-	-	$<2\times10^{-21}$	-
$*OH + NH_3 \rightarrow H_2O + NH_2$	3.5×10^{-12}	925±200	1.6×10^{-13}	1.4

* Indicates a change from the previous Panel evaluation (JPL 83-62).
\# Indicates a new entry that was not in the previous evaluation.
≠ $OH + HNO_3$ pressure and temperature dependence fit by

$$k(M,T) = k_0 + \frac{k_3[M]}{1 + \frac{k_3[M]}{k_2}}$$

with $k_0 = 7.2 \times 10^{-15} \exp(785/T)$, $k_2 = 4.1 \times 10^{-16} \exp(1440/T)$, $k_3 = 1.9 \times 10^{-33} \exp(725/T)$

Table 1. (Continued)

Reaction	A-Factor	E/R±Δ(E/R)	k(298K)	Uncertainty Factor/298K
$NH_2 + HO_2 \rightarrow$ products	-	-	3.4×10^{-11}	2
*$NH_2 + NO \rightarrow$ products	3.8×10^{-12}	-(450±150)	1.7×10^{-11}	2
*$NH_2 + NO_2 \rightarrow$ products	2.1×10^{-12}	-(650±250)	1.9×10^{-11}	3
$NH_2 + O_2 \rightarrow$ products	-	-	$<3 \times 10^{-18}$	-
*$NH_2 + O_3 \rightarrow$ products	4.8×10^{-12}	930±500	2.1×10^{-13}	3
	Hydrocarbon Reactions			
*$OH + CO \rightarrow CO_2 + H$	-		$1.5 \times 10^{-13}(1+0.6P_{atm})$	1.3
$OH + CH_4 \rightarrow CH_3 + H_2O$	2.4×10^{-12}	1710±200	7.7×10^{-15}	1.2
*$OH + C_2H_6 \rightarrow H_2O + C_2H_5$	1.1×10^{-11}	1090±250	2.8×10^{-13}	1.25
$OH + C_3H_8 \rightarrow H_2O + C_3H_7$	1.6×10^{-11}	800±250	1.1×10^{-12}	1.5
$OH + C_2H_4 \rightarrow$ products	(See Table 2)			
$OH + C_2H_2 \rightarrow$ products	(See Table 2)			
$OH + H_2CO \rightarrow H_2O + HCO$	1.0×10^{-11}	0±200	1.0×10^{-11}	1.25
$OH + CH_3OOH \rightarrow$ products	1.0×10^{-11}	0±200	1.0×10^{-11}	2.0
$OH + HCN \rightarrow$ products	1.2×10^{-13}	400±150	3.1×10^{-14}	3.0
*$OH + CH_3CN \rightarrow$ products	4.5×10^{-13}	900±400	2.2×10^{-14}	2.0
$HO_2 + CH_2O \rightarrow$ adduct	-	-	4.5×10^{-14}	10.0
$O + C_2H_2 \rightarrow$ products	2.9×10^{-11}	1600±300	1.4×10^{-13}	1.3
$O + H_2CO \rightarrow$ products	3.0×10^{-11}	1550±250	1.6×10^{-13}	1.25
$O + CH_3 \rightarrow$ products	1.1×10^{-10}	0±250	1.1×10^{-10}	1.3
$CH_3 + O_2 \rightarrow$ products	-	-	$<3 \times 10^{-16}$	-
$CH_3 + O_2 \xrightarrow{M} CH_3O_2$	(See Table 2)			
$CH_2OH + O_2 \rightarrow CH_2O + HO_2$	-	-	2×10^{-12}	10
*$CH_3O + O_2 \rightarrow CH_2O + HO_2$	8.4×10^{-14}	1200±300	1.5×10^{-15}	2

*Indicates a change from the previous Panel evaluation (JPL 83-62).
#Indicates a new entry that was not in the previous evaluation.

Table 1. (Continued)

Reaction	A-Factor	E/R±Δ(E/R)	k(298K)	Uncertainty Factor/298K
$HCO + O_2 \rightarrow CO + HO_2$	3.5×10^{-12}	-(140±140)	5.5×10^{-12}	1.3
$CH_3 + O_3 \rightarrow$ products	5.4×10^{-12}	220±150	2.6×10^{-12}	2
$CH_3O_2 + O_3 \rightarrow$ products	-	-	$<1\times10^{-17}$	-
$CH_3O_2 + CH_3O_2 \rightarrow$ products	1.6×10^{-13}	-(220±220)	3.4×10^{-13}	1.25
*$CH_3O_2 + NO \rightarrow CH_3O + NO_2$	4.2×10^{-12}	-(180±180)	7.6×10^{-12}	1.2
$CH_3O_2 + NO_2 \xrightarrow{M} CH_3O_2NO_2$	(See Table 2)			
$CH_3O_2 + HO_2 \rightarrow CH_3OOH + O_2$	7.7×10^{-14}	$-(1300^{+500}_{-1300})$	6.0×10^{-12}	3.0
#$NO_3 + CO \rightarrow$ products	-	-	$<1\times10^{-15}$	-
#$NO_3 + CH_2O \rightarrow$ products	-	-	6×10^{-16}	1.5
	Cl_x Reactions			
$Cl + O_3 \rightarrow ClO + O_2$	2.8×10^{-11}	257±100	1.2×10^{-11}	1.15
$Cl + H_2 \rightarrow HCl + H$	3.7×10^{-11}	2300±200	1.6×10^{-14}	1.25
$Cl + CH_4 \rightarrow HCl + CH_3$	9.6×10^{-12}	1350±150	1.0×10^{-13}	1.1
$Cl + C_2H_6 \rightarrow HCl + C_2H_5$	7.7×10^{-11}	90±90	5.7×10^{-11}	1.1
$Cl + C_3H_8 \rightarrow HCl + C_3H_7$	1.4×10^{-10}	-(40±250)	1.6×10^{-10}	1.5
$Cl + C_2H_2 \rightarrow$ products	-	-	1×10^{-12}	10
$Cl + CH_3OH \rightarrow CH_2OH + HCl$	6.3×10^{-11}	0±250	6.3×10^{-11}	2.0
$Cl + CH_3Cl \rightarrow CH_2Cl + HCl$	3.4×10^{-11}	1260±200	4.9×10^{-13}	1.2
$Cl + CH_3CCl_3 \rightarrow CH_2CCl_3 + HCl$	-	-	$<4\times10^{-14}$	-
$Cl + H_2CO \rightarrow HCl + HCO$	8.2×10^{-11}	34±100	7.3×10^{-11}	1.15
$Cl + H_2O_2 \rightarrow HCl + HO_2$	1.1×10^{-11}	980±500	4.1×10^{-13}	1.5
$Cl + HOCl \rightarrow$ products	3.0×10^{-12}	130±250	1.9×10^{-12}	2.0
$Cl + HNO_3 \rightarrow$ products	-	-	$<1.7\times10^{-14}$	-
$Cl + HO_2 \rightarrow HCl + O_2$	1.8×10^{-11}	-(170±200)	3.2×10^{-11}	1.5

*Indicates a change from the previous Panel evaluation (JPL 83-62).
#Indicates a new entry that was not in the previous evaluation.

Table 1. (Continued)

Reaction	A-Factor	E/R±Δ(E/R)	k(298K)	Uncertainty Factor/298K
→ OH + ClO	4.1×10^{-11}	450±200	9.1×10^{-12}	2.0
$Cl + Cl_2O \rightarrow Cl_2 + ClO$	9.8×10^{-11}	0±250	9.8×10^{-11}	1.2
$Cl + OClO \rightarrow ClO + ClO$	5.9×10^{-11}	0±250	5.9×10^{-11}	1.25
$Cl + ClONO_2 \rightarrow$ products	6.8×10^{-12}	-(160±200)	1.2×10^{-11}	1.3
$Cl + NO \xrightarrow{M} NOCl$	(See Table 2)			
$Cl + NO_2 \xrightarrow{M} ClONO\ (ClNO_2)$	(See Table 2)			
$Cl + ClNO \rightarrow NO + Cl_2$	2.3×10^{-11}	$0^{\pm500}_{\pm250}$	2.3×10^{-11}	3.0
$Cl + O_2 \xrightarrow{M} ClOO$	(See Table 2)			
$Cl + ClOO \rightarrow Cl_2 + O_2$	1.4×10^{-10}	0±250	1.4×10^{-10}	3.0
→ ClO + ClO	8.0×10^{-12}	0±250	8.0×10^{-12}	3.0
*$ClO + O \rightarrow Cl + O_2$	4.7×10^{-11}	50±100	4.0×10^{-11}	1.3
$ClO + NO \rightarrow NO_2 + Cl$	6.2×10^{-12}	-(294±100)	1.7×10^{-11}	1.15
$ClO + NO_2 \xrightarrow{M} ClONO_2$	(See Table 2)			
$ClO + HO_2 \rightarrow HOCl + O_2$	4.6×10^{-13}	$-(710^{\pm250}_{\pm700})$	5.0×10^{-12}	1.4
$ClO + H_2CO \rightarrow$ products	$\sim1.0\times10^{-12}$	>2060	$<1.0\times10^{-15}$	-
*$ClO + OH \rightarrow$ products	1.0×10^{-11}	-(120±150)	1.5×10^{-11}	1.6
$ClO + CH_4 \rightarrow$ products	$\sim1.0\times10^{-12}$	>3700	$<4.0\times10^{-18}$	-
$ClO + H_2 \rightarrow$ products	$\sim1.0\times10^{-12}$	>4800	$<1.0\times10^{-19}$	-
$ClO + CO \rightarrow$ products	$\sim1.0\times10^{-12}$	>3700	$<4.0\times10^{-18}$	-
$ClO + N_2O \rightarrow$ products	$\sim1.0\times10^{-12}$	>4260	$<6.0\times10^{-19}$	-
$ClO + ClO \rightarrow$ products	-	-	-	-
$ClO + O_3 \rightarrow ClOO + O_2$	1.0×10^{-12}	>4000	$<1.0\times10^{-18}$	-
→ $OClO + O_2$	1.0×10^{-12}	>4000	$<1.0\times10^{-18}$	-
*$OH + HCl \rightarrow H_2O + Cl$	2.6×10^{-12}	350±100	8.0×10^{-13}	1.2

*Indicates a change from the previous Panel evaluation (JPL 83-62).
#Indicates a new entry that was not in the previous evaluation.

Table 1. (Continued)

Reaction	A-Factor	E/R±Δ(E/R)	k(298K)	Uncertainty Factor/298K
$OH + HOCl \rightarrow H_2O + ClO$	3.0×10^{-12}	150^{+850}_{-150}	1.8×10^{-12}	10
$OH + CH_3Cl \rightarrow CH_2Cl + H_2O$	1.8×10^{-12}	1112±200	4.3×10^{-14}	1.2
$OH + CH_2Cl_2 \rightarrow CHCl_2 + H_2O$	4.5×10^{-12}	1032±200	1.4×10^{-13}	1.2
$OH + CHCl_3 \rightarrow CCl_3 + H_2O$	3.3×10^{-12}	1034±200	1.0×10^{-13}	1.2
$OH + CHFCl_2 \rightarrow CFCl_2 + H_2O$	8.9×10^{-13}	1013±200	3.0×10^{-14}	1.3
$OH + CHF_2Cl \rightarrow CF_2Cl + H_2O$	7.8×10^{-13}	1530±200	4.6×10^{-15}	1.2
$OH + CH_2ClF \rightarrow CHClF + H_2O$	2.0×10^{-12}	1134±150	4.4×10^{-14}	1.2
$OH + CH_3CCl_3 \rightarrow CH_2CCl_3 + H_2O$	5.4×10^{-12}	1820±200	1.2×10^{-14}	1.3
$OH + C_2Cl_4 \rightarrow$ products	9.4×10^{-12}	1200±200	1.7×10^{-13}	1.25
$OH + C_2HCl_3 \rightarrow$ products	5.0×10^{-13}	-(445±200)	2.2×10^{-12}	1.25
$OH + CFCl_3 \rightarrow$ products	$\sim1.0\times10^{-12}$	>3650	$<5.0\times10^{-18}$	-
$OH + CF_2Cl_2 \rightarrow$ products	$\sim1.0\times10^{-12}$	>3560	$<6.5\times10^{-18}$	-
$OH + ClONO_2 \rightarrow$ products	1.2×10^{-12}	333±200	3.9×10^{-13}	1.5
$O + HCl \rightarrow OH + Cl$	1.0×10^{-11}	3340±350	1.4×10^{-16}	2.0
$O + HOCl \rightarrow OH + ClO$	1.0×10^{-11}	2200±1000	6.0×10^{-15}	10
$O + ClONO_2 \rightarrow$ products	3.0×10^{-12}	808±200	2.0×10^{-13}	1.5
$O + Cl_2O \rightarrow ClO + ClO$	2.9×10^{-11}	630±200	3.5×10^{-12}	1.4
$O + OClO \rightarrow ClO + O_2$	2.5×10^{-11}	1160±300	5.0×10^{-13}	1.5
$NO + OClO \rightarrow NO_2 + ClO$	2.5×10^{-12}	600±300	3.4×10^{-13}	1.5
$\#Cl + CH_3CN \rightarrow$ products	-	-	$<2.0\times10^{-15}$	-
$\#Cl + NO_3 \rightarrow ClO + NO_2$	-	-	7.6×10^{-11}	2.0
$\#ClO + NO_3 \rightarrow$ products	-	-	4.0×10^{-13}	2.0
$\#OH + Cl_2 \rightarrow HOCl + Cl$	-	-	6.5×10^{-14}	1.2

*Indicates a change from the previous Panel evaluation (JPL 83-62).
#Indicates a new entry that was not in the previous evaluation.

Table 1. (Continued)

Reaction	A-Factor	E/R±Δ(E/R)	k(298K)	Uncertainty Factor/298K
#$HCl + ClONO_2 \rightarrow$ products	-	-	$<1.0\times10^{-18}$	-
#$HCl + HO_2NO_2 \rightarrow$ products	-	-	$<1\times10^{-20}$	-
		BrO_x Reactions		
$Br + O_3 \rightarrow BrO + O_2$	1.4×10^{-11}	755±200	1.1×10^{-12}	1.2
$Br + H_2O_2 \rightarrow HBr + HO_2$	1.0×10^{-11}	>2500	$<2.0\times10^{-15}$	-
$Br + H_2CO \rightarrow HBr + HCO$	1.7×10^{-11}	800±200	1.1×10^{-12}	1.3
*$Br + HO_2 \rightarrow HBr + O_2$	-	-	8.0×10^{-13}	3.0
$BrO + O \rightarrow Br + O_2$	3.0×10^{-11}	0±250	3.0×10^{-11}	3.0
$BrO + ClO \rightarrow Br + OClO$	6.7×10^{-12}	0±250	6.7×10^{-12}	2.0
$\rightarrow Br + Cl + O_2$	6.7×10^{-12}	0±250	6.7×10^{-12}	2.0
$BrO + NO \rightarrow NO_2 + Br$	8.7×10^{-12}	-(265±130)	2.1×10^{-11}	1.15
$BrO + NO_2 \xrightarrow{M} BrONO_2$	(See Table 2)			
$BrO + BrO \rightarrow 2\ Br + O_2$	1.4×10^{-12}	-(150±150)	2.3×10^{-12}	1.25
$\rightarrow Br_2 + O_2$	6.0×10^{-14}	-(600±600)	4.4×10^{-13}	1.25
$BrO + O_3 \rightarrow Br + 2\ O_2$	$\sim1\times10^{-12}$	>1600	$<5.0\times10^{-15}$	-
$BrO + HO_2 \rightarrow$ products	-	-	5.0×10^{-12}	3.0
$BrO + OH \rightarrow$ products	-	-	1.0×10^{-11}	5.0
*$OH + HBr \rightarrow H_2O + Br$	1.1×10^{-11}	0±250	1.1×10^{-11}	1.3
$OH + CH_3Br \rightarrow CH_2Br + H_2O$	6.1×10^{-13}	825±200	3.8×10^{-14}	1.25
$O + HBr \rightarrow OH + Br$	6.6×10^{-12}	1540±200	3.7×10^{-14}	1.3
#$OH + Br_2 \rightarrow HOBr + Br$	-	-	4.8×10^{-11}	1.3
		FO_x Reactions		
$F + O_3 \rightarrow FO + O_2$	2.8×10^{-11}	226±200	1.3×10^{-11}	2.0
$F + H_2 \rightarrow HF + H$	1.6×10^{-10}	525±250	2.7×10^{-11}	1.3

*Indicates a change from the previous Panel evaluation (JPL 83-62).
#Indicates a new entry that was not in the previous evaluation.

Table 1. (Continued)

Reaction	A-Factor	E/R ± Δ(E/R)	k(298K)	Uncertainty Factor/298K
$F + CH_4 \rightarrow HF + CH_3$	3.0×10^{-10}	400±300	8.0×10^{-11}	1.5
*$F + H_2O \rightarrow HF + OH$	4.2×10^{-11}	400±200	1.1×10^{-11}	3.0
$F + O_2 \xrightarrow{M} FO_2$	(See Table 2)			
$F + NO \xrightarrow{M} FNO$	(See Table 2)			
$F + NO_2 \xrightarrow{M} FNO_2(FONO)$	(See Table 2)			
$NO + FO \rightarrow NO_2 + F$	2.6×10^{-11}	0±250	2.6×10^{-11}	2.0
$FO + FO \rightarrow 2\ F + O_2$	1.5×10^{-11}	0±250	1.5×10^{-11}	3.0
$FO + O_3 \rightarrow F + 2\ O_2$	-	-	-	-
$\rightarrow FO_2 + O_2$	-	-	-	-
$FO + NO_2 \xrightarrow{M} FONO_2$	(See Table 2)			
$O + FO \rightarrow F + O_2$	5.0×10^{-11}	0±250	5.0×10^{-11}	3.0
$O + FO_2 \rightarrow FO + O_2$	5.0×10^{-11}	0±250	5.0×10^{-11}	5.0
#$CF_3O_2 + NO \rightarrow CF_3O + NO_2$	3.9×10^{-12}	-(400±200)	1.5×10^{-11}	1.3
#$CF_2Cl_2O_2 + NO \rightarrow CF_2Cl_2O + NO_2$	3.1×10^{-12}	-(500±200)	1.6×10^{-11}	1.3
#$CFCl_2O_2 + NO \rightarrow CFCl_2O + NO_2$	3.5×10^{-12}	-(430±200)	1.5×10^{-11}	1.3
#$CCl_3O_2 + NO \rightarrow CCl_3O + NO_2$	5.7×10^{-12}	-(330±200)	1.7×10^{-11}	1.3
	SO_x Reactions			
$OH + H_2S \rightarrow SH + H_2O$	5.9×10^{-12}	65±65	4.7×10^{-12}	1.2
*$OH + OCS \rightarrow$ products	3.9×10^{-13}	1780±500	1.0×10^{-15}	10
$OH + CS_2 \rightarrow$ products		-	-	-
$OH + SO_2 \xrightarrow{M} HOSO_2$	(See Table 2)			
$O + H_2S \rightarrow OH + SH$	1.0×10^{-11}	1810±550	2.2×10^{-14}	1.7
$O + OCS \rightarrow CO + SO$	2.1×10^{-11}	2200±150	1.3×10^{-14}	1.2
$O + CS_2 \rightarrow CS + SO$	3.2×10^{-11}	650±150	3.6×10^{-12}	1.2

*Indicates a change from the previous Panel evaluation (JPL 83-62).
#Indicates a new entry that was not in the previous evaluation.

Table 1. (Continued)

Reaction	A-Factor	E/R±Δ(E/R)	k(298K)	Uncertainty Factor/298K
$O + SH \rightarrow H + SO$	-	-	1.6×10^{-10}	5.0
$S + O_2 \rightarrow SO + O$	2.3×10^{-12}	0±200	2.3×10^{-12}	1.2
$S + O_3 \rightarrow SO + O_2$	-	-	1.2×10^{-11}	2.0
$S + OH \rightarrow SO + H$	-	-	6.6×10^{-11}	3.0
$SO + O_2 \rightarrow SO_2 + O$	2.4×10^{-13}	2370±500	8.4×10^{-17}	2
$SO + O_3 \rightarrow SO_2 + O_2$	3.6×10^{-12}	1100±200	9.0×10^{-14}	1.2
$SO + OH \rightarrow SO_2 + H$	-	-	8.6×10^{-11}	2.0
$SO + NO_2 \rightarrow SO_2 + NO$	-	-	1.4×10^{-11}	1.3
$SO + ClO \rightarrow SO_2 + Cl$	-	-	2.3×10^{-11}	3.0
$SO + OClO \rightarrow SO_2 + ClO$	-	-	1.9×10^{-12}	3.0
$SO + BrO \rightarrow SO_2 + Br$	-	-	$>4.0\times10^{-11}$	-
$SO_2 + HO_2 \rightarrow$ products	-	-	$<1.0\times10^{-18}$	-
$CH_3O_2 + SO_2 \rightarrow$ products	-	-	$<5.0\times10^{-17}$	-
*$SH + O_2 \rightarrow OH + SO$	-	-	$<1.0\times10^{-17}$	-
$Cl + H_2S \rightarrow HCl + SH$	-	-	7.3×10^{-11}	1.4
$Cl + OCS \rightarrow SCl + CO$	-	-	$<1.1\times10^{-16}$	-
$ClO + OCS \rightarrow$ products	-	-	$<2.4\times10^{-16}$	-
$ClO + SO_2 \rightarrow Cl + SO_3$	-	-	$<4.0\times10^{-18}$	-
#$SH + H_2O_2 \rightarrow$ products	-	-	$<5\times10^{-15}$	-
#$SH + O_3 \rightarrow HSO + O_2$	-	-	3.2×10^{-12}	3.0
#$HSO + O_3 \rightarrow$ products	-	-	1×10^{-13}	5.0
#$SH + NO_2 \rightarrow HSO + NO$	-	-	3.2×10^{-11}	1.5
#$SH + NO \xrightarrow{M} HSNO$	(See Table 2)			
#$HOSO_2 + O_2 \rightarrow HO_2 + SO_3$	-	-	4.0×10^{-13}	3.0

*Indicates a change from the previous Panel evaluation (JPL 83-62).
#Indicates a new entry that was not in the previous evaluation.

Table 1. (Continued)

Reaction	A-Factor	E/R ± Δ(E/R)	k(298K)	Uncertainty Factor/298K
#$SO_2 + NO_2 \rightarrow$ products	-	-	$<2\times10^{-26}$	-
#$SO_3 + NO_2 \rightarrow$ products	-	-	1.0×10^{-19}	10
#$SO_2 + O_3 \rightarrow SO_3 + O_2$	3.0×10^{-12}	>7000	$<2\times10^{-22}$	-
#$CS + O_2 \rightarrow OCS + O$	-	-	2.9×10^{-19}	2.0
#$CS + O_3 \rightarrow OCS + O_2$	-	-	3.0×10^{-16}	3.0
#$CS + NO_2 \rightarrow OCS + NO$	-	-	7.6×10^{-17}	3.0
	Metal Reactions			
#$Na + O_3 \rightarrow NaO + O_2$	5×10^{-10}	0±400	5×10^{-10}	1.5
$\rightarrow NaO_2 + O$	$<3\times10^{-11}$	0±400	$<3\times10^{-11}$	-
#$Na + O_2 \xrightarrow{M} NaO_2$	(See Table 2)			
#$NaO + HCl \rightarrow$ products	2.8×10^{-10}	0±400	2.8×10^{-10}	3.0
#$NaOH + HCl \rightarrow NaCl + H_2O$	2.8×10^{-10}	0±400	2.8×10^{-10}	3.0

*Indicates a change from the previous Panel evaluation (JPL 83-62).
#Indicates a new entry that was not in the previous evaluation.

Table 2. Rate Constants for Three-Body Reactions

Reaction	Low Pressure Limit $k_0(T) = k_0^{300}(T/300)^{-n}$		High Pressure Limit $k_\infty(T) = k_\infty^{300}(T/300)^{-m}$	
	k_0^{300}	n	k_∞^{300}	m
$O + O_2 \xrightarrow{M} O_3$	(6.0±0.5)(-34)	2.3±0.5	-	-
$O(^1D) + N_2 \xrightarrow{M} N_2O$	(3.5±3.0)(-37)	$0.6^{+2}_{-.6}$	-	-
$*H + O_2 \xrightarrow{M} HO_2$	(5.5±0.5)(-32)	1.6±0.5	(7.5±4.0)(-11)	0±1
$OH + OH \xrightarrow{M} H_2O_2$	(6.9±3.0)(-31)	$0.8^{+2.0}_{-0.8}$	(1.0±0.5)(-11)	1.0±1.0
$*O + NO \xrightarrow{M} NO_2$	(9.0±2.0)(-32)	1.5±0.3	(3.0±1.0)(-11)	0±1
$O + NO_2 \xrightarrow{M} NO_3$	(9.0±1.0)(-32)	2.0±1.0	(2.2±0.3)(-11)	0±1
$OH + NO \xrightarrow{M} HONO$	(7.0±2.0)(-31)	2.6±1.0	(1.5±1.0)(-11)	0.5±0.5
$OH + NO_2 \xrightarrow{M} HNO_3$	(2.6±0.3)(-30)	3.2±0.7	(2.4±1.2)(-11)	1.3±1.3
$*HO_2 + NO_2 \xrightarrow{M} HO_2NO_2$	(2.0±0.5)(-31)	2.7±1.5	(4.2±1.0)(-12)	2.0±2.0
$*NO_2 + NO_3 \xrightarrow{M} N_2O_5$	(2.2±0.5)(-30)	4.3±1.3	(1.5±0.8)(-12)	0.5±0.5
$Cl + NO \xrightarrow{M} ClNO$	(9.0±2.0)(-32)	1.6±0.5	-	-
$*Cl + NO_2 \xrightarrow{M} ClONO$	(1.3±0.2)(-30)	2.0±1.0	(1.0±0.5)(-10)	1.0±1.0
$\xrightarrow{M} ClNO_2$	(1.8±0.3)(-31)	2.0±1.0	(1.0±0.5)(-10)	1.0±1.0
$Cl + O_2 \xrightarrow{M} ClOO$	(2.0±1.0)(-33)	1.4±1.4	-	-
$ClO + NO_2 \xrightarrow{M} ClONO_2$	(1.8±0.3)(-31)	3.4±1.0	(1.5±0.7)(-11)	1.9±1.9
$BrO + NO_2 \xrightarrow{M} BrONO_2$	(5.0±2.0)(-31)	2.0±2.0	(1.0±0.5)(-11)	1.0±1.0
$F + O_2 \xrightarrow{M} FO_2$	(1.6±0.8)(-32)	1.4±1.0	-	-
$F + NO \xrightarrow{M} FNO$	(5.9±3.0)(-32)	1.7±1.7	-	-
$*F + NO_2 \xrightarrow{M}$ Products	(1.1±0.6)(-30)	2.0±2.0	(3.0±2.0)(-11)	1.0±1.0
$FO + NO_2 \xrightarrow{M} FONO_2$	(2.6±2.0)(-31)	1.3±1.3	(2.0±1.0)(-11)	1.5±1.5
$*CH_3 + O_2 \xrightarrow{M} CH_3O_2$	(4.5±1.5)(-31)	2.0±1.0	(1.8±0.2)(-12)	1.7±1.7

Note: $k(Z) = k(M,T) = \left(\frac{k_0(T)[M]}{1 + k_0(T)[M] / k_\infty(T)}\right) 0.6^{\{1 + [\log_{10}(k_0(T)[M]/k_\infty(T))]^2\}^{-1}}$

The values quoted are suitable for air as the third body, M.

*Indicates a change from the previous Panel evaluation (JPL 83-62).

Table 2. (Continued)

Reaction	Low Pressure Limit $k_0(T) = k_0^{300}(T/300)^{-n}$		High Pressure Limit $k_\infty(T) = k_\infty^{300}(T/300)^{-m}$	
	k_0^{300}	n	k_∞^{300}	m
$CH_3O_2 + NO_2 \xrightarrow{M} CH_3O_2NO_2$	(1.5±0.8)(-30)	4.0±2.0	(6.5±3.2)(-12)	2.0±2.0
*OH + $SO_2 \xrightarrow{M} HOSO_2$	(3.0±1.0)(-31)	3.3±1.5	(1.5±0.5)(-12)	0^{+2}_{-2}
*OH + $C_2H_4 \xrightarrow{M} HOCH_2CH_2$	(1.5±0.6)(-28)	0.8±2.0	(8.8±0.9)(-12)	0^{+2}_{-2}
*OH + $C_2H_2 \xrightarrow{M} HOCHCH$	(5.5±2.0)(-30)	0.0±0.2	(8.3±1.0)(-13)	$-2.0^{+2.8}_{-1.8}$
#$CF_3 + O_2 \xrightarrow{M} CF_3O_2$	(4.5±1.0)(-29)	2±2	(8±6)(-12)	1±1
#$CFCl_2 + O_2 \xrightarrow{M} CFCl_2O_2$	(5.0±0.8)(-30)	2±2	(6.0±1.0)(-12)	1±1
#$CCl_3 + O_2 \xrightarrow{M} CCl_3O_2$	(1.0±0.7)(-30)	2±2	(2.5±2)(-12)	1±1
#$CFCl_2O_2 + NO_2 \xrightarrow{M} CFCl_2O_2NO_2$	(3.5±0.5)(-29)	4±2	(6.0±1.0)(-12)	2±2
#HS + NO $\xrightarrow{M}$ HSNO	(2.4±0.4)(-31)	3±1	(2.7±0.5)(-11)	0^{+2}_{-2}
#Na + $O_2 \xrightarrow{M} NaO_2$	(1.9±1)(-30)	1.1±0.5	(2.0±1.8)(-10)	0±1

Note: $k(Z) = k(M,T) = \left(\frac{k_0(T)[M]}{1 + k_0(T)[M] / k_\infty(T)}\right) 0.6^{\{1 + [\log_{10}(k_0(T)[M]/k_\infty(T))]^2\}^{-1}}$

The values quoted are suitable for air as the third body, M.
*Indicates a change from the previous Panel evaluation (JPL 83-62).
#Indicates a new entry that was not in the previous evaluation.

Table 3. Equilibrium Constants

Reaction	A/cm³ molecule⁻¹	B/°K	Log K_{eq}(300)
$HO_2 + NO_2 \rightarrow HO_2NO_2$	2.33×10^{-27}	10,870	-10.90
$*NO_2 + NO_3 \rightarrow N_2O_5$	1.52×10^{-27}	11,153	-10.68
$Cl + O_2 \rightarrow ClOO$	2.43×10^{-25}	2,979	-20.30
$ClO + O_2 \rightarrow ClO \cdot O_2$	$<1.3 \times 10^{-26}$	<5,230	<-18.30
$F + O_2 \rightarrow FOO$	5.32×10^{-25}	7,600	-13.27
	1.15×10^{-25}	3,582	-19.75
$CH_3O_2 + NO_2 \rightarrow CH_3O_2NO_2$	1.30×10^{-28}	11,192	-11.68

K/cm^3 molecule^{-1} = A exp (B/T) [200 < T/K < 300]
*Indicates a change from the previous Panel evaluation (JPL 83-62).

APPENDIX B

SPECTROSCOPIC DATABASE

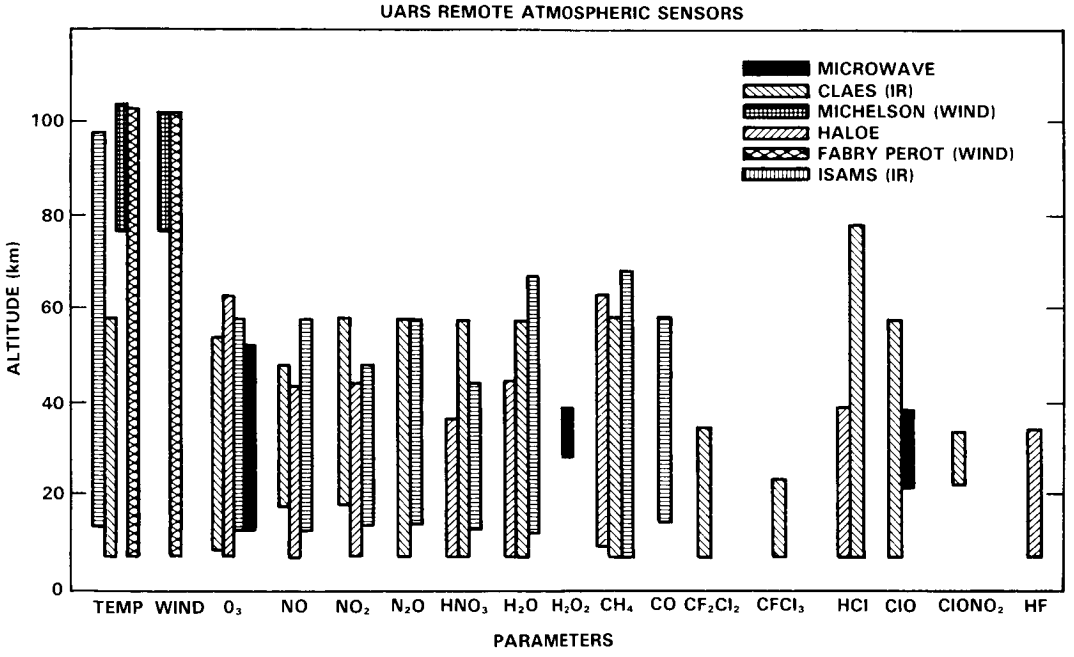

Panel Members

N. Husson, Chairperson

A. Barbe
L. R. Brown
B. Carli
A. Goldman
H. M. Pickett
A. E. Roche
L. S. Rothman
M. A. H. Smith

APPENDIX B

SPECTROSCOPIC DATABASE: INFRARED TO MICROWAVE

TABLE OF CONTENTS

B-0 INTRODUCTION

It is now well recognized that accurate modeling of radiative transfer phenomena in a planetary atmosphere requires very good knowledge of the parameters describing the radiation absorption or emission properties of the optically active gases involved in the medium considered. The increasing impact of physical techniques for the remote sensing of the thermal structure and composition of the earth's atmosphere requires continuous research to achieve a better understanding of molecular spectra of radiatively active gases and necessitates the compilation of accurate relevant spectroscopic data.

The purpose of the appendix is to review the status of spectroscopic database and current laboratory spectroscopy in the infrared to the microwave for atmospheric remote sensing. Reviews of this type have been given by the WMO as part of a meeting on potential climatic effects of ozone and other minor trace gases (WMO, 1983) and by NASA (Smith, 1985), and in the proceedings of a CMA-NBS workshop on atmospheric spectra held in 1983 (CMA-NBS, 1985).

This appendix is divided into eight sections beginning with the introduction in Section B-0. In Sections B-1 and B-2, several aspects of quantitative atmospheric spectroscopy are considered, using a classification of the molecules according to the gas amounts in the stratosphere and upper troposphere, and reviews of quantitative atmospheric high-resolution spectroscopic measurements and field measurements systems are given. Laboratory spectroscopy and spectral analysis and prediction are presented in Section B-3 with a summary of current laboratory spectroscopy capabilities. Spectroscopic data requirements for accurate derivation of atmospheric composition are discussed in Sections B-4 and B-5, where examples are given for space-based remote sensing experiments of the atmosphere: the ATMOS (Atmospheric Trace Molecule Spectroscopy) and UARS (Upper Atmosphere Research Satellite) experiments. Section B-6 is devoted to a database assessment including:

- a review of the basic parameters involved in the data compilations;
- a summary of information on line parameter compilations already in existence: the AFGL (Air Force Geophysics Laboratory) catalog (McClatchey *et al.*, 1973; Rothman *et al.*, 1983 a,b; 1985), the GEISA (Gestion et Etude des Informations Spectroscopiques Atmospheriques; word translation: Management and Study of Atmospheric Spectroscopic Information) catalog (Chedin *et al.*, 1980; 1985, Husson *et al.*, 1982; 1985), the JPL catalog (Poynter *et al.*, 1981, 1984);
- a summary of current laboratory spectroscopy studies.

Finally, the major recommendations for further work in laboratory spectroscopy to support atmospheric measurements are presented in Section B-7.

B-1 OVERVIEW OF ATMOSPHERIC SPECTROSCOPY

During the last twenty years, atmospheric spectroscopy has proven to be a powerful tool for the identification and quantification of previously unknown stratospheric gases as well as for more accurate quantification and monitoring of known species. The initial detection of stratospheric HNO_3 (Murcray *et al.*, 1968) and NO_2 (Goldman *et al.*, 1970) and the increased interest in stratospheric chemistry in relation to the effects of supersonic transports (SST) and chlorofluorocarbons (CFC) on the ozone layer have served to intensify the atmospheric spectroscopy studies. Indeed, most of the atmospheric species involved in the various photochemical cycles of the stratosphere, and particularly in the ozone photochemistry, are currently being measured, or scheduled to be measured, with high sensitivity spectrometers from the ground, aircraft, balloon and spacecraft.

SPECTROSCOPIC DATABASE

Simultaneous measurements of O_3 and related species are required for a more complete evaluation of the ozone problem. Therefore, the discussion of atmospheric spectroscopy and ozone has to include all of the possibly related species.

Traditionally, classical spectroscopy has focused mostly on spectral line positions and energy levels. Modern theoretical and experimental developments made spectroscopy a very effective quantitative tool, and the identification and quantification of atmospheric species from their spectra has become a major part of today's atmospheric science. This requires the study of absolute line intensities and line shapes in addition to line positions.

The atmospheric long geometric path obtainable at large zenith angles is a major factor in increasing the sensitivity of spectroscopic measurements to trace constituents. Some species are not observable from the ground and require high altitude platforms such as balloons or aircraft to minimize the interference by other species (especially H_2O). Most of the measurements are made in either solar absorption or atmospheric emission modes. In general, the absorption measurements yield higher spectral resolution, but the emission measurements yield larger dynamic range. In ground-based measurements, signal-to-noise ratios over 1,000 have been achieved. In aircraft and balloon borne measurements, a signal-to-noise ratio of ~ 100 is typical.

In this text, several aspects of quantitative atmospheric spectroscopy, its current status and accuracies, and its anticipated developments as a part of modern atmospheric measurements are presented. The discussion will concentrate on the infrared to microwave spectral region, but many of the concepts addressed apply to the entire electromagnetic spectrum. The evaluation will be made mostly in relation to the assessment of current knowledge and the requirements for future measurements and interpretation of ozone and related species.

B-2 QUANTITATIVE HIGH-RESOLUTION ATMOSPHERIC SPECTROSCOPY

The major quantitative spectral parameters include:

- individual line parameters;
- total and spectral band model parameters;
- approximate line or band absorption coefficients;
- continuum coefficients;

The line parameters include:

- line positions, energy levels, absolute transition probabilities, and energy level populations;
- quantum number dependence and temperature dependence of Lorentz halfwidths;
- non-Lorentzian line shapes (cores and wings).

The two series of above parameters are classified in order of decreasing accuracy.

A complete knowledge of the line parameters allows line-by-line simulations of atmospheric spectra which can lead to very accurate quantification of atmospheric gases. Indeed, this has become a standard tool of modern atmospheric spectroscopy, and extensive improvements in line parameter data banks are currently being made. The existing line parameters compilations and their accuracies are discussed separately

in this Appendix. Considerable research is also being devoted to semi-empirical quantification methods for line wings and the various coefficients which are needed to supplement the line-by-line simulations.

In general, the molecules of interest can be classified according to their optical depths in the stratosphere and upper troposphere as in Table B-1.

Table B-1. Classification of Atmospheric Molecules[1]

Category	Constituent Type	Optical Path	Molecules
[1]	"major"	long	H_2O, CO_2, O_3, N_2O, CO, CH_4, O_2, N_2, atomic O
[2]	"minor"	medium	NO, NO_2, NH_3, HNO_3, HF, HCl, OCS, H_2CO, HCOOH, HCN, C_2H_2, C_2H_6, CF_2Cl_2, $CFCl_3$, CF_4, CCl_4, CHF_2Cl
[3]	observed "trace"	small	ClO, $ClONO_2$, HO_2, OH
[4]	predicted "trace"	small	N_2O_5, CH_3Cl, HOCl, HNO_4, HNO_2, H_2O_2, HBr, SO_2, H_2S, H_2SO_4, C_3H_8, C_2H_4.

[1]According to the optical depths of the molecules in the stratosphere and upper troposphere.

In category [1] of Table B-1, the long geometric path, relative to the optical depth, of field measurements gives rise to spectral features of many weak transitions (isotopes, hot bands, etc.) not usually encountered in ordinary laboratory spectroscopy. For the infrared active molecules such as H_2O, CO_2, O_3, N_2O, CO and CH_4, this means that high rotational and vibrational quantum numbers for the participating energy levels, high order terms in the Hamiltonian expansions, and various resonance interactions between specific levels must be known. Indeed, for the polyatomic molecules in this list, it has proven necessary to do simultaneous analysis of several bands, taking into account high-order rotational terms and extensive vibration-rotation interactions. In addition, hyperfine line parameters are now needed not only for the microwave lines, but also for light diatomic molecules (e.g., NO and OH) observed in the infrared. For the infrared inactive molecules, such as N_2 and O_2, electric quadrupole line transitions and pressure-induced transitions are significant (pressure-induced transitions of CO_2, N_2O and CH_4 should have only a small effect on atmospheric spectra).

In category [2], the medium geometric path involves relatively simpler spectra for the small molecules (NH_3, HCN). However, the spectra of the larger molecules (CCl_4, $ClONO_2$) can be quite complex. The spectroscopic analysis of some of the larger molecules where the full line structure cannot be resolved requires the application of semi-empirical methods, such as band models, for quantification of these molecules from atmospheric spectra.

In categories [3] and [4], the small geometric path implies much simpler spectroscopic analysis. However, some of these molecules are unstable, and others are large molecules, so that the quantitative analysis can be quite complicated. Nevertheless, the "linear region of the curve of growth" approximation is applicable to most of these species so that the halfwidth and line shape dependence are not very significant for their quantification in the atmosphere.

The above list includes all of the species that have been measured to date in the stratosphere and upper troposphere by infrared and/or microwave spectroscopy. Other stratospheric infrared active species not listed here, such as NO_3, have been identified and quantified by their visible and ultraviolet (UV) spectra. It is important to realize, however, that with the current improvement in instrumental and theoretical techniques, it is anticipated that new species will be identified which may have strong catalytic effects. Thus, category [4] includes several potential species predicted by current photochemical/dynamic models but not yet confirmed. While the line parameters for some of these species are accurately known, only a first order quantification is needed for the initial identification.

The spectral resolution of the measurements is an important parameter in atmospheric spectroscopy. While many quantitative measurements can be made successfully from medium resolution spectra, the true stratospheric halfwidth of spectral lines is of the order of 0.001 to 0.02 cm^{-1}. Only 10 years ago, none of the field spectrometers were capable of measuring infrared atmospheric spectra at this resolution. Currently, a number of such high resolution field instruments are available and used for more sensitive quantitative atmospheric spectroscopy, for both absorption and emission spectra. These include grating, Fourier, laser and microwave spectrometers as well as others.

An extensive summary of the last 10 years [1975-1985] of atmospheric spectroscopic measurements of the species in Table B-1 is given in Table B-2; it is limited to spectral measurements of medium to high resolution only (better than 0.5 cm^{-1}), thus excluding lower resolution spectrometers and wide band filter instruments used extensively in many atmospheric measurements. Only results published in refereed journals and papers in preparation have been included. Table B-3 includes spectroscopic systems now under development for stratospheric and upper tropospheric species measurements, with classifications similar to those in Table B-2. The explanations of the instrumental abbreviations used in Tables B-2 and B-3, as well as the institution abbreviations of Table B-3, are given in Annex B-1 and Annex B-2, respectively, at the end of this appendix.

Despite the large number of spectral lines involved in the atmospheric spectrum (more than 500,000 lines), it is usually effective to perform detailed laboratory measurements only on a relatively small number of lines in preselected regions. Such measurements can yield relative or absolute intensity and line shape quantification with accuracy on the order of 1% to 5%. Combining such results with modern spectroscopic theories allows, in many cases, determination of line parameters in much wider spectral regions with accuracies of 10% or better. The selection of intervals for quantitative analysis will be specific to the planned experiment. Several laboratories are now equipped with high resolution quantitative spectroscopy systems, and are suited for such measurements. These include grating, Fourier, laser and microwave spectrometers with specialized absorption cells for various temperatures, pressures and optical paths for stable as well as unstable and corrosive gases. These are described separately in the following section.

Table B-2. Review of High-Resolution Microwave to Infrared Spectroscopic Field Measurements of Atmospheric Gases (1975-1985).

Spectral Region (cm^{-1})	Measurement Accuracy	Reference	Vehicle†	Instrument‡	Resolution* (cm^{-1})	Method**
H_2O						
20-130	50%	Clark & Kendall (1976)	Balloon	FTS	0.2	Emiss.
20-120		Kendall & Clark (1978)	Balloon	FTS	0.06	Emiss.
36-85		Carli *et al* (1980)	Balloon	FTS	0.003	Emiss.
1600-1610		Niple *et al* (1980)	Balloon	FTS	0.02	Absorp.
1599-1608	30%	Louisnard *et al* (1980)	Balloon	Grille	0.1	Absorp.
3229-3238	20%	Farmer *et al* (1980)	Balloon	FTS	0.15	Absorp.
30-110		Kendall & Clark (1981)	Balloon	FTS	0.06	Emiss.
30-80	10%	Naylor *et al* (1981)	Balloon	FTS	0.15	Absorp.
1323-1327,1602-1608	15%	Girard *et al* (1983)	Aircraft	Grille	0.1	Absorp.
794-798, 945-950	15%	Goldman *et al* (1983a)	Ground	FTS	0.02	Absorp.
1288-1326, 1595-1600, 1840-1846, 2860-2870, 2940-2950	10-20%	Louisnard *et al* (1983)	Balloon	Grille	0.1	Absorp.
1600-1608		Girard and Louisnard (1984)	Balloon	Grille	0.1	Absorp.
3815-3825		Lippens *et al* (1984)	Spacelab	Grille	0.1	Absorp.
3949-3951	15%	Park *et al* (1984)	Balloon/	FTS/	0.04/	Absorp./
			Balloon	FTS	0.15	Absorp.
1350-1570	15-20%	Rinsland *et al* (1984b)	Balloon/	FTS/	0.02/	Absorp./
			Aircraft	FTS	0.06	Absorp.
1335-1350,		Murcray *et al* (1985a)	Balloon/	Grating/	0.5/	Emiss./
278-400,			Balloon/	Grating/	0.25/	Emiss./
1600-1608,			Balloon/	Grille/	0.1/	Absorp./
80-220,	15%		Balloon/	FTS/	0.03/	Emiss./
2900-3000			Balloon	Grating	0.04	Absorp.
1450-1650		Kunde *et al* (1985)	Balloon	FTS	0.05	Emiss.
1450-1650		Murcray *et al* (1985b)	Balloon	FTS	0.08	Emiss.
HDO						
7-85		Carli *et al* (1980)	Balloon	FTS	0.003	Emiss.
1469-1513	15-20%	Rinsland *et al* (1984b)	Balloon/	FTS/	0.02/	Absorp./
1450-1486			Aircraft	FTS	0.06	Absorp.
CO_2						
2382-2392	10%	Farmer *et al* (1980)	Balloon	FTS	0.15	Absorp.
794-798, 945-950	5%	Goldman et al (1983a)	Ground	FTS	0.02	Absorp.
2046-2056		Louisnard *et al* (1983)	Balloon	Grille	0.1	Absorp.
3505-3509	15%	Park *et al* (1984)	Balloon/	FTS/	0.15/	Absorp./
			Balloon	FTS	0.04	Absorp.
700-800		Kunde *et al* (1985)	Balloon	FTS	0.05	Emiss.
700-800		Murcray *et al* (1985b)	Balloon	FTS	0.08	Emiss.
O_3						
20-90	40%	Clark & Kendall (1976)	Balloon	FTS	0.2	Emiss.
1011-1012		Frerking *et al* (1977)	Ground	LHS	0.007	Absorp.
20-120		Kendall & Clark (1978)	Balloon	FTS	0.06	Emiss.

Table B-2. Review of High-Resolution Microwave to Infrared Spectroscopic Field Measurements of Atmospheric Gases (1975-1985). — Continued

Spectral Region (cm^{-1})	Measurement Accuracy	Reference	Vehicle†	Instrument‡	Resolution* (cm^{-1})	Method**
O_3 — Continued						
1043.14-1043.18		Abbas *et al* (1978)	Ground	LHS	0.0002	Absorp.
7-85		Carli *et al* (1980)	Balloon	FTS	0.003	Emiss.
1720-1725		Goldman *et al* (1980)	Balloon	FTS	0.02	Absorp.
2778-2804, 3044-3056	25%	Farmer *et al* (1980)	Balloon	FTS	0.15	Absorp.
30-80	10%	Kendall & Clark (1981)	Balloon	FTS	0.06	Emiss.
30-80		Naylor *et al* (1981)	Balloon	FTS	0.15	Emiss.
6.876, 7.032	15%	Waters *et al* (1981)	Balloon	MWS		Absorp.
1001-1004	10%	Goldman *et al* (1983a)	Ground	FTS	0.02	Absorp.
1045-1085, 2046-2056, 2130-2138	10%	Louisnard *et al* (1983)	Balloon	Grille	0.1	Absorp.
2084-2085		Marche *et al* (1983)	Ground	SISAM	0.02	Absorp.
1080-1085	10%	Girard *et al* (1983)	Aircraft	Grille	0.1	Absorp.
2130-2135		Girard and Louisnard (1984)	Balloon	Grille	0.1	Absorp.
700-800, 1100-1200		Kunde *et al* (1985)	Balloon	FTS	0.05	Emiss.
900-1060, 80-220		Robbins *et al* (1985)	Balloon/ Balloon	Grating/ FTS	0.25/ 0.03	Emiss./ Emiss.
975-994, 1044-1090, 1109-1172		Rinsland *et al* (1985c)	Ground	FTS	0.005	Absorp.
700,800, 1100-1200		Murcray *et al* (1985b)	Balloon	FTS	0.08	Emiss.
N_2O						
2200-3500	10-30%	Farmer *et al* (1980)	Balloon	FTS	0.15	Absorp.
10-40		Carli *et al* (1980)	Balloon	FTS	0.003	Emiss.
1177-1187	20%	Coffey *et al* (1981a)	Aircraft	FTS	0.06	Absorp.
1878-1881	15-20%	Rinsland *et al* (1982c)	Balloon	FTS	0.02	Absorp.
1247-1249	5%	Goldman *et al* (1983a)	Ground	FTS	0.02	Absorp.
1323-1327, 2134-2143	15%	Girard *et al* (1983)	Aircraft	Grille	0.1	Absorp.
1288-1295	10-30%	Louisnard *et al* (1983)	Balloon	Grille	0.1	Absorp.
2205-2212		Muller *et al* (1985)	Spacelab	Grille	0.1	Absorp.
1150-1300		Kunde *et al* (1985)	Balloon	FTS	0.05	Emiss.
1150-1300		Murcray *et al* (1985b)	Balloon	FTS	0.08	Emiss.
CO						
40-65		Carli *et al* (1980)	Balloon	FTS	0.003	Emiss.
2145-2167	20-50%	Farmer *et al* (1980)	Balloon	FTS	0.15	Absorp.
2040-2050, 2134-2143	10%	Girard *et al* (1983)	Aircraft	Grille	0.1	Absorp.
2046-2056, 2130-2138	10-25%	Louisnard *et al* (1983)	Balloon	Grille	0.1	Absorp.
Solar CO						
2046-2056, 2134-2143		Girard *et al* (1983)	Aircraft	Grille	0.1	Absorp.
2130-2138		Louisnard *et al* (1983)	Balloon	Grille	0.1	Absorp.
CH_4						
2900-3030	10-30%	Ackerman *et al* (1978/79)	Balloon	Grille	0.1	Absorp.
3000	15-25%	Farmer *et al* (1980)	Balloon	FTS	0.15	Absorp.
1228-1249	10%	Goldman *et al* (1983a)	Ground	FTS	0.02	Absorp.

Table B-2. Review of High-Resolution Microwave to Infrared Spectroscopic Field Measurements of Atmospheric Gases (1975-1985). – Continued

Spectral Region (cm^{-1})	Measurement Accuracy	Reference	Vehicle†	Instrument‡	Resolution* (cm^{-1})	Method**
CH_4 — Continued						
1323-1327, 2863-2871, 2929-2947	15%	Girard *et al* (1983)	Aircraft	Grille	0.1	Absorp.
1288-1326, 2860-2870, 2940-2950		Louisnard *et al* (1983)	Balloon	Grille	0.1	Absorp.
3010-3020		Lemaitre *et al* (1984)	Spacelab	Grille	0.2	Absorp.
1350-1570	15-20%	Rinsland *et al* (1984b)	Balloon/ Aircraft	FTS/ FTS	0.2/ 0.6	Absorp./ Absorp.
2974-3020		Muller *et al* (1985)	Spacelab	Grille	0.2	Absorp.
1335-1350, 2821-3385		Zander *et al* (1985)	Balloon/ Balloon	Grating/ FTS	0.5/ 0.1	Emiss./ Absorp.
1200-1400		Kunde *et al* (1985)	Balloon	FTS	0.05	Emiss.
1200-1400		Murcray *et al* (1985b)	Balloon	FTS	0.08	Emiss.
O_2						
20-100		Clark & Kendall (1976)	Balloon	FTS	0.2	Emiss.
6-85		Carli *et al* (1980)	Balloon	FTS	0.003	Emiss.
30-110		Clark & Kendall (1980)	Balloon	FTS	0.05	Emiss.
30-110		Kendall & Clark (1981)	Balloon	FTS	0.06	Emiss.
1603-1604		Goldman *et al* (1981b)	Balloon	FTS	0.02	Absorp.
1440-1680		Rinsland *et al* (1982b)	Balloon	FTS	0.02	Absorp.
80-220		Traub & Chance (1985)	Balloon	FTS	0.03	Emiss.
Atomic O						
68.6-68.9, 158.2-158.4		Carli *et al* (1985a)	Balloon	FTS	0.003	Emiss.
157-159		Clark *et al* (1985)	Balloon	FTS	0.01	Emiss.
NO						
1902-1917	25-50%	Ackerman *et al* (1975)	Balloon	Grille	0.1	Absorp.
1890-1892, 1908-1910, 1914-1916	40%	Fontanella *et al* (1975)	Aircraft	Grille	0.1	Absorp.
1898-1903		Bradford *et al* (1976)	Ground	FTS	0.06	Absorp.
1846, 1857, 1915	20-50%	Blatherwick *et al* (1980)	Balloon	FTS	0.02	Absorp.
1845-1860, 1910-1925	20-30%	Murcray *et al* (1980)	Balloon	FTS	0.02	Absorp.
1845-1848, 1859-1863, 1913-1917	20%	Coffey *et al* (1981a)	Aircraft	FTS	0.06	Absorp.
1913-1917		Girard *et al* (1983)	Aircraft	Grille	0.01	Absorp.
1840-1846	15-25%	Louisnard *et al* (1983)	Balloon	Grille	0.1	Absorp.
36-64		Carli *et al* (1983)	Balloon	FTS	0.003	Absorp.
1897-1903	20%	Rinsland *et al* (1984a)	Ground	FTS	0.01	Absorp.
1987		Webster & Menzies (1984)	Balloon	TDL	0.0002	Absorp.
1914-1919		Laurent *et al* (1985)	Spacelab	Grille	0.1	Absorp.
NO_2						
1595-1601	20-30%	Ackerman *et al* (1975)	Balloon	Grille	0.1	Absorp.
1603-1608	20%	Fontanella *et al* (1975)	Aircraft	Grille	0.1	Absorp.
1604-1607	20-50%	Blatherwick *et al* (1980)	Balloon	FTS	0.02	Absorp.

Table B-2. Review of High-Resolution Microwave to Infrared Spectroscopic Field Measurements of Atmospheric Gases (1975-1985). — Continued

Spectral Region (cm^{-1})	Measurement Accuracy	Reference	Vehicle†	Instrument‡	Resolution* (cm^{-1})	Method**
NO_2 — Continued						
1600-1610		Niple *et al* (1980)	Balloon	FTS	0.02	Absorp.
1600-1610	20%	Coffey *et al* (1981a)	Aircraft	FTS	0.06	Absorp.
36.5-39.0		Kendall & Clark (1981)	Balloon	FTS	0.06	Emiss.
1602-1608	15%	Girard *et al* (1983)	Aircraft	Grille	0.1	Absorp.
1595-1600	6-50%	Louisnard *et al* (1983)	Balloon	Grille	0.1	Absorp.
2880-2930	15-25%	Camy-Peyret *et al* (1983)	Ground	FTS	0.01	Absorp.
67-68		Carli *et al* (1983)	Balloon	FTS	0.003	Emiss.
2880-2930		Flaud *et al* (1983)	Ground	FTS	0.01	Absorp.
2890-2930	25-50%	Kendall & Buijs (1983)	Balloon	FTS	0.04	Absorp.
1595-1600		Girard & Louisnard (1984)	Balloon	Grille	0.1	Absorp.
1575-1610		Kunde *et al* (1985)	Balloon	FTS	0.05	Emiss.
1595-1599		Laurent *et al* (1985)	Spacelab	Grille	0.1	Absorp.
1600-1615		Roscoe *et al* (1985a)	Balloon	Grating	0.5	Emiss.
OH						
60-90		Kendall & Clark (1979)	Balloon	FTS	0.06	Emiss.
61.0-61.4, 83.6-84.0		Carli *et al* (1983)	Balloon	FTS	0.003	Emiss.
80-220		Chance & Traub (1985)	Balloon	FTS	0.03	Emiss.
61-62, 83-84		Carli *et al* (1985a)	Balloon	FTS	0.003	Emiss.
118-189						
Solar OH						
825-960	50%	Goldman *et al* (1981c)	Balloon	FTS	0.02	Absorp.
810-960		Goldman *et al* (1983b)	Balloon/	FTS/	0.02/	Absorp./
			Ground	FTS	0.01	Absorp.
2400-3300		Grevesse *et al* (1984)	Ground	FTS	0.01	Absorp.
HF						
4038-4040	20%	Zander (1975)	Balloon	Grating	0.08	Absorp.
4038-4040		Farmer & Raper (1977)	Balloon	FTS	0.15	Absorp.
41.0-41.2		Carli *et al* (1980)	Balloon	FTS	0.003	Emiss.
3833-4040	25%	Buijs *et al* (1980)	Balloon	FTS	0.05	Absorp.
4038-4040	20%	Farmer *et al* (1980)	Balloon	FTS	0.15	Absorp.
160-250	20%	Traub & Chance (1981)	Balloon	FTS	0.03	Emiss.
4038-4041	6-20%	Zander (1981a,b)	Balloon	Grating	0.04	Absorp.
4038-4041	50%	Girard *et al* (1982)	Aircraft	Grille	0.2	Absorp.
3944-4009	40%	Girard *et al* (1983)	Aircraft	Grille	0.2	Absorp.
4039-4041,	20%/	Park *et al* (1984)	Balloon/	FTS/	0.02/	Absorp./
3877-3878	30%		Balloon	FTS	0.04	Absorp.
160-250	20%	Farmer *et al* (1985)	Balloon	FTS	0.03	Emiss.
163.9-164.1		Carli *et al* (1985a)	Balloon	FTS	0.003	Emiss.
HCl						
2923-2947	40%	Ackerman *et al* (1976)	Balloon	Grating	0.22	Absorp.
2923-2928		Bradford *et al* (1976)	Ground	FTS	0.06	Absorp.
2929-2947	25%/	Farmer *et al* (1976)	Ground/	FTS/	0.15/	Absorp./

Table B-2. Review of High-Resolution Microwave to Infrared Spectroscopic Field Measurements of Atmospheric Gases (1975-1985). — Continued

Spectral Region (cm^{-1})	Measurement Accuracy	Reference	Vehicle†	Instrument‡	Resolution* (cm^{-1})	Method**
HCl — Continued						
	10%		Aircraft	FTS	0.15	Absorp.
2926-2927	25-50%	Farmer and Raper (1977)	Balloon	FTS	0.15	Absorp.
2841-2844, 2924-2946	30%	Raper *et al* (1977)	Balloon	FTS	0.15	Absorp.
2925-2946	15%	Buijs *et al* (1980)	Balloon	FTS	0.05	Absorp.
40-83		Carli *et al* (1980)	Balloon	FTS	0.003	Emiss.
2841-2844, 2924-2946	20-50%	Farmer *et al* (1980)	Balloon	FTS	0.15	Absorp.
124-126, 144-146	27%	Chance *et al* (1980)	Balloon	FTS	0.03	Emiss.
140-250	20%	Traub & Chance (1981)	Balloon	FTS	0.03	Emiss.
2775-2776, 2942-2943	20-25%	Marche *et al* (1980a,b)	Ground	SISAM	0.03	Absorp.
103.0-105.5		Kendall & Clark (1981)	Balloon	FTS	0.06	Absorp.
2942-2946	17-24%	Zander (1981a,b)	Balloon	Grating	0.04	Absorp.
2942-2946	25-30%	Girard *et al* (1982)	Aircraft	Grille	0.1	Absorp.
2942-2946	25%	Girard *et al* (1983)	Aircraft	Grille	0.1	Absorp.
40-83,110-187		Carli *et al* (1985a)	Balloon	FTS	0.003	Emiss.
140-250,	15%/	Farmer *et al* (1985)	Balloon/	FTS/	0.03/	Emiss./
2821-3385	22-27%		Balloon	FTS	0.1	Absorp.
2803-3057		Fast *et al* (1985)	Balloon	FTS	0.1	Absorp.
HBr						
49.9-50.1, 83.3		Carli *et al* (1985a)	Balloon	FTS	0.003	Emiss.
ClO						
853.122	30%	Menzies (1979)	Balloon	LHS	0.001	Absorp.
6.816	25%	Parrish *et al* (1981)	Ground	MWS	<0.001	Emiss.
6.816	40%	Waters *et al* (1981)	Balloon	MWS	<0.001	Emiss.
853.125	30-40%	Menzies (1983)	Balloon	LHS	0.001	Absorp.
856.5, 859.8		Mumma *et al* (1983)	Ground	LHS	0.001	Absorp.
6.8163-9.2941	5-25%	Solomon *et al* (1984)	Ground	MWS	<0.001	Emiss.
22.8-23.0		Carli *et al* (1985b)	Balloon	FTS	0.003	Emiss.
OCS						
2050-2060	10-30%	Mankin *et al* (1979)	Aircraft	FTS	0.06	Absorp.
2046-2056	30-50%	Louisnard *et al* (1983)	Balloon	Grille	0.1	Absorp.
2040-2050	15%	Girard *et al* (1983)	Aircraft	Grille	0.1	Absorp.
H_2CO						
2806-2808, 2868-2871	75%	Barbe *et al* (1979)	Ground	SISAM	0.03	Absorp.
HCOOH						
1100-1108	75%	Goldman *et al* (1984a)	Balloon	FTS	0.02	Absorp.
NH_3						
825-935		Murcray *et al* (1978)	Ground	FTS	0.06	Absorp.
927.22-927.30	20-25%	Hoell *et al* (1980)	Ground	LHS	−0.001	Absorp.

C-4

Table B-2. Review of High-Resolution Microwave to Infrared Spectroscopic Field Measurements of Atmospheric Gases (1975-1985). — Continued

Spectral Region (cm^{-1})	Measurement Accuracy	Reference	Vehicle†	Instrument‡	Resolution* (cm^{-1})	Method**
HNO_3						
1324-1336	30%	Fontanella *et al* (1975)	Aircraft	Grille	0.1	Absorp.
860-890		Bradford *et al* (1976)	Ground	FTS	0.006	Absorp.
9-25		Carli *et al* (1980)	Balloon	FTS	0.003	Emiss.
1720-1725		Goldman *et al* (1980)	Balloon	FTS	0.02	Absorp.
1720-1725	20%	Coffey *et al* (1981a)	Aircraft	FTS	0.06	Absorp.
875-900	22%	Lippens & Muller (1981)	Ground	FTS	0.13	Absorp.
1323-1327	20-30%	Girard *et al* (1982)	Aircraft	Grille	0.1	Absorp.
1323-1327	20-30%	Girard *et al* (1983)	Aircraft	Grille	0.1	Absorp.
1320-1326	10-20%	Louisnard *et al* (1983)	Balloon	Grille	0.1	Absorp.
867-873	50%	Goldman *et al* (1984c)	Balloon	FTS	0.02	Absorp.
1320-1326		Girard & Louisnard (1984)	Balloon	Grille	0.1	Absorp.
884		Murcray *et al* (1985b)	Balloon	Grating	0.25	Emiss.
850-925		Kunde *et al* (1985)	Balloon	FTS	0.05	Emiss.
870-900		Pollitt *et al* (1985)	Balloon	Grating	0.25	Emiss.
860-900		Murcray *et al* (1985b)	Balloon	FTS	0.08	Emiss.
N_2						
2395-2420		Camy-Peyret *et al* (1981)	Ground	FTS	0.01	Absorp.
2395-2420		Goldman *et al* (1981b)	Ground	FTS	0.06	Absorp.
2395-2420		Rinsland *et al* (1981)	Balloon	FTS	0.15	Absorp.
HCN						
3270-3290	10%	Coffey *et al* (1981b)	Aircraft	FTS	0.06	Absorp.
25-60		Carli *et al* (1982)	Balloon	FTS	0.003	Emiss.
3287-3287.5, 3299-3300	25%	Rinsland *et al* (1982a)	Ground	FTS	0.01	Absorp.
3270-3300	50-75%	Smith & Rinsland (1985)	Balloon	FTS	0.15	Absorp.
CH_3Cl						
2870-3010		Kendall & Buijs (1983)	Balloon	FTS	0.04	Absorp.
H_2O_2						
6.83	50%	Waters *et al* (1981)	Balloon	MWS	<0.001	Emiss.
51-54, 93-96, 111-113		Kendall & Clark (1981)	Balloon	FTS	0.06	Emiss.
90-150		Chance & Traub (1984)	Balloon	FTS	0.06	Emiss.
$CFCl_3$ (F-11)						
830-860	20%	Wlliams *et al* (1976)	Balloon	Grating	0.3	Absorp.
830-860		Bradford *et al* (1976)	Ground	FTS	0.06	Absorp.
830-860	8%	Lippens & Muller (1981)	Ground/ Ground	FTS/ FTS	0.13/ 0.13	Absorp./ Emiss.
824-864	16-24%	Zander *et al* (1983)	Ground	FTS	0.01	Absorp.
840-860		Kunde *et al* (1985)	Balloon	FTS	0.05	Emiss.
840-860		Murcray *et al* (1985b)	Balloon	FTS	0.08	Emiss.

Table B-2. Review of High-Resolution Microwave to Infrared Spectroscopic Field Measurements of Atmospheric Gases (1975-1985). — Continued

Spectral Region (cm^{-1})	Measurement Accuracy	Reference	Vehicle†	Instrument‡	Resolution* (cm^{-1})	Method**
CF_2Cl_2 (F-12)						
918-925		Bradford *et al* (1976)	Ground	FTS	0.06	Absorp.
900-940	20%	Williams *et al* (1976)	Balloon	Grating	0.3	Absorp.
920-940, 1160-1162	24%	Zander *et al* (1983)	Ground	FTS	0.01	Absorp.
920-925		Kunde *et al* (1985)	Balloon	FTS	0.05	Emiss.
910-930		Murcray *et al* (1985b)	Balloon	FTS	0.08	Emiss.
$ClONO_2$						
1291-1293	25%	Murcray *et al* (1979)	Balloon	FTS	0.02	Absorp.
779-781	60-80%	Rinsland *et al* (1985b)	Balloon	FTS	0.02	Absorp.
CHF_2Cl (F-22)						
828-830	75%	Goldman *et al* (1981d)	Balloon	FTS	0.02	Absorp.
828-830	20-24%	Zander *et al* (1983)	Ground	FTS	0.01	Absorp.
C_2H_2						
776-778	40%	Goldman *et al* (1981a)	Balloon	FTS	0.02	Absorp.
776-777	22%	Zander *et al* (1982)	Ground	FT5	0.01	Absorp.
3250.5-3251, 3304.8-3305.3	15%	Rinsland *et al* (1985a)	Ground	FTS	0.01	Absorp.
C_2H_6						
822-823	17%	Zander *et al* (1982)	Ground	FTS	0.01	Absorp.
821-823	40%	Goldman *et al* (1984b)	Balloon/ Aircraft	FTS/ FTS	0.02/ 0.06	Absorp./ Absorp.
2975-2990, 2976-2977		Coffey *et al* (1985)	Aircraft/ Ground	FTS/ FTS	0.06/ 0.01	Absorp./ Absorp.
CCl_4						
785-810	30%	Williams *et al* (1976)	Balloon	Grating	0.3	Absorp.
CF_4						
1275-1290		Goldman *et al* (1979)	Balloon	FTS	0.02	Absorp.
HO_2						
8.859-8.866	15%	De Zafra *et al* (1984)	Ground	MWS	<0.001	Emiss.

† Type of instrument platform.

‡ See Annex B-1 for explanation of the instrument abbreviations.

* For interferometric spectra, this is either the apodized or the unapodized resolution, depending on how the data were analyzed.

** Emission or absorption measurements.

A slash (/) indicates that two experiments were treated in the article. A comma (,) indicates multiple spectral regions.

Note: It is inevitable, in any extensive compilation such as this, that a few works will inadvertently be overlooked. Our apologies to any authors whose publications have thus been accidentally omitted.

Table B-3. Some Examples of High Resolution Infrared to Microwave Atmospheric Spectrometer Systems in Progress

Institution¶	Instrument*	Resolution†	Spectral Interval[s]	Vehicle‡	Method**
JPL	FTS	10	500 - 5000	Shuttle	Absorp.
	FTS	10	500 - 5000	Balloon	Absorp.
	TDL	0.2	330 - 3300	Balloon	Absorp.
MET.FRANCE	Grille	100	1000 - 4000	Aircraft	Absorp.
NASA Goddard	Cold FTS	20	650 - 2000	Balloon	Emiss.
NCAR	TDL	1	800 - 1300	Aircraft	Absorp.
LPMOA Orsay	FTS	10	650 - 4000	Balloon	Absorp.
LPM Reims	FTS	3	1000 - 1600	Ground	Absorp.
	LHS	0.3	1000	Ground	Absorp.
SAO Harvard	FTS	4	80 - 250	Balloon	Emiss.
U. Calgary	FTS	15	20 - 90	Balloon	Absorp.
U. Denver/AFGL	Cold FTS	60	650 - 2500	Balloon	Emiss.
U. Denver	FTS	3	650 - 2500	Balloon	Absorp.
	LHS	0.3	1000	Ground	Absorp.
U. München	Cold FTS	100	650 - 2000	Balloon	Emiss.

¶ see Annex B-2 for explanation of the institution abbreviation
* see Annex B-1 for explanation of the instrument abbreviation
† Resolution in units of 10^{-3} cm^{-1}. For interferometric spectra, it is either the apodized or the unapodized resolution, depending on how the data were analyzed.
s spectral interval in units of cm^{-1}
‡ type of instrument platform.
** emission or absorption measurements

B-3 LABORATORY SPECTROSCOPY BY SPECTRAL ANALYSIS AND PREDICTIONS

Laboratory measurement capabilities in the infrared and microwave regions have undergone significant evolution in the past ten years. Examples of current laboratory spectroscopy capabilities are listed in Table B-4. Where the exact frequency range was not known we have used near infrared (IR) to mean the region near 2μm, mid-IR to mean the region near 10 μm, and far-IR to mean the region near 100 μm. There are approximately 60 microwave groups of similar capability. Rather than list them all, we have summarized them in the last entry in the table. Instrument and institutional abbreviations are expanded in Annex B-1 and B-2, respectively.

With the advent of computer assisted data analysis, it is now possible to reproduce the experimental absorption profile with model lineshapes to within experimental errors. However, due to our lack of understanding of the systematic errors in instrument performance, the significance of the derived lineshape parameters is less certain. With care, line positions can be retrieved to 1/20 to 1/100 of the instrumental width, and intensities and collisional widths can be retrieved to 5%. Systematic effects which degrade these accuracies include multiple lines, channeling, source power variations with frequency, and continuum contributions. Development of believable capabilities for measurement of intensities and widths which are more accurate than 5% will require much more work and a coordinated program of intercomparisons between different laboratories. Moreover, it should be emphasized that accurate laboratory data are more readily obtained for the more stable trace species such as CH_4, etc., compared to the reactive compounds such as $ClONO_2$ and HNO_3, due to the difficulty in manipulating these compounds in the laboratory.

Use of predictive models has always been an essential part of interpreting the spectrum. A model Hamiltonian is used to assign the spectrum and predict the relative intensities and energies of the levels involved in the transition. The complexity of the model varies with the complexity of the molecule, but challenges the state of the art only when there are multiple interacting vibrational states. Typically, line positions can be fit to better than one part in 10^7 in frequency. Prediction of line centers can be made with known errors deduced from the fit, although care must be taken in extrapolating out of the range of measured quantum numbers.

Relative intensities within a band can also be predicted from the molecular Hamiltonian. Absolute intensities require measurements of gas concentration in the infrared or permanent dipole moments in the rotational region. In the case of resonances or severe centrifugal interaction, corrections to the predicted intensities may be required. Halfwidth predictions require collision theory which is not as well developed as the theory used for frequency and intensity predictions. Current approximate theories, such as the Anderson-Tsao-Curnutte (ATC) method (Anderson, 1949; Tsao and Curnutte, 1962) or the Quantum Fourier transform (QFT) method (Davies, 1975), reproduce widths to 10% if adjustable parameters are used (Robert and Bonamy, 1979; Lacome *et al.*, 1983; Gamache and Davies, 1985). More exact available theories require several orders of magnitude more computing resources.

Table B-4. Examples of Some Current Infrared to Microwave Laboratory Spectroscopy Capabilities.

Institution†	Instrument*	Resolution‡	Spectral Interval¶	Sample Cells
AFGL	FTS	3	400–4000	
Duke U.	Submillimeter	0.003	3–35	2 m
IROE	FTS	1.3	10–200	1.4 m
ISM-CNR	FTS	20	IR	20 m
JPL	Laser Sideband	0.01	10–100	2 m cooled, DC discharge
	Submillimeter	0.003	3–35	
	TDL	1	mid-IR	
	FTS (Bomem)	4	400–4000	0.8 m
	FTS (Nicolet)	60	8–4000	
JRC Ispra	TDL	1	mid-IR	cooled cells
	FTS (Bruker)	30	mid-IR	60 m, 256 m
Kitt Peak NSO	FTS	5	500–4000	384 m White cell
LIR Orsay	FTS	3	600–4000	cooled cells
	TDL	1	mid-IR	
LPM Reims	SISAM	20	IR	
	FTS	2	800–4000	4 m cooled, 30 m,
	LHS heterodyne	0.1	mid-IR	3 km
LPMOA Orsay	FTS (Bomem)	20	400–9000	
LSM-ENEA	TDL	3	620–760	1 m
LSM Paris	FTS (Bomem)	1	600–10000	40 m cooled
	TDL	1	mid-IR	
NASA Ames	FTS (Bomem)	4,60	400–4000	30 cm cryogenic, 35 m, 3000 m
	FTS (Nicolet)	60		35 m, 3000 m White cells
	TDL	1	mid-IR	
NASA Goddard	TDL	1	mid-IR	
	FTS	60	4–4000	
	CO_2 laser heterodyne	0.1	900–1100	
NASA Langley	TDL	1	mid-IR	5, 10, 25,
	FTS (Nicolet)	60	400–4000	50 cm cooled
NBS Boulder	CO_2 difference laser	0.01	10–200	

Table B-4. Examples of Some Current Infrared to Microwave Laboratory Spectroscopy Capabilities. — Continued

Institution†	Instrument*	Resolution‡	Spectral Interval¶	Sample Cells
NBS Washington	FTS (Bomem)	4	8–4000	cooled cells
	FTS (Nicolet)	60		35 m, 3000 m White cells
	TDL	0.1, 1	mid-IR	
	difference frequency	1	near-IR	
NCAR	FTS	20	IR	atmospheric spectra
NOAA/NESDIS	TDL	1	mid-IR	8 m cooled
	grating spectrometer			
NPL	FTS	15	10–200	13 m
NRC Canada	FTS (Bomem)	4	400–4000	
OSU	FTS (Nicolet)	60	400–4000	2 km cooled
RAL	FTS (Bomem)	4	400–4000	cooled 5 m, 20 m, 1000 m
U. Bologna	FTS	12	IR-Visible	20 m
U. Denver	grating spectrometers			
	FTS (Eocom)	60	500–400	atmospheric spectra
	FTS (Bomem)	20		
	FTS (Bomem)	4		
U. Louvain	Intracavity (CO_2,CO)	0.01		
	Laser Stark spectrometer			
U. Oulu	FTS	3	far-IR	
			up to 1000	
U. Stony Brook	grating spectrometer	100	IR	5 cm to 100 m
	TDL	1		cooled
(+60 institutions) see text	microwave	0.001	0.3–3	2 m some cooled

† See Annex B-2 for explanation of the institution abbreviation.
* See Annex B-1 for explanation of the instrument abbreviation.
‡ unapodized in units of $10^{-3}cm^{-1}$
¶ in units of cm^{-1}

B-4 USE OF SPECTROSCOPIC DATA TO DERIVE ATMOSPHERIC COMPOSITION

Analysis of atmospheric data consists of identifying the species that give rise to individual features in the atmospheric spectra and retrieving important atmospheric parameters as a function of altitude (vertical profiles). The general tasks involved are:

- line-by-line identification of observed features (including detection of new species);
- upper limits of species not directly observed;
- retrieval of volume mixing ratios of observed species;
- retrieval of pressure and temperature profiles.

To accomplish these tasks, the observed spectra are often compared to synthetic spectra, the computation of which requires good knowledge of:

- the spectroscopic parameters and line shapes;
- the instrumental effects of the spectrometer;
- the pressure and temperature profiles of the atmosphere;
- the estimates of the concentrations or volume mixing ratios of species as a function of altitude;
- the geometric path.

In an analysis of atmospheric data, identifications of spectral features are often made by computer matching of the observed line centers of the spectral lines to values given in the spectroscopic database and by visual inspection of plots computed with approximate atmospheric parameters. Once the features in a spectrum are generally identified, then one can say with confidence that the absorptions of a particular species are not observed and obtain upper limits of concentration.

The retrievals of vertical concentration profiles and pressure or temperature profiles from the spectra are done using various methods (such as least squares techniques, equivalent-width method, etc.). The measurements are made for altitudes from sea level to 120 km where atmospheric pressures range from 1 to 10^{-6} atm and temperatures from 300 K to 180 K. In practice, the vertical profiles can be obtained through the "onion-peel" approach; in this, parameters for the uppermost altitudes (pressure, temperature, number density, etc.) are retrieved first and then held fixed in the computed spectra when determining the parameters at lower altitudes. A complimentary method of retrieving vertical profiles involves the fitting of an observed radiance profile to a simulated profile, with the fitting done simultaneously at every altitude point over the range of intensity. The simultaneous spectral radiance profiles are generated using available spectroscopic data and assuming an atmospheric model for the gas (or gases) of interest. As a practical matter, researchers may select small spectral intervals that contain absorptions of just a few (or one) species whose vertical profiles are to be obtained by the retrieval technique. The interval may be as small as 1 cm^{-1} or as large as a few hundred cm^{-1}, depending on the application.

As indicated in Section B-3, the essential molecular parameters required for the interpretation of atmospheric data are positions, strengths, widths and lower state energies of those species which contribute to the atmospheric spectrum. The required accuracies of these molecular parameters will vary according to how they are to be used. The identification of the spectral features and determination of upper limits can be readily accomplished with only moderately accurate parameters. In a spectrum recorded at 0.01 cm^{-1} resolution, with a signal-to-noise ratio of 100:1, features can be readily matched by computer if the line positions in the database are given to only 0.003 cm^{-1} and strengths to only $\pm$ 20% with ground

state energies known to 5%. In fact, many of the features in the ongoing atmospheric atlases, such as those from the University of Denver (Blatherwick, *et al.*, 1982; Goldman *et al.*, 1982), the Kitt Peak Solar Atlas (Delbouille *et al.*, 1981) and the IROE-CNR Atlas (Baldecchi *et al.*, 1984) have been assigned and quantified using current database compilations. These databases must be as complete as possible and contain the parameters of all lines that might be observed. For the trace species, this can generally be achieved by study of the fundamentals and a few of the weaker overtones and hot bands. For the major gases, parameters of many bands and several isotopes with strengths ranging over four to six orders of magnitude are needed. In all, the database appropriate for today's technologies probably consists of over 500,000 entries.

Molecular parameters of features in the selected intervals will be utilized in the computer retrieval of atmospheric parameters and therefore must be known with better accuracies. For example, Figure B-1 shows a comparison between observed and computed spectra overlaid with the differences between the two (the residuals labelled O-C) plotted below. The observed spectrum is a laboratory spectrum of CH_4 recorded at 0.01 cm^{-1} resolution with a signal-to-noise ratio of 500:1 using the FTS (Fourier transform spectrometer) at Kitt Peak NSO. As an illustration, different types of errors have been introduced in the parameters of the computed spectrum. In the left panel, the positions of the three strong lines (a, b, c) are in error by 0.0001, 0.0005 and 0.0030 cm^{-1}, respectively, while at the right, the strengths of the same three lines (d, e, f) are in error by 1%, −5% and 15%, respectively. Visually, the two spectra appear to be in good agreement in both panels, but the residuals in the difference plots are considerably different around each line. Whether or not these errors will adversely affect the retrieval of atmospheric parameters depends on the signal-to-noise ratio of the observed spectrum. If the signal-to-noise ratio of the observed spectrum of Figure B-1 were 100:1, the errors in lines b and e would be substantially masked. However, the errors in lines c and f would still interfere with the functioning of an algorithm which uses the residuals to direct its action. The retrieval mechanism would try to adjust atmospheric parameters to compensate for errors in the molecular parameters, thus resulting in an incorrect retrieval of atmospheric physical and chemical properties.

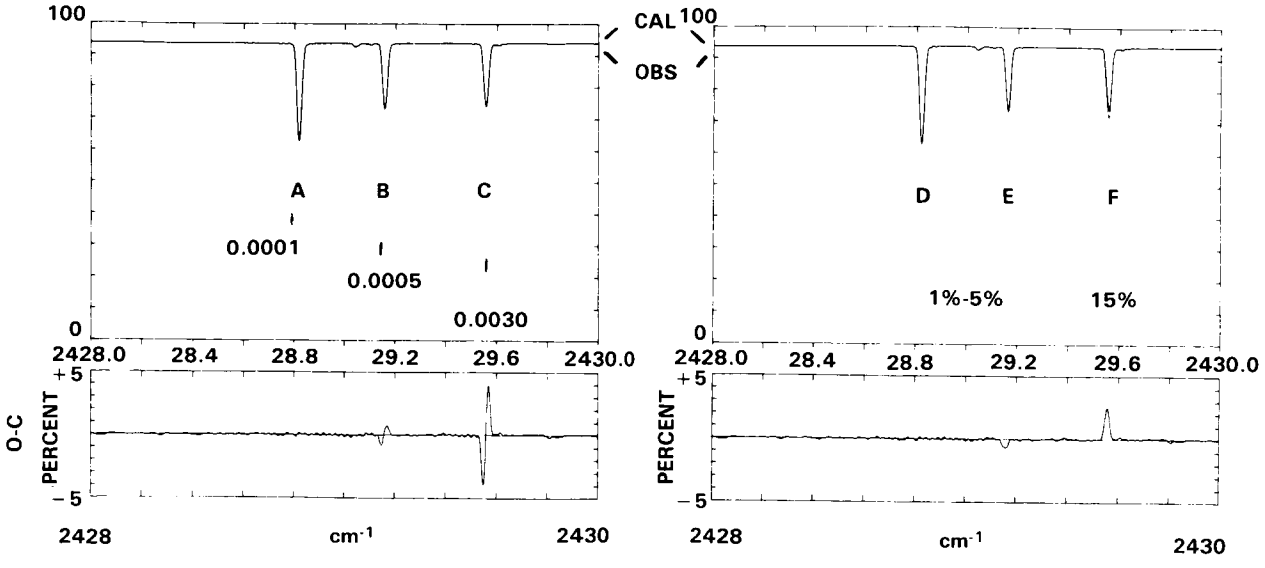

Figure B-1. A Comparison of Observed and Synthetic Spectra of CH_4.

SPECTROSCOPIC DATABASE

An example of how uncertainties in a particular spectroscopic parameter (line strengths) impact the accuracy of a retrieved vertical profile is shown by Figure B-2. For this, a profile of ozone was generated using a specific value of strengths for a series of lines and a particular profile. The profile was then recalculated, but included a 3% change in the strengths of all O_3 lines, and the ozone profile was adjusted to force a fit between the two calculations. In Figure B-2, the standard deviation in percent between the adjusted ozone profile and the assumed profile is shown (on the vertical axis) versus altitude. The uncertainty in the line strengths is seen to give rise to errors of 2.5% to 3% over the altitude range of 20 to 50 km, and there is, to first order, a one-to-one correspondence between the uncertainty in the spectroscopic parameter and the induced error in the retrieved ozone. For reference, the impact of adding an 0.5 K bias and an 0.25 K random error to the temperature knowledge is also shown (lower trace), along with the errors associated with the combination of the two (upper trace).

As discussed in the main body of this document, understanding of the atmospheric chemistry and circulation requires detailed knowledge of vertical profiles of many diverse molecular species. The detection of some of the important trace species, which contribute only a small percentage of intensity to an atmospheric spectrum, can be achieved only with complete spectroscopic knowledge of all species whose transitions overlap the region of the target species. A good example is provided by the recent detection of ClO at 22.9 cm^{-1} (Carli *et al.*, 1985b). This feature has been observed in emission spectra recorded with the same instrument during two balloon flights, one in 1979 and another, with a better signal-to-noise ratio, in 1983. This identification was made possible only after new laboratory data of ozone isotopes and vibrationally-excited ozone became available. These species contribute to the submillimeter stratospheric spectrum with features that have an intensity comparable to that of ClO and cause a background structure which, if not identified, must be considered as measurement noise. Without these new laboratory data, even the 1983 field measurements, with better signal-to-noise ratio, could not be interpreted.

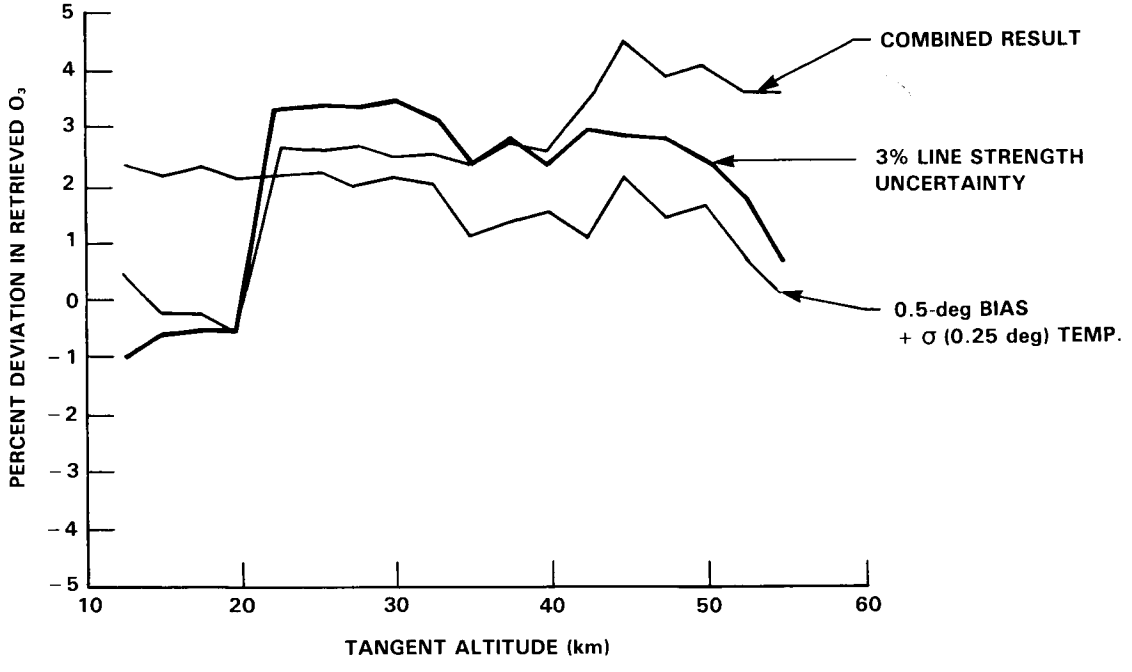

Figure B-2. Effect of Line Strength and Temperature Uncertainties on the Retrieval of Atmospheric Ozone Density.

Another example is provided by the recent study of $ClONO_2$ in the 780 cm^{-1} region (Rinsland *et al.*, 1985b). After balloon-borne spectra (recorded at 0.02 cm^{-1} resolution and long geometric path) revealed several inadequacies in the database for this region, new laboratory research was done to improve the positions and strengths of O_3 and to provide a semi-empirical spectral model for $ClONO_2$ parameters. Once completed, it also became clear that the atmospheric spectrum also contained features arising from the solar atmosphere. In particular, solar OH, $\Delta v = 1$, lines were found to be important in the $ClONO_2$ region, and new work on this species was done. Finally, the improved database was used to do a least squares fitting of the balloon spectra involving O_3 and CO_2 with residuals to 1% and $ClONO_2$ with residuals to 4%.

Thus it should be emphasized that the complete spectroscopic needs of remote sensing are difficult to specify completely until the data from a specific application are examined in detail. One may predict the needs according to species known to be found in the atmosphere or from chemical models that predict the probability of their existence, but quite often a new and interesting analysis of atmospheric data also results in a redefinition of the spectroscopic parameters required.

B-5 EXAMPLES OF SPECTROSCOPIC DATA REQUIREMENTS FOR SPACE-BASED REMOTE SENSING OF THE ATMOSPHERE

B-5.1 The Spectroscopic Requirements of ATMOS

The objective of the ATMOS (Atmospheric Trace Molecule Spectroscopy) investigation is to measure the concentrations and distribution of gases in the upper atmosphere. In May 1985, the ATMOS instrument, a modified Michelson interferometer, orbited the earth aboard the space shuttle at an altitude of 350 km to record the infrared absorption spectrum in the 2 to 16 um region at a resolution of 0.01 cm^{-1} (unapodized). This spectrometer obtained an interferogram every 1.1 seconds with signal-to-noise ratios in the transformed spectrum of 100:1 or better, using the sun as the optical source and optical filters with widths of 600 to 1500 cm^{-1}. The mission provided data from 19 occultations (sunrise and sunset) for a total of 2000 individual spectra. In a typical orbit, the atmospheric data covered altitudes ranging from 16 to 350 km with a vertical resolution of better than 2 km. Yearly reflights are planned.

The species to be investigated during 1985 are shown in Table B-5. They include the major gases (which account for 85% of the observed absorption features), several chemical families of species (nitrogen, hydrogen, halogen) and also hydrocarbons and sulfur compounds.

Analysis will include retrieval by least squares techniques of the pressure-temperature vertical profiles and volume mixing ratios of detected species, as well as upper limits of species not observed, and identification of spectral features. For the first two tasks, small portions of spectra containing unblended, single transitions of one of the targeted species, will be carefully selected from the large volume of available ATMOS spectra and used in the least squares retrieval of parameters. These regions are generally one to two cm^{-1} wide. Efforts will be made to choose windows in which only absorptions of an individual target molecule appear, if possible. Table B-6 lists the general spectral regions where tentative windows are found along with the molecule targeted for detection in each interval.

The interpretation of ATMOS data requires accurate line positions, strengths, widths, and lower state energies of the species listed in Table B-5. Additional parameters may be required for radicals of major gases, species that arise from the outgassing of the shuttle and species previously undetected in the upper atmosphere as well as features from the solar spectrum. As summarized in Table B-7, the required ac-

Table B-5. Species to be Investigated by ATMOS

Major gases	
	H_2O, CO_2, O_3, N_2O, CO, CH_4, N_2, O_2
Minor and Trace gases	
Nitrogen family:	NH_3, NO, NO_2, N_2O_5, HNO_2, HNO_3, HNO_4, HCN
Hydrogen family:	H_2O_2, HO_2, H_2CO, HCOOH, HDO
Halogen family:	Chlorofluorocarbons [$CFCl_3$ (F-11), CF_2Cl_2 (F-12), CF_2HCl (F-22)], CH_3CCl_3, CH_3Cl, CCl_4, HCl, HF, ClO, HOCl, $ClONO_2$, COF_2, COClF, CH_3F, CF_4
Hydrocarbons, Sulfur compounds and others:	
	C_2H_2, C_2H_4, C_2H_6, C_3H_8, OCS, SO_2

curacies of individual parameters vary greatly according to the use made of them. Positions must be known at least to a third of a line width so that the spectral features can be identified and detection windows selected. For the retrieval of vertical profiles, it is desirable that positions be good to 0.0005 cm^{-1} (or better), although in practice, one can often recognize and compensate for small errors in positions through computer software.

Knowledge of line shapes and Doppler and Lorentz widths are needed for data covering the lower part of the stratosphere. Below 35 km, where the pressure is greater than 0.01 atm, the Lorentz contribution to the line profile becomes increasingly important, particularly at longer wavelengths. The accuracies needed for general feature identification are crude (50%), but better accuracies (2% to 5%) are needed for the retrieval of vertical profiles.

The line strengths are needed with accuracies of 20% to 2%, depending on usage. To identify the spectral features, select detection windows for targeted species, and determine upper limits, strengths to 20% are sufficient. However, for transitions used in the vertical profile retrievals, requirements are much more stringent. With the ATMOS data, the volume mixing ratios are obtained using 5 to 25 transitions per molecule for which strengths (and widths) are known to 5% (a total of 1000 lines). For the retrieval of pressure-temperature profiles, some one hundred CO_2 lines are to be used for which line strength accuracies of 1% to 2% are needed.

Over the next decade, the ATMOS project will generate a wealth of atmospheric data which can be analyzed in a reasonable time period only if computerized methods of data reduction and analysis are employed. The task requires (among other things) that a comprehensive computer-accessed database be available. The majority of the parameters can be of modest accuracies (0.003 cm^{-1} for positions and 20% for strengths in the worst case), but for some 1000 selected transitions, accuracies of 0.0005 cm^{-1} for positions and 1 to 5% for strengths are needed.

Table B-6. General Spectral Regions of the ATMOS Analysis

Region†	Targeted Species
650- 750	CO_2
750- 880	CO_2, HNO_2, HNO_3, HNO_4, ClO, $ClONO_2$, $CFCl_3$ (F-11), CF_3Cl (F-13), C_2H_2, C_2H_6, COClF, $COCl_2$, COF_2, CCl_4, OCS
920- 960	NH_3, C_2H_4
1040-1080	O_3
1100-1120	HCOOH
1150-1180	CF_2Cl_2 (F-12)
1200-1400	H_2O, H_2O_2, HOCl, CH_4, CF_4, N_2O_5, N_2O, SO_2, HNO_3
1460-1540	H_2O, O_2
1600-1700	H_2O, NO_2, O_2
1890-1930	CO_2, N_2O, NO
2000-2100	CO_2, OCS
2140-2200	N_2O, CO, O_3
2230-2240	N_2O
2300-2450	CO_2, N_2O, N_2
2580-2590	N_2O
2670-2690	CH_4
2720-2740	HCl
2800-2870	O_3, H_2CO
2900-3080	CH_4, CH_3Cl, HCl, H_2CO, O_3, C_2H_6
3200-3310	H_2O, HCN
3380-3445	N_2O
3800-3870	H_2O
4030-4150	HF
4495-4510	CH_4
4600-4630	CH_4, CO_2

† cm^{-1}

Table B-7. ATMOS Spectroscopic Parameter Accuracy Requirements

Uses	Positions†	Strengths	Widths‡	Lower States	# of Lines
a. Identify species	0.003	20%	50%	20%	4×10^5
b. Upper limits	0.003	20%	50%	20%	10^3
c. VMR profiles*	0.0005	5%	5%	5%	10^3
d. P-T profiles**	0.0005	2%	2%	1%	10^2

† cm^{-1}
‡ air-broadened
* volume mixing ratios
** pressure-temperature profiles

B-5.2 UARS Program Spectroscopic Requirements

The Upper Atmosphere Research Satellite (UARS), which is scheduled for launch in the fall of 1989, will provide global synoptic monitoring of the earth's upper atmosphere from a 600 km orbit for a period of two years.

The goals of the UARS program have been defined (Banks, 1978) as:

- to understand the mechanisms that control upper atmosphere structure and variability;
- to understand the response of the upper atmosphere to natural and anthropogenic perturbations;
- to define the role of the upper atmosphere in climate and climate variability.

To accomplish these goals, three categories of measurements will be performed (Reber, 1985):

- *atmospheric composition and structure:* This involves the measurement of upper atmospheric species distribution and temperature and is directed towards the study of global photochemistry with emphasis on ozone layer chemical cycles;
- *dynamics:* Involving the measurement of upper atmospheric wind and temperature fields;
- *energy input:* Involved primarily with the measurement of solar irradiance and particle energy deposition.

To illustrate the spectroscopic requirements of the UARS project and to keep within the infrared to microwave guidelines of this report, only the four experiments dealing with chemical species are discussed here; comprehensive details of all of the experiments, and their requirements are available as part of the UARS Project Spectroscopy Requirements Document (Roche, 1985), being generated by the UARS spectroscopy working group.

A list of all species to be measured by the four composition/structure experiments, CLAES (Cryogenic Limb Array Etalon Spectrometer), ISAMS (Improved Stratospheric and Mesospheric Sounder), MLS (Microwave Limb Sounder), and HALOE (Halogen Occultation Experiment), is given in Table B-8 with associated spectral intervals. Figure B-3 displays this information on an altitude grid along with details of two other UARS experiments. As seen from this table and figure, UARS will provide (in certain cases, for the first time) global measurements of stratospheric and lower mesospheric chlorine species including ClO, $ClONO_2$, HCl, CF_2Cl_2(F-12), and $CFCl_3$(F-11). It will also provide more complete measurements of the global distribution of ozone and important species in the stratospheric O_x, NO_x and HO_x chemistry and should provide improved measurements of global temperature and pressure.

All four experiments view the earth limb between approximately 10 and 100 km altitude and depend on the inversion of either emitted or absorbed radiances to infer the altitude distribution of species concentrations and temperature. As discussed previously, the inversion process requires data on spectroscopic line parameters including line position, intensity, halfwidth, and line shape for all species of interest over a temperature range of at least 180 to 300 K and an atmospheric pressure range from a few to several hundred millibars. Furthermore, since two of the experiments (HALOE and ISAMS) employ gas cells with relatively high concentrations of the target gases, self-broadened halfwidths and line shapes will be required for these species in addition to air-broadened data.

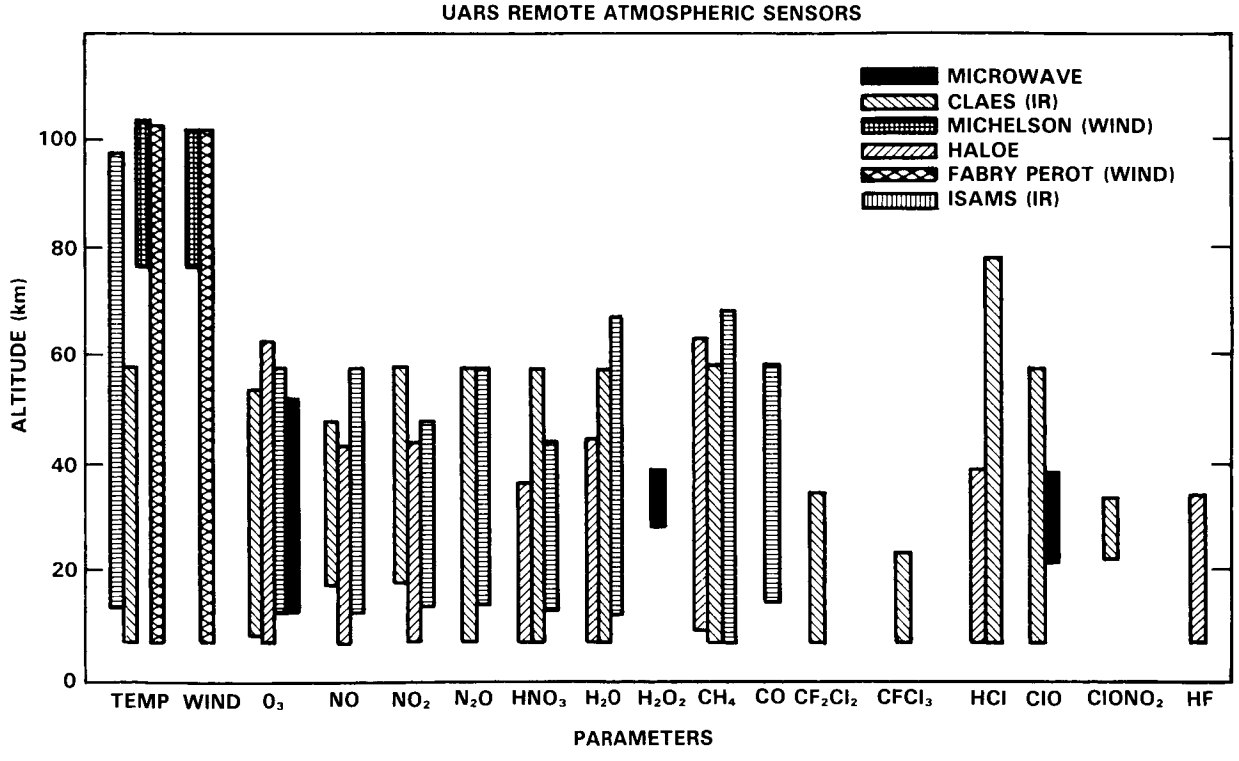

Figure B-3. UARS Remote Atmospheric Sensors.

Table B-8. UARS Atmospheric Spectroscopy Measurements

Atmospheric Composition and Structure				
Instrument	**Description**	**Species/Parameter**		**Spectral Interval/ Line Frequency [cm^{-1}]**
CLAES Cryogenic Limb Array Etalon Spectrometer	Solid-hydrogen cooled spectrometer sensing atmospheric infrared emissions	HCl		2838-2848
		NO		1892-1902
		NO_2, H_2O		1600-1610
		N_2O, CH_4, $ClONO_2$		1288-1298
		CF_2Cl_2 (Fl2), CO_2		920-930
		HNO_3		874-884
		$CFCl_3$ (F11), O_3, Aerosol		835-845
		O_3, Pressure, Temperature		787-797
ISAMS Improved Stratospheric and Mesospheric Sounder	Mechanically cooled spectrometer sensing atmospheric infrared emissions	CO_2	Pressure Modulated Radiometer	2325, 666
		H_2O, NO_2		1590
		CO		2174
		NO		1887
		N_2O		1266
		CH_4		1298
		O_3	Radiometric	1030
		HNO_3		884
MLS Microwave Limb Sounder	Microwave radiometer sensing atmospheric emissions	ClO		6.866
		H_2O_2		6.874
		O_3		6.926
		H_2O		6.159
		O_2 - Pressure		2.117
HALOE Halogen Occultation Experiment	Gas filter/radiometer sensing sunlight occulted by the atmosphere	HF	Gas Correlation	4047-4109
		HCl		2910-2970
		CH_4		2870-2912
		NO		1883-1917
		CO_2/Pressure	Radiometric	3537-3608
		NO_2		1591-1607
		H_2O		1506-1522
		O_3		976-1017

To assess the accuracy requirements for these spectroscopic parameters, each experiment has to exercise specific inversion algorithms against simulated data, in a similar manner to that described above in Section B-4, and establish the impact of uncertainties in spectroscopic input data on the accuracy of retrieved geophysical parameters. As Table B-8 indicates, this is a nontrivial task in view of the number of species and spectral intervals being studied. Further, each spectral interval containing one or more target species will have a set of interfering species whose line parameters need to be known, and selected spectral intervals may also require accurate knowledge of continua such as collision-induced O_2 and N_2 absorption bands, continuum absorption in H_2O, and aerosol effects.

In general, the more complete and accurate the spectroscopic parameters are, the more accurate the geophysical parameters will be (at least to the inherent sensitivity and calibration limits of the individual experiment). It is also important to note that, in many instances, the availability of improved spectroscopic data even after launch and orbital data acquisition can be used to advantage to upgrade geophysical data.

The specialized and detailed accuracy requirements of these four diverse experiments will constitute the major portion of the UARS requirements document mentioned above. General accuracy requirements over stratospheric temperature (T_{strat}) and pressure (P_{strat}) ranges are summarized in Table B-9. However, many common requirements exist for all the experiments, and most of these are included in Section B-7.

B-6 DATABASE ASSESSMENT

There are several spectroscopic databases for high resolution atmospheric transmission and emission simulations. The AFGL compilation became available in 1973 (McClatchey *et al.*, 1973) and has since been updated on the average of every two years (Rothman *et al.*, 1983a,b). The GEISA compilation began in 1976 for internal use and was published for the first time in 1980 (Chedin *et al.*, 1980); most of its data (Chedin *et al.*, 1985: Husson *et al.*, 1985) are in common with the AFGL compilation. In addition, an atlas of microwave and submillimeter transitions is available from JPL (Poynter and Pickett, 1984). The initial emphasis of each of the three compilations varied. The AFGL compilation was intended for terrestrial atmospheric problems, the GEISA compilation for terrestrial and giant planetary atmospheres, and the JPL catalog for astrophysical studies. The GEISA compilation also provided software for efficient use of its database. These databases now overlap in that they include many of the same molecular transitions relevant to remote sensing. Table B-10 summarizes the parameters that are currently incorporated into the compilations. The parameters are given in order of frequency for all significant transitions of molecular and atomic species of interest (provided that they are available in a suitably quantitative form).

Until 1984, the AFGL and GEISA compilations included for each absorption line of a given molecule, the following parameters:

- the resonant frequency in vacuum cm^{-1};
- the intensity in $cm^{-1}/(molecule\ cm^{-2})$ at 296 K;
- the collision halfwidth HWHM (halfwidth at half-maximum), in $cm^{-1}\ atm^{-1}$ at 296 K;
- the lower state energy of the associated transition in cm^{-1};
- the quantum identifications (vibrational, rotational, electronic level, hyperfine, and splitting designation if necessary);
- the entry date, isotope and molecule codes.

Table B-9. Typical Spectroscopic Parameter Accuracy Requirements for UARS Composition Measurement Experiments

Parameter	CLAES	HALOE	ISAMS	MLS
Line Position	± 0.001 cm^{-1}	± 0.001 cm^{-1}	± 0.001 cm^{-1}	± 30 kHz
Line Intensity	$<5\%$ over T_{strat}	$<5\%$ over T_{strat}	$<6\%$ over T_{strat}	$<2\%$ over T_{strat}
Collision-Broadened Halfwidths	$<5\%$ over T_{strat} and P_{strat} *Air-Broadening* for all species	$<5\%$ over T_{strat} and P_{strat} *Air-Broadening* for all species *Self-Broadening* for HF, HCl, NO, CH_4	$<5\%$ over T_{strat} and P_{strat} *Air-Broadening* for all species *Self-Broadening* for PMR species	$<2\%$ over T_{strat} and P_{strat} *Air-Broadening* for all species
Absorption Continua	Collision-induced O_2 band, H_2O continua, $<5\%$	Collision-induced O_2 band, H_2O continua, $\simeq <3\%$	Collision-induced O_2 band, H_2O continua, $<5\%$	

However, some basic modifications have been made recently in the compilations (in addition to inclusion of new species). For example, the impact of the temperature variation of the halfwidth $\gamma(T)$ of a line on the accuracy of radiative transfer computation is now accepted to be very important (as explained by Chedin *et al.*, 1985). As a result, in 1984, the temperature-dependence of halfwidth has been introduced as a new parameter in the GEISA catalog by giving the value of the exponent "n" in the expression $\gamma(T) = \gamma(T_O)(T_0/T)^n$, where $\gamma(T)$ is the collision halfwidth at T, and T_O is a reference temperature (e.g., 296K).

In addition, five new parameters will be included (or at least are to be considered when reliable information becomes available) in the 1985 new AFGL format:

- the transition moment in debyes;
- the self-broadened halfwidth in cm^{-1} atm^{-1} at 296 K;
- the pressure shift of the line in cm^{-1} atm^{-1} at 296 K;
- approximate error estimates for frequency, intensity and halfwidth;
- references for frequency, intensity and halfwidth.

The major part of all the above-mentioned line parameters is also included in the JPL catalog (see Table B-10).

As can be seen, the compilations attempt to present for each transition, molecule-dependent unique parameters from which synthetic spectra can be calculated. Issues such as line shape or coupling between the radiation field and matter have been left to individual computer algorithms used in calculating synthetic spectra. Likewise, phenomena such as continua which are not amenable to discrete quantization

Table B-10. Spectroscopic Database Parameters

Parameter†			Database			
	Type	**Unit**	**AFGL GEISA**	**JPL**	**GEISA84**	**AFGL85**
MOL	molecular specie index		x	x	x	x
ISO	isotopic variant index		x	x	x	x
ν	resonant frequency	cm^{-1}	x	x	x	x
S	intensity of transition	$cm^{-1}/(molecule\ cm^{-2})$	x	x	x	x
R	transition moment	Debye				○
g	upper state degeneracy			x		
γ	air-broadened halfwidth	$cm^{-1}\ atm^{-1}$	x		x	x
γ_s	self-broadened halfwidth	$cm^{-1}\ atm^{-1}$				○
E″	lower state energy	cm^{-1}	x	x	x	x
n	temperature-dependence of halfwidth				○	○
δ	pressure shift of transition	$cm^{-1}\ atm^{-1}$				○
v′	upper vibrational quanta		x	x	x	x
v″	lower vibrational quanta		x	x	x	x
Q′	upper rotational quanta		x	x	x	x
Q″	lower rotational quanta		x	x	x	x
e	error estimates for major parameters			x		○
ref	citations for major parameters					○

† Reference temperature 296 K
○ New parameter for GEISA (1984 Edition) or AFGL (1985 Edition)

are not included on the databases. In some cases, bands of heavier molecules whose transitions are separated by a fraction of a Doppler width and are hence unresolvable by most laboratory and field instruments have been relegated to a separate file on the most recent AFGL compilation where pseudo-band models have been supplied.

Table B-11 summarizes the present situation with respect to the molecules classified in Table B-1. These species are a subset of those available on the compilations. In the second column, arbitrary spectral intervals have been given (in reciprocal centimeters) which roughly correspond to the submillimeter region (if present) and various regions of the infrared spectrum, further subdivided for important species where different qualities of the data prevailed. The third column presents the log of the minimum and maximum line intensities in units cm^{-1}/(molecule cm^{-2}) at 296 K. This information is given as a very good guide in evaluating the effect of a species on long path attenuation problems and includes the extremes of the three databases. In some cases, very weak transitions have been retained due to either consideration of hot bands necessary for nonlocal thermodynamic equilibrium problems, or flame spectra, or transitions in the millimeter region. The number of transitions, again, represent the union of the databases. The fifth column (under quality) gives an evaluation of the three most significant parameters in terms of calculating atmospheric spectra and retrieval of atmospheric profiles, namely the frequencies (ν), strengths (S), and halfwidths (γ) of the transitions. The designation "A" is a judgement that the data are good for many applications; "B" signifies that the data are good for some applications considered here but need improvement; and "C" indicates that the data require major improvement. It must be realized that for major constituents, the classification of A, B, or C in a particular spectral region is, for the most part, very difficult since regions containing strong transitions, with very accurate parameters, usually also contain less accurate parameters for hot bands, isotopic lines, or weak bands in resonance. The sixth column lists the current availability of data in each interval on the AFGL, GEISA, and JPL databases, respectively. Under the comments heading, remarks on present deficiencies, problems, and other highlights of a species have been given. The need for self-broadened widths, which are required by some of the experiments discussed in Section B-5-2, has been abbreviated as "SB."

In addition to current work involved with adding completed work to the databases, there are many laboratory measurements which are in progress. A sampling of this work is listed in Table B-12. (Instrument and institutional abbreviations are expanded in Annex B-1 and B-2.) Because it was necessary to suppress many of the details of these investigations, it may appear that there is considerable overlap in the studies in progress. In the case of linewidth and intensity measurements, this duplication is desirable as a check for systematic errors, as discussed above. In addition, measurements using different techniques often provide complimentary data sets. For example, diode laser systems are typically used to measure a few lines to high resolution, while Fourier instruments typically are used to measure many more lines at necessarily lower resolution.

B-7 CONCLUSIONS AND RECOMMENDATIONS

The status of the spectroscopic database and current laboratory research given in this appendix is related to the accuracies with which atmospheric composition can be determined from spectral measurements. Further limitations are imposed by the inherent uncertainties of different atmospheric experiments and by the optical paths involved. With the present capabilities available for laboratory spectroscopic measurements and calculation of those spectroscopic parameters which cannot be measured, it is now routine to obtain line positions with high absolute accuracy (± 30 kHz in the microwave, 0.001 cm^{-1} or better in the infrared). Intensity and halfwidth measurements are more difficult. While relative intensities can

Table B-11. Summary of Spectroscopic Databases

Specie	Spectral Interval†	Intensity Range‡	Number of Transitions	Quality* ν	S	γ	Database** A	G	J	Comments***
H_2O	0-500	-32,-18	49000	A	A	B	x	x	x	Better precision needed due to
	500-5000	-27,-19		B	B	B	x	x		interference with other species
	5000-17900	-27,-20		C	C	C	x	x		$\lvert \Delta K \rvert > 2$ lines need improvement; SB
CO_2	400-1400	-27,-19	60000	A	B	B	x	x		Strengths to 1% needed for P,T
	1800-2400	-37,-18		A	B	B	x	x		retrievals for ATMOS and UARS; SB
	2400-9700	-27,-20		A	B	B	x	x		
O_3	0-300	-26,-21	49000	A	B	B	x	x	x	Better precision needed due to
	500-1200	-25,-20		A	B	B	x	x		interference with other species;
	1600-2900	-26,-21		B	B	B	x	x		Missing transitions needed between
	2900-3100			C	C	B	x	x		8.3-6.3 μm and $<$ 3.2 μm
N_2O	0-50	-25,-22	16000	A	A	A	x	x	x	Not all available measurements
	500-1400	-24,-19		A	A	A	x	x		have been incorporated; SB
	1600-5200	-24,-19		B	B	A	x	x		
CO	0-150	-24,-21	600	A	A	B	x	x	x	SB
	1900-6400	-24,-19		A	A	B	x	x		
CH_4 and CH_3D	0-100	-29,-27	27000	A	A	B	x	x	x	Some hot bands missing
	900-2000	-29,-19		A	B	B	x	x		
	2200-3200	40,-19		A	B	B	x	x		Some transitions missing between
	4100-6100	-23,-20		C	C	B	x	x		2-1.6 μm; SB
O_2	0-300	-35,-25	2200	A	A	B	x	x	x	Pressure induced bands needed;
	1400-16000	-30,-23		A	B	B	x	x		coefficients available
N_2	2000-2600	-34,-28	100	A	B	C	x	x		Pressure induced bands needed
O	68-158	-22,-21	2	A	A	C			x	
NO	0-100	-35,-22	7400	A	A	B	x	x	x	SB
	1500-4000	-44,-19		A	B	B	x	x		
NO_2	0-100	-25,	26000	A	A	C			x	SB
	600-3000	-24,-19		A	B	B	x	x	x	
NH_3	0-400	-29,-21	7000	A	A	B	x	x	x	6 μm region to be revised; 3 μm
	400-2200	-28,-19		B	B	B	x	x		region needed
HNO_3	0-100	-26,-21	57000	A	A	C	x	x	x	Several strong fundamentals missing;
	840-1750	-23,-17		C	C	C	x	x		7.7 μm bands needed
HF	0-8000	-24,-17	60	A	A	B	x	x		SB

Table B-11. Summary of Spectroscopic Databases (continued)

Specie	Spectral Interval†	Intensity Range‡	Number of Transitions	Quality* ν	S	γ	Database** A	G	J	Comments***
HCl	0-400	-24,-18	200	A	A	B	x	x	x	SB
	2400-8500	-24,-19		A	A	B	x	x		
OCS	0-40	-28,-21	700	A	A	B	x	x	x	
	800-2100	-23,-18		A	B	B	x	x		3.4 and 2.4 μm bands needed
H_2CO	0-100	-38,-19	2700	A	A	C	x	x	x	
	2700-3000	-20,-19		A	A	C	x	x		5.7 μm band needed
HCOOH	0-100	-28,-21	1888	B	A	C			x	Available data not yet incorporated
	1060-1160	-22,-20	3388	B	B	C		x		
HCN	0-150	-24,-18	800	A	A	B	x	x	x	
	550-3450	-25,-19		A	A	B	x	x		
C_2H_2	600-3400	-25,-18	1200	A	A	B	x	x		
C_2H_6	700-1000	-25,-21	5400	C	C	C	x	x		Major improvement required; 3.3 μm Q-branch strengths needed
CF_2Cl_2, $CFCl_3$, CF_4, CCl_4, CHF_2Cl										Band models and cross sections are available
ClO	0-100	-29,-21	6000	A	A	B	x	x	x	
	760-900	-24,-20		A	C	B	x	x		
$ClONO_2$	0-100	-24,-22	8500	A	A	C			x	
HO_2	0-100	-25,-20	6200	A	A	C			x	high resolution IR data needed
OH	0-100	-31,-18	8500	A	A	C	x	x	x	New extended rotational prediction forthcoming
	1250-10000	-81,-19		A	B	C	x	x		
N_2O_5	—	—	—		—			—		Cross sections available
CH_3Cl	2900-3200	-25,-21	6700	A	B	C	x	x		Incomplete vibrational spectrum
HOCl	0-300	-26,-19	15600	A	A	C			x	Missing fundamental
	1150-3800	-23,-20		A	B	C	x	x		
HNO_4 — HNO_2 —		—	—		—			—		Incomplete data
H_2O_2	0-300	-26,-20	3300	A	A	C			x	Missing data for high quantum numbers
	1150-1350	-23,-20		A	B	C	x	x		Only one IR band at present, 3 μm region needed

Table B-11. Summary of Spectroscopic Databases (continued)

Specie	Spectral Interval†	Intensity Range‡	Number of Transitions	Quality* ν	S	γ	Database** A	G	J	Comments***
HBr	0-350	-24,-18	300	A	A	B	x	x	x	
	2200-9800	-24,-19		A	A	B	x	x		
SO_2	0-200	-24,-20	18200	A	A	C	x	x	x	
	400-2550	-23,-19		A	B	C	x	x		
H_2S	0-600	-27,-19	4100	A	A	C	x	x	x	Missing fundamentals
	990-1600	-23,-21		A	A	C	x	x		Available data not yet incorporated
H_2SO_4	—	—	—		—			—		No data
C_2H_4	900-1100	-21,-18	200	B	B	C		x		Only a single band at present
C_3H_8	—	—	—		—			—		No data

† Spectral intervals are given in units of cm^{-1}.
NB: 1 μm corresponds to 10,000 cm^{-1}.

‡ Spectral intensities range is the log of the minimum and maximum line intensities in units of cm^{-1}/(molecule cm^{-2}).

* The quality codes indicate: A, good for many applications; B, good for some applications but needs improvements; C, needs major improvements. The three columns refer to line position (ν), line strength (S), and halfwidth (γ).

** Database codes are: A, AFGL (1985); G, GEISA (1984); J, JPL (1984) catalog.

*** The need for self-broadened widths has been abbreviated as "SB".

Table B-12. Some Examples of Infrared to Microwave Current Laboratory Spectroscopy Efforts

Molecule	Spectral Coverage (cm^{-1})	Instrument[1]	Data Type[2]	Accuracy[3]	Institution[4]
H_2O	2-4	MW	line shapes	2%	JPL
	20-350	FTS	F	0.0001 cm^{-1}	NRC Canada
	0-300(H_2O,HDO)	MW,FTS	F	0.00001 cm^{-1}	JPL
	500-2000(HDO)	FTS	F	0.004 cm^{-1}	AFGL
	700-1200(continuum)	grating,TDL	I,W	10%, 5%	U. Stony Brook
	900-5000($\Delta K > 1$)	FTS	I	5%	JPL
	1000-2000	FTS	F(calib.)	0.0001 cm^{-1}	JPL
	1250-1380(H_2O,HDO)	TDL	I,air-W,N_2-W	3%	NASA Langley, CWM
	1400-1800	grating,TDL	I,W	10%, 5%	U. Stony Brook
	1500-1523	TDL	I,N_2-W,self-W	3%	NOAA/NESDIS,CWM
	1523-1600	TDL	I,N_2-W,self-W	3%	NOAA/NESDIS
	1600(HDO)	FTS	F	0.001 cm^{-1}	JPL
	2100-2900(HDO)	FTS	F,I	0.001 cm^{-1}, 5%	LPMOA Orsay
	5000-5500(^{18}O)	FTS	F,I	0.001 cm^{-1}, 5%	LPMOA Orsay
	7550-7660	FTS	air-W,self-W	10%	Douglas RL, Kitt Peak NSO
	16000-25000	FTS	F,I	0.001 cm^{-1}	LPMOA Orsay
	10000-25000	FTS	F,I	0.001 cm^{-1}	JPL

Table B-12. Some Examples of Infrared to Microwave Current Laboratory Spectroscopy Efforts (continued)

Molecule	Spectral Coverage (cm^{-1})	Instrument[1]	Data Type[2]	Accuracy[3]	Institution[4]
CO_2	500-4000(high temp)	FTS	F	0.0005 cm^{-1}	AFGL
	600-750	grating,TDL	I,W	10%, 5%	U. Stony Brook
	670-720	TDL	self-,N_2-W		NOAA/NESDIS
	700-800(hot band)	FTS	F	0.005 cm^{-1}	LSM Paris
	700-800(hot band)	TDL	I,self-W,N_2-W	5%	LIR Orsay
	700-1100	FTS	F,I	0.001 cm^{-1}, 5%	JPL
	800-1100	FTS	F,I,W,	0.002 cm^{-1}, 5%	OSU
	900-1000	CO_2 laser	self-W,N_2-W,O_2-W	3%-5%	LIR Orsay
	1800-4200(isotopes)	FTS	F,I	0.0004 cm^{-1}, 2%	NASA Langley, CWM
	1900-4000(isotopes)	FTS	F	0.0004 cm^{-1}	AFGL
	2086-2307	FTS	F	0.0005 cm^{-1}	LIR Orsay
	2270-2600	FTS	F,I, self-W,N_2-W	0.005 cm^{-1}, 3%	LSM Paris
	2200-2400	grating,TDL	I,W	10%, 5%	U. Stony Brook
	2300-2400	FTS	I	2%	NRC Canada
	2400-2600(continuum)	FTS	self-W,N_2-W		U. Rennes, LSM Paris
	7550-7660	FTS	F	0.005 cm^{-1}	Douglas RL, Kitt Peak NSO
O_3	FIR-500	MW,FTS	F,I	0.0001 cm^{-1}	JPL,IROE, U. Bologna
	500-900	FTS	F,I	0.001 cm^{-1}, 10%	JPL, U. Denver LPM Reims, NASA Langley, CWM
	600-5000	FTS	F,I,W	0.001 cm^{-1}, 5%, 3%	RAL
	950-1200	FTS,LHS	I,N_2-W,O_2-W	2%, 2%	LPM Reims
	950-1400(isotopes)	FTS,TDL	F,I,W	0.004 cm^{-1}, 10%, 2%	LPMOA Orsay NASA Langley, CWM
	2050-2150	FTS	N_2-W,O_2-W	5%	LPM Reims
	3000-3200	FTS	F,I	0.001 cm^{-1}, 10%	LPM Reims
N_2O	900-5000	FTS	F,I	0.0001 cm^{-1}, 2%-5%	JPL
	1000-1350 (hot band)	FTS	F	0.001 cm^{-1}	LSM Paris
	1100-1110	FTS,TDL	F,I	0.002 cm^{-1}, 10%	NBS Washington
	1100-1300	grating,TDL	I,W	10%, 5%	U. Stony Brook
	1830-1950	FTS,TDL	F,I	0.002 cm^{-1}, 10%	NBS Washington, U. Oulu
	2160-2270	FTS	F,I,self-W,N_2-W,O_2-W	0.001 cm^{-1}, 3%	LSM Paris
	2200-2400	FTS	F,I	0.001 cm^{-1}, 2%	JPL
	2200-2400	grating,TDL	I,W	10%, 5%	U. Stony Brook
	2400-2900	TDL	F,I,W	0.001 cm^{-1}, 2%	JPL
	3000-5000	TDL	F,I,W	0.001 cm^{-1}, 2%	JPL
CO	30-100	SMM	F	10^{-4} cm^{-1}	NBS Boulder
	2000-2200	grating,TDL	I,W	10%, 5%	U. Stony Brook
CH_4	1000-2000	FTS	F,I	$10^{-4}cm^{-1}-10^{-3}cm^{-1}$, 2%-10%	JPL, U. Dijon
	1000-1500	FTS	F,I,self-W,air-W	0.0005 cm^{-1}, 5%, 3%	RAL
	1000-1300(CH_3D)	TDL,FTS	F,I	0.005 cm^{-1}	LIR Orsay, JRC Ispra
	1100-1500(isotopes)	FTS,TDL	I,air-W,N_2-W	3%	NASA Langley, CWM
	1200-1400	grating,TDL	I,W	10%, 5%	U. Stony Brook
	2800-3200	grating,TDL	I,W	10%, 5%	U. Stony Brook
	3750-4750	FTS	F,I	2×10^{-4}-$2\times10^{-3}cm^{-1}$, 2%-10%	JPL, U. Dijon
	5800-6150	FTS	F,I	4×10^{-4}cm, 2%-15%	JPL
	7601-7606	Photoacoustic	air-W		Douglas RL, Kitt Peak NSO
O_2	6-30 (singlet delta)	SMM	F	0.1 MHz	JPL

Table B-12. Some Examples of Infrared to Microwave Current Laboratory Spectroscopy Efforts (continued)

Molecule	Spectral Coverage (cm^{-1})	Instrument[1]	Data Type[2]	Accuracy[3]	Institution[4]
N_2	---				
O atom	---				
NO	1800-1950	FTS	N_2-W,Ar-W	3%	LSM Paris
	1800-2000	FTS	F,I,self-W,air-W	0.0005 cm^{-1}, 5%-3%	RAL
	1800-1950	grating,TDL	I,W	10%, 5%	U. Stony Brook
	3700-3880	DFL	I,self-W	2%	NBS Washington
NO_2	10-200	FTS	F	0.0001 cm^{-1}	IROE, LPMOA Orsay, U. Bologna
	1570-1620	FTS	F,I	0.001 cm^{-1}, 2%-15%	JPL
NH_3	900	FTS	F	0.001 cm^{-1}	JPL
	1400-1490	FTS	F,I	0.0002 cm^{-1}, 2%-10%	JPL
	1500	FTS	F,I	0.001 cm^{-1}, 10%	JPL
HNO_3	850-1740	TDL,FTS	F,I	0.001 cm $^{-1}$, 20%	NBS Washington, U. Denver
	850-1350	FTS	F	0.001 cm $^{-1}$	LSM Paris, LPMOA Orsay
	1240-1370	FTS	F	0.002 cm $^{-1}$	RAL
	1310-1340	TDL	I	10%	JPL
HF	40-160	FTS	N_2-W,O_2-W	5%	IROE, SAO Harvard, U. Bologna
	3500-4300	DFL	I,self-W,N_2-W	1%	NBS Washington
HCl	20-160	FTS	N_2-W,O_2-W	5%	IROE, U. Bologna, SAO Harvard
	2600-3100	FTS	HF-W	10%	NASA Langley
	2600-3000	FTS	N_2-W	3%	RAL
	2650-3080	FTS	I,self-W,N_2-W	2%	NASA Ames
	2700-3050	DFL	I,self-W,N_2-W	1%	NBS Washington
	2900-3100	grating,TDL	I,W	10%, 5%	U. Stony Brook
OCS	490-1920	FTS,TDL	F,I	0.0002 cm^{-1}, 10%	NBS Washington, U. Oulu
	839-887	TDL	self-W,N_2-W	5%	LIR Orsay
	1050	Stark	I		U. Louvain
	2000-2200	grating,TDL	I,W	10%, 5%	U. Stony Brook
H_2CO	1800	FTS	F,I	0.001 cm^{-1}	JPL
HCOOH	---				
HCN	3200-3400	FTS	F,W	0.02 cm^{-1}, 10%	NASA Langley
C_2H_2	650-800	grating,TDL	I,W	10%, 5%	U. Stony Brook
	1250-1350	TDL	air-W,N_2-W	3%	NASA Langley, CWM
C_2H_6	---				
CF_2Cl_2	860-950	grating,TDL	I,W	10%, 5%	U. Stony Brook
	700-1200	FTS	band	5%	NBS Washington
	1050-1200	grating,TDL	I,W	10%, 5%	U. Stony Brook
$CFCl_3$	150-1100	grating,TDL	I,W	10%, 5%	U. Stony Brook
	700-1200	FTS	band	5%	NBS Washington
	810-850	grating,TDL	I,W	10%, 5%	U. Stony Brook

Table B-12. Some Examples of Infrared to Microwave Current Laboratory Spectroscopy Efforts (continued)

Molecule	Spectral Coverage (cm $^{-1}$)	Instrument[1]	Data Type[2]	Accuracy[3]	Institution[4]
CF_4	---				
CCl_4	---				
CHF_2Cl	---				
ClO	---				
$ClONO_2$	10-200	FTS	F	0.0001 cm^{-1}	IROE, U. Bologna
HO_2	1040-1140	TDL	F,I,W	0.001 cm^{-1}, 20%	Aerodyne Research
	1340-1440	TDL	F,I,W	0.001 cm^{-1}, 20%	Aerodyne Research
	3370-3500	TDL	F,I,W	0.001 cm^{-1}, 20%	Aerodyne Research
OH	30-105(OH,OD)	SMM	F	0.5 MHz	JPL
	60-200	DFL	air-W	5%	SAO Harvard, NBS Boulder
N_2O_5	3-30	MW,SMM	F,I	0.05 MHz	JPL
	800-2800	FTS	I		LPMOA Orsay
CH_3Cl	---				
HOCl	10-200	FTS	F	0.0001 cm^{-1}	IROE, U. Bologna
HNO_4	1-10	MW	F,I	0.05 MHz	NBS Washington, JPL
HNO_2	1240-1280	TDL	F,I	0.001 cm^{-1}, 10%	NBS Washington
H_2O_2	10-200	FTS	F	0.0001 cm^{-1}	IROE, U. Bologna
	1250-1380	TDL	air-W	5%	NASA Langley, CWM
SO_2	3-100	SMM	F	0.1-0.5 MHz	Duke U., JPL
H_2S	10-100	FTS	F	0.0001 cm^{-1}	IROE, U. Bologna
	2000-2800	FTS	F,I	0.001 cm^{-1}, 10%	LPMOA Orsay
	6100-6500	FTS	F,I	0.001 cm^{-1}, 10%	LPMOA Orsay
H_2SO_4	---				
C_3H_8	500-4000	FTS	band		NBS Washington
C_2H_4	800-1100($^{13}C,^{12}C$)	FTS	F	0.001 cm^{-1}	U. Louvain, LSM Paris
	1780-2380($^{13}C,^{12}C$)	FTS	F	0.001 cm^{-1}	U. Louvain, LIR Orsay
CH_3CCl_3	1000-1200	grating,TDL	I,W	10%, 5%	U. Stony Brook

Notes: 1. See Annex B-1.
2. Data Type: F = frequency, I = intensity, W = linewidths, Band = random band model.
3. The accuracy, when available, refers to F in cm^{-1} or MHz and to I or W in %.
4. See Annex B-2.
5. 0.0001 cm^{-1} $\cong$ 1 MHz

It is inevitable, in any extensive compilation such as this, that works will inadvertently be overlooked. Our apologies to any authors whose works have thus been accidentally omitted.

often be determined with a precision of 2 to 5%, absolute intensities are usually known with confidence to only 10 to 15% for stable molecules. With particularly careful measurements, accuracies of 5% can be achieved, but greater absolute accuracy (1 to 3%) requires intensive collaborative effort by several laboratories to reduce systematic errors. The situation is similar for halfwidths, where the present measurements result in absolute accuracies usually no better than 5%. Many of the spectroscopic parameters needed for the future UARS program require greater accuracy than can be achieved at the present time.

The major requirements for further work in laboratory spectroscopy for atmospheric measurements and climate modeling are summarized below, in order of importance. Specific details for many of these requirements will be found in Tables B-7, B-9, and B-11 of this appendix, in Chapter 15 of this report, in the report of Smith (1985), and in the UARS Spectroscopic Requirements document (Roche, 1985). The first two of the requirements given here have much greater importance than those in the remainder of the list.

1. *Line Positions and Intensities.* Accurate line positions and intensities are important for many of the atmospheric remote sensing techniques and for climate studies. However, the spectral parameters for several infrared bands of major and trace constituents are either totally missing or of poor accuracies. This problem, in general, is more severe between 3000 to 10,000 cm^{-1} where significant contributions from molecules such as O_3, CH_4, and HNO_3 are not available. Even where intensities are available, for example, in the 15 μm band system of CO_2, improvements are needed in both the experimental accuracies and the theoretical modeling of these data.

2. *Line Widths.* Knowledge of spectral line halfwidths and their dependence on temperature is deficient for nearly all the atmospheric gases. Accurate measurements of air-broadened halfwidths (and self-broadened and N_2-broadened halfwidths in special cases [see Table B-9] are needed). Efforts to improve theoretical calculations of line widths for atmospheric molecules should also be encouraged.

3. *Line Shapes.* Deviations from the Lorentz lineshape can be critical for analysis of atmospheric spectral data (see Chedin and Scott, 1984) and for calculation of atmospheric heating and cooling rates in almost all wavelength regions, such as in the 15 μm region and the 4.3 μm band head of CO_2, the 6.3 μm H_2O band and in many regions in the microwave. Continued laboratory and theoretical studies of these deviations are needed.

4. *Unresolved Bands.* The use of band models to represent unresolved rotational structure is required for heavy molecules such as chlorofluorocarbons. More accurate measurements of band intensities or absorption coefficients and integrated intensities of strong isolated features such as Q-branches are desired. Accurate band model representations for radiatively important trace gases are also needed in climate studies where line-by-line calculations over very large spectral regions are impractical or impossible.

5. *Pressure Induced Bands.* The currently available absorption coefficients for the important pressure induced bands of O_2 and N_2 (in the 6 μm and 4 μm regions, respectively) are quite approximate, especially at typical stratospheric temperatures. Additional laboratory measurements and modeling efforts are needed.

6. *Water Vapor Continuum.* H_2O continuum absorption is important in the interpretation of tropospheric absorption spectra and in climate studies, but presently available representations do not adequately model the temperature-pressure dependence of the continuum. More work in this area is needed.

7. *Non-LTE Radiative Transfer.* Emission or absorption by molecules such as O_2, O_3, HCl, OH, NO, H_2O and CO_2, which are not in local thermodynamic equilibrium (LTE) at certain altitudes in the upper atmosphere, can significantly affect atmospheric measurements in many cases. Improvements are needed in parameters for transitions between the high vibrational levels involved in non-LTE radiative transfer.

8. *Other Effects.* Several other effects such as pressure induced line shifts, collisional narrowing, and line mixing, which are normally neglected in most atmospheric spectroscopic studies, can be significant in some cases. Measurements and theoretical modeling of these effects should be encouraged. In particular, accurate measurements of pressure induced line shifts would be useful for validation of theoretical line width calculations.

There are also several comments and recommendations which may be made in regard to the maintenance and improvement of the spectroscopic database.

- Since the analysis of atmospheric spectral measurements increasingly involves the use of computers, the entire database should be computer accessible.
- Laboratory investigators should consistently report absolute accuracies along with measured values for line positions, intensities, and halfwidths.
- Where multiple measurements exist for a given set of parameters (e.g., CO_2 line positions and intensities), a critical evaluation of the measurements should be made, and the best possible set of parameters (with error bars) should be determined and incorporated in the database.
- As can be seen from section B-5-2, several UARS investigations desire line intensity and halfwidth accuracies better than those reported in this document or routinely measured in the community. Since improved line parameter accuracies directly benefit the accuracy of retrieved geophysical parameters, there should be an organized effort, involving many laboratories, to establish absolute line intensity standards in the infrared. A related effort should be made for line widths in the infrared and microwave.

In this appendix the status of spectroscopic data in the visible and ultraviolet regions has not been addressed, except to the extent that some visible-region line parameters are included in the AFGL and GEISA compilations. However, a number of ground-based, balloon-borne, rocket-borne or space-based atmospheric ultraviolet and visible remote sensing experiments are presently in operation or are planned for the future. As in the infrared to microwave region, the accuracy of the results derived from these short-wavelength atmospheric observations is also affected by the uncertainties in the available spectroscopic data. Therefore it is recommended that the database in the visible to ultraviolet region be reviewed and evaluated in the near future.

Increasingly more sophisticated atmospheric remote sensing experiments are being discussed for possible implementation in the later part of this century and beyond. Examples of the types of instruments under discussion may be found in the Earth Observing System (EOS) science and missions requirements working group report (Butler, 1984). The increasing number of observations from space will require better knowledge of spectroscopic parameters at conditions prevalent in the upper stratosphere, mesosphere, and possibly at even higher altitudes. Efforts toward remote sensing of the troposphere from space will also require improved knowledge of halfwidths, line shapes, continua, and aerosol extinction, as well as line parameters for additional molecules which are not important in the stratosphere. Improved knowledge of these same spectroscopic parameters, along with accurate representations of absorption and emission in broad spectral regions covering many molecular bands, will also be required for climate studies.

Acknowledgements

Thanks are expressed to Drs. A. Chedin, K. Chance, and V. Ramanathan for valuable comments to preliminary versions of this appendix.

Annex B-1
Explanation of Instrument Abbreviations

FTS:	Fourier Transform Spectrometer (Michelson Interferometer)
TDL:	Tunable Diode Laser Spectrometer
MW:	Microwave Spectrometer
SMM:	Submillimeter (Far-Infrared) Spectrometer
DFL:	Difference Frequency Laser
LHS:	Laser Heterodyne Spectroscopy
SISAM:	French interferometer (spectromètre interférentiel à selection par l'amplitude de modulation)

Annex B-2
Explanation of the Institution Abbreviations

Aerodyne Research:	Aerodyne Research, Inc., Billerica, MA, USA
AFGL:	Air Force Geophysics Laboratory, Hanscom Field, MA, USA
Douglas RL:	MacDonnell Douglas Research Laboratories, St. Louis, MO, USA
CWM:	College of William and Mary, Williamsburg, VA, USA
Duke U:	Duke University, Durham, NC, USA
IROE	Istituto di Ricerca sulle onde Elettromagnetiche del CNR, Firenze, ITALY
ISM CNR:	Istituto di Spettroscopia Molecolare del CNR, Bologna, ITALY
JPL:	Jet Propulsion Laboratory, California Institute of Technology, Pasadena, CA, USA
JRC Ispra:	Joint Research Center, EEC, Ispra, ITALY
Kitt Peak NSO:	National Solar Observatory, Kitt Peak, Tucson, AZ, USA

LIR Orsay:	Laboratoire d'Infrarouge, Université d'Orsay, FRANCE
LPM Reims:	Laboratoire de Physique Moléculaire, Faculté de Sciences des Reims, FRANCE
LPMOA Orsay:	Laboratoire de Physique Moléculaire et d'Optique Atmosphérique, Campus d'Orsay, FRANCE
LSM-ENEA:	Laboratoria di Spettroscopia Molecolare del ENEA, Frascati, ITALY
LSM Paris:	Laboratoire de Spectronomie Moléculaire, Université de Paris 6, FRANCE
MET. FRANCE:	Météorologie Nationale, FRANCE
NASA Ames:	NASA Ames Research Center, Moffett Field, CA, USA
NASA Langley:	NASA Langley Research Center, Hampton, VA, USA
NASA Goddard:	NASA Goddard Space Flight Center, Greenbelt, MD, USA
NBS Boulder:	National Bureau of Standards, Boulder, CO, USA
NBS Wash.:	National Bureau of Standards, Washington, DC, USA
NCAR:	National Center for Atmospheric Research, Boulder, CO, USA
NOAA/NESDIS:	National Oceanic and Atmospheric Administration, National Environmental Satellite Data and Information Service, Washington, DC, USA
NPL:	National Physical Laboratory, Teddington, UNITED KINGDOM
NRC Canada:	National Research Council of Canada, Herzberg Institute of Astrophysics, Ottawa, Ontario, CANADA
OSU:	Ohio State University, Columbus, OH, USA
RAL:	Rutherford Appleton Laboratory, Chilton, Didcot, Oxon, UNITED KINGDOM
SAO Harvard:	Smithsonian Astrophysical Observatory, Harvard, Cambridge, MA, USA

U. Bologna:	Instituto Chimica Fisica e Spectroscopia, Università, Bologna, ITALY
U. Calgary:	University of Calgary, Calgary, Alberta, CANADA
U. Denver:	University of Denver, Department of Physics, Denver, CO, USA
U. Dijon:	Laboratoire de Spectronomie Moléculaire de l'Université de Dijon, Dijon, FRANCE
U. München:	München Universität, München, FRG
U. Louvain:	Université Catholique de Louvain, Département de Physique, Louvain la Neuve, BELGIUM
U. Oulu:	University of Oulu, Physics Department, Oulu, FINLAND
U. Rennes	Département de Physique Atomique et Moléculaire, Université de Rennes, Rennes, FRANCE
U. Stony Brook:	Laboratory for Planetary Atmospheres Research, State University of New York at Stony Brook, Stony Brook, NY, USA

APPENDIX C

INSTRUMENT INTERCOMPARISONS AND ASSESSMENTS

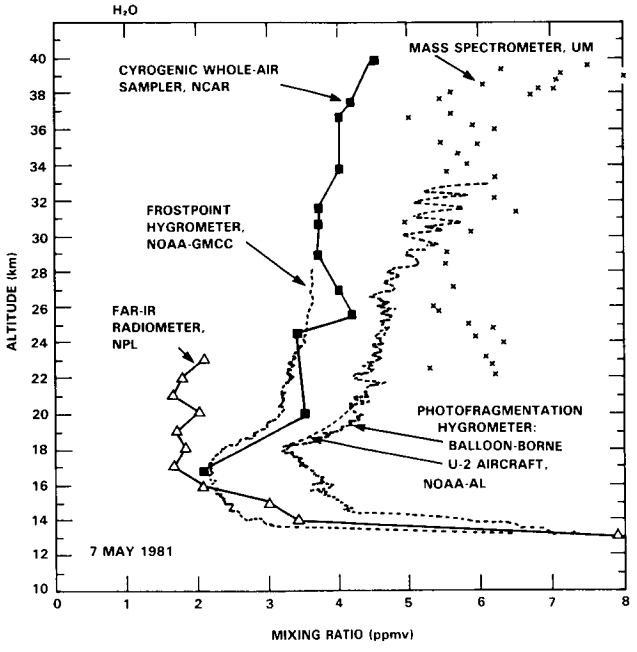

Panel Members

D.L. Albritton and R.J. Zander, Co-Chairmen

C.B. Farmer
E. Hilsenrath
W.G. Mankin
D.G. Murcray
S. Pollitt
D.E. Robbins
H. Roscoe

APPENDIX C

INSTRUMENT INTERCOMPARISONS AND ASSESSMENTS

TABLE OF CONTENTS

C-0 INTRODUCTION

The word "stratospheric" means different things to different people. For the layperson, *Webster's Thesaurus* has expanded on the meaning of this adjective by listing several synonyms:

> "*stratospheric* adj syn EXCESSIVE, dizzy, exorbitant, extravagant, immoderate, sky-high, steep, stiff, unconscionable, unmeasurable."

While it would be interesting to see how well each of these translates over to the field of stratospheric research, the synonym that does indeed strike at the heart of an important scientific issue is the last one: "unmeasurable".

To be sure, not all of the stratospheric trace constituents are unmeasurable, as experimentalists would quickly and correctly point out. But the lexicographers have indeed caught a germ of truth; such measurements are generally extremely challenging to carry out and often end up being somewhat equivocal. Yet, it is vital to have reliable estimates of the uncertainty in the observations, since they are the touchstone against which the theoretical understanding is tested.

In the series of assessments that have addressed the status of this understanding of the physics and chemistry of the atmosphere (e.g., WMO, 1982), several questions have generally arisen regarding the quality of the measurements of stratospheric trace constituents:

- Are the current data of adequate quality to constrain the models in useful ways?
- Are the rather large differences between measurements that have been made at different times, at different places, and with different methods due to atmospheric variability or instrumental uncertainty (or both)?
- Have the estimates of experimental uncertainty been tested quantitatively?
- Recognizing the growing need for simultaneous and comprehensive data on a photochemically coupled suite of trace gases, is measurement reliability currently at a state such that only one instrument or method need be included for each key species in a campaign?

In recent years, the community has devised a way to address these questions in an arduous, but effective way: a formal and rigorous intercomparison of instruments and techniques.

The features of the most successful (i.e., the most instructive) of these instrument intercomparisons have been the following:

- involve several different techniques for measuring the same species,
- measure at the same place and time and under typical operating conditions, insofar as possible,
- state the accuracy and precision estimates in advance of the intercomparison,
- each investigator prepare his/her results independently and separately (i.e., "blind") from the others and in a publication-ready status,
- jointly (or via an independent party) compile the separate results and assess the state of agreement,
- publish all results and conclusions in a refereed journal, and
- repeat the whole process occasionally.

Over the past few years, there have been several field campaigns devoted specifically to this goal, namely, the assessment of instrument reliability, as opposed to solely obtaining data to answer a geophysical question. Some of these intercomparison campaigns have been carried out in a fashion close to the above "ideal".

INTERCOMPARISONS

Table C-1 lists chronologically some examples of the formal instrument intercomparisons that have occurred in the past decade and those that are planned for the very near future. Moreover, numerous research institutions have participated, as the list in the table demonstrates. In this Appendix, the focus is on the middle group of campaigns, for which published or publication-ready results are available. These are the ones that have been carried out in recent years, but yet sufficiently long ago to permit a definitive assessment of some of the results. Furthermore, most of these campaigns have incorporated many of the features of the "ideal" noted above.

Table C-1. Examples of past and planned instrument intercomparisons and the participating research institutions

Intercomparison Campaigns:

• Ozonesondes: Hohenpeissenberg	1970, 1978
• Balloon-borne Ozone Instruments: UV absorption photometer and mass spectrometer	1978
• International Ozone Campaign: variety of ozone instruments	1981*
• Water Vapor Instrumentation: primarily balloon-borne *in situ* methods	1981, 1983*
• Balloon Ozone Intercomparison Campaign: primarily balloon-borne *in-situ* and remote methods	1983*, 1984*
• Balloon Intercomparison Campaign: remote methods addressing several species	1982*, 1983*
• Global Tropospheric Experiment - Chemical Instrumentation Tests and Evaluation:	
— aircraft-borne OH, NO, and CO methods	1983, 1984
— aircraft-borne NO_2, HNO_3, and PAN methods	1986
• The Middle Atmosphere Program: Global Budget of Stratospheric Trace Constituents (MAP-GLOBUS): variety of methods and species	1983, 1985

Participating Research Institutions*

AES	Atmospheric Environment Service (Canada)
CNRS-FSR	Centre Nationale de la Recherche Scientifiques, Faculte des Sciences de Reims (France)
CNRS-SA	Centre Nationale de la Recherche Scientifique, Service d'Aeronomie (France)
DU	Denver University (U.S.A.)
HU	Harvard University (U.S.A.)
IASB	Institut d'Aeronomie Spatiale de Belgique (Belgium)
IROE	Instituto de Ricerca sulle Onde Electromatnetiche (Italy)
JPL	Jet Propulsion Laboratory (U.S.A.)
MN	Meteorologie Nationale (France)
MOH	Meteorologisches Observatorium Hohenpeissenberg (Federal Republic of Germany)
NASA-GSFC	National Aeronautics and Space Administration, Goddard Space Flight Center (U.S.A.)
NASA-JSC	National Aeronautics and Space Administration, Johnson Space Center (U.S.A.)

Table C-1 (Continued)

NASA-WFC	National Aeronautics and Space Administration, Goddard Space Flight Center, Wallops Flight Facility (U.S.A.)
NBS	National Bureau of Standards (U.S.A.)
NCAR	National Center for Atmospheric Research (U.S.A.)
NOAA-AL	National Oceanic and Atmospheric Administration, Aeronomy Laboratory (U.S.A.)
NOAA-GMCC	National Oceanic and Atmospheric Administration, Geophysical Monitoring for Climate Change (U.S.A.)
NPL	National Physical Laboratories (U.K.)
ONERA	Office Nationale d'Etudes et de Recherches Aerospatiales (France)
SAO	Smithsonian Astrophysical Observatory (U.S.A.)
UL	Universite de Liege (Belgium)
UM	University of Minnesota (U.S.A.)
UO	University of Oxford (U.K.)
UT	University of Tokyo (Japan)

*Emphasized in this Appendix

This Appendix emphasizes balloon-borne techniques and instruments that address the height profiles of the trace species in the lower stratosphere. Although ground-based total-column methods offer an independent and valuable constraint, most of the recent campaigns have not completed a full intercomparison of the integrated vertical profiles and the groundbased results. Lastly, the comparison of vertical-profile data with satellite measurements is a challenging study in itself and is outside the scope of this summary.

Some of the chemical species have been addressed rather thoroughly in more than one campaign. Beginning with the most extensively studied trace constituent, this Appendix describes the approach taken and the results that have been obtained. Lastly, the conclusions reached regarding the current status of the measurement capabilities are summarized, and the needs for future intercomparisons and assessments are listed.

C-1 OZONE (O_3)

For obvious reasons that are developed in this and previous reports, there has been substantial effort directed toward an assessment of the reliability with which stratospheric ozone can be measured. Indeed, more intercomparisons have addressed this species than any other. There have been three major research efforts in this regard in the last few years, each having a rather different focus:

- INTERCOMPARISON OZONE CAMPAIGN - the first integrated intercomparison of a *wide variety of techniques*,

- BALLOON OZONE INTERCOMPARISON CAMPAIGN - primarily *in situ balloon-borne instruments*, and

- BALLOON INTERCOMPARISON CAMPAIGN - primarily *remote balloon-borne instruments.*

The goals, approach, and results of each are summarized here.

C-1.1 Intercomparison Ozone Campaign

The multi-faceted, three-week, Intercomparison Ozone Campaign has been the most extensive investigation of the experimental aspects of atmospheric ozone (Chanin, 1983a and 1983b and accompanying papers).

Characteristics

(a) *Organization and location:* Figure C-1 gives a graphical summary of the campaign. The study, which was conducted at several sites located across southern France, combined ground-based observing stations with several ozonesonde launches and two large-gondola balloon launches. This approach was to include as many different methods as possible, with the goal of obtaining the first overall "status report" on how well ozone can be measured.

(b) *Variety of ozone instruments:* The observational techniques included not only those that had been used routinely as part of network operations, but also those newly developed ones still undergoing field

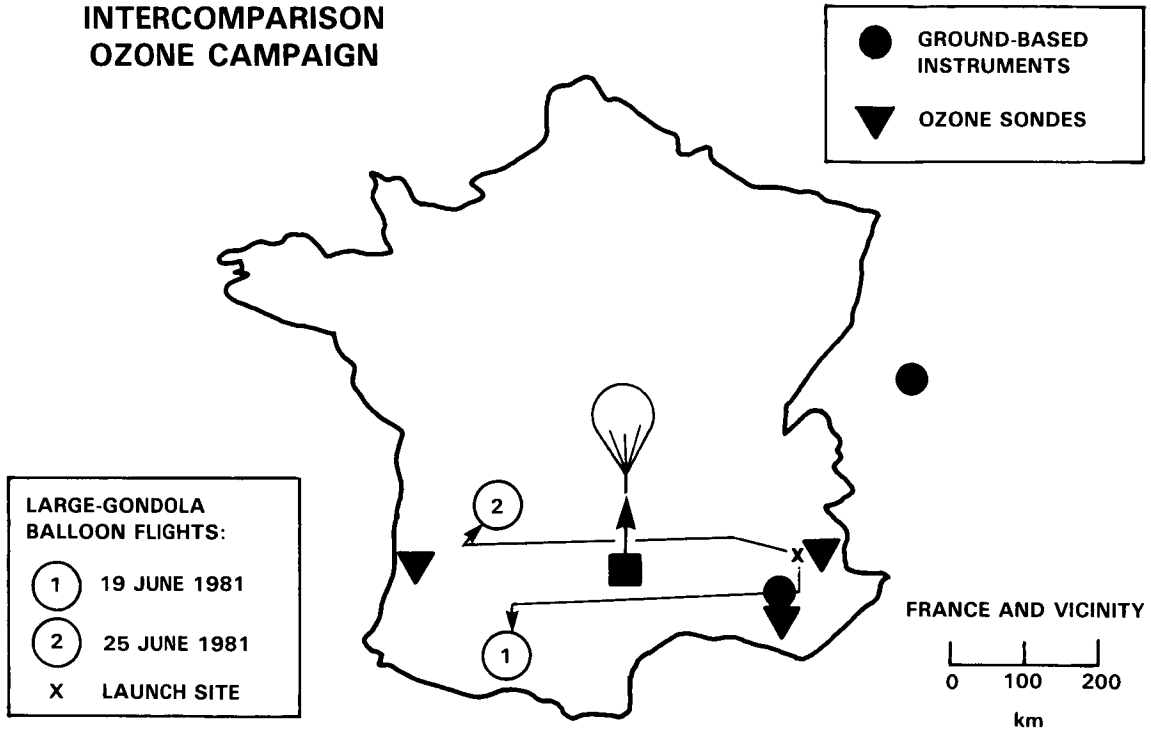

Figure C-1. Geographical locations of the components of the Intercomparison Ozone Campaign. (Adapted from Chanin [1983a]).

trials. Several research institutions were represented and both vertical-profile and total-column instruments were employed:

- ground-based:
  - CNRS-FSR: Dobson spectrometer (column)
  - CNRS-FSR: high-resolution IR absorption interferometer (column)
  - CNRS-FSR: Umkehr method (profile)
  - CNRS-SA: differential absorption lidar (profile)

- balloon-borne:
  - NASA-WFC: electrochemical concentration cell (ECC) sonde (*in situ,* profile)
  - MN: Brewer-Mast sonde (*in situ,* profile)
  - NASA-JSC: UV absorption photometer (*in situ,* profile)
  - CNRS-SA: chemiluminescence ozonometer (*in situ,* profile)
  - IASB and NASA-GSFC: solar UV absorption photometers (*in situ,* remote)

The large gondola carried the last four types of balloon-borne methods.

There were a total of fourteen ozonesondes launched on small balloons during the three weeks (four Brewer-Mast and ten ECC) from western and eastern France, respectively. Each set of soundings had sequential launches, with time separations of hours or greater, since the goal was to compare the ozonesondes to other types of instruments, rather than to compare sonde versus sonde. The other techniques were represented by a single instrument each, except for the solar UV absorption photometers, of which there were two from different institutions on the gondola.

Results

The price paid for variety was, of course, a resulting set of observations that were somewhat separated in space and time and a modest number of samples, both of which hindered some of the intercomparisons. Nevertheless, there had never been such an extensive look at how well ozone can be measured. The results stand as a benchmark in experimental science.

(a) *Total column:* The four ground-based instruments - Dobson, IR and UV spectrometers, and lidar - gave total-column ozone values that agreed within $\pm 5\%$ during the three-week period, *provided* the data were taken at the same place and time. On one day during one of the large-balloon flights, twelve different methods (ground-based and balloon-borne) were used to deduce the total column of ozone, and the values obtained were with $\pm 10\%$. If the results from the ECC sondes were excluded, the dispersion was reduced to $\pm 5\%$.

(b) *Vertical profile:* Because of larger variability of ozone in the region below about 20 km and because so few of the observations were coincident in space and time, the assessment of the performance of the instruments in this lower part of the atmosphere was limited to noting general agreement. However, above 25 km, which was the emphasis of the campaign, several results stand out:

(i) The electrochemical sondes exhibit substantial discrepancies among themselves. The dispersion between the results increased with increasing altitude, reaching a factor of two at 33 km for one day's series. While the soundings were at different times during that day, it is unlikely that all of these discrepancies could be rationalized by atmospheric variability alone.

(ii) The *in situ* UV absorption and chemiluminescence instruments differed by as much as ±15% at the ozone maximum, the major uncertainty being attributed to the lack of inflight calibration in the latter.

(iii) The data from both of the remote solar UV absorption photometers were consistently about 20% larger than those from the *in situ* UV absorption instrument. Figure C-2 shows this reproducible difference, which had been seen on earlier balloon flights also.

(iv) The profiles obtained from the Umkehr method scattered ±20% from the others in the height range 15-30 km, but the correction for aerosols had not been made completely.

C-1.2 Balloon Ozone Intercomparison Campaign (BOIC)

This series of three balloon campaigns were conducted at Palestine, Texas, in three parts:

BOIC 1 - June, July 1983
2 - October 1983
3 - March 1984.

The primary goal was to assess the ability to perform stratospheric ozone measurements by balloon-borne instruments (Hilsenrath *et al.*, 1985).

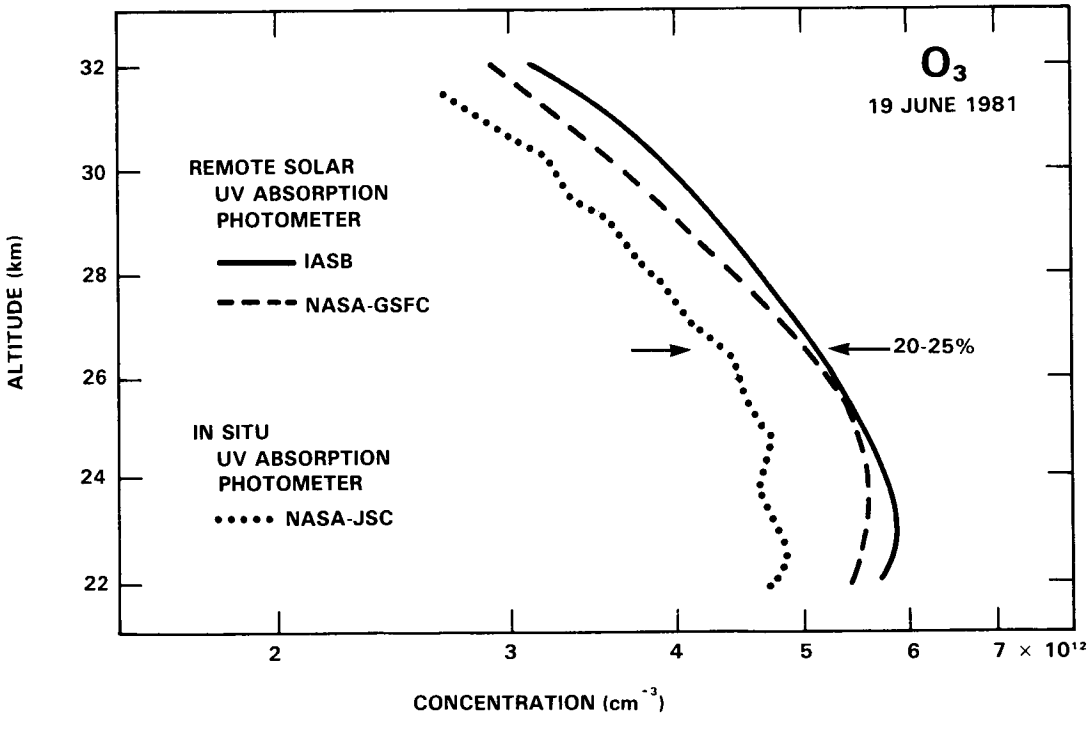

Figure C-2. Comparison of results of two remote solar UV absorption photometers with those taken simultaneously by an *in situ* UV absorption photometer. The data are from the Intercomparison Ozone Campaign. The result of the *in situ* UV absorption photometer are from one profile. The results of the NASA-GSFC and IASB remote UV absorption photometers are averages of data from three and two profiles (ascents and descents), respectively. (Adapted from Aimedieu *et al.*, [1983]).

Characteristics

(a) *Organization:* The campaign employed three instrument ensembles: a large multi-instrument gondola, a smaller gondola with fewer instruments, and a series of small ballons, each carrying a set of three electrochemical ozonesondes. Specifically, the institutions and techniques were:

- multi-instrument gondola:
  - — HU, NASA-GSFC (2), NASA-JSC, and NOAA-AL (2): *in situ* UV absorption photometer, six instruments,
  - — NASA-GSFC and NASA-WFC: remote solar UV absorption photometer, two instruments, and
  - — NASA-WFC and NOAA-GMCC: ECC sondes, several instruments.

- secondary gondola, one of each of the following:
  - — UM: mass spectrometer,
  - — NASA-JSC: *in situ* UV absorption photometer,
  - — NASA-WFC: remote solar UV absorption photometer, and
  - — NASA-WFC and NOAA-GMCC: ECC sonde, one from each institution.

- triplets; a set of three sondes flown together and representing four institutions and different methods:
  - — AES, NASA-WFC, and NOAA-GMCC: ECC, and
  - — MOH: Brewer-Mast.

The optimum plan was to have simultaneous flights of both gondolas to 40 km, accompanied by a series of triplet flights, thereby intercomparing measurements of all of the methods and research groups. However, two successive balloon failures for the multi-instrument gondola forced BOIC into three parts:

• BOIC 1:	multi-instrument gondola	10 July, 1983	(only to 26 km)
	secondary gondola	18 July	
	triplets	19 June - 7 July	
• BOIC 2:	multi-instrument gondola	24 October, 1983	(only to 22 km)
	triplets	1 week	
• BOIC 3:	multi-instrument gondola	21 March, 1984	(to 42 km)
	secondary gondola	24 March	

Only on the third attempt did the main gondola reach 42 km. Because of this lengthening of the time required to complete the campaign, not all of the institutions could participate in all aspects, as indicated. The primary data for the high altitudes are from BOIC 3 and the best statistics for the ozonesondes are from BOIC 1.

(b) *Ground-based observations:* Total ozone and Umkehr profiles were taken by Dobson and Brewer spectrophotometers, which were located at Palestine to limit the effect of spatial variations on the intercomparisons.

(c) *Ground-based comparison with an ozone reference:* Most of the *in situ* instruments were compared with the ozone reference photometer of NBS, both in advance of BOIC at the Gaithersburg, Maryland laboratory and at the launch site on BOIC 1 and 2. The ozone concentrations employed were those that would be encountered in the stratosphere, but the pressure remained at one atmosphere.

(d) "*Blindness*": In almost all cases, the flight data were reduced separately, each group being unaware of the other's data, and the results were submitted to an independent party and then intercompared jointly. Some data were corrected for errors that this initial intercomparison revealed. The comparisons at the launch site with the NBS reference were also done "blind".

Results

By focusing only on balloon-borne instruments, BOIC could enhance the statistics of the observations by having multiple instruments of a given type and by having numerous launches of the triplets of electrochemical sondes. Therefore, even though only one of the three attempts with the main gondola reached optimum altitude, BOIC has revealed several key features of the current ability to measure ozone from balloon platforms:

(a) *Comparison with NBS reference:* The largest differences between the *in situ* instruments and the NBS reference occurred for the electrochemical sondes. The departures were often systematic for each method/institution and ranged from 20% low to 10% high. The sondes exhibited response times on the order of a minute.

Four of the *in situ* UV absorption photometers (NOAA-AL #1 and #2 and NASA-JSC #1 and #2) agreed with the reference within $\pm 2\%$. The two photometers of NASA-GSFC consistently were about 8 to 12% lower than the NBS reference for both BOIC 1 and 2. The flow requirements of the HU photometer precluded a comparison with the reference

(b) *In situ* UV absorption photometers: The six *in situ* photometers of HU, NASA-GSFC (2), NASA-JSC, and NOAA-AL (2) were on the main gondola on BOIC 3 and hence could be intercompared at altitudes to 42 km. The left-hand side of Figure C-3 shows the percentage differences of the results of five of the photometers (NASA-GSFC #2 reported no data) from the average of the measured profiles on ascent. The salient feature is that four of the five photometers agreed within about $\pm 3\%$ over much of the middle stratosphere. The NASA-GSFC #1 instrument, which was low compared to the NBS reference, was also low in the stratosphere by about the same amount; hence, it is not unreasonable to assume that a yet-unknown, persistent error of 5-10% exists in that particular instrument. The NOAA-AL #1 photometer was designed to operate only up to 30 km, and the increasing discrepancy between it and its partner (NOAA-AL #2) at altitudes above 35 km is attributed to inlet wall losses, as described below. Therefore, if the data from the NASA-GSFC #1 and NOAA-AL #1 photometers are excluded from the set for these reasons, the right-hand side of Figure C-3 likely reflects the state of the art with which ozone can be measured in the stratosphere by *in situ* UV absorption photometry.

(c) *Electrochemical sondes:* The ECC sondes (NASA-WFC and NOAA-GMCC) that accompanied the main gondola gave results that agreed to $\pm 10\%$ with the average of the *in situ* UV absorption photometer data in the region of the ozone maximum. Above about 30 km, the sonde data drop to values much lower than the photometer results, exceeding 20% at 38 km and higher.

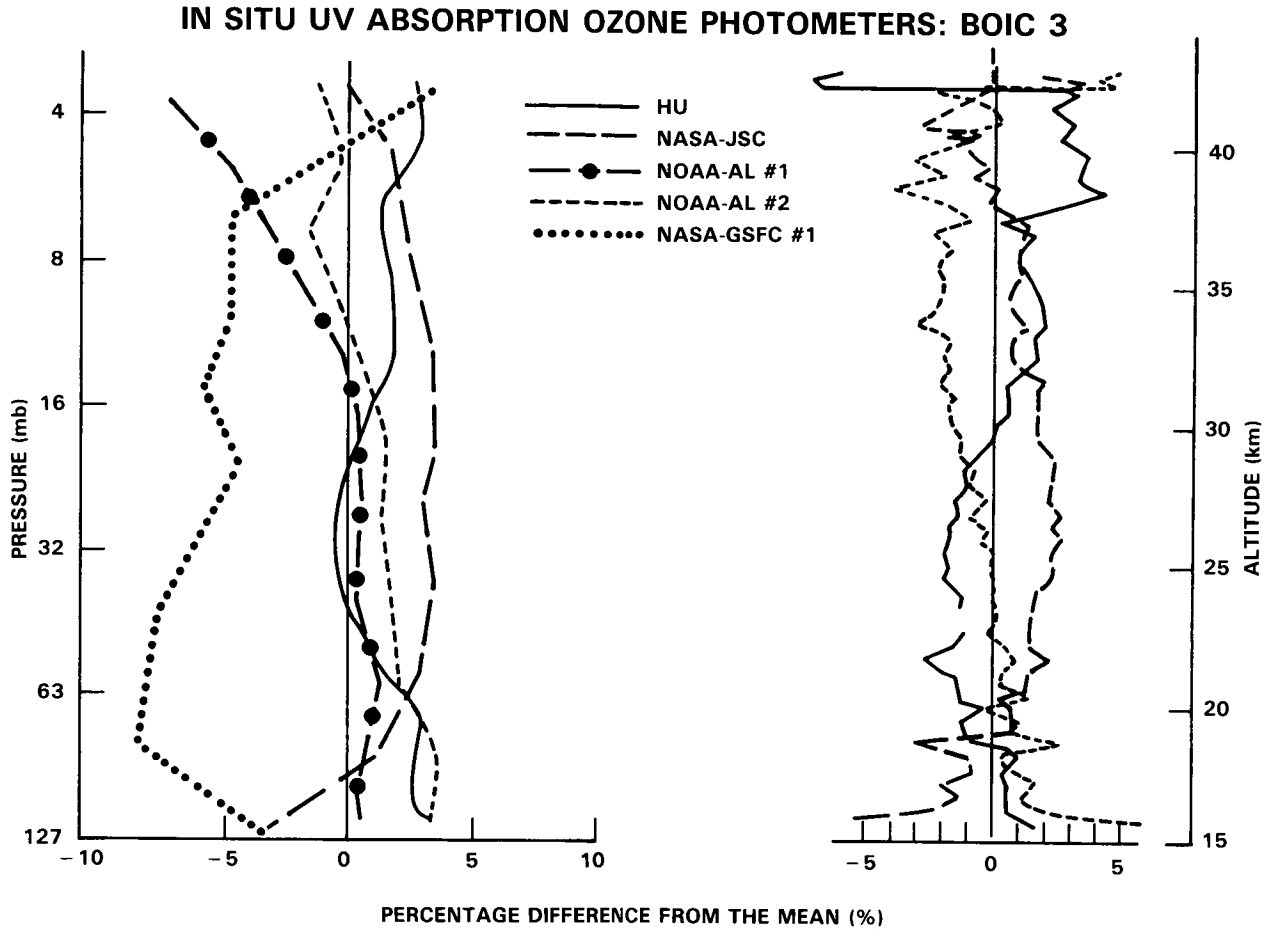

Figure C-3. Percentage difference of the results of *in situ* UV absorption photometers from the mean. The right-hand diagram contains the same data as the left-hand diagram, except that the results from the NASA-GSFC #1 and NOAA-AL #1 instrument have been deleted from the former (see text for reasons). Note the different ordinates: left-hand, pressure, and righthand, altitude. The data are from the Balloon Ozone Intercomparison Campaign 3 and are averages over height intervals. (Adapted from Hilsenrath *et al.*, [1985]).

Since numerous sondes flew in the triplet series of BOIC 1, reliable precision estimates are now possible. For the sondes of a given research group, the sonde-to-sonde difference for simultaneous measurements was typically 5% in the stratosphere, but with occasional outliers. This figure is almost doubled when those of different groups were flown together. The agreement between the sondes of different groups is reflected in Figure C-4, which shows the average departure, by Umkehr layer, of the sondes from each institution from a mean profile from all soundings (a) before, and (b) after normalization to the ground-based measurements of the total ozone column.

(d) *Remote UV absorption photometers:* Balloon and instrument failures almost thwarted a BOIC testing of the remote UV absorption method, a technique that the earlier intercomparisons had found wanting. However, on the BOIC 3 flight of the small gondola, one of these instruments was intercompared with an *in situ* UV absorption photometer. The result was consistent with the earlier observations; namely, the remote method gave results that were 5-10% higher over much of the altitude range covered.

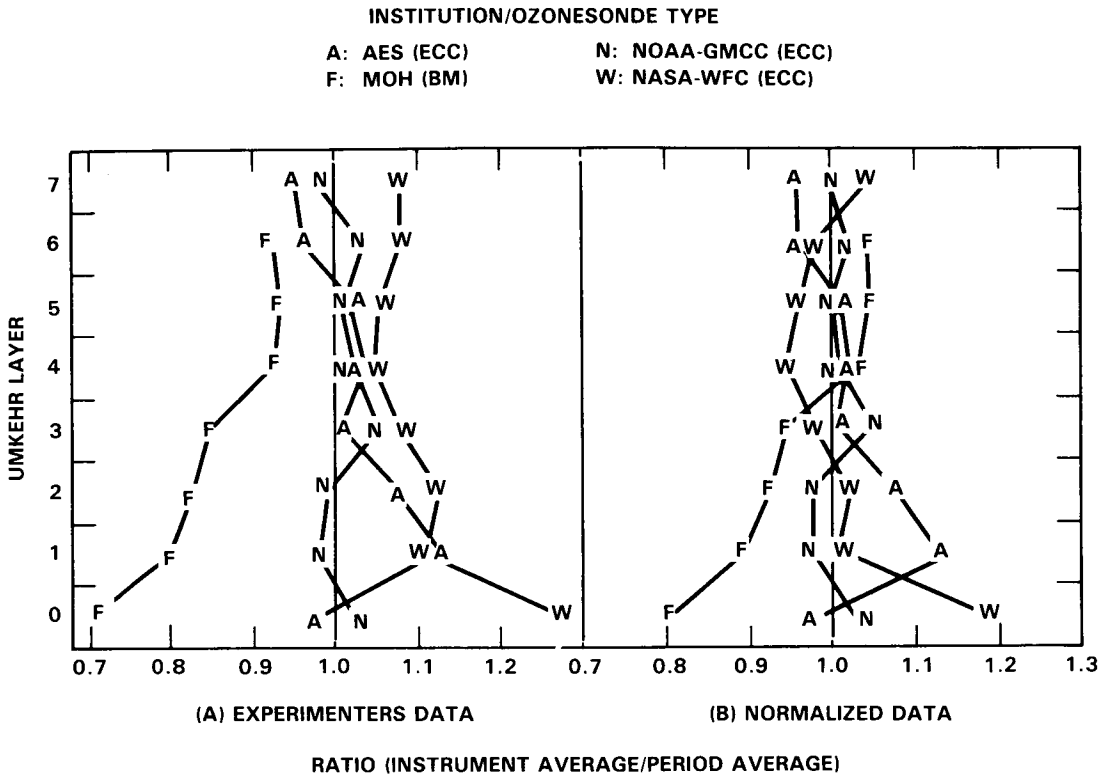

Figure C-4. Average percentage departure of each electrochemical sonde type from the mean of all soundings. Left-hand diagram: before normalizing to separately measured total ozone column. Right-hand diagram: after normalization. The sonde types are Brewer-Mast (BM) and electrochemical concentration cell (ECC). The data are from the Balloon Ozone Intercomparison Campaign 1. (Adapted from Hilsenrath *et al.,* [1985]).

(e) *Gondola and inlet-tube losses:* BOIC made a special effort to explore the oft-discussed, but rarely quantified *in situ* measurement uncertainties of losses of ozone to surfaces. At float, the differences between the *in situ* UV photometers nearly doubled and preliminary analyses suggest correlations with gondola orientation. Three of the UV instruments (HU, NASA-JSC, and NOAA-AL #2) could change their flow rates while inflight by ground command and thereby could assess whether ozone loses were occurring internally in the instrument. None showed any discernable effects even at 42 km. The NOAA-AL #1 UV photometer was not designed for measurements above 30 km and, when carried above this altitude on BOIC 3, showed distinctly lower values than its partner above 35 km (dot-dash line in Figure C-3) strongly suggesting losses on its smaller-diameter inlet lines.

C-1.3 Balloon Intercomparison Campaign

The Balloon Intercomparison Campaign (BIC) a Palestine, Texas was an ambitious and complex program whose primary goal was to assess the accuracy with which balloon-borne remote-sensing instruments can determine the composition of the stratosphere (Watson, 1986). The full implementation required a set of near-simultaneous launches of heavy gondolas on separate large balloons. Each gondola carried several instruments, many of which could measure the stratospheric abundance of numerous species.

However, balloons are not trains, and a gap of 13 days occurred between the launches of some of the main gondolas in the first BIC program in 1982. However, the launches in the second BIC program in 1983 were much closer together:

- BIC 1: 3 gondolas 22 September 1982
  1 gondola 5 October 1982
  aircraft
  ground sites

- BIC 2: 2 gondolas 17 June 1983
  2 gondolas 20 June 1983
  aircraft
  ground sites

Understandably, the time span that occurred in BIC 1 complicated some of the assessments of the intercomparisons, as did the fact that the aerosols from the El Chichon volcano were present in the lower part of the stratosphere at the balloon-site latitude during that time period. Consequently, this Appendix relies heavily on the BIC 2 data, since the more detailed analyses required for some of the BIC 1 data are still underway. Nevertheless, the whole BIC series was a logistical tour de force and has provided an unprecedented examination of the performances of balloon-borne remote-sensing techniques.

Simultaneous aircraft flights and sequences of ground-based observations provided vertical column abundances of many species, and these data could be compared to an integration of the height-profile data from the balloons. This Appendix includes only the results from the aircraft flights in BIC 2 and the Palestine ground site, for which the comparisons are the most straightforward.

Characteristics

(a) *Organization:* A number of laboratories used a total of seven different techniques to measure ozone, and their distributions among the primary BIC launch dates are the following (Robbins *et al.*, 1986):

	BIC 1	BIC 2
• balloon-borne *in situ*:		
— AE: ECC sondes	8 launches	8 launches
— NASA-JSC: UV absorption photometer	22 Sept.	14 June
• balloon-borne remote:		
— NPL: mid-IR emission grating spectrometer	5 Oct.	20 June
— JPL: microwave emission spectrometer	22 Sept.	17 June
— AES: solar UV absorption spectrophotometer	22 Sept.	
— ONERA: IR grille absorption spectrometer		20 June
— SAO: far-IR emission spectrometer		20 June

A study of the ozone data from ground-based, ECC, and satellite measurements indicated that little change occurred in the ozone structure above about 22 km between 22 September and 5 October on BIC 1; hence, the NPL data are considered comparable to the others that were obtained earlier on 22 September, but the intercomparisons were limited to higher altitudes. A Brewer spectrophotometer was operated by AES at Palestine for measurements of the total vertical column of ozone for both BIC 1 and 2.

(b) *Uncertainty analysis:* A unique feature of BIC was the detailed uncertainty analyses that each of the investigators applied to their technique. Altitude-dependent uncertainties for each known random and systematic component were combined to construct a 95% confidence interval expected for the flight data. Figure C-5 shows these confidence levels, expressed as a percentage, for the seven techniques that addressed ozone in BIC. The IR techniques exhibit substantial possible uncertainty, greater than 25%. The others anticipated lower uncertainties, 10% or less at the ozone maximum. The key utility of these careful estimates is that the instrumental differences observed inflight can be assessed in terms of whether they are larger than the combined uncertainties, i.e., whether they are significant. Disagreement beyond such conservative confidence limits for a pair of data sets would clearly indicate a highly significant discrepancy.

Results

(a) *Overall agreement:* If one disregards the ECC measurements above 29 km on BIC 1, the results of all techniques, with one exception, agree to within ±15% for 22-38 km for BIC 1 and 2. This agreement is within the 95% confidence limits; in fact, it is well within, which suggest that these limits are conservative.

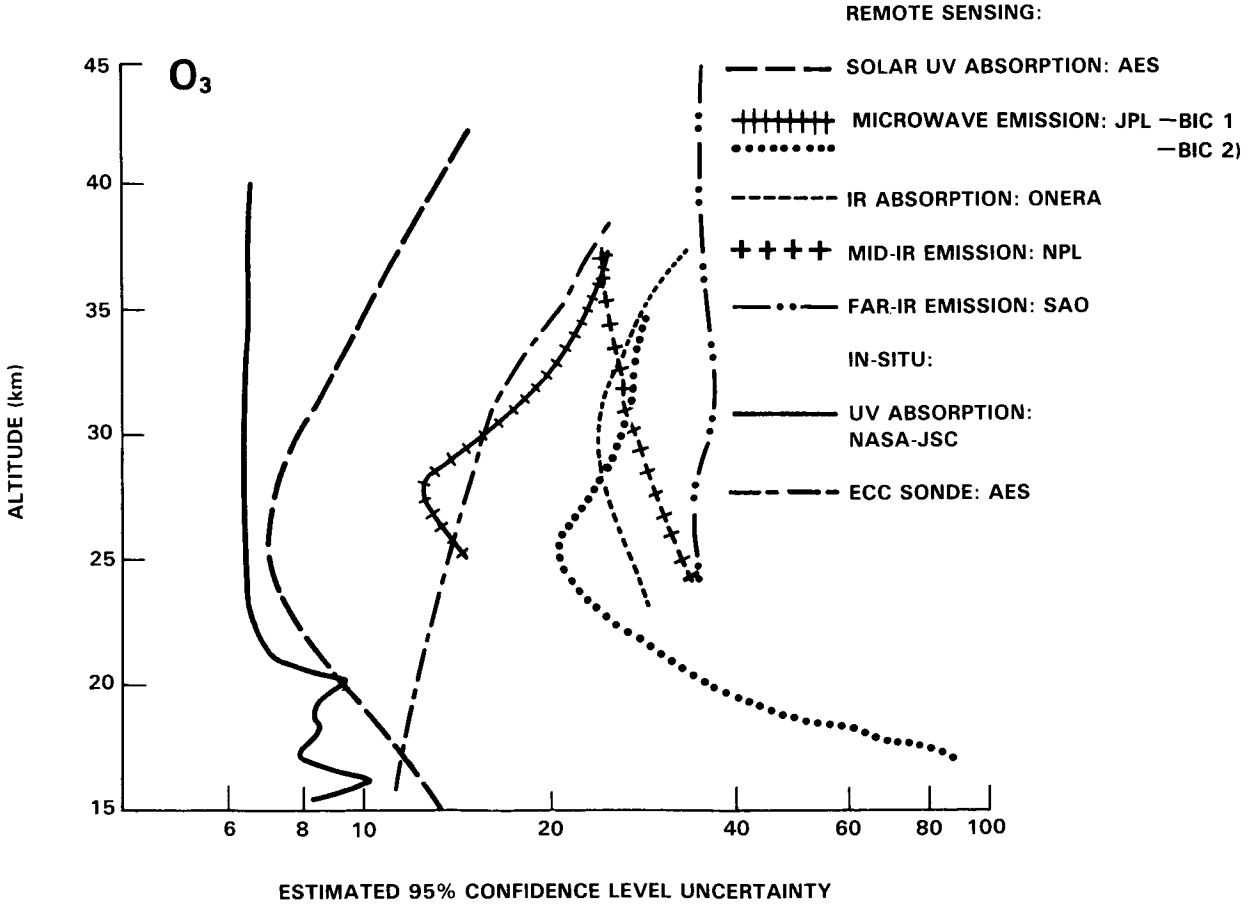

Figure C-5. The altitude-dependent, 95%-confidence-level uncertainties estimated for the ozone instruments in the Balloon Intercomparison Campaign. (Adapted from Robbins *et al.,* [1986]).

(b) *Particulars:* The solar UV absorption technique was the exception noted above. Its data at 31 km were higher than the others, a direction that the results of this technique have tended in the past. Furthermore, the ECC data were lower than the others at the highest altitudes, a tendency that is also consistent with earlier observations.

C-2 WATER VAPOR (H_2O)

The measurement of stratospheric water vapor by *in situ* techniques is difficult due to the potential problems of local contamination arising from outgassing in and around the instrument. Remote instruments are relatively less sensitive to contamination from this particular source, but could be influenced by outgassing from the balloon or gondola. The measurements that had been made over the past decade at different times and places by the various methods had shown differences as large as an order of magnitude. Consequently, there has been a keen interest in assessing the reliability of balloon-borne stratospheric water vapor measurements. Two major research efforts have addressed this question:

- *INTERNATIONAL INTERCOMPARISON OF STRATOSPHERIC WATER VAPOR INSTRUMENTATION* - primarily *in situ* methods, and
- *BALLOON INTERCOMPARISON CAMPAIGN* - remote methods.

The results of each are described here.

C-2.1 International Intercomparison of Stratospheric Water Vapor Instrumentation

The goal of this campaign was to better characterize the difference between the results of the different balloon-borne *in situ* methods that address stratospheric water vapor (Watson *et al.*, 1986). Some remote methods were also included, however.

Characteristics

(a) *Organization:* The campaign was conducted in Palestine, Texas,in two parts. The first was in 1981 and the second was in 1983. Eight different types of instrumentation were involved:

	1981 gondola and date	**1983 gondola and date**
• *in situ:*		
— NCAR: cryogenic whole-air sampler	A, 7 May	A, 13 Oct.
— UM: mass spectrometer	B, 7 May	B, 11 Oct.
— NOAA-AL: photofragmentation hygrometer	C, 7 May	C, 11 Oct.
— NOAA-GMCC: frostpoint hygrometer (free flyer)	7 May	11 Oct.
• remote:		
— DU: emission spectrometer	D, 7 June	D, 11 Oct.
— AES: scanning radiometer	D, 7 June	D, 11 Oct.
— NPL: far-IR radiometer	C, 7 May	

INTERCOMPARISONS

The methods whereby the different instruments acquire their samples (e.g., at float, on ascent, or on descent) were sufficiently different that four separate gondolas and balloons, designated above as A, B, C, D, as well as a small payload on handlaunched balloons, were required. In addition, several water vapor instruments were onboard a U-2 research aircraft that was to rendezvous with the balloons. The goal was, of course, to have all of these in the air at nearly the same time, but this could not be done. Here, only the results that were taken very nearly at the same time are intercompared.

Results

After the May 1981 flight, the investigators separately reduced their data and then examined the results as a group. While the differences were not the factor-of-ten variation from the individual studies of the previous decade, there were striking discrepancies between the data sets, as large as a factor of four. This situation prompted an intense re-evaluation by each investigator of their method and instrument. Several minor and major problems were caught in this soul-searching. Figure C-6 shows the May 1981 results,

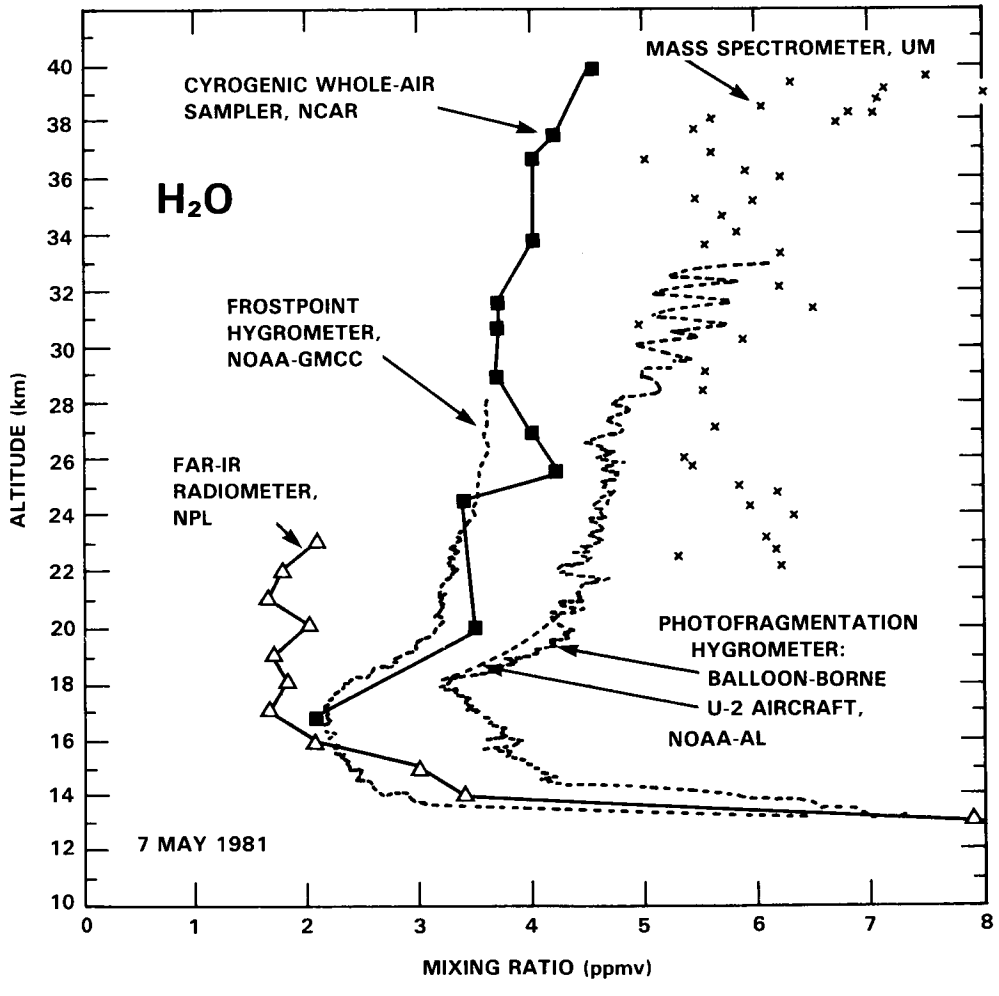

Figure C-6. Water vapor mixing ratios obtained in the first flight series of the international intercomparison of stratospheric water vapor instrumentation. (Adapted from Watson *et al.*, [1986]).

once these errors were corrected. While this re-examination resulted in a modest improvement in the overall agreement (factor-of-three worst case), there are still substantial differences. The stated error limits touch in most cases, but nevertheless there are intriguing regularities that suggest systematic problems with magnitudes of tens of percent.

Since the soul-searching presumably had improved the methods and instruments, a second flight series was carried out to see if the state of affairs portrayed by Figure C-6 was indeed the current state of the art of stratospheric water measurements. Figure C-7 shows the results of the October 1983 flights. Since the differences are comparable to those of the earlier study, both data sets are likely to be a fairly definitive statement regarding the reliabiity of *in situ* water vapor measurements in the stratosphere.

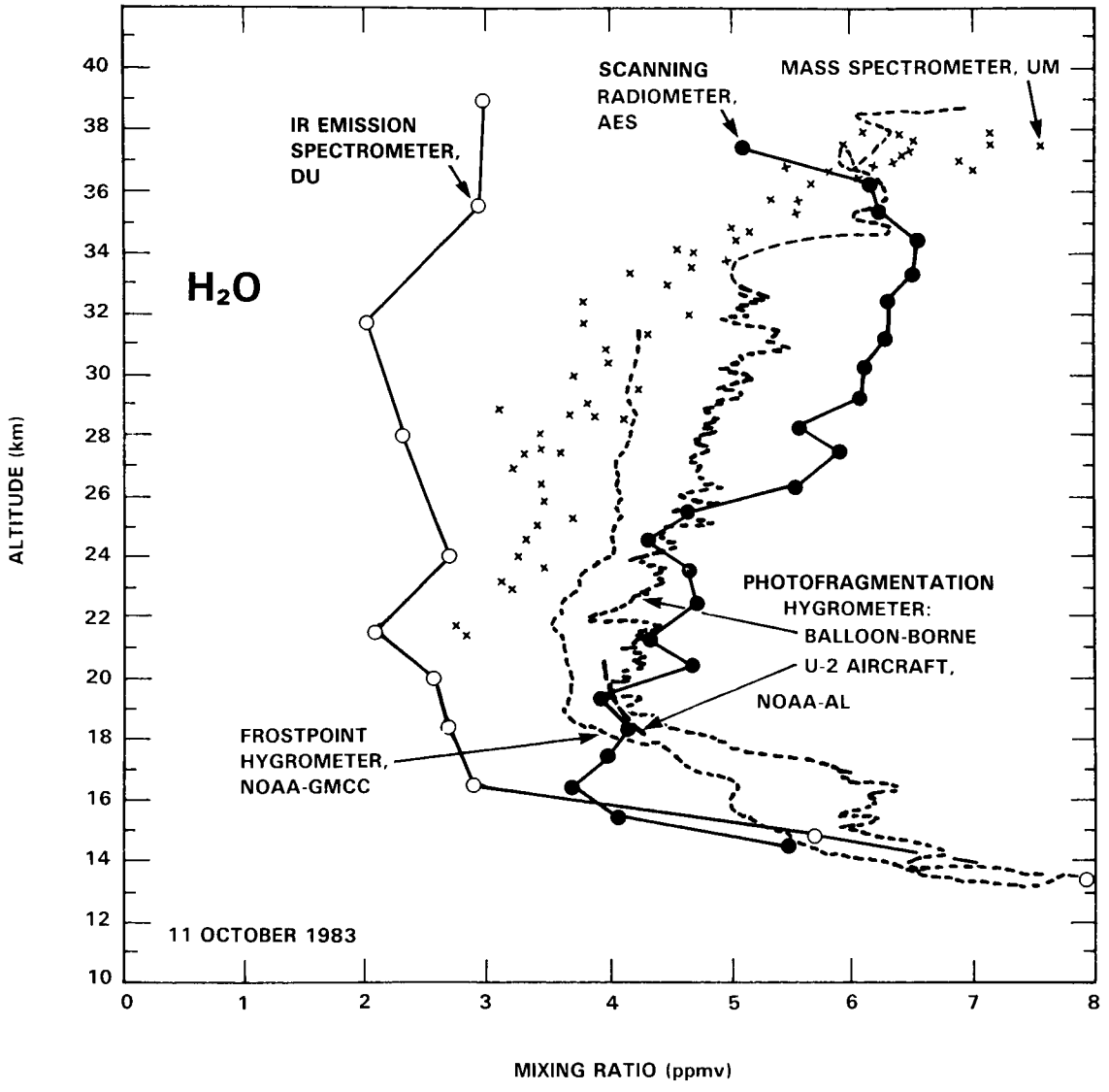

Figure C-7. Water vapor mixing ratios obtained in the second flight series of the international intercomparison of stratospheric water vapor instrumentation. (Adapted from Watson *et al.*, [1986]).

The patterns (or lack thereof) in Figure C-6 and C-7 are fairly clear. First, the photofragmentation and frostpoint hygrometers differ in a regular fashion, the latter being lower by 0.5 to 0.75 ppmv. The same magnitude and sign of this difference was also observed on simultaneous flights of these two instruments from Laramie, Wyoming in February 1983. This consistency has occurred even though different frostpoint instruments have been used in the studies, demonstrating that the problem does not lie in one particular frostpoint instrument. The mass spectrometer data are consistent with neither the photofragmentation nor the frostpoint data. The results of the three remote techniques, although not flown together on the same series, are both lower and higher than the *in situ* data.

C-2.2 Balloon Intercomparison Campaign

The Balloon Intercomparison Campaign (BIC) was carried out to assess the ability to measure remotely a number of compounds other than water vapor; however, this species has strong absorption features throughout the IR and mm-wave regions of the spectrum. Hence, many of the investigators had absorption or emission features due to water vapor in their data and have reported these results for intercomparison. While more data was, in fact, available for water vapor than any other species addressed in BIC, the spectral regions were generally chosen to optimize the measurement of species other than water vapor. Nevertheless, BIC does provide a useful first look at the level of agreement between remote techniques (Murcray *et al.*, 1986), hence complementing the earlier comparison of *in situ* methods.

Characteristics

As explained in Part 1.3 above, BIC was conducted in two parts, the first in 1982 and the second in 1983. Furthermore, in neither case were all of the gondolas launched on one day, but rather they were separated by 13 days in 1982 and 3 days in 1983. Since the latter is much more favorable for intercomparison, we focus here on it. The four emission and two absorption remote-measurement techniques were:

Group	Instrument	Method	Wavelength	Gondola and date
UL	Mid-IR grating spectrometer	absorption	4044 cm^{-1}	A, 17 June
DU	IR grating spectrometer	emission	25, 26 μm	B, 17 June
AES	IR scanning	emission	6.3 μm	C, 20 June
SAO	Far-IR Fourier spectrometer	emission	111, 188 cm^{-1}	D, 20 June
ONERA	IR grille spectrometer	absorption	1600–1608 cm^{-1}	D, 20 June
NPL	Mid-IR grating spectrometer	emission	1339–1350 cm^{-1}	E, 20 June

Results

Figure C-8 presents the results obtained. The data appear to split into two sets at the higher altitudes, a "high" set from ONERA and SAO and a "low" set from AES, DU, NPL, and UL. While the "high" pair were indeed on the same gondola, some of the data of the "low" set were taken, nevertheless, on the same day. Furthermore, the two sets do not reflect a division between emission and absorption methods.

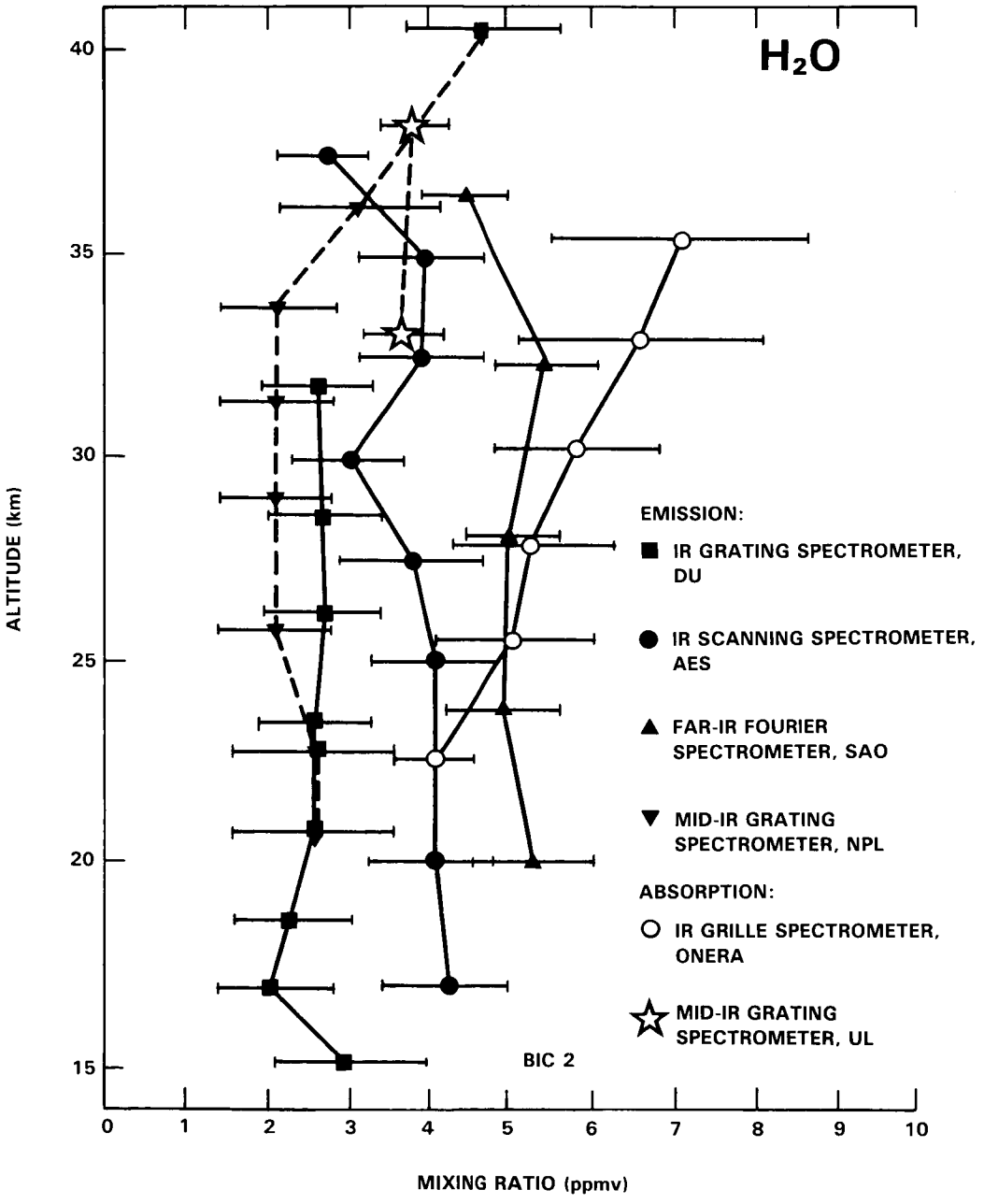

Figure C-8. Water vapor mixing ratios as observed in the Balloon Intercomparison Campaign 2. (Adapted from Murcray *et al.*, [1986]).

Thus, it is difficult to find a simple rationalization of the differences and, indeed, no satisfactory explanation is known currently. The discrepancy is a real one, since the uncertainty limits in Figure C-8 are deemed conservative estimates of the possible random and systematic errors. The differences were smaller on the BIC flights the year earlier, but the time spread over which those data were taken clouds the issue of whether the change reflects better instrumental performance. Thus, on the basis of one sample, the discrepancies among the results of non-optimized remote methods for measuring stratospheric water vapor are up to a factor of 3.5. One positive point can be made: the AES and DU results are in far better agreement in BIC 2 than they were in the October 1983 flights of the *in situ* water-vapor campaign (Figure C-7).

C-3. OTHER SPECIES

The direct assessment of the reliability with which other stratospheric species can be measured has been done only in the Balloon Intercomparison Campaign (BIC). As described in Sec. 1.3, BIC concentrated predominately on evaluating balloon-borne remote-sensing methods. The program was conducted in two parts; September-October 1982 (BIC 1) and June 1983 (BIC 2). Problems forced the BIC 1 flights to be separated by over two weeks, whereas all of the BIC 2 flights occurred within a 3-day period. Consequently, the data from BIC 2 are the emphasis in the intercomparisons described below.

C-3.1 Nitric Acid (HNO_3)

Characteristics

During BIC, remote-sensing methods using both emission and absorption spectroscopy were assessed for their reliability in determining height-profile and vertical-column abundances of HNO_3 (Pollitt *et al.*, 1986):

Height-profile, balloon-borne

Group	Instrument	Technique	Spectral Region (cm^{-1})	BIC
AES	cooled radiometer	emission, ascent	870–900	1&2
DU	cooled-grating spectrometer	emission, ascent	Q-branch 873.73	1&2
NPL	cooled-grating spectrometer	emission, limb-scanning	870–900	2
ONERA	grille spectrometer	absorption limb-scanning	1325.7	2

Total-column, balloon-borne

Group	Instrument	Technique	Spectral Region (cm^{-1})	BIC
DU	IR Fourier spectrometer	absorption, occulation	1720–1730	1&2

Total-column, aircraft

Group	Instrument	Technique	Spectral Region (cm^{-1})	BIC
NCAR	IR Fourier spectrometer	absorption, occultation	1720–1730	1&2

Special care was taken by the BIC investigators to intercompare only those data from the same air mass, wherever possible. For example, the AES radiometer and the DU spectrometer were on two gondolas that were launched on the same day in BIC 1 and hence were deemed comparable. Furthermore, the sunset solar absorption measurements of ONERA and the westward-looking emission measurements of NPL during BIC 2 were paired. While some possible effects of spatial variation could not be ruled out, the measurements of the HNO_3 column made in the region round the launch site showed little variation with latitude and time, thereby giving confidence that samples of dissimilar parts of an inhomogeneous distribution were not a significant source of differences between instruments.

Results

The initial comparisons of the results revealed substantial agreement for most of the data sets, but there were two notable exceptions. First, the emission data obtained by the cooled radiometer of AES at altitudes less than 22 km were significantly lower than the other data. The cause of this discrepancy was traced to spectral contamination by chlorofluorocarbons and hence corrections were made in the final data. The second anomaly was the absorption data set from the grille spectrometer of ONERA, which was significantly different in magnitude and shape from all of the other profile data. Despite preliminary re-examination of the laboratory calibration that was used to reduce the flight data, the cause of the discrepancy remains unknown.

The left-hand portion of Figure C-9 compares the percentage differences of the AES and DU data from their common mean for the averages over four altitude ranges in BIC 1. The $\pm 20\%$ differences are well within the possible uncertainties, except perhaps at the lowest elevations. However, both are emission measurements employing the 11.3 micron band of HNO_3 and reduced using the same band model; hence, systematic errors in the spectral parameters are common to both.

In BIC 2, a much more extensive intercomparison could be made: three emission techniques (AES, DU and NPL) and one absorption technique (ONERA). The right-hand portion of Figure C-9 shows the percentage deviations of these data sets from the mean of the emission data. The three emission experiments, which used similar wavelength regions, gave results that were in substantial harmony, generally $\pm 25\%$ and well within the possible uncertainties, except perhaps at the lowest altitudes. However, the absorption data of ONERA are quite different, being a factor of two larger at 27 km. It is not currently clear whether this is a problem associated with the ONERA instrument and/or techniques in particular or an unknown problem with emission and/or absorption methods in general.

An average of the three emission data sets on BIC 2 gave an integrated column abundance above 21 km that agrees satisfactorily with that that determined in one "best" scan by the absorption measurement of the balloon-borne IR Fourier transform spectrometer of DU. The aircraft absorption measurements of the HNO_3 above 13 km are 20% lower than those obtained from an integration of the height-profile data from the balloon-borne emission instruments, but this difference may not be outside of the combined uncertainties.

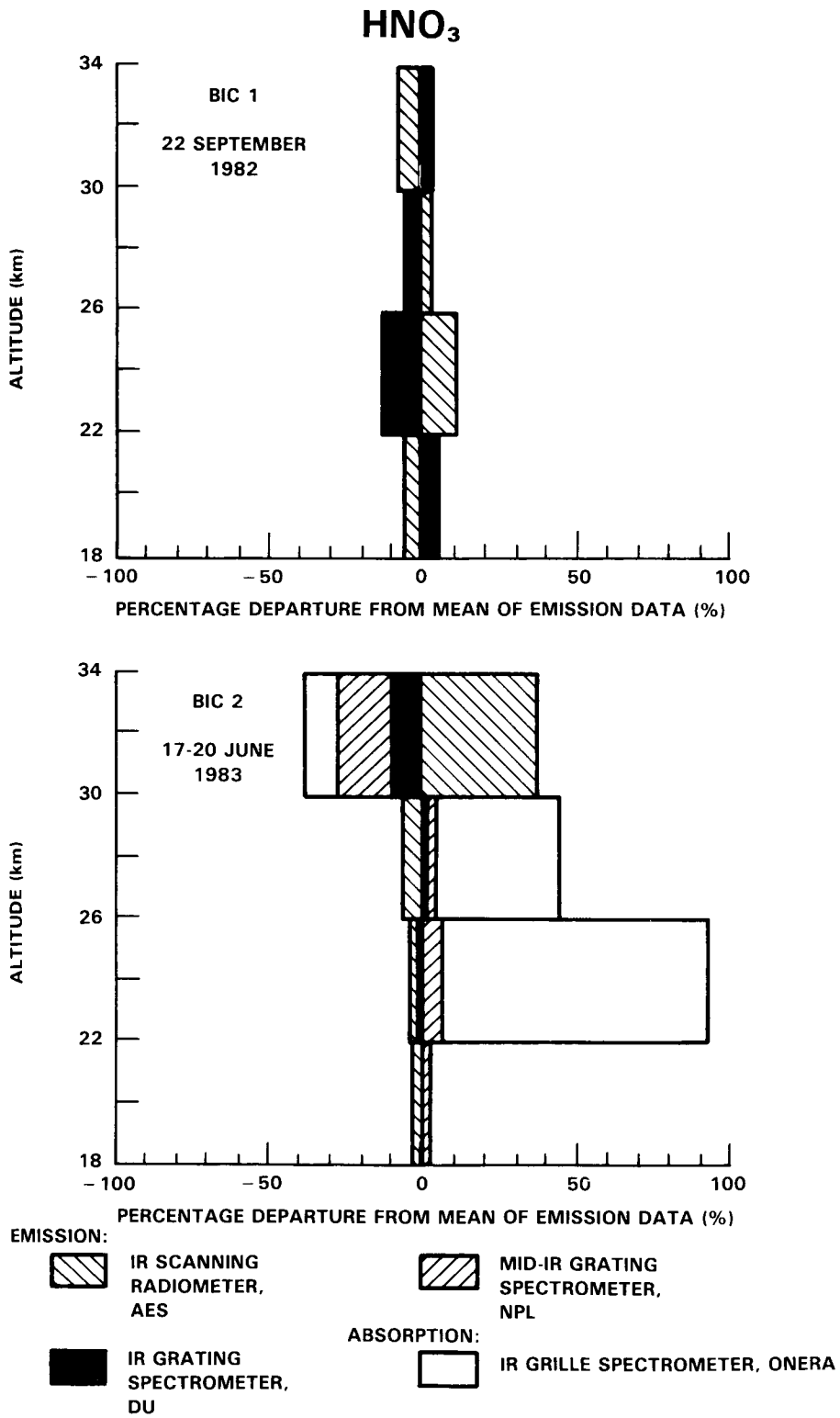

Figure C-9. Departures of the 4-km averages of the HNO_3 data from the mean in the Balloon Intercomparison Campaign. (Adapted from Pollitt *et al.*, [1986]).

C-3.2 Hydrogen Chloride (HCl) and Hydrogen Fluoride (HF)

Apart from its importance in the chemistry of the stratosphere, HCl provides an excellent test of the spectroscopic remote sensing methods that are currently used for measuring the composition of the upper atmosphere. HF also provides a useful test of such methods. Their lines are widely spaced, have well-known positions, are fairly clear from interferences, and have relatively well-understood spectral shapes and strengths. Hence, this spectroscopic "best case" was one of the primary focuses in BIC. There were a total of eight different instruments involved in the HCl and HF measurements (Farmer *et al.*, 1986; Mankin *et al.*, 1986). The most definitive test of the reliability with which HCl and HF can be quantified occurred in BIC 2.

Characteristics

HCl height-profiles were obtained by five balloon-borne instruments: three limb scanning in absorption and two in emission:

Group	Instrument	Technique	Spectral Region (cm^{-1})
AES	IR Fourier spectrometer	absorption	3000 (HCl)
ONERA	IR grille spectrometer	absorption	3000 (HCl)
UL	Mid-IR grating spectrometer	absorption	3000 (HCl), 4040 (HF)
IROE	Far-IR Fourier spectrometer	emission	41 and 62 (HCl), 164 (HF)
SAO	Far-IR Fourier spectrometer	emission	124, 145, and 165 164 (HF)

In addition to these ballon-borne instruments, there were vertical-column measurements of HCl made from balloons and aircraft, as well as ground sites. These data, however, are not yet fully available.

Results

Figure C-10 shows the height-profile data obtained for HCl by five instruments. It is clear that there is excellent agreement, generally within $\pm 20\%$ and well within the experimental uncertainties. The agreement for HF among three instruments was not quite as good, perhaps generally $\pm 35\%$.

C-3.3 Methane (CH_4)

Although CH_4 was not a main emphasis in BIC, some of the instruments, especially those making optical remote-sensing measurements in the mid-IR, could examine vibration-rotation bands of this molecule (Zander *et al.*, 1986). The more-coincident balloon flights of BIC 2 provided the best opportunity to intercompare the results of the instruments that could observe CH_4.

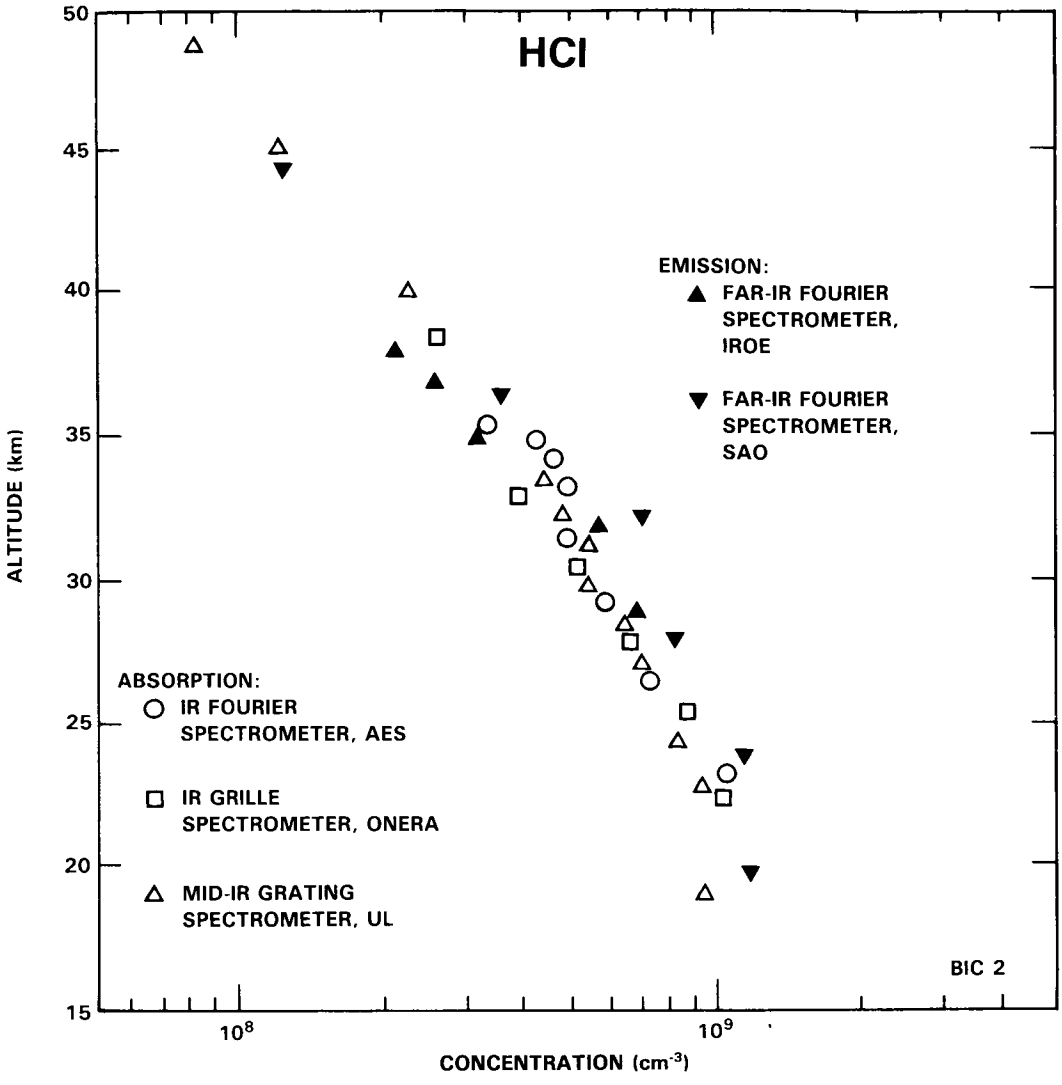

Figure C-10. The HCl concentrations measured in the Balloon Intercomparison Campaign. (Adapted from Farmer *et al.*, [1986]).

Characteristics

CH_4 height profiles were recorded by three instruments on BIC 2, two operating in absorption and one in emission:

Group	Instrument	Technique	Spectral Range (cm^{-1})
UL	Mid-IR grating spectrometer	solar absorption, occultation	2948
NPL	Mid-IR grating spectrometer	atmospheric emission, limb scan	1335–1350
ONERA	IR grille spectrometer	solar absorption, occultation	1322, 2927, 2948

Results

Figure C-11 shows the BIC results. A significant discrepancy is apparent. While both of the absorption studies, UL and ONERA, are in excellent agreement, the emission data of NPL are substantially lower. The emission technique was re-examined carefully, since it was the "outlier" and since its results for H_2O, which were from the same spectral region, also tend to be lower than others (Figures C-6 and C-8). However, the difference has not been rationalized satisfactorily at the present.

C-3.4 Nitrogen Oxides (NO and NO_2)

Nitric oxide and nitrogen dioxide were considered as prime targets in the BIC campaign. Not only are they the key reactive species in the stratospheric nitrogen chemistry that leads to ozone destruction,

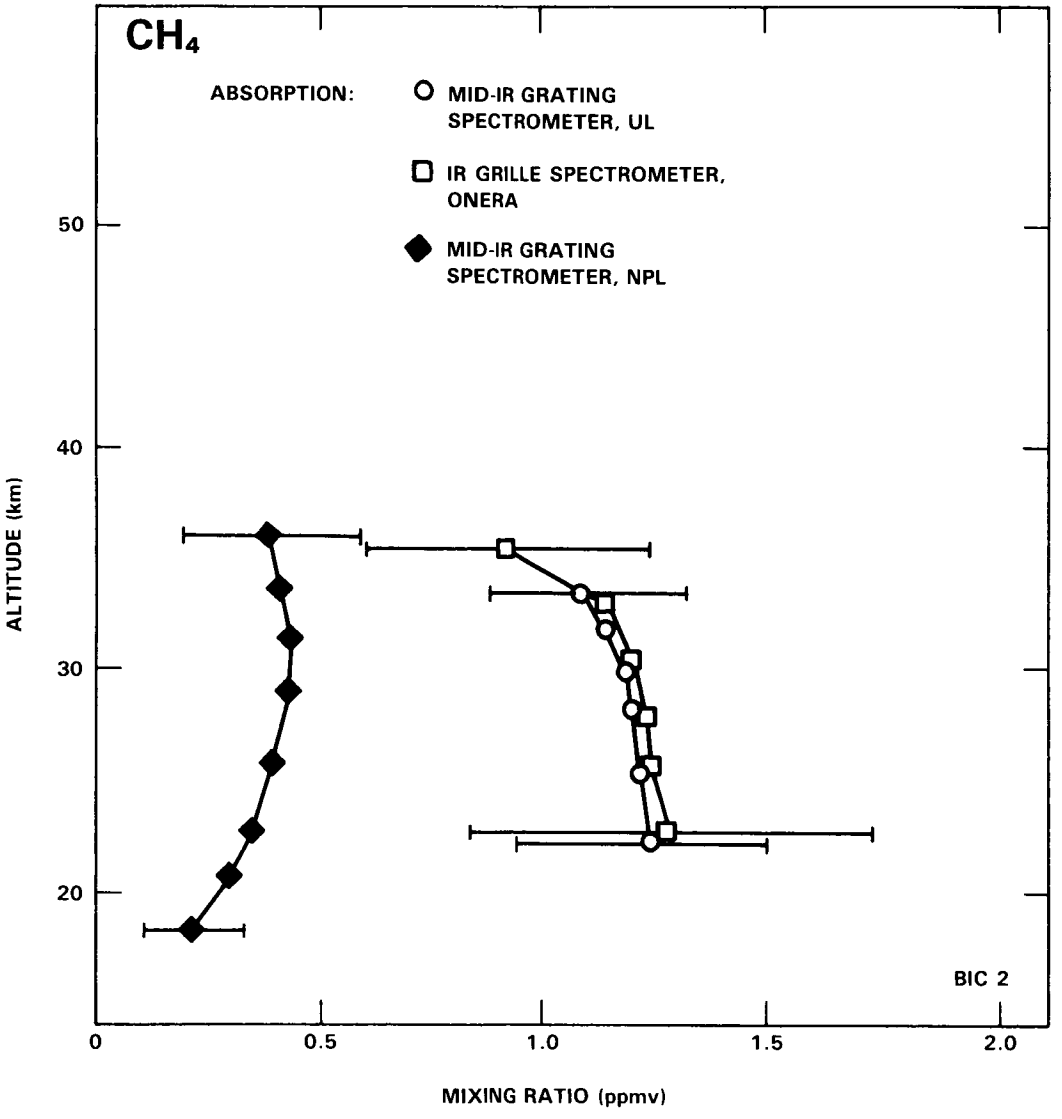

Figure C-11. The CH_4 mixing ratios measured in the Balloon Intercomparison Campaign 2. (Adapted from Zander *et al.*, [1986]).

but also a number of remote-sensing methods and instruments are capable and available to measure these species (Roscoe *et al.*, 1986).

Characteristics

BIC 1 and 2 involved not only balloon-borne instruments that obtained vertical-profile data, but also aircraft-borne and ground-based instruments that could obtain vertical-column data. Of particular concern for the species NO and NO_2 is the fact that the absorption measurements that use the sun as a source are generally made at sunrise and sunset, just at the time when the concentrations of these species are changing rapidly. Therefore, emission methods, which do not require the sun as a source and hence can be made at any time of the day, are an important complement to the more-common absorption instruments.

The suite of balloon-borne methods that were included in BIC for NO_2 were the following:

Group	Instrument	Technique	Spectral Range	BIC
UO	IR pressure modulated radiometer	emission	1570–1650 (cm^{-1})	1&2
NPL	Mid-IR grating spectrometer	emission	1600–1615	1&2
ONERA	IR grille spectrometer	absorption	1600–1608	2
AES	Visible spectrometer	absorption	437–450 (nm)	2
UT	Visible spectrometer	absorption	429–452	2
CNRS-SA	Visible spectrometer	absorption	432–450	2

The total-column data are only partially available at the present.

Results

There is still a considerable amount of analysis and scrutiny that must be done on the BIC data for the nitrogen oxides, and hence a complete picture is not yet available. However, it is clearly a very interesting and puzzling picture.

(a) *NO:* The nitric oxide observations were limited to two instruments on BIC 2: the UO emission radiometer and the ONERA absorption spectrometer. The results agree very well, $\pm 15\%$, over the 30–40 km altitude range, which is very significant since the two approaches are so different.

(b) *NO_2*: The puzzle arises for NO_2. The BIC 2 data from the four absorption instruments (ONERA in the infrared and AES, UT, and CNRS-SA in the visible) agree very well, typically within $\pm 25\%$, over the 20–40 km altitude range. Furthermore, the results of the NPL emission spectrometer are in accord with this absorption data set. However, the other emission instrument, UO's IR pressure modulated radiometer, gave results that are substantially less than the others at altitudes below about 30 km.

Although the discrepancy is only slightly larger than the (rather broad) limits of uncertainty, the pattern is similar to that seen in BIC 1 in the UO and NPL data and in the "historic" data sets that preceded BIC. Despite extensive searching for consistent reasons, none have been found. Thus far, the comparison to the vertical-column data has not shed any light.

C-4 CONCLUSIONS

Although not all of the analyses from the intercomparison campaigns have been completed, several conclusions presently stand out and are unlikely to change substantially when the picture is completed.

C-4.1 Ozone

(a) *UV absorption photometry appears to be able to measure the mixing ratios of ozone with a precision and relative accuracy of $\pm 4\%$ at stratospheric altitudes up to 40 km.*

The BOIC 3 data demonstrate that three very differently constructed and independently operated UV absorption photometers can agree to $\pm 3\%$, using a common measurement of ambient pressure and the same absorption cross section. Assuming that this one flight was not simply a fortuitous anomaly and indeed reflects approximately the current state of UV absorption photometry, then these results can be generalized as follows into an assessment of the state of the art of *in situ* stratospheric measurement capability. Pressure should be quantifiable to $\pm 1\%$. The uncertainty in the cross section is considered commonly to be about $\pm 2\%$. Therefore, UV absorption photometry should be capable of $\pm 4\%$ uncertainty relative to the cross section and $\pm 6\%$ uncertainty absolute. Since this technique has been woven deliberately as a common thread through all of the ozone intercomparisons (indeed, one of the NASA-JSC instruments has been on every campaign), it allows a common basis with which to assess the uncertainties of the other methods.

(b) *The electrochemical sondes, with state-of-the-art preflight preparation, are generally reliable to about $\pm 10\%$ overall uncertainty in the stratosphere at altitudes up to approximately 30 km, above which the readings are erroneously low.*

The extensive triplet intercomparisons of BOIC 1 and the sonde-to-UV intercomparison on BOIC 3 are the rationale for this $\pm 10\%$ figure of merit for the general monitoring-type sonde. All ozone intercomparison campaigns demonstrate the loss of sensitivity at the higher altitudes. While this figure of merit applies to the average performance, individual sondes are occasionally much better or much worse. The electrochemical sondes are "operator sensitive", as demonstrated in BOIC 1 and 3, and those of a single group can have a one-standard-deviation precision of $\pm 5\%$ in the stratosphere.

(c) *The remote solar UV absorption technique gives results that appear to be erroneously high by 5–20%.*

Every one of the recent intercomparisons campaigns have verified this pattern. Different types of solar absorption instruments operated by different groups were involved in these campaigns. Hence, the prob-

lem is very likely to be a property of the method. Since this remote solar UV absorption method could, in principle, have the same high accuracy as its *in situ* cousin, it remains an enigma why it does not.

(d) *The total vertical column of ozone can be measured to an absolute uncertainty of* $\pm 5\%$.

Several intercomparisons of ground-based methods for measuring the vertical column of ozone have shown the high precision of the Dobson and Brewer techniques and instruments. However, the balloon-borne studies summarized in this Appendix have afforded height-profile data of unparalleled accuracy. Hence, since ground-based total-column measurements were also a part of these studies, comparisons of these data to the integrations of the independent vertical-profile data provides a more sensitive test of the absolute accuracy of both approaches than was heretofore available. The analyses completed thus far provide the $\pm 5\%$ figure of merit.

C-4.2 Water Vapor

(a) *Concurrent stratospheric water vapor measurements by various balloon-borne methods differ by a factor 3 to 4, reflecting differences of 2–5 ppmv.*

While this is an improvement over the factor-of-ten differences reported over the earlier decade, the discrepancies among the results of nine different methods, if all are taken at face value, demonstrate that water vapor still remains a very difficult stratospheric constituent to measure with high absolute accuracy.

(b) *The frostpoint and photofragmentation in situ results differ consistently by 0.5 to 0.75 ppmv, with the latter being the larger values.*

This consistency is worth noting for two reasons. First, it is the only consistency among the water vapor intercomparison results. Secondly, these are the methods whereby the bulk of stratospheric water vapor data have been acquired. The consistency of the difference strongly indictates a bias in one or both of the methods, which has defied discovery thus far.

C-4.3 Other Species

(a) *Current balloon-borne measurements of* HNO_3 *by three instruments using emission spectroscopy in the same wavelength region agree within* $\pm 10\%$ *at altitudes between 22 and 30 km and* $\pm 25\%$ *between 30 and 37 km.*

In addition, these data yield column abundances above 21 km that agree to within 30% with a separate absorption measurement. It is tempting to conclude that this harmony represents the current ability to measure HNO_3 with remote sensing methods, but an unexplained serious discrepancy (factor of two) between these data and the height-profile measurements in absorption by another instrument currently prevent this.

(b) *Remote sensing techniques can determine the height profile of* HCl *over the altitude ranges 20–45 km to within* $\pm 20\%$ *and can determine* HCl *mixing ratios at 30 km to within* $\pm 35\%$.

HCl and HF pose a "best case" for remote sensing methods and BIC 2 states strongly that the best is indeed quite good. No systematic differences were observed between emission and absorption and between the two spectral regions that were employed.

(c) *Unresolved discrepancies among members of a small data set prevent an unequivocal assessment of remote methods for measuring stratospheric CH_4.*

Taking the 21 data points and their uncertainty estimates from the three instruments at face value, the methane mixing ratio at altitudes of 20–35 km lies between 0.2 and 1.5 ppmv, which is not a useful constraint.

(d) *The IR pressure modulated radiometer appear to rather consistenty give results for NO_2 that are significantly less than the results from other remote balloon-borne measurements at altitudes below about 30 km.*

This pattern was seen in both BIC 1 and 2 and in much of the "historic" data as well. Yet this emission method yields NO results that are consistent with those of other methods. The cause, if indeed it lies solely in IR pressure modulated radiometry, has resisted discovery thus far.

C-4.4 General

(a) *The intercomparison campaigns have improved the quality of the measurements of stratospheric trace gases.*

This is undoubtedly true. Specific examples of deficiencies that were discovered and corrected are the following: an error in a primary standard, an incorrectly measured length, a spectroscopic interference from chlorofluorocarbons, large and variable losses to the walls of inlet tubes at high elevations at night, a misapplied algorithm, an incorrect preception of the number of path lengths in a multipass cell, and a small persistent leak in a vacuum line. In the complex and challenging task of balloon-borne measurements of stratospheric trace gases, it is by no means surprising that some problems of this sort have occurred. It is very unlikely that they would have been discovered in the near future had the rigorous intercomparisons not been done. Many of the problems caused errors in the awkward 20–40% range, which is small enough to not be immediately obvious in the results of separate flights, but large enough to be of consequence.

C-5 FUTURE RESEARCH NEEDS

Although it is clear that the past intercomparison campaigns have been instructive and useful in assessing and improving stratospheric measurement capabilities, it is also clear that much still needs to be done in this regard. This includes, first of all, simply finishing the analyses and assessments of the large body of intercomparison data already in hand and, secondly, initiating new studies based on what has then been learned. The major short-term needs are as follows, expressed here as a series of questions:

C-5.1 Ozone

(a) *Does $\pm 3\%$ precision and relative accuracy indeed reflect the standard performance of in situ UV absorption photometry at stratospheric altitudes up to 40 km?*

While very encouraging, BOIC 3 is only one sampling of this technique's performance. Opportunities should not be missed to intercompare these instruments a few more times and with other techniques like lidar. If this performance is indeed standard, then the demonstration of that will be highly significant in future monitoring or ground-truth strategies.

(b) *What is the origin and cure for the operator sensitivity of the electrochemical monitoring sondes?*

Realistically, BOIC only represents a "best-case" assessment of the sondes, since they were lovingly prepared in the field by the leading authorities. The differences between the data of the institutions involved that occurred even under these ideal circumstances suggest that the sonde-to-sonde variation will likely be larger in a network of far-flung sites operated by a variety of people. Laboratory tests seem to be in order to seek the cause of these differences, so that network operation could have a smaller potential variance.

(c) *What are the details of the agreement between the integrals of the best height-profile data and the simultaneous total-column measurements?*

Although a preliminary examination has been done, the BOIC, and to a lesser extent the BIC, data have only just begun to be mined for this important information on these two separately measured quantities.

C-5.2 Water Vapor

(a) *What is the origin of the systematic 0.5–0.75 ppmv difference between the photofragment and frost-point hygrometers?*

Further flight investigations are not needed. Laboratory comparisons of the two methods under conditions were potential artifacts could be systematically tested would seem to be more fruitful. If these two methods were to agree eventually, they would serve as a benchmark against which the other methods, both *in situ* and remote, could be assessed in future balloon-borne intercomparisons, particularly ones in which the remote methods are optimized for water vapor.

C-5.3 Other Species

(a) *Is the discrepancy among the remote methods for measuring HNO_3 a problem with one instrument, the IR absorption grille spectrometer, or a more subtle difference between absorption and emission techniques in general?*

The laboratory calibration spectra used with the grille spectrometer are currently being examined in this regard, including effects of pressure dependence. This is an example of a need that is more broad and fundamental than this current discrepancy; namely, the remote methods, and HNO_3 in particular, could use better-quality spectroscopic data.

(b) *Since the vertical-profile data for HCℓ and HF appear to be very accurate, what are the details of the agreement with the total column data?*

This spectroscopic "best case" should be mined for all the information that it contains. Clearly, the stage is nearly set for an in situ vis-a-vis remote balloon-borne intercomparison.

(c) *The weight of evidence suggests that the IR pressure modulated spectrometer produces results that are too small at the stratospheric altitudes below about 30 km. Why?*

Laboratory tests are addressing this question, e.g., the possible temperature dependence of the NO_2 line shape. Emission methods for NO_2 are not plentiful and the daytime capability is important. This discrepancy is a key one.

C-5.4 General

Clearly there remains much more to be done and learned about instrument assessment via intercomparison. In addition to completing what has been started, there are the more general comparisons of *in situ* and remote methods for most of the BIC species. Furthermore, some of the key radical species, like ClO, are ripe for balloon-borne and ground-based intercomparisons. The pacing element is the existence of different techniques that address the same species with instruments that have completed the separate field-trial stage. Even with that necessary condition, the road to harmony can be long and twisting. For example, there is no one recipe for what to do when two or more methods significantly disagree.

Since both individual instrument development and tracking down the origin of will-o-the-wisp discrepancies are both arduous, time-consuming, and costly tasks, it should continue to be recognized that (a) multiple techniques are essential (and are not "wasteful" duplication) and that rigorous and blind intercomparisons under field conditions are vital (and are indeed as much a part of doing atmospheric science as is gathering data to test a geophysical hypothesis). The need is as simple as being able to unequivocally demonstrate that what we measure is correct.

APPENDIX D

MONTHLY MEAN DISTRIBUTION OF OZONE AND TEMPERATURE

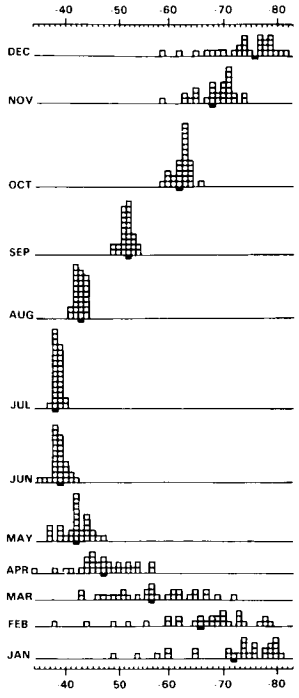

Panel Members

K. Labitzke, Chairperson

J. K. Angell
J. J. Barnett
P. Bowman
M. Corney
G. M. Keating
A. J. Krueger
A. J. Miller
R. M. Nagatani

APPENDIX D

MONTHLY MEAN DISTRIBUTION OF OZONE AND TEMPERATURE

TABLE OF CONTENTS

D-0 INTRODUCTION

This Appendix is provided because global monthly mean charts of ozone and temperature have become available, covering for the first time the height range 30 to 0.1-mbar, (approximately 24 to 64 km).

For both hemispheres these charts are given for the four mid-season months, and for the pressure levels 30, 10, 1, and 0.1 mbar for temperature, and 0.4 mbar for ozone. Charts of total ozone are provided separately. This set of charts shows clearly the very close coupling between the temperature and ozone distributions and demonstrates the influence of the large-scale planetary waves which give rise to very large longitudinal variations.

A discussion of the regular and interannual variability of temperature and ozone precedes the description of the mean state.

D-1 DATA

D-1.1 Temperature

The temperatures presented here are data which were prepared for a new REFERENCE ATMOSPHERE, published as *MAP-Handbook, Vol. 16*, by a COSPAR-SCOSTEP Task Group. These temperatures are based largely on satellite observations made by the Selective Chopper Radiometer (SCR) and the Pressure Modulator Radiometer (PMR) which both are nadir-viewing instruments which measure the infra-red emission from the carbon dioxide υ_2 band at about 15μm. These data are an average of the 5 year period 1973, 1974, July 1975 to June 1978, (Barnett and Corney, 1984). The 30-mbar temperatures are based on radiosonde observations, and are a 20-years average for the Northern Hemisphere (July 1964 to June 1984), *Meteorologische Abhandlungen, F.U.Berlin*, and a 5-years average for the Southern Hemisphere (1968 to 1972), Knittel, 1976.

D-1.2 Ozone

The ozone data presented here are based on measurements from the Solar Backscatter Ultraviolet (SBUV) Ozone Measurement System and on the Total Ozone Mapping Spectrometer (TOMS), covering the period October 1978 to September 1982, (R.M. Nagatani and A.J. Miller, personal communication).

SBUV, a nadir-viewing double monochromator, measures the radiances backscattered from the atmosphere at 12 discrete wavelengths from the 255 nm to 340 nm with a 1-nm bandpass (Heath *et al.*, 1975; McPeters *et al.*, 1984; Fleig *et al.*, 1982). Radiances between 255 nm and 306 nm are used in the ozone profile inversion, while radiances between 312 nm and 340 nm are used to calculate total ozone. In order to calculate backscattered albedo, the ratio of backscattered radiance to extraterrestrial solar irradiance must be measured daily by deploying a diffuser plate. The scan-to-scan precision of the albedo measurement is very high, a few tenths of a percent. A detailed discussion on the accuracy of these data is given in Chapter 8.

A comparison of results of different experiments measuring ozone during the period November 1978 - May 1979 is under preparation and will be published as a MAP-Handbook; (J.R. Russel *et al;* Middle Atmosphere Composition Revealed by Satellite Observations). Only one example is given here, pointing out the differences between LIMS and SBUV during January and February 1979, Figure D-1. It should be recalled that February 1979 was a month with a major stratospheric warming.

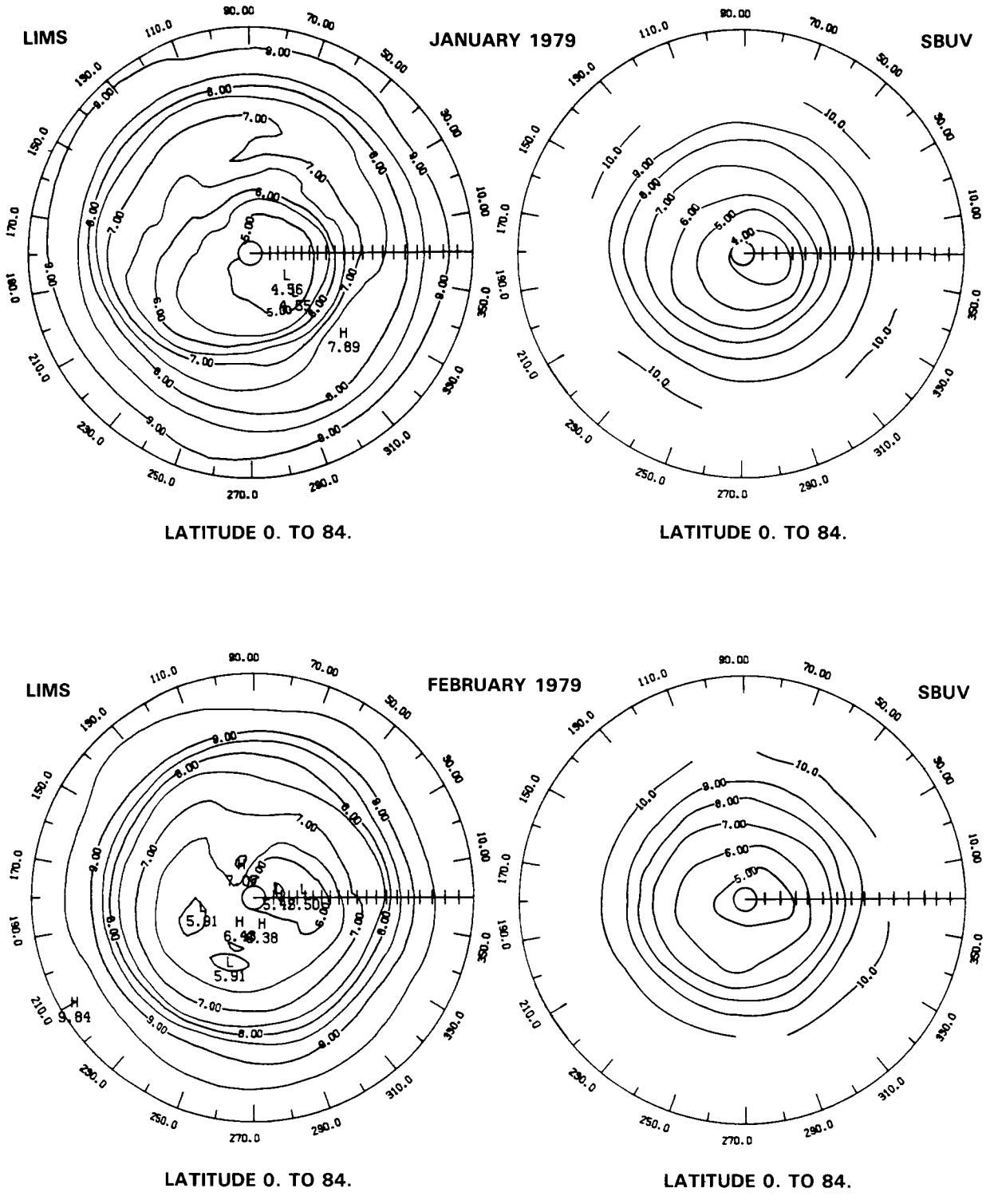

Figure D-1. Comparison of monthly mean values of ozone mixing ratio(ppmV) as measured at the 10-mbar level by LIMS and SBUV: upper part = January 1979; lower part = February 1979. (Russell *et al.*, 1986.)

Looking at the maps for January, we see that the overall placement of the major trough-ridge systems agree quite favorably, but LIMS shows a bit more detail than does SBUV. For example, the secondary high values at about 70 °E and 330 °E are not evident in SBUV. This is, most likely, due to the increased vertical resolution of LIMS as discussed in Chapter 8. A similar situation exists for the February maps with the LIMS indicating more detail in the high latitudes at about 100 °E, but with general agreement of the patterns. In general, the SBUV data as presented in Section D-4 tend to show a more detailed structure in the ozone distribution for the regions above and below the maximum of the ozone mixing ratio.

TOMS is similar in concept to the SBUV with two important distinctions, (Fleig *et al.*, 1982). The first is that it is limited to total ozone only. The second is that it incorporates a side scan feature with approximately 50×50 km field of view. This coupled with the several hundred thousand data points obtained in a single day provides considerable detail not generally observed by the nadir only SBUV.

Error sources of TOMS are very similar to those for SBUV and comparison with total ozone measurements from Dobson stations indicates that TOMS is lower, on average, by about 6%.

D-2 REGULAR COMPONENTS: ANNUAL, SEMI-ANNUAL AND QUASI-BIENNIAL WAVES

D-2.1 Temperature

D-2.1.a Annual and Semi-Annual Waves

The SCR/PMR monthly mean temperature values have been Fourier analysed at each latitude and pressure level to obtain the annual mean and the amplitude and phase of the annual and semi-annual cycles, Figure D-2. The phase is the month of the maximum, such that 1=January 1, 1.5=January 16, 2=February 1, etc. There are some very marked hemispheric differences, notably:

a) At 80 °N there is a maximum amplitude of the annual cycle of 26K at 2.5 mbar, the corresponding maximum at 80 °S is much stronger (35K) and at a lower altitude (11 mbar), Figure D-2.b. This is because in the middle stratosphere summers are warmer and winters colder over the Antarctic than over the Arctic, as shown in Section D-4.

(b) A semi-annual wave in temperature is found over both polar regions, Figure D-2.c. The one in the Arctic is 2-3 times larger than the one in the Antarctic. The latter is as large as the one over the equator.

(c) The annual mean, Figure D-2.a, shows a minimum at 50 °S, 1 mbar, and a corresponding weaker minimum at 60 °N. This is a general feature of the Southern Hemisphere winter, occurring to a smaller extent in the Northern Hemisphere, and clearly strong enough to affect the annual mean.

The annual wave reaches its maximum mostly during the summer solstices. The phase of the equatorial semi-annual wave in temperature is equinoctial and propagates downward, Figure D-2.c, while the first maximum of this wave in the polar regions falls in winter. This confirms earlier analyses (van Loon *et al.*, 1972).

In general the hemispheres are remarkably similar and six months out of phase above about 0.3 mbar (56 km). It will be shown in Section D-4 that the two hemispheres are significantly different especially in winter. However, changes from summer to winter are so large by comparison that the annual cycles appear to be very similar.

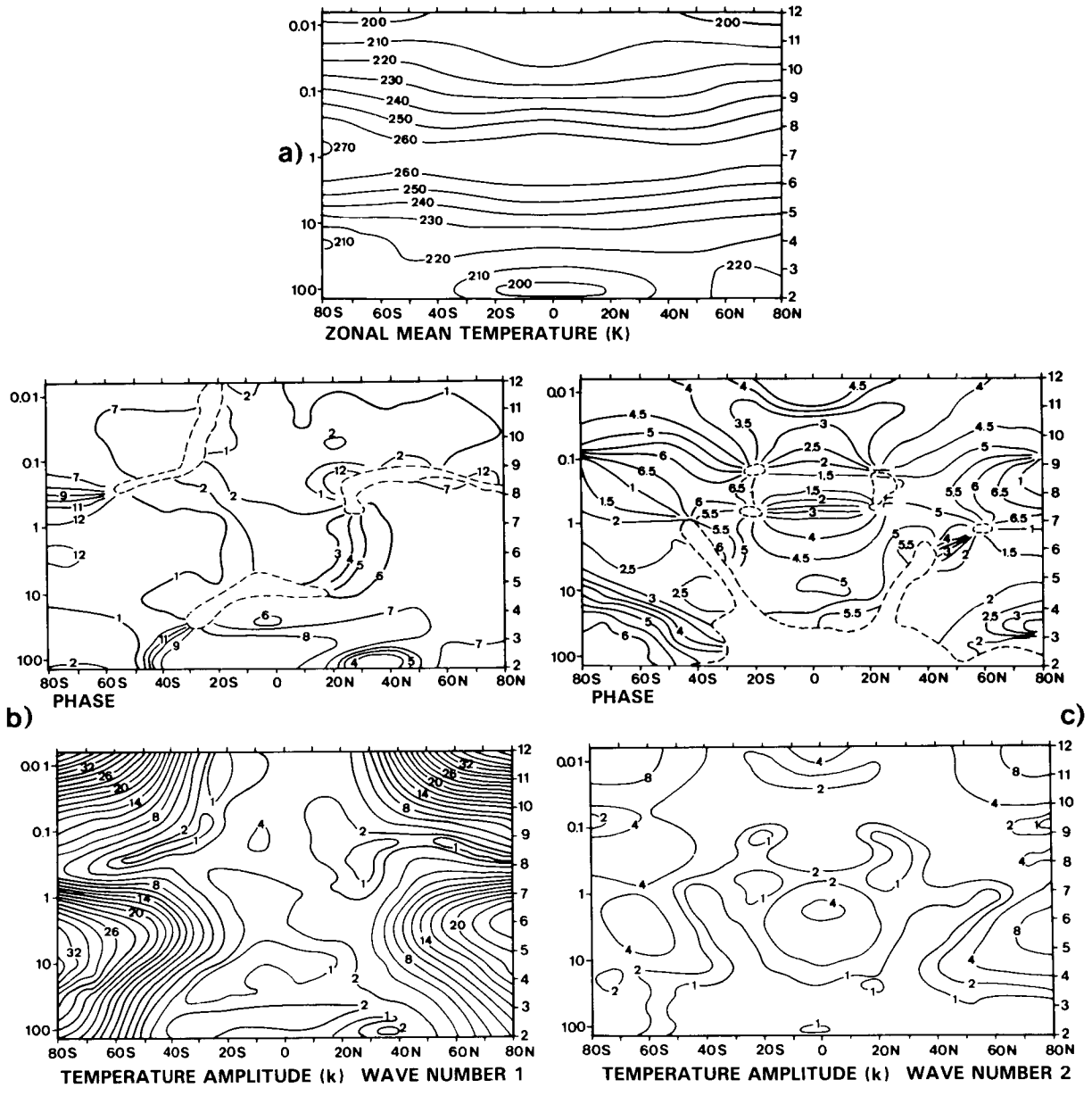

Figure D-2. Components of the annual variation of temperature (K) derived from the SCR/PMR combined means.

a) annual mean;
b) phase and amplitude of annual cycle;
c) phase and amplitude of semi-annual cycle; (Phase is given as the month of maximum temperature, e.g. 12 means December 1. (Barnett and Corney, 1984.)

Because of the existence in winter of large longitudinal temperature variations which are repeatedly in the same phase for several months, a given longitude might be consistently warm at some levels and cold at others, leading to annual and semi-annual cycles which differ markedly from those of the zonal mean. This is shown for the annual wave by means of horizontal maps of the 30-mbar level, Figure D-3, (Labitzke, 1977).

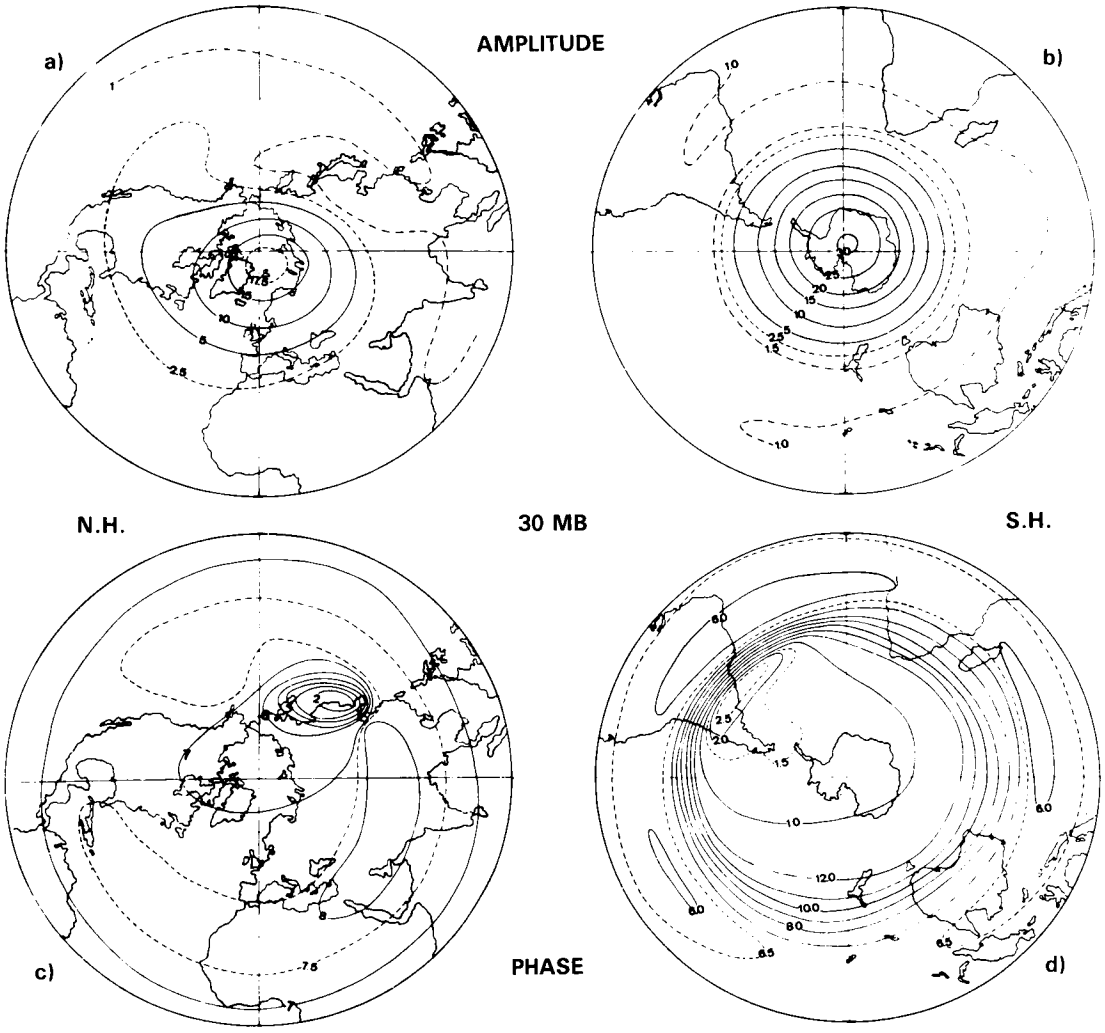

Figure D-3. a) and b): amplitude (K); c) and d) phases (month of maximum) of the annual temperature wave at the 30-mbar level. (Labitzke, 1977.)

Over the Northern Hemisphere large changes in phase occur within the regime of the Aleutian anticyclone. Here, the amplitude of the annual wave is small because it is warm in winter as well as in summer.

Over the Southern Hemisphere large phase changes occur over the southern part of South America. Here the maximum of the annual wave is reached late because the "Final Warmings" are starting over the Australian sector of the Antarctic and the transition into summer is finished last over South America, (Knittel, 1976). A similar pattern can be seen in the total ozone data, (cf. Section D-2.2 and Figure D-8).

The variations around the globe of annual and semi-annual cycles should be largest at 60–70 °S or N where planetary wave amplitudes are largest (cf. Section D-3), and Figure D-4 shows the temperature amplitudes and phases (time of maxima) for 64 °N as a function of longitude and pressure. Phase variations are relatively minor (except where the amplitudes are very small). However there are large amplitude variations, e.g. from 16 to 26 K at 3 mbar for the annual cycle, 5 to 8.3 K at 5 mbar for the semi-annual cycle.

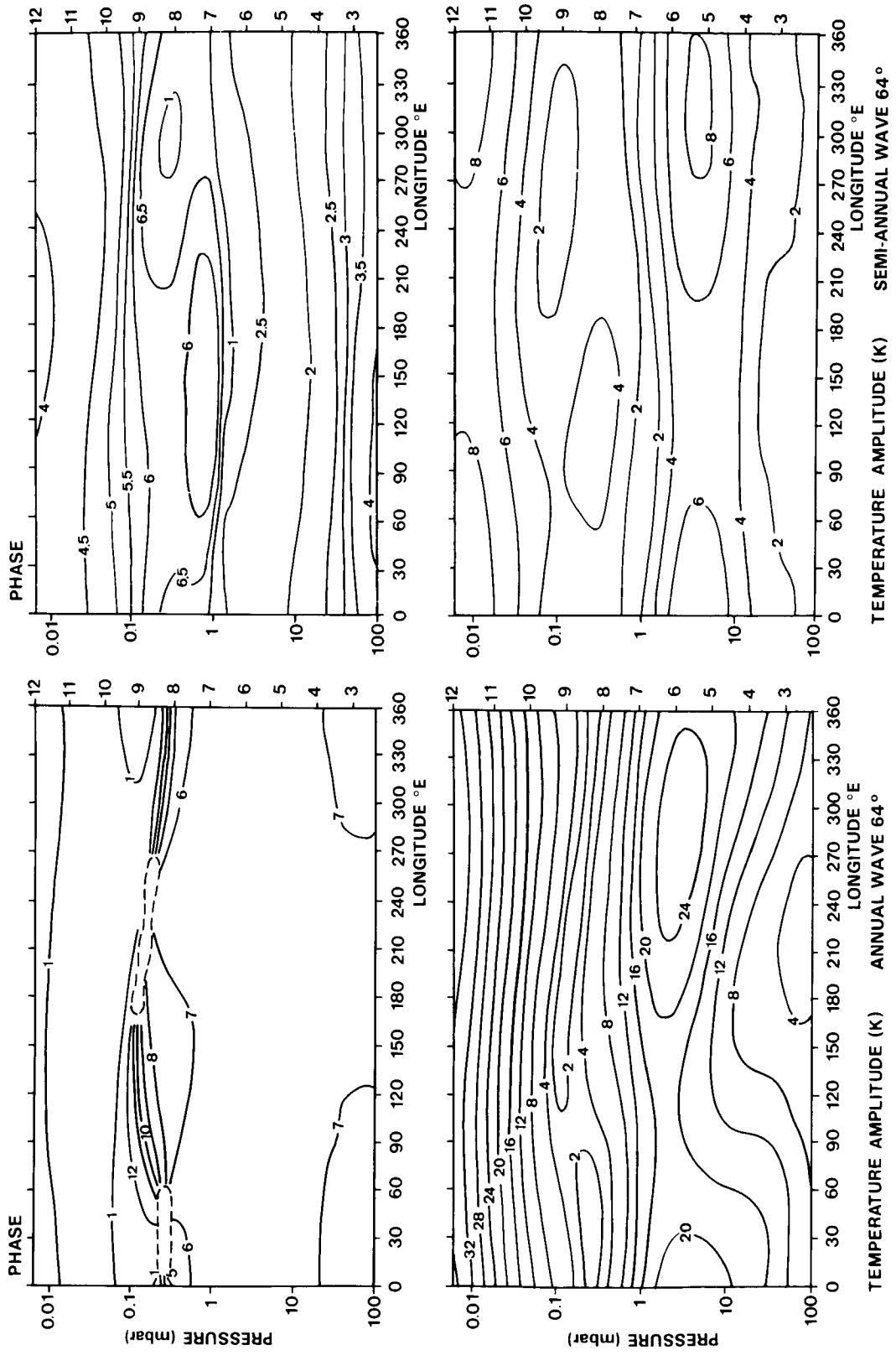

Figure D-4. Amplitude (K) and phase (month of maximum) of the annual and semi-annual cycles of temperature at 64°N as functions of longitude and pressure. (Barnett and Corney, 1984.)

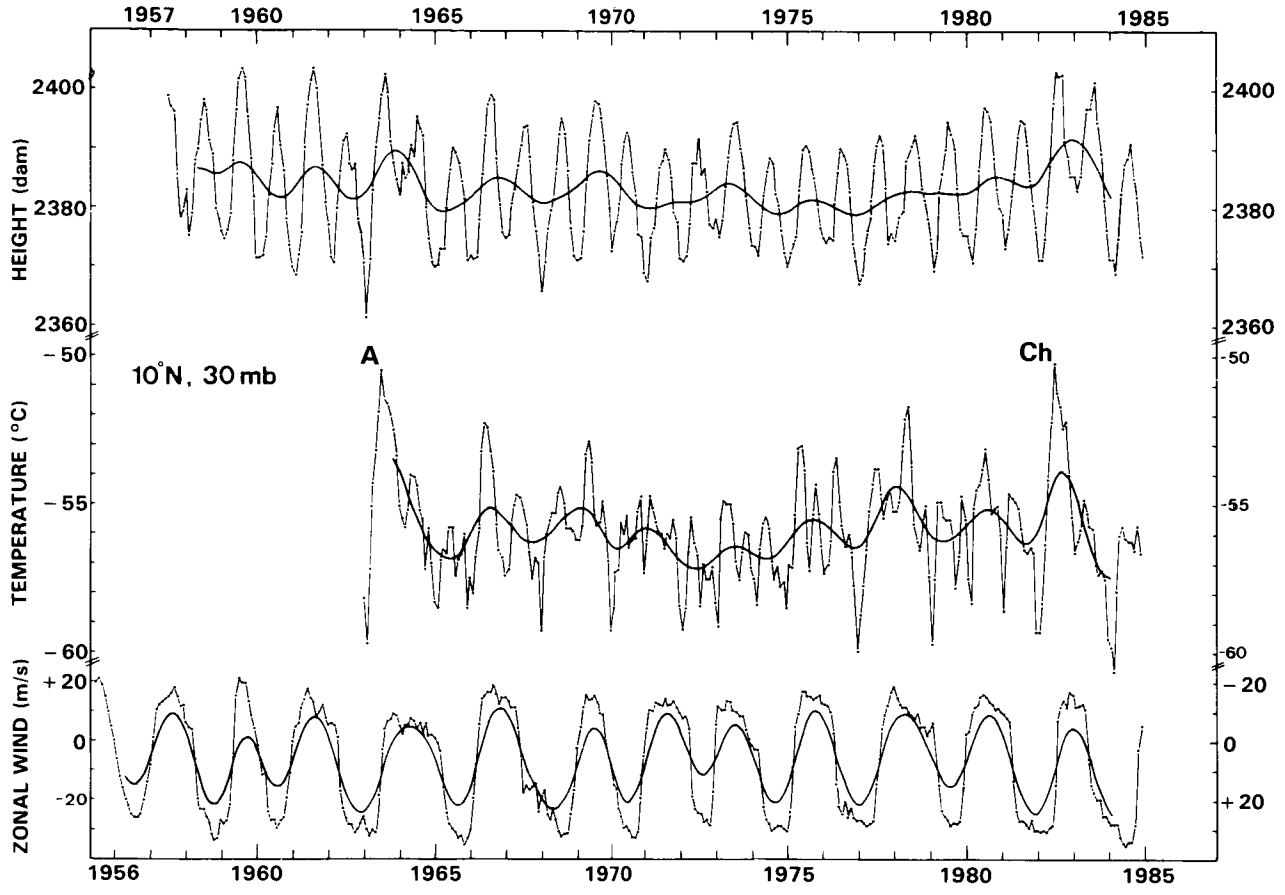

Figure D-5. Zonal means of monthly mean 30-mbar heights (a) and temperatures (b) for 10°N, (thin lines), together with a curve giving the filtered data (13-point filter to remove the annual and semi-annual wave, after Naujokat, 1981) (c) Monthly mean zonal winds over the equator based on different radiosonde stations, thin lines, (Naujokat, 1986) and filtered as above, heavy lines. (Labitzke and Naujokat, 1986.)

D-2.1.b Quasi-Biennial Wave (QBO)

The well known Quasi-Biennial Wave in the winds over the tropics has been discussed already in Chapter 6.

But this wave is also clearly pronounced in the temperatures of the stratosphere. This has been shown before, e.g., by Newell *et al.*, 1974. Here we show an update for the 30-mbar level at 10°N, Figure D-5. The zonal mean heights (curve a) and zonal mean temperatures (curve b) are plotted for each month and also after being filtered in such a way that the annual and semi-annual components are removed. These data are based on daily hemispheric analyses, using largely radiosondes, (F.U. Berlin). These series of data can be compared with a series of monthly mean winds over the equator (curve c) which is based on an analysis of Naujokat (1986), using different radiosonde stations close to the equator. Obviously, higher temperatures lead to westerlies and lower temperatures to easterlies, in accordance with the thermal wind relationship, (Reed, 1962).

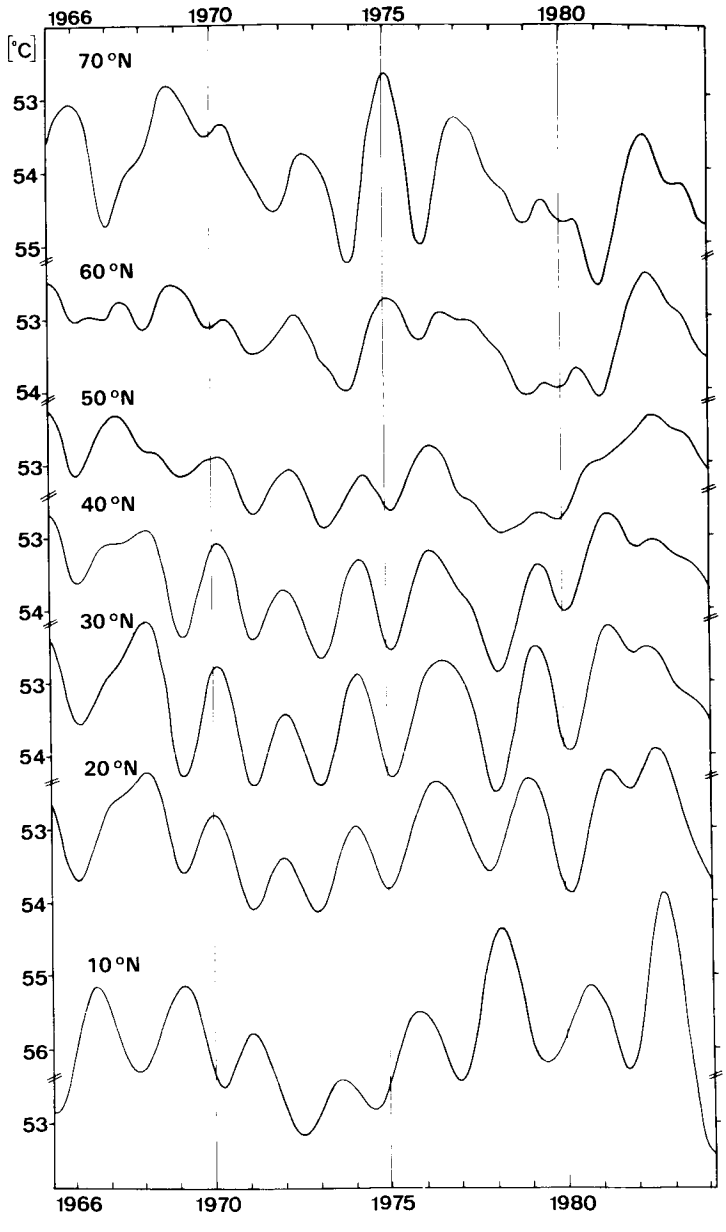

Figure D-6. Zonal mean 30-mbar temperatures (filtered to remove the annual and semi-annual wave) from 10 to 70°N. (Labitzke and Naujokat, 1986.)

The horizontal structure of the QBO in the temperature is shown for the 30-mbar level in Figure D-6. Here only the filtered temperatures are given, for every ten degrees latitude between 10 and 70 °N, (Labitzke and Naujokat, 1986).

The QBO in the 30-mbar temperatures is very well developed, with largest amplitudes at 30 °N. The amplitudes are leading at 10 °N, while they appear to be well in phase from 20 to 50 °N. Further north the signal is less clear, although evident, and the phase appears to be out of phase here, compared with the region 20 to 50 °N.

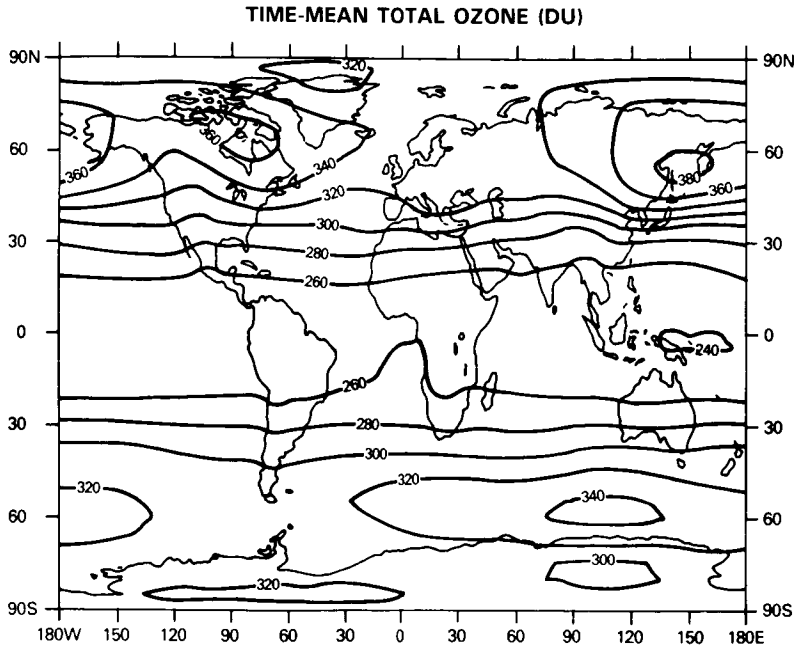

Figure D-7. TOMS time-mean total ozone, computed for the 4 year period 1978–1982, (Dobson units). (Bowman and Krueger, 1985.)

D-2.2 Total Ozone

D-2.2.a Annual and Semi-Annual Wave

Based on a global climatology of total ozone data as measured by the TOMS (Bowman and Krueger, 1985) global maps of the time-mean total ozone and of the amplitudes and phases of the annual and semi-annual waves are presented in Figures D-7–D-9. (For a detailed discussion of the quality of the data see Bowman and Krueger, 1985.)

In the Northern Hemisphere the amplitude of the annual wave in ozone increases nearly uniformly away from the equator, Figure D-8. There are two regions with large annual variations (fraction of variance) over the Sea of Okhotsk and the Canadian Arctic. Both are located coincident with maxima in the time mean ozone, Figure D-7. The minimum of the annual wave is located at about 10°S. The maximum of the annual wave in the Southern Hemisphere is also co-located with the maximum in the time mean. There is a very low minimum in the annual wave straddling the Antarctic penninsula. This coincides with the region of large phase changes of the annual wave of the 30-mbar temperature, as discussed above, Figure D-3.d. Obviously, the spring build up of ozone is weak here due to the delayed Final Warmings.

The annual harmonic in the Northern Hemisphere reaches a maximum in late winter to early spring. The earliest maximum occurs where the amplitude is largest, over the Sea of Okhotsk. The phase of the annual harmonic increases southward across the equator so that maxima in the Southern Hemisphere also occur in winter to early spring. Phase is difficult to determine near the poles, but there appear to be large differences between the annual harmonics in the Arctic and Antarctic regions. The annual harmonic explains a large fraction of the variance over much of the earth, especially in middle and high latitudes of the Northern Hemisphere and in the Northern Hemisphere tropics.

The amplitude, phase, and fraction of the variance explained by the semi-annual harmonic are shown in Figure D-9. The amplitude is flat throughout the tropics and generally increases towards the poles. At high latitudes the semi-annual wave becomes very unreliable due to the large amount of missing data and is probably largely an artifact of the analysis method. Hopkins (1975) has suggested that the semi-annual wave in the tropics results from the absorption of equartorward propagating planetary waves at the zero wind line. The total ozone shows no evidence for a maximum in the amplitude of the semi-annual harmonic in the tropics, although such a feature could occur locally in the vertical.

The maximum in the fraction of the variance explained over Asia appears to be associated with a real maximum in the amplitude of the semi-anual wave, but the maxima over the Indian Ocean stretching toward the west and over the Weddel Sea appear to be caused by the absence of a strong annual harmonic, Figure D-8.

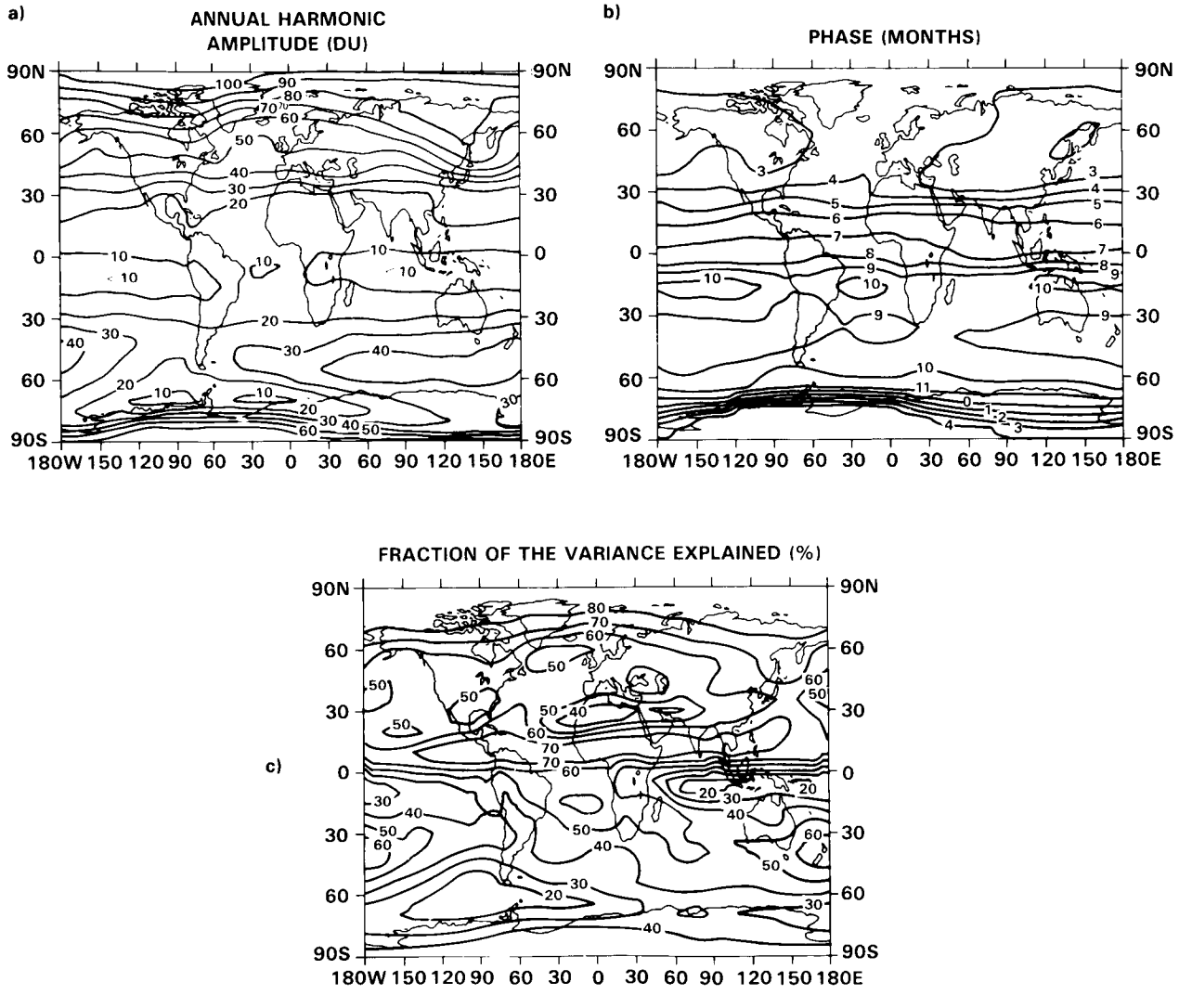

Figure D-8. (a) Amplitude (Dobson units),(b) Phase (months of maximum, after 1 January), and (c) fraction of the total variance explained by the annual harmonic (%). (Bowman and Krueger, 1985.)

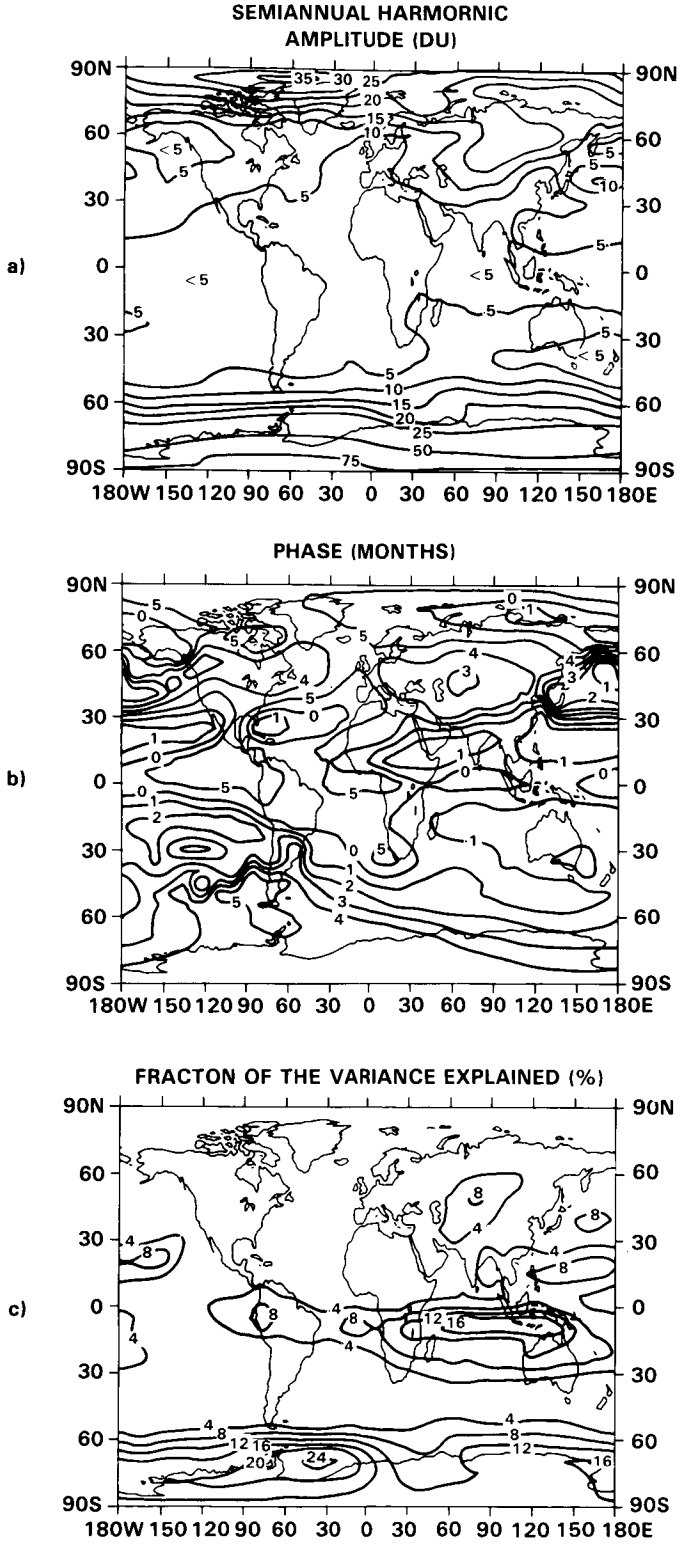

Figure D-9. (a) Amplitude (Dobson units), (b) Phase (month of first maximum after 1 January), and (c) fraction of the total variance explained by the semi-annual harmonic (%). (Bowman and Krueger, 1985.)

D-2.2.b Quasi-Biennial Wave

The quasi-biennial variation in ozone is thought to be related to the quasi-biennial variation in equatorial zonal winds (Oltmans and London, 1982). Shown in Figure D-10 (Tolson, 1981) is the biennial component of the zonal mean total ozone variation based on 7 years of Nimbus 4 BUV data. The contour interval is 2 Dobson units with the solid lines positive and the shaded area with dashed lines negative. However, since the variation is only quasi-biennial, the phase indicated in Figure D-10 will change with time. There is also evidence that the period of the quasi-biennial variation may vary somewhat with latitude (Hilsenrath and Schlesinger, 1981) and that the latitude of maximum quasi-biennial variation may vary somewhat with time (Hasebe, 1983).

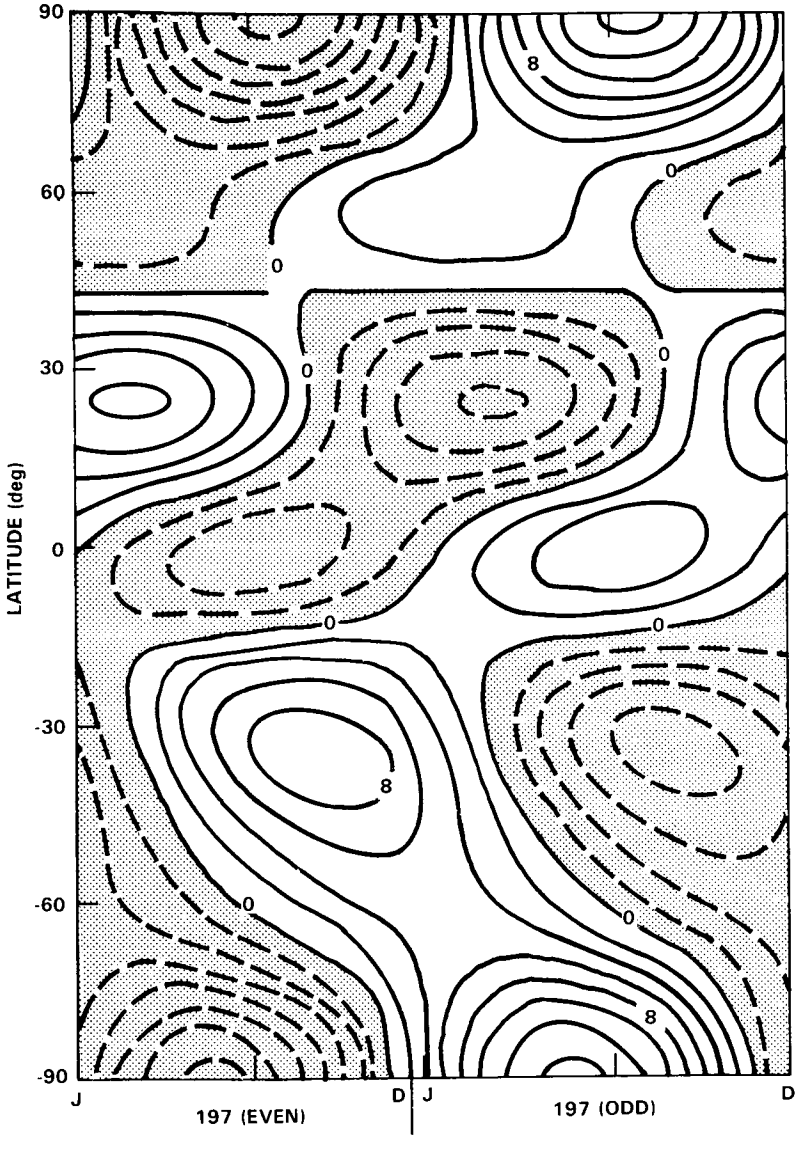

Figure D-10. Biennial component of zonal mean total ozone variation based on 7 years of Nimbus 4 BUV measurements. Contour interval is 2 Dobson units; solid lines are positive and shaded area negative. (Tolson, 1981.)

D-2.3 Vertical Ozone Profiles

D-2.3.a Annual and Semi-Annual Waves

Using data from the ozonesonde and Umkehr stations listed in Table D-1, standard harmonic analyses have been computed for the mandatory pressure surfaces of 700, 500, 300, 200, 150, 100, 70, 50, 30, 20 and 10 mbar from ozonesonde data, and for layer 6 (centered at 12 mbar), layer 7 (centered at 6 mbar), layer 8 (centered at 3 mbar) and layer 9 (centered at 1.5 mbar) from Umkehr data. Insofar as possible, stations were chosen about 15 degrees of latitude apart.

Table D-1. List of stations used in analysis of annual, semi-annual and biennial ozone components. Umkehr records have been terminated at the end of 1981 because of the biasing of the measurements by El Chichon volcanic eruption in the spring of 1982. (J.K. Angell, personal communication.)

Station	Latitude	Record Length
Ozonesonde		
Resolute	75°N	1967-1983
Churchill	59°N	1974-1983
Hohenpeissenberg	47°N	1967-1983
Kagoshima	31°N	1969-1983
Natal	6°S	1980-1981
Aspendale	38°S	1966-1981
Syowa	69°S	1966-1982*
Umkehr		
Edmonton	54°N	1970-1981
Arosa	47°N	1965-1981
New Delhi	28°N	1965-1981
Singapore	1°N	1981
Brisbane	27°N	1965-1981
Aspendale	38°S	1965-1981
Invercargill	46°S	1973-1981

* No data between 1974 and 1978.

OZONE AND TEMPERATURE DISTRIBUTIONS

Figure D-11 shows the annual amplitude of ozone in units of partial pressure (left) and percent of the average value at the given surface (middle). The latter is presented because at upper levels the values become very small and patterns are hard to discern otherwise. These results from ground-based data (Table D-1) are supplemented on the right by an analysis of the 4-year SBUV data set available from Nimbus 7, expressed in percent. The latter, while based on a limited time interval, has better spatial coverage than the ground-based data.

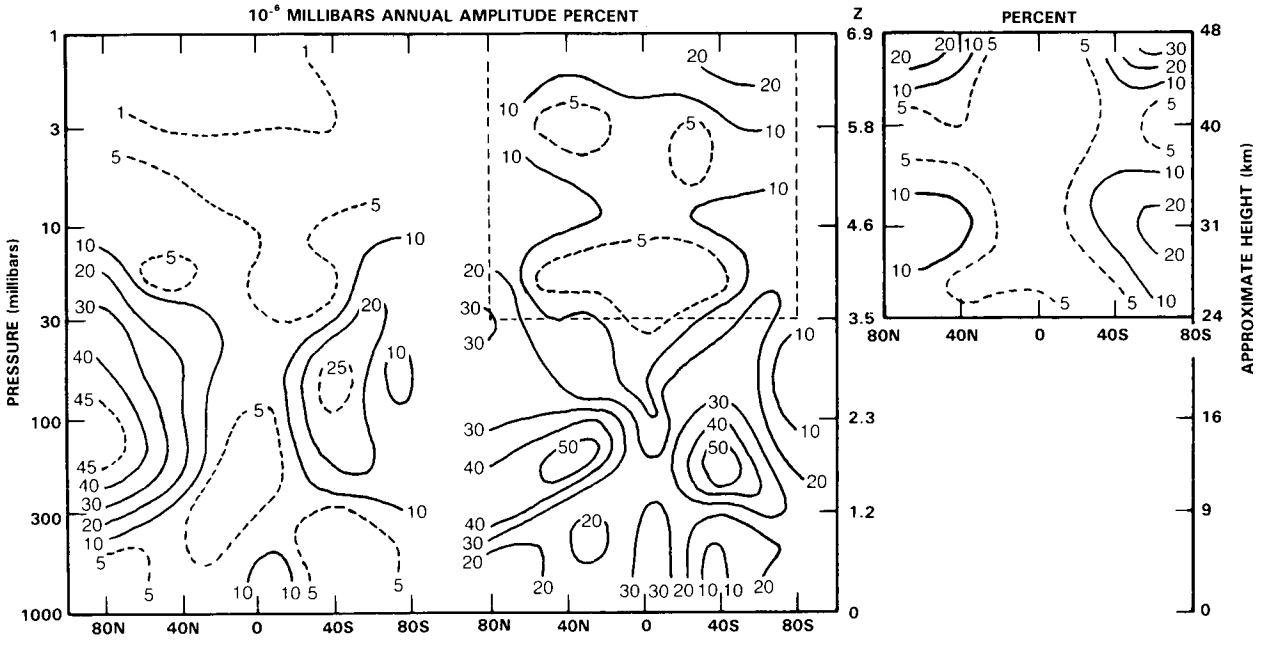

Figure D-11. Annual amplitude of ozone as a function of pressure and latitude from ground-based data and from SBUV data (right). The amplitude in units of mixing ratio (ppmv) is obtained by dividing the partial pressure in units of 10^{-6} mbar by the ordinate pressure in mbar; (J.K. Angell, private communication.)

In terms of partial pressure, the annual amplitude of ozone is a maximum between 100 and 200 mbar in north polar latitudes. In middle latitudes of the Southern Hemisphere the amplitude is indicated to be only half as large between 50 and 100 mbar. In these units the annual amplitude is not the same in the two hemispheres, either in magnitude or distribution. In the case of percent, however, the annual amplitude is a maximum near the tropopause, with a value of 50% at about 40 degrees latitude in both hemispheres. Here, the amplitude in the two hemispheres appears more nearly the same. At upper levels both ground-based and satellite data indicate a consistent analysis with a relative minimum in the tropics and the minimum at about 3 mbar in the vertical. At 1 mbar the SBUV shows a larger amplitude in the polar areas by about 10%.

The phase of the annual cycle determined from ground-based data is shown in Figure D-12. At the specified latitudes the phase is given as the time of maximum ozone. In middle and polar latitudes of the Northern Hemisphere the time of maximum ozone varies from June near the surface to March in the 30–100 mbar layer. At 30°N, however, there is little change in time of ozone maximum between the surface and low stratosphere. At 1–3 mbar the ozone is a maximum near the winter solstice, in agreement with SBUV results. The sparse Southern Hemisphere data suggest a similar variation with height, but 6 months out of phase.

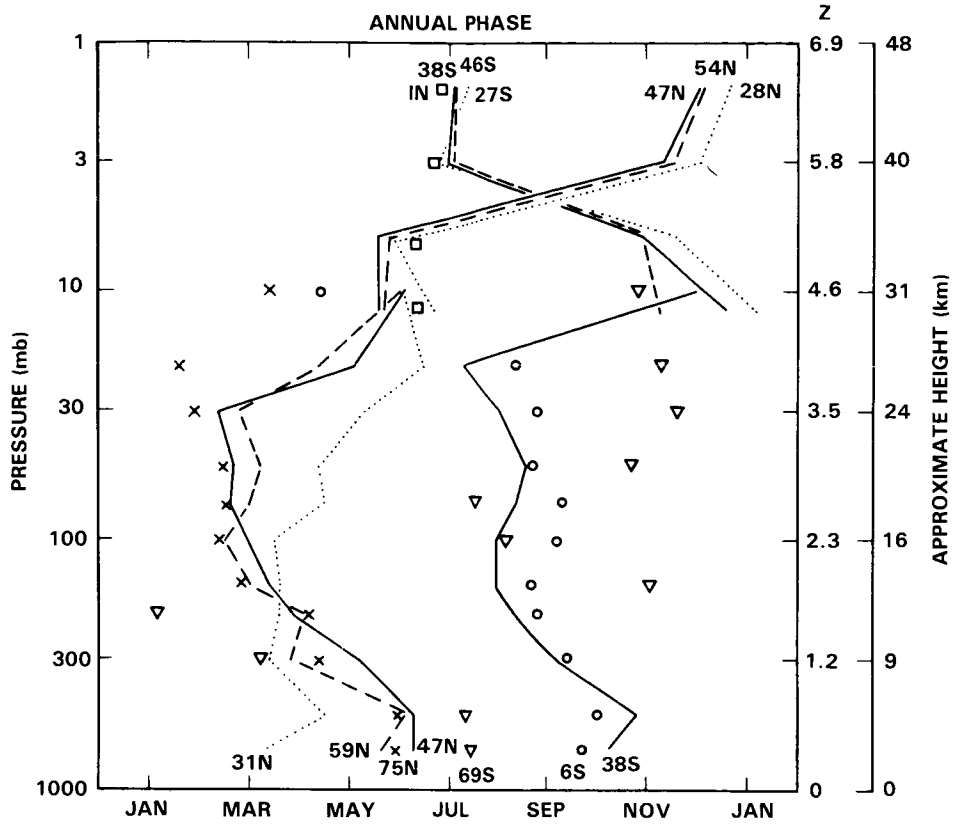

Figure D-12. Times of maximum ozone values for annual component. Latitude of ozonesonde and Umkehr stations indicated at bottom and top; (J.K. Angell, private communication.)

In Figure D-13 results for the semi-annual component are presented. The values tend to be much smaller than for the annual component. In terms of partial pressure, a polar maximum is observed in both hemispheres in the 30–100 mbar layer, with evidence for another maximum in the equatorial zone above 30 mbar. In the case of percent, the ground-based data indicate a maximum in the tropics of at least 12% between 100 and 300 mbar. At higher altitudes the semi-annual amplitudes are small and different from those calculated from the SBUV data. In the latter, a tropical maximum of about 5% is observed between 1 and 3 mbar, together with polar maxima of about 10% in the same layer, whereas polar maxima are not apparent from the ground-based data.

The phase of the semi-annual cycle determined from ground-based data is shown in Figure D-14. In the Northern Hemisphere the time of the earlier ozone maximum varies from about May near the surface to March at the tropopause. From the tropopause to the stratopause there is no compelling evidence of a change in phase. Southern Hemisphere phases are so scattered it is difficult to say whether semi-annual variations are in phase or out of phase in the two hemispheres. With such small amplitudes, the confidence of the phase depiction is rather low.

D-2.3.b Biennial Wave

In Figure D-15 are presented the results for the biennial (not quasi-biennial) component. In the Southern Hemisphere only the ozonesonde station at Aspendale has a record of sufficient length for consideration

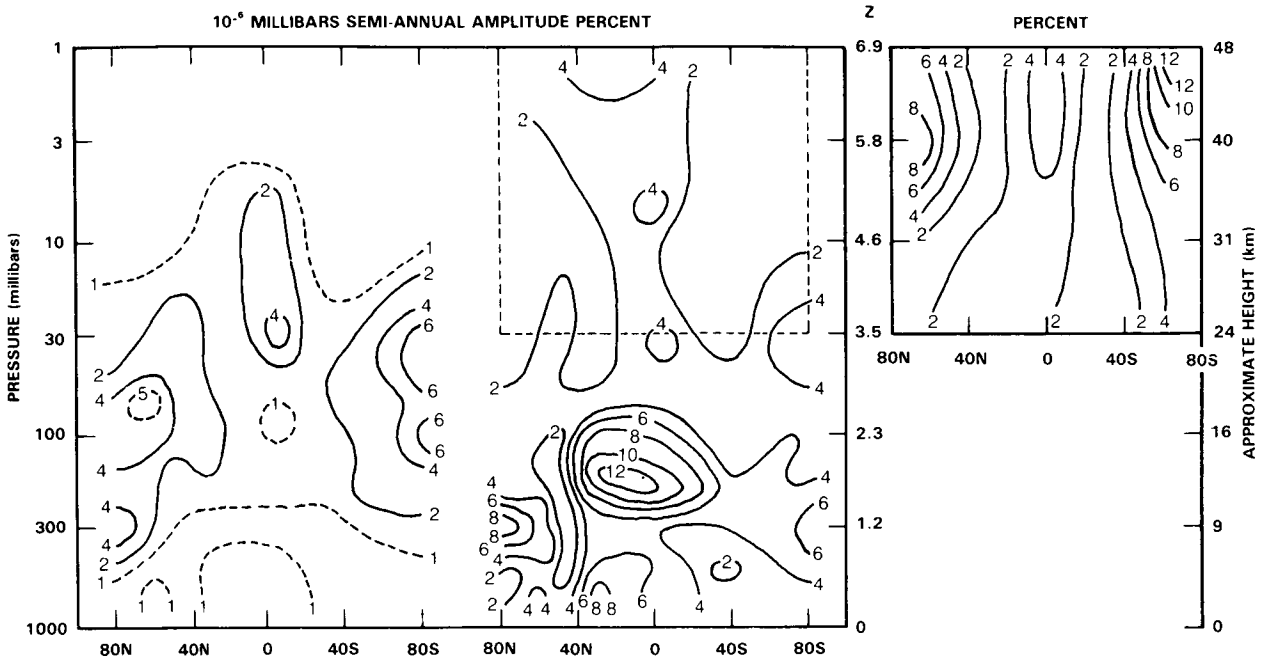

Figure D-13. Same as Figure D-11 for semi-annual component.

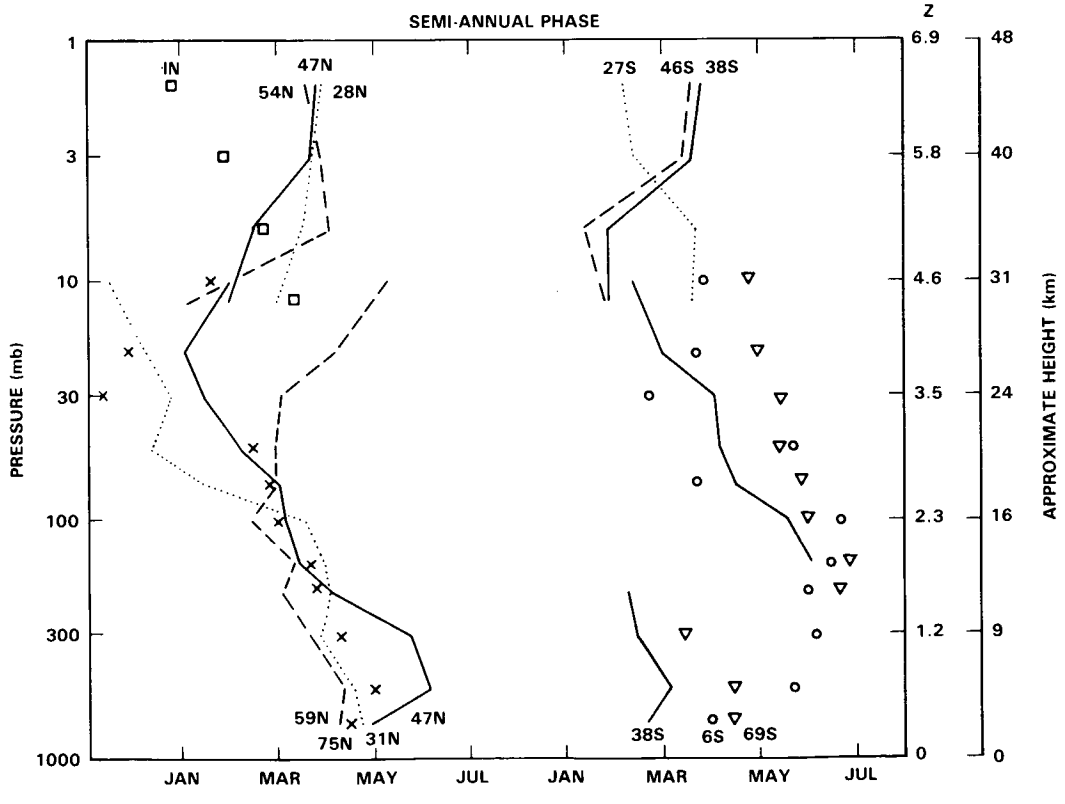

Figure D-14. Same as Figure D-12 for semi-annual component.

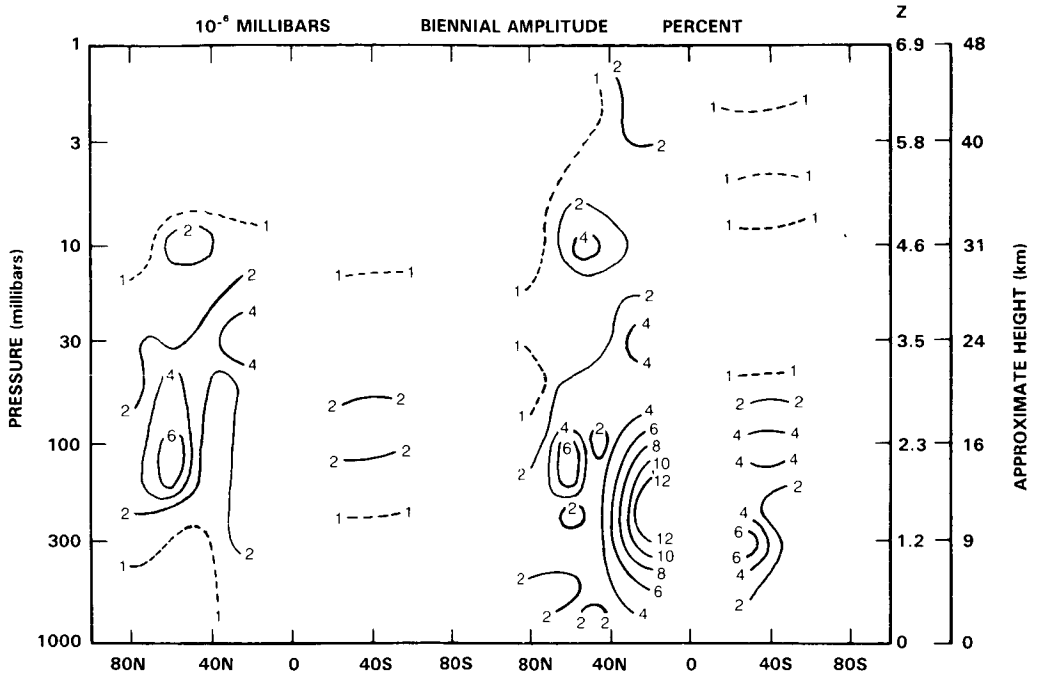

Figure D-15. Same as Figure D-11 for biennial component.

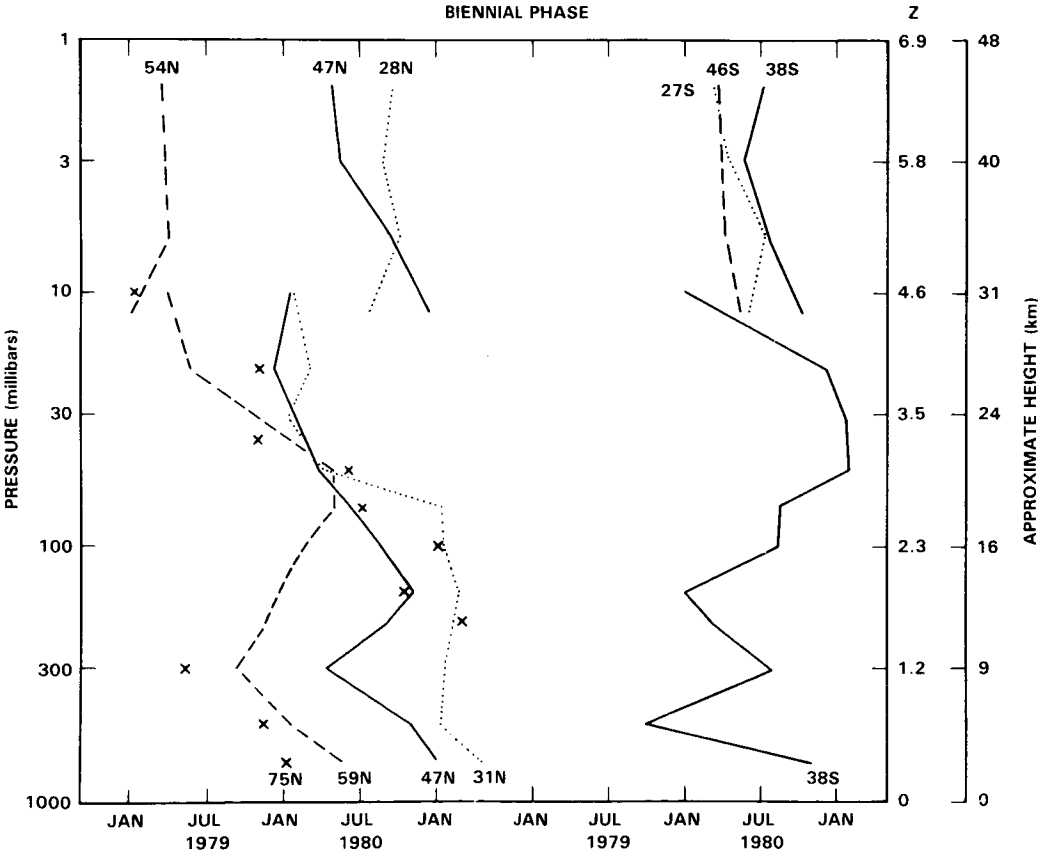

Figure D-16. Same as Figure D-12 for biennial component.

here. The absence of long-term records in the tropics makes the analysis particularly difficult. In terms of partial pressure, a maximum is observed around 100 mbar in northern mid-latitudes, but in the case of percent the maximum is indicated to be in the tropics between 100 and 300 mbar. With such small amplitudes the confidence of the biennial phase depiction in Figure D-16 is also low. In general, the ozone amount has been greater in even years (1980) than in odd years (1979) in both hemispheres.

D-3 INTERANNUAL VARIABILITY

The climatology which will be presented in Section D-4 is based on global satellite data and forms a very useful basis for climatological studies. When using such climatologies it is important to be aware of the interannual variability which in the middle atmosphere is particularly large during the northern winters and southern springs.Then the standard deviations of the monthly mean temperatures are particularly large.

D-3.1 Temperature

D-3.1.a Lower Stratosphere

For the discussion of the interannual variability of the lower stratosphere a long-term series of temperature data is available for the Northern Hemisphere. This series is based on daily maps derived largely from radiosonde data,(Free University Berlin). For the Southern Hemisphere only data of single radiosonde stations are available.

Variability of the Polar Region

For a comparison of the two polar regions, the monthly mean temperature data for 90°N and 90°S are shown in Figures D-17 (update of Figure 1 of Naujokat , 1981) and D-18 (Figure 1b, Labitzke and Naujokat, 1983) in the form of frequency distributions. The time-scale is shifted by 6 months so that both polar regions can be compared easily.The monthly mean values for the North Pole are based on daily 30-mbar charts derived from radiosonde data, while for the South Pole a radiosonde station is available directly.

The main features to be noted and which have been pointed out previously (e.g., Barnett, 1974; Labitzke, 1974; Knittel, 1976) are:

(1) In the *lower stratosphere* the interannual variability during the northern midwinters, Figure D-17, is much larger than during the southern midwinters, Figure D-18, due to the major midwinter warmings which take place only during the northern winters; the largest interannual variations over Antarctica are observed during late spring,i.e., October and November when very intense "Final Warmings" bring about the transition into summer.
(2) The variability in the middle stratosphere is very small in summer when the planetary waves of the troposphere cannot propagate upwards into the stratosphere due to the prevailing easterly winds. This is true for both polar regions.

Standard Deviations of Monthly Means

Figure D-19 gives the latitudinal distribution of the standard deviations of the 30-mbar temperatures for the Northern Hemisphere. This drawing indicates clearly where the interannual variability is smallest: at 60–70°N, *in summer*; as well where it is largest: at 80–90°N in *winter* and *spring*.

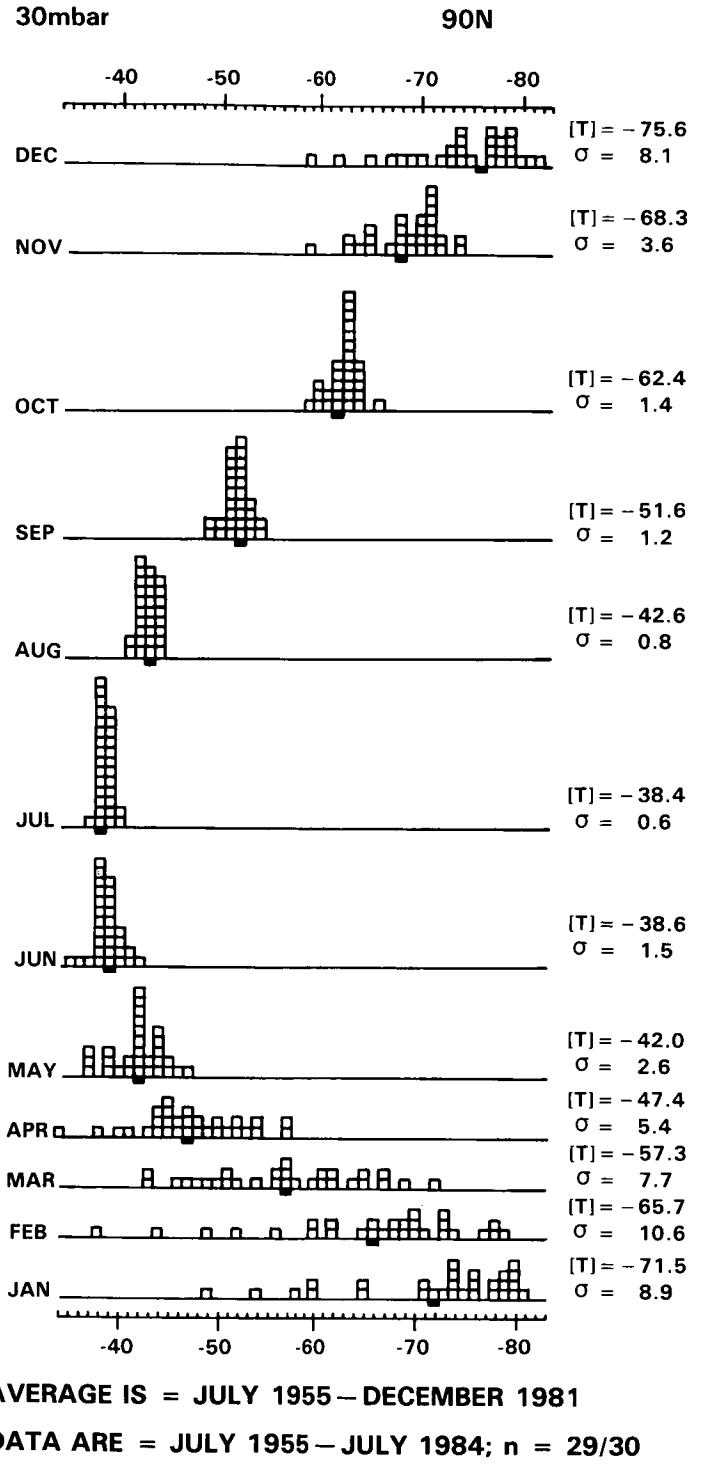

Figure D-17. Frequency distribution of the monthly mean 30-mbar temperatures (°C) over the North Pole, for the period July 1955 through July 1984. Interval is 1 K. The long-term average T is given at the right hand side of the picture, together with the standard derivation, and T is also marked as a black box in the frequency distribution. (Update of Figure 1, Naujokat, 1981.)

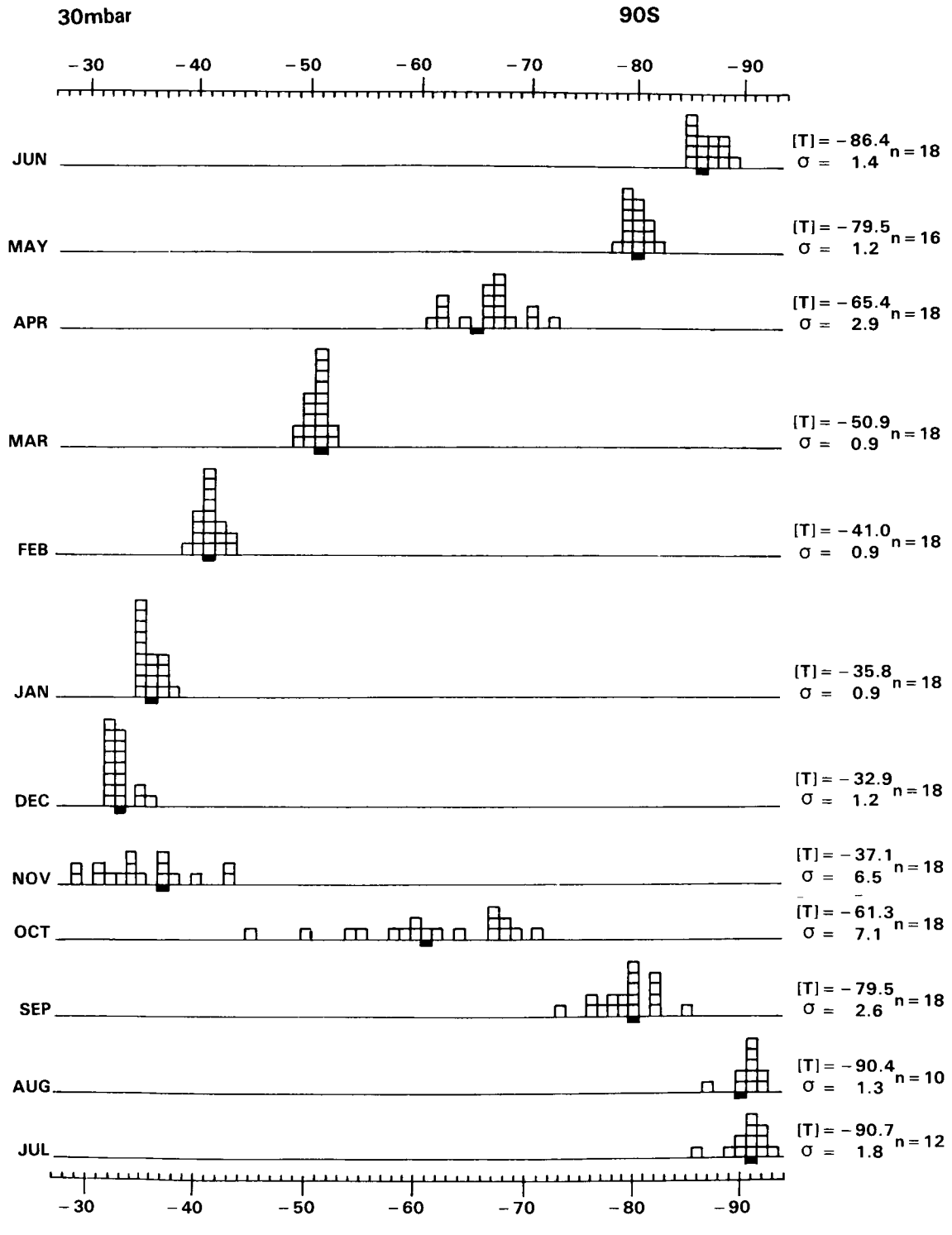

Figure D-18. Frequency distribution of the monthly mean 30-mbar temperatures (°C) over the South Pole, for the period 1961–1978. (Based on radiosonde data, not all months are complete, because of the very low temperatures in winter.) Otherwise same notation as in Figure D-17 (Figure 1b, Labitzke and Naujokat, 1983.)

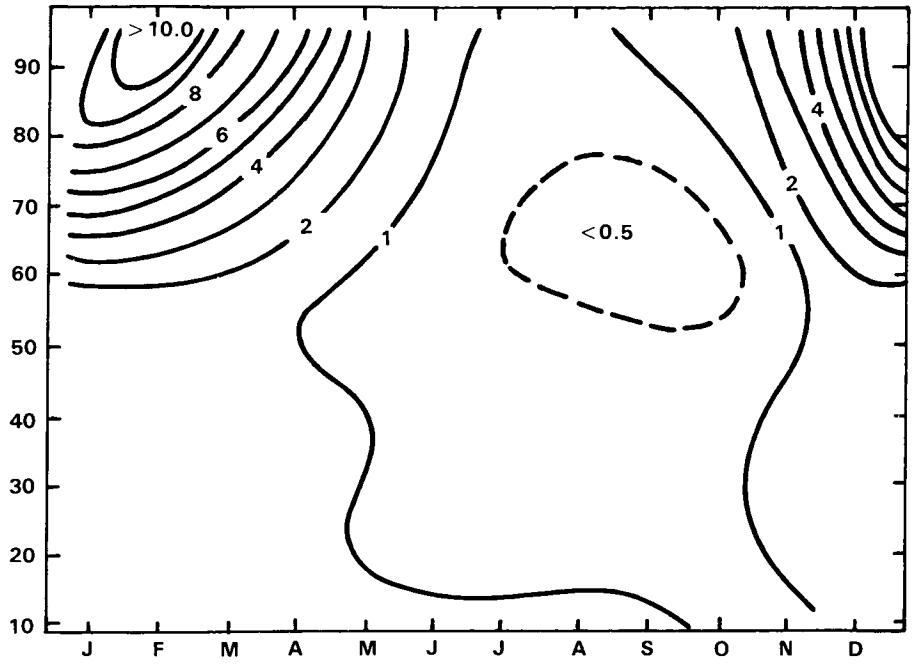

Figure D-19. Latitudinal distribution of the standard deviations (K) of the monthly mean 30-mbar temperatures throughout the year. (90°N: July 1955–December 1981, n = 26 or 27 years; 80–10°N: July 1964–December 1981, n = 17 or 18 years.) (Figure 3, Labitzke and Naujokat, 1983.)

D-3.1.b Upper Stratosphere

The discussion of the interannual variability of the upper stratosphere will concentrate on satellite data which are available for this region since the winter of 1970/71.

Variability of the Polar Regions

The same features as discussed for the lower stratosphere can be found in the upper stratosphere, namely highly disturbed northern winters. This is shown with daily zonal means of radiances at 80 deg.N from different upper stratospheric channels of the SCR (Selective Chopper Radiometer) and PMR (Pressure Modulated Radiometer) (Nimbus 4, 5, 6), Figure D-20. They are compared with the 10- and 30-mbar temperatures over the North Pole, (Labitzke, 1983). The data-set used for the preparation of the climatology, (as presented in Section D-4), includes most of these winters.

This survey over 8 northern winters illustrates distinctly the high variability of the stratospheric winters with the different timing and intensity of the stratospheric warmings. The "major warmings(*)" are connected with a break-down of the stratospheric polar vortex, followed by a "late winter cooling", thus influencing the whole winter season. (Definition of major warmings see, e.g., Labitzke, 1981).

In contrast, the southern winters show very little variation from year to year over the polar region. The temperature minimum is reached in early winter and therefore in the *upper stratosphere* the transition into summer starts much earlier over the Antarctic than over the Arctic. This is shown in Figure D-21, where the march of radiances at 80°N and 80°S is compared, (Labitzke, 1977).

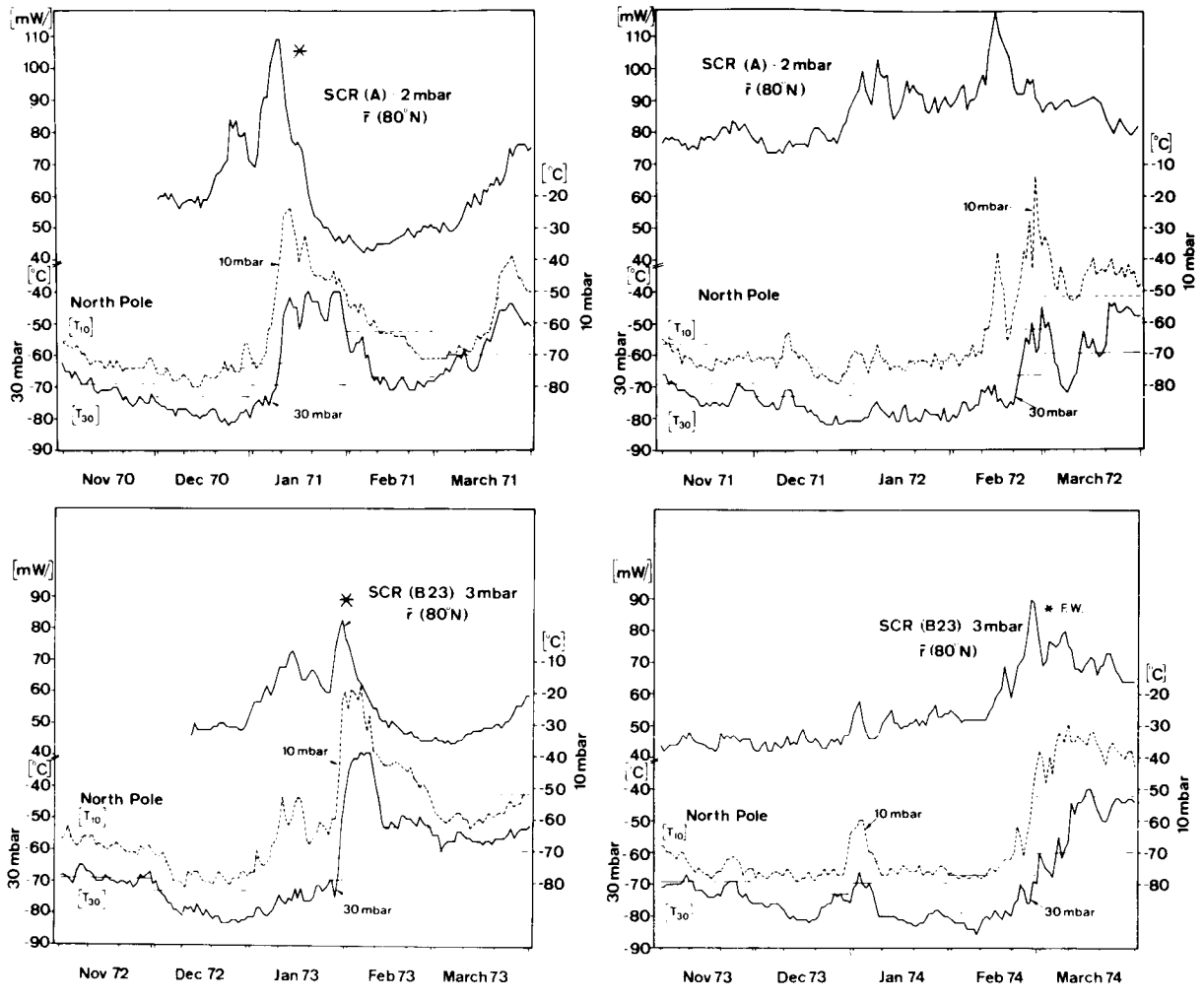

Figure D-20. Course of radiances or temperatures over the polar region: zonal mean radiances at 80°N in ($mW(m^2sr(cm^{-1})^{-1}$) or (K), i.e., equivalent blackbody temperature, from different experiments representing the upper stratosphere as indicated. Temperatures (°C) of the 10- and 30-mbar level over the North Pole. (Radiance data: Oxford University, U.K.; temperature data: Free University Berlin.) (Labitzke, 1983.)

These differences are most obvious in spring. Therefore, the 30- and 1-mbar temperature charts of March/N.H. and September/S.H. are compared in Figure D-22.

For the N.H. the temperature distributions show that the transition into spring is *well advanced in the lower stratosphere* while the cold wintertime polar vortex is still dominant in the upper stratosphere, Figure D-22, upper part.

This is very different from the developments in the S.H., Figure D-22, lower part. Here, the cold polar vortex of the lower stratosphere is still very strong in September while the transition into spring is *well advanced in the upper stratosphere* with the warm polar region, a reversed temperature gradient and the remnants of the cold polar vortex over middle latitudes.

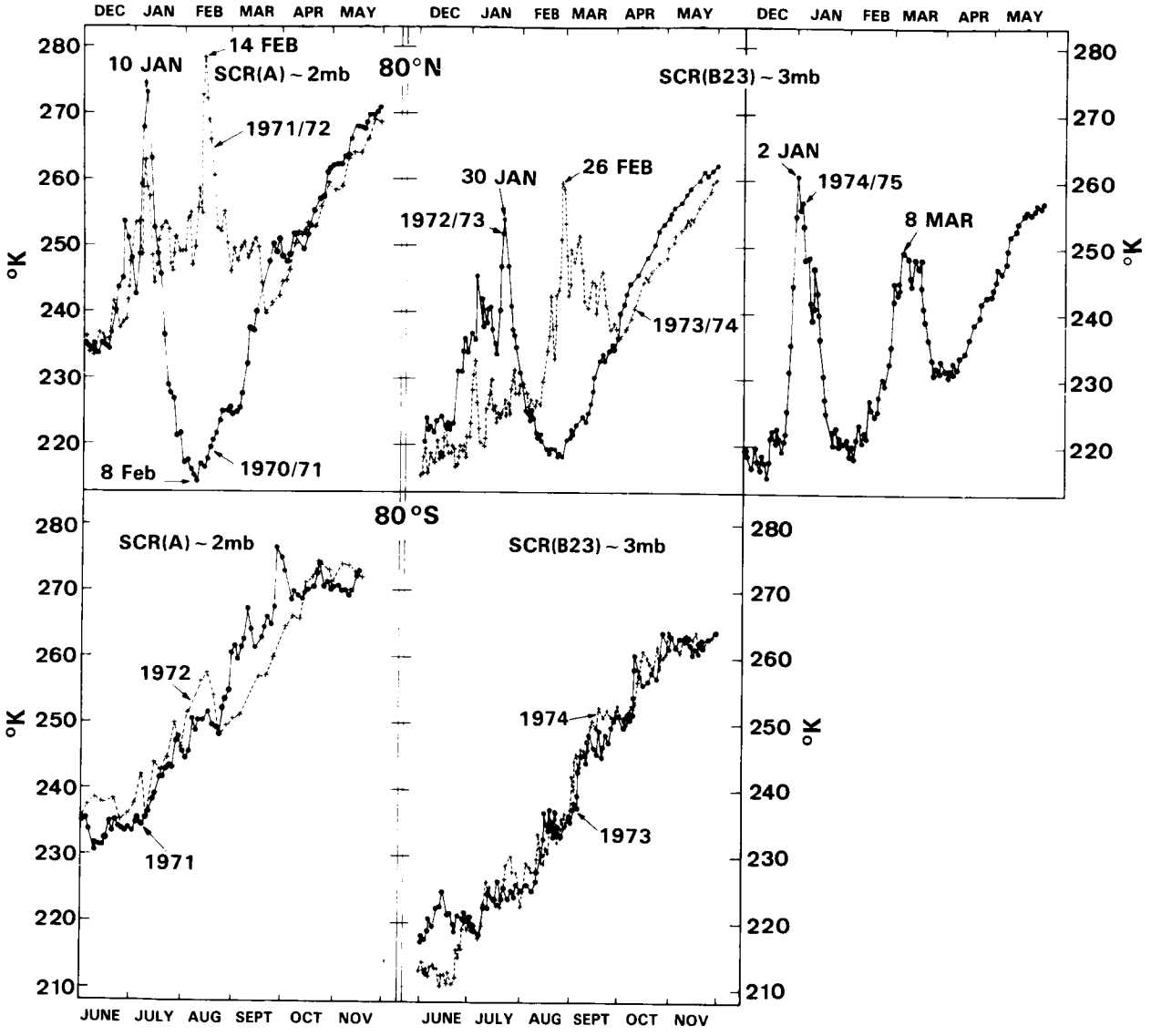

Daily zonal means at 80 deg. latitude of radiances of upper stratospheric channels of the SCR, flown on Nimbus 4 and 5.

(The radiances are converted into equiv. black body temperatures (°K)).

Figure D-21. Daily zonal means at 80° latitude of radiances of upper stratospheric channels of the SCR flown on Nimbus 4 and 5. The radiances are converted into equivalent blackbody temperatures. (Labitzke, 1977.)

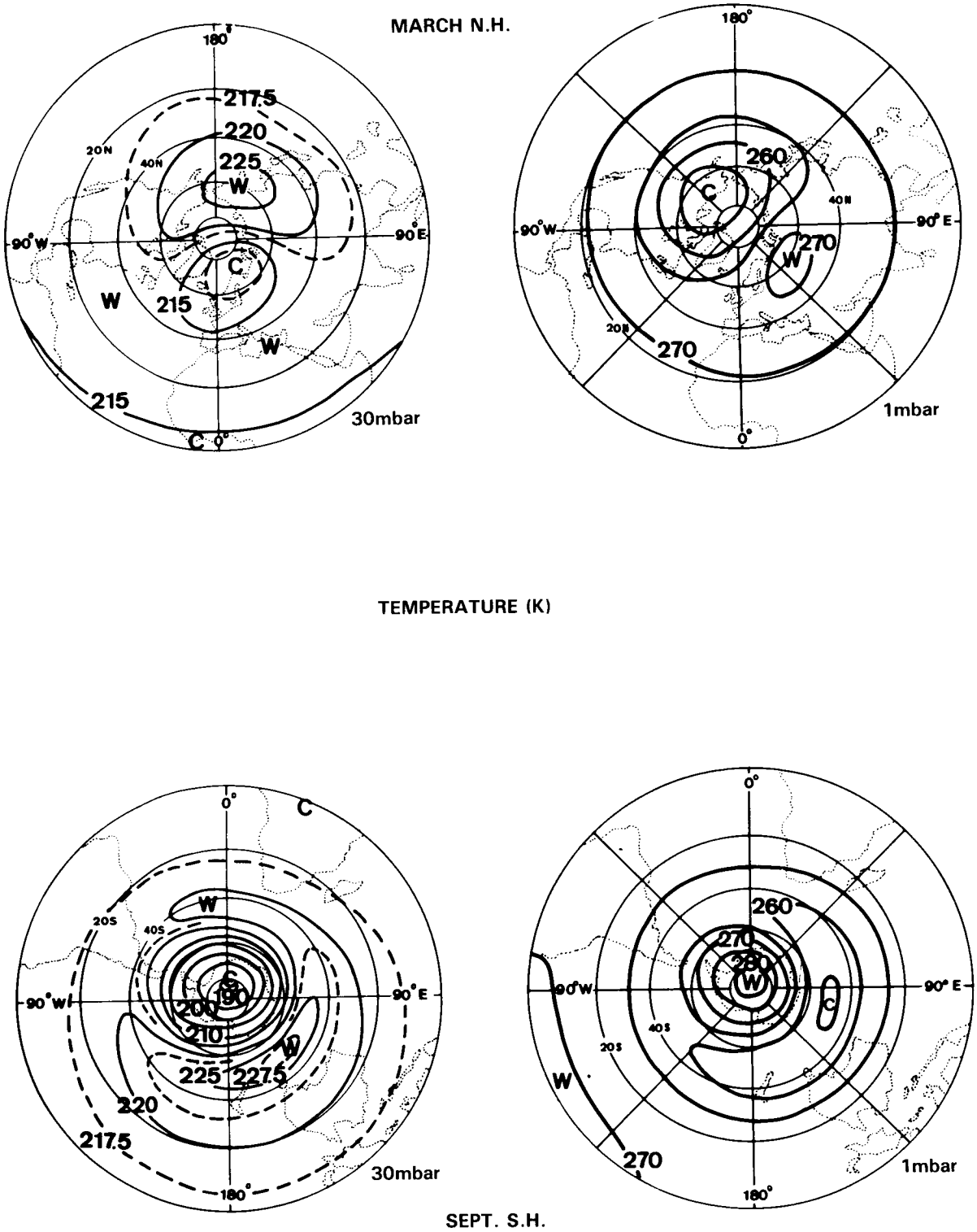

Figure D-22. Monthly mean 30- and 1-mbar temperatures for March, N.H. and September, S.H. (Data: F.U. Berlin and New Reference Atmosphere, MAP-Handbook, 16.)

D-3.2 Total Ozone

For a discussion of the interannual variability of ozone, data for many years are required but are not easily available.

But one excellent example is given here with Figure D-23, which shows the series of total ozone measurements in Arosa, Switzerland. This series of annual mean values starts by 1926, (Duetsch, 1985) and shows clearly very large interannual variations which are closely connected with the variability of the winter polar vortex, but also with volcanic eruptions like Mt. Agung in March 1963 and El Chichon in April 1982, which are responsible for the large minima in total ozone occurring after the eruptions.

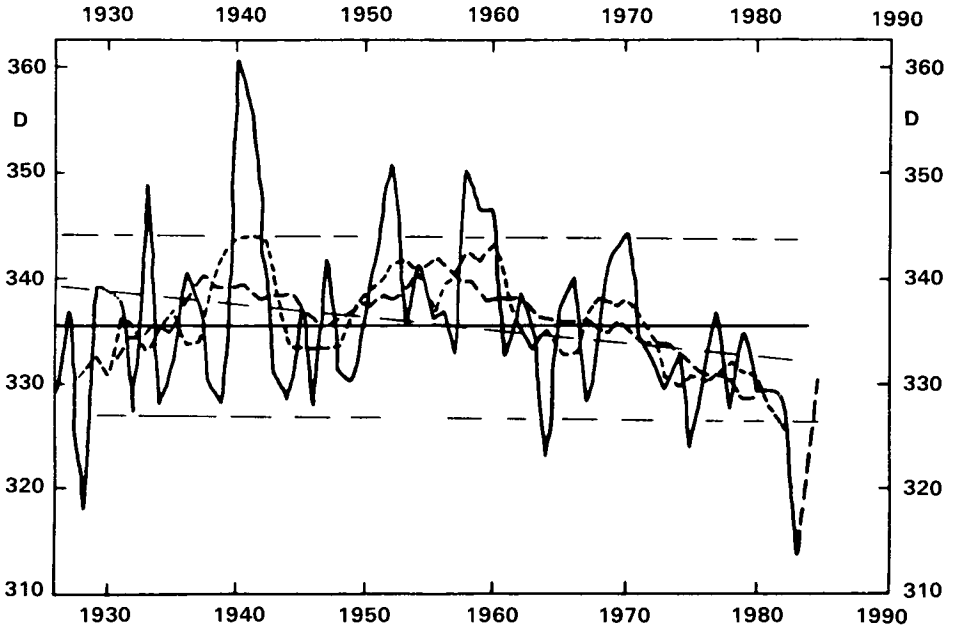

Figure D-23. Arosa total ozone series; annual mean values (C-wavelength pair): Full line; 5 year overlapping means: short dashed line; ten year overlapping means: dashed line; regression line: fine dashed. (Duetsch, 1984.)

D-3.3 Vertical Distribution of Ozone

Although there is interannual variability, comparison of the SBUV data over the 4-year period of measurements shows a remarkable similarity of structure from year to year. For example, shown in Figure D-24 is the vertical structure at 0°, 20°N, 40°N and 60°N for November of 1978, 1979, 1980 and 1981. Note how the 0° and 20°N profiles come together near 4 mbar. The 60°N profile changes in each case from the lowest profile at 4 mbar to the highest at 1.5 mbar.

Shown in Figure D-25 is the interannual variability of zonal mean ozone expressed as standard deviation (in percent) relative to the mean 4 years of SBUV data as a function of pressure and latitude for the months of November and July. As indicated in the previous Figure, the interannual variability of zonal means in November is very low, generally less than 4%. In contrast, the month of July gave the largest variability over this 4-year period with the maximum variability occurring at high southern winter latitudes. The interannual variability over the tropics appears to be strongly related to the quasi-biennial oscillation.

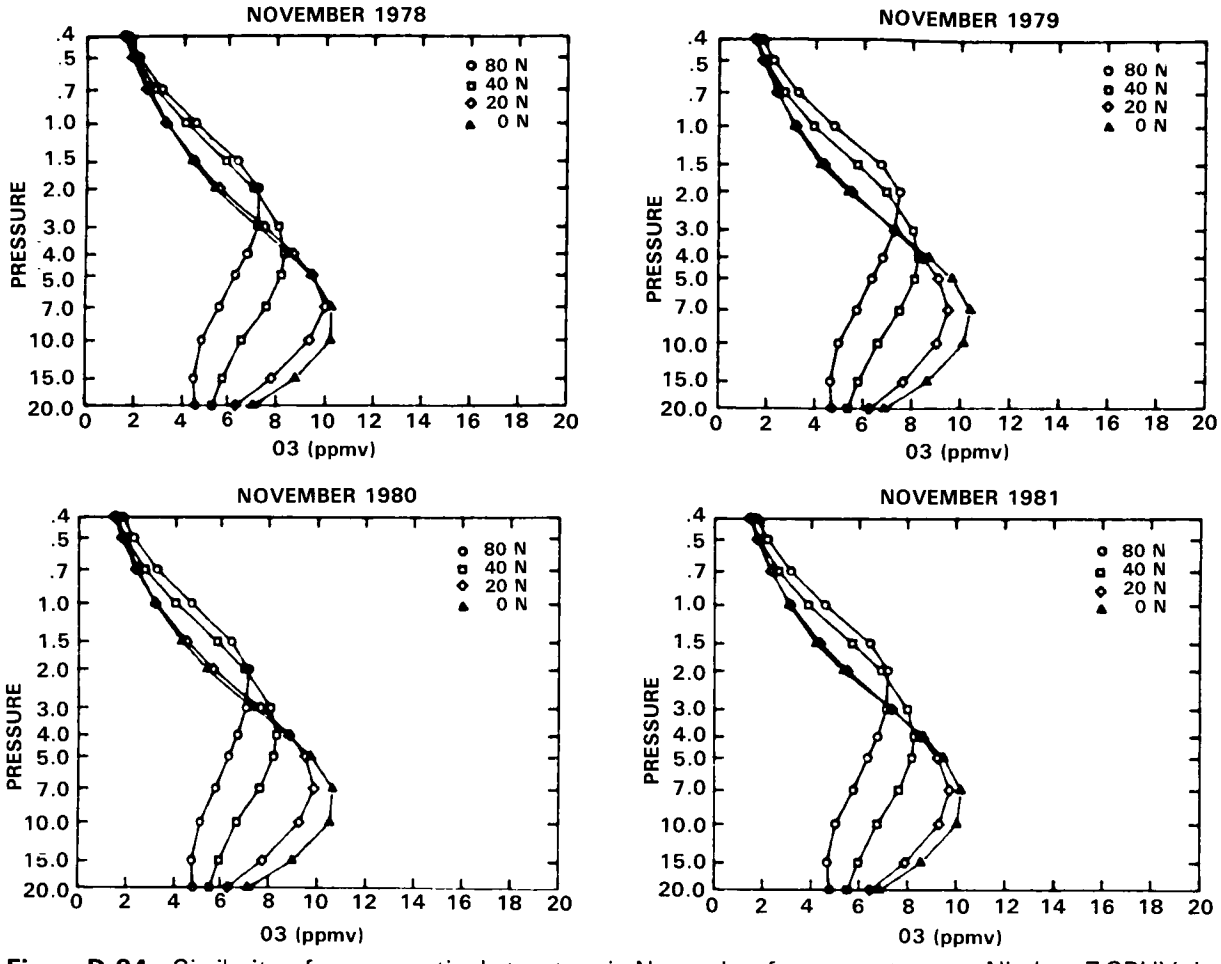

Figure D-24. Similarity of ozone vertical structure in November from year to year; Nimbus 7 SBUV data. (Keating and Young, 1985.)

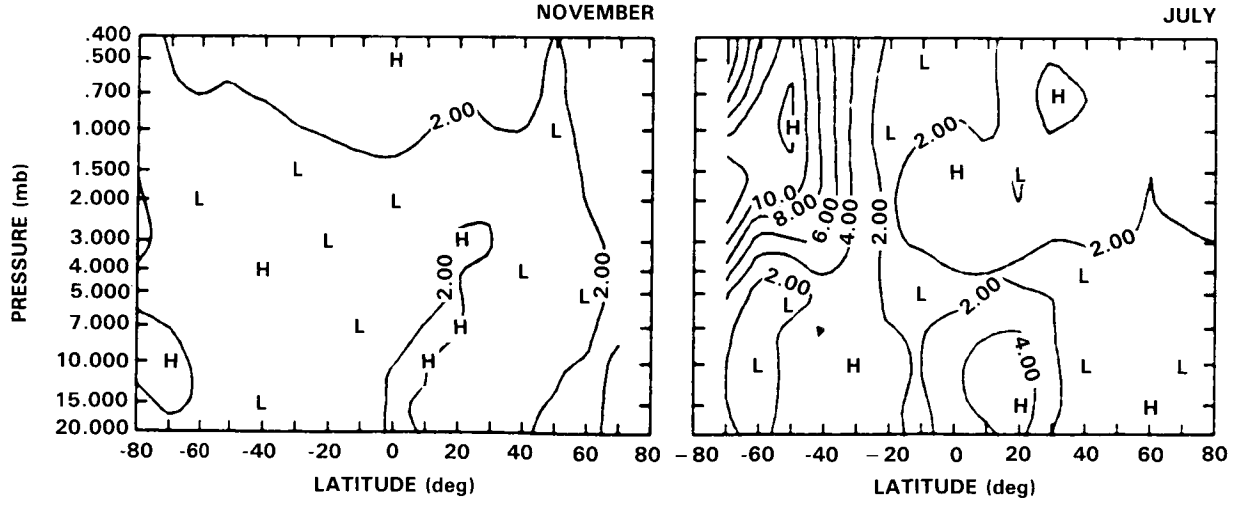

Figure D-25. Interannual variability of ozone vertical structure expressed as yearly standard deviation (percent) from 4-year zonal means for the months of November and July; Nimbus 7 SBUV data. (Keating and Young, 1985.)

D-4 MONTHLY MEAN CHARTS OF TOTAL OZONE, AND OF OZONE MIXING RATIOS AND TEMPERATURES AT SELECTED PRESSURE LEVELS

Based on the data described above, monthly mean charts of total ozone, Figure D-26 and of ozone mixing ratio and temperatures at selected pressure levels, Figures D-27–D-30, are presented for the mid-season months, together with meridional sections of the amplitudes and phases of the quasi-stationary planetary temperature waves 1 and 2, Figure D-31.

When comparing these temperature fields with the respective ozone fields, the following features are evident:

During summer the influence of the dynamics in connection with the planetary waves is negligable and we find a strong temperature dependance of ozone, i.e., minima of ozone mixing ratio are connected with the temperature maxima over the polar regions.

During all other seasons, however, when planetary waves are developed, the ozone distribution is coupled strongly to the horizontal and vertical motions in connection with the planetary waves. In the lower stratosphere (30 mbar) *maxima of ozone mixing ratio are connected with high temperatures*, (which are a result of sinking motions), and vice versa. The same is valid for the pattern of the total ozone.

In the upper stratosphere, 1-mbar, and lower mesosphere, 0.4-and 0.1-mbar, respectively, photochemical processes dominante and we find a negative correlation between ozone and temperature, and *high temperatures are connected with ozone minima*, and vice versa.

D-4.1 Total Ozone: Mid-Season Months, Northern and Southern Hemisphere

The charts of total ozone, Figure D-26, support the discussion in the previous Sections, particularly with respect to the differences between the hemispheres during the spring transition time. The distribution of total ozone is highly correlated with the temperature of the lower stratosphere and with the large-scale planetary waves. This will be discussed in more detail in Section D-4.2, where the ozone distribution is presented at selected pressure levels.

D-4.2 Ozone Mixing Ratios and Temperatures at Selected Pressure Levels

D-4.2.a January:

Northern Hemisphere

During the northern winters the large-scale planetary waves 1 and 2 can penetrate from the troposphere into the stratosphere as long as the mean zonal winds are from the west, (Charney and Drazin, 1961). The most prominent features of the stratosphere in winter are the well developed cold polar vortex and the strong quasi-stationary planetary wave 1. This wave which causes large longitudinal variability over middle and high latitudes, is most pronounced in the lower and middle stratosphere at the 30-and 10-mbar levels (23 and 30km), respectively, Figure D-27.2. The warm region over approx. 150 °E is connected with the well known Aleutian anticyclone which is responsible for the displacement of the polar vortex away from the North Pole.

Following are the charts for Section D-4.1 and D-4.2, Figures 26.1–31.4.

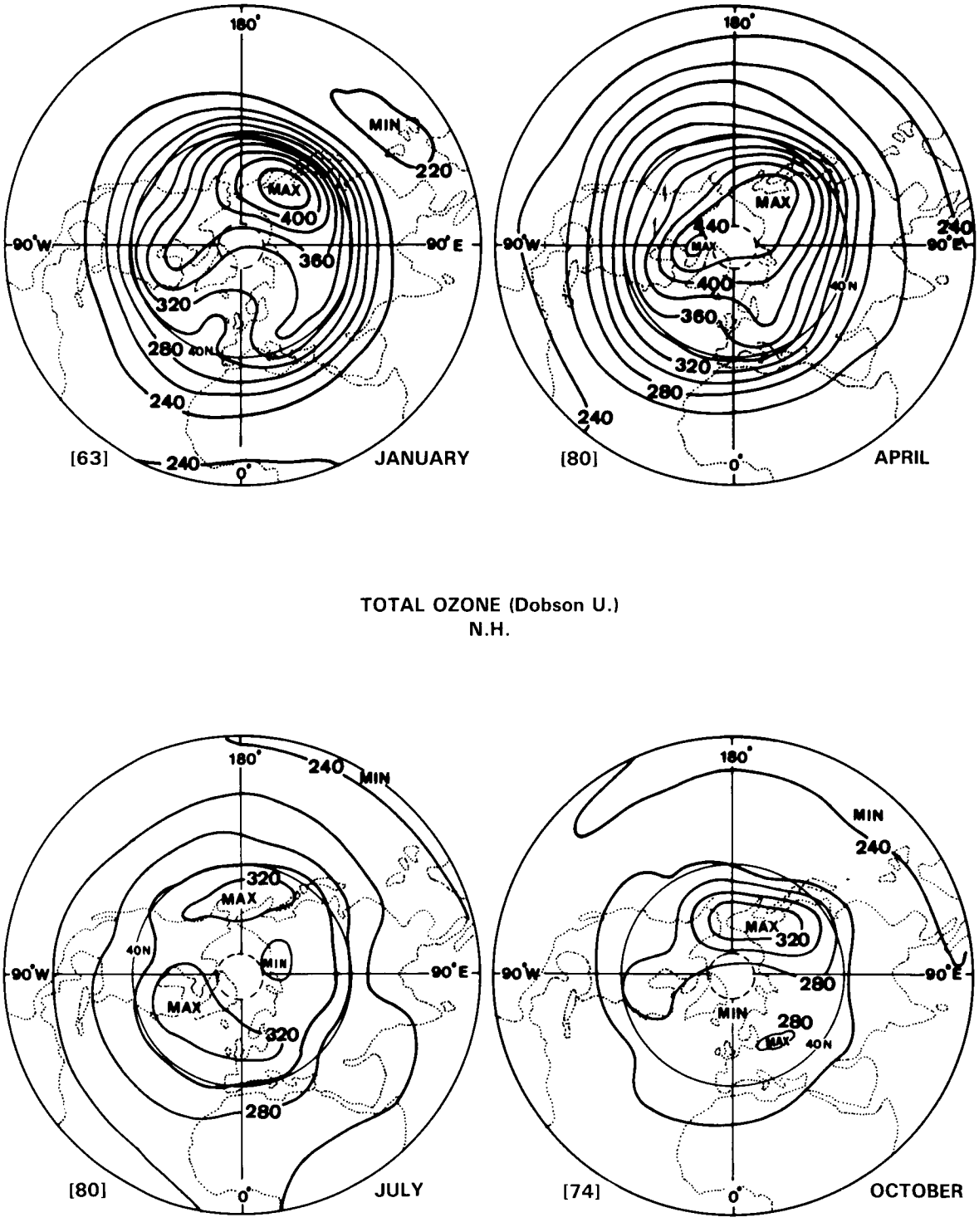

Figure D-26.1. Monthly average total ozone charts for the Northern Hemisphere from 1978–1982, for the mid-season months. Values in brackets outside of the charts indicate the latitude from which the analyses were extrapolated polewards. (R.M. Nagatani and A.J. Miller, personal communication.)

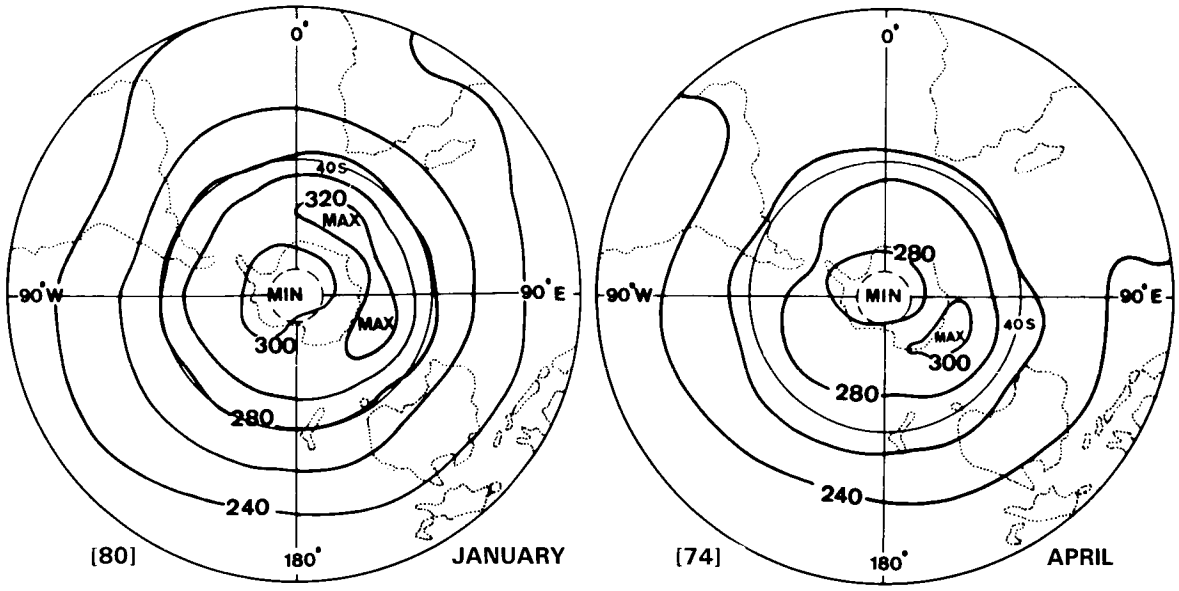

TOTAL OZONE (Dobson U.)
S.H.

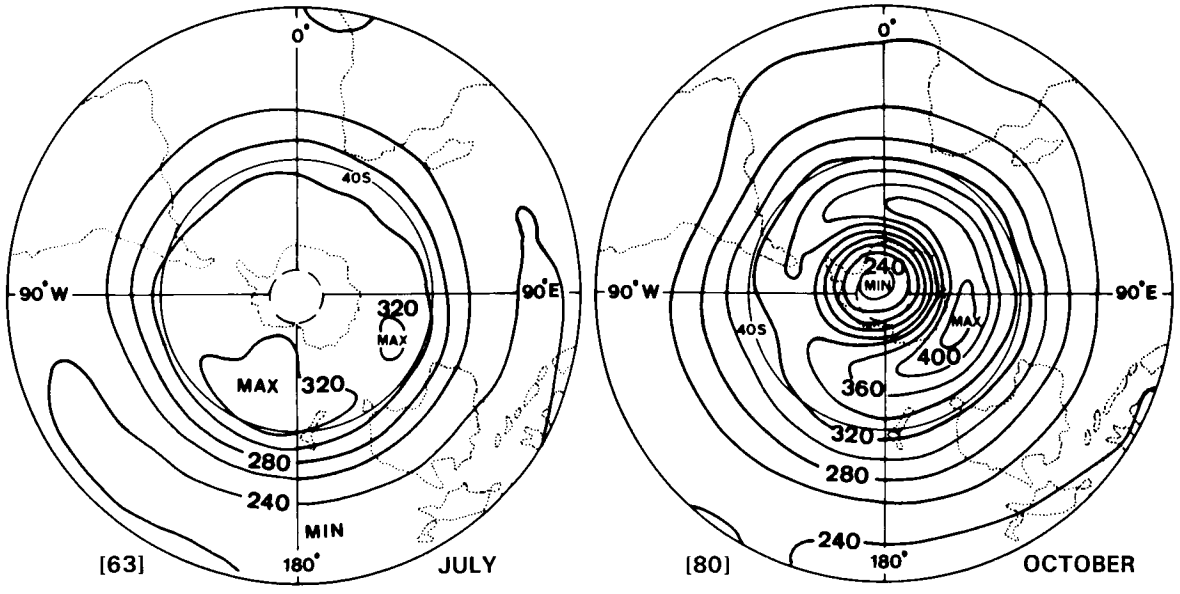

Figure D-26.2. Monthly average total ozone charts for the Southern Hemisphere from 1978–1982, for the mid-season months. For values in brackets see Figure D-26.1. (R.M. Nagatani and A.J. Miller, personal communication.)

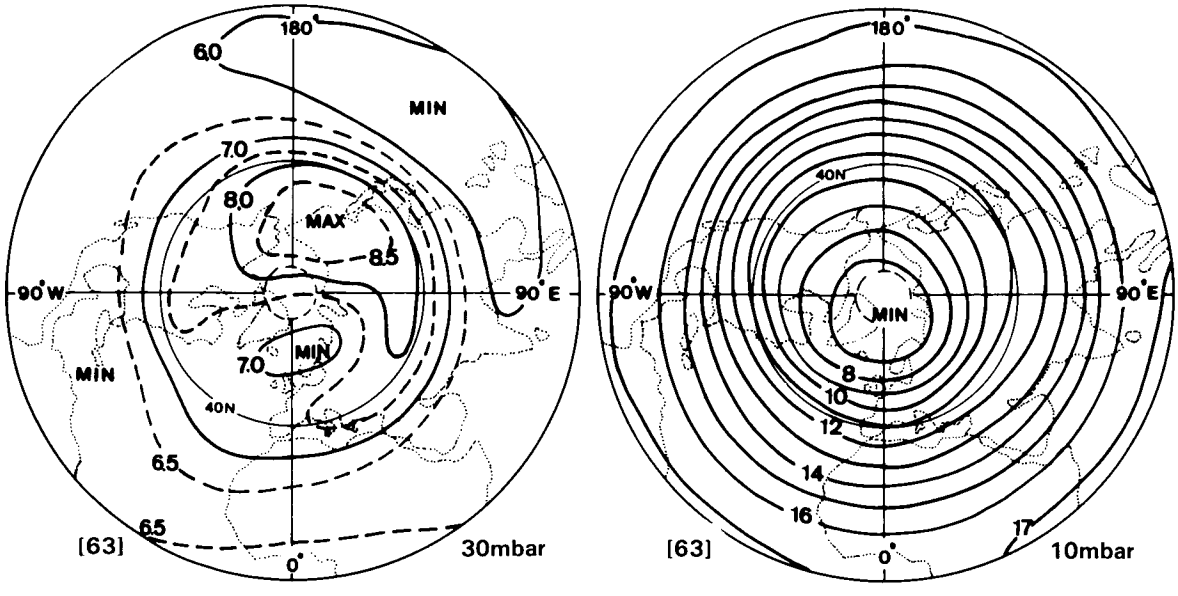

OZONE MASS MIXING RATIO (ppm)
JANUARY N.H.

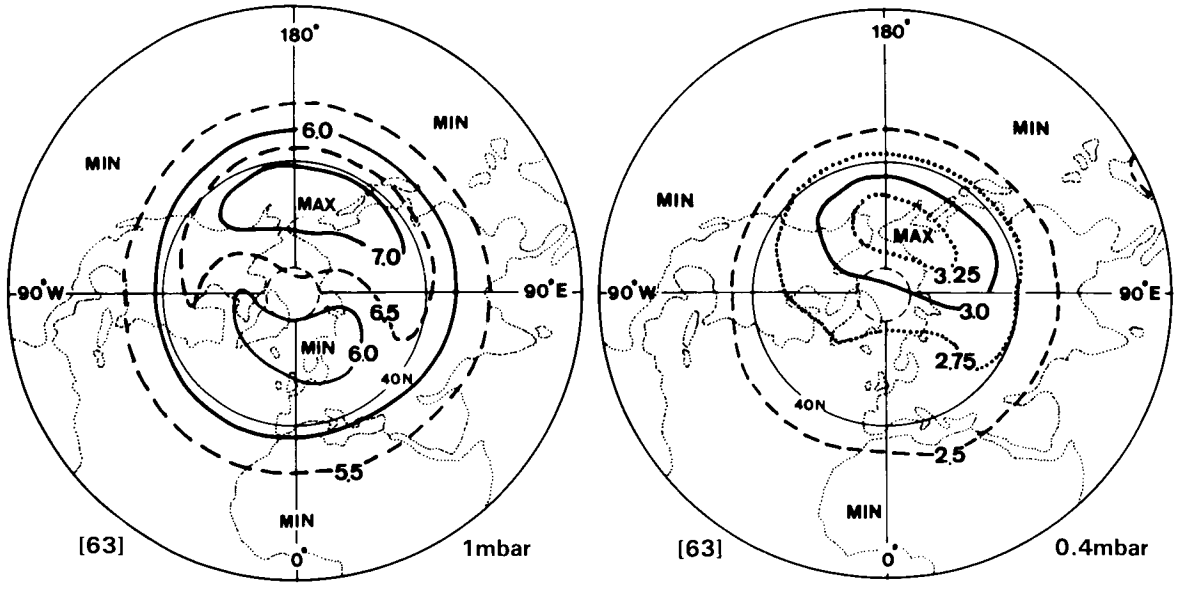

Figure D-27.1. Monthly average ozone mass mixing ratio (ppm) for the Northern Hemisphere from 1978–1982, for January. For values in brackets see Figure D-26.1. (R.M. Nagatani and A.J. Miller, personal communication.)

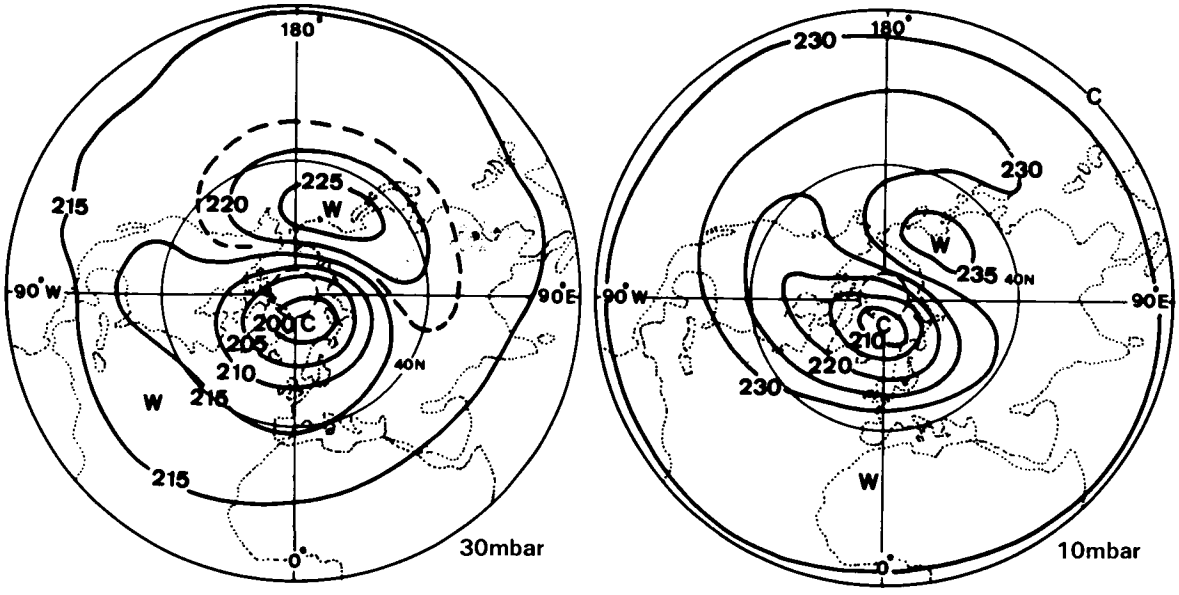

TEMPERATURE (K)
JANUARY N.H.

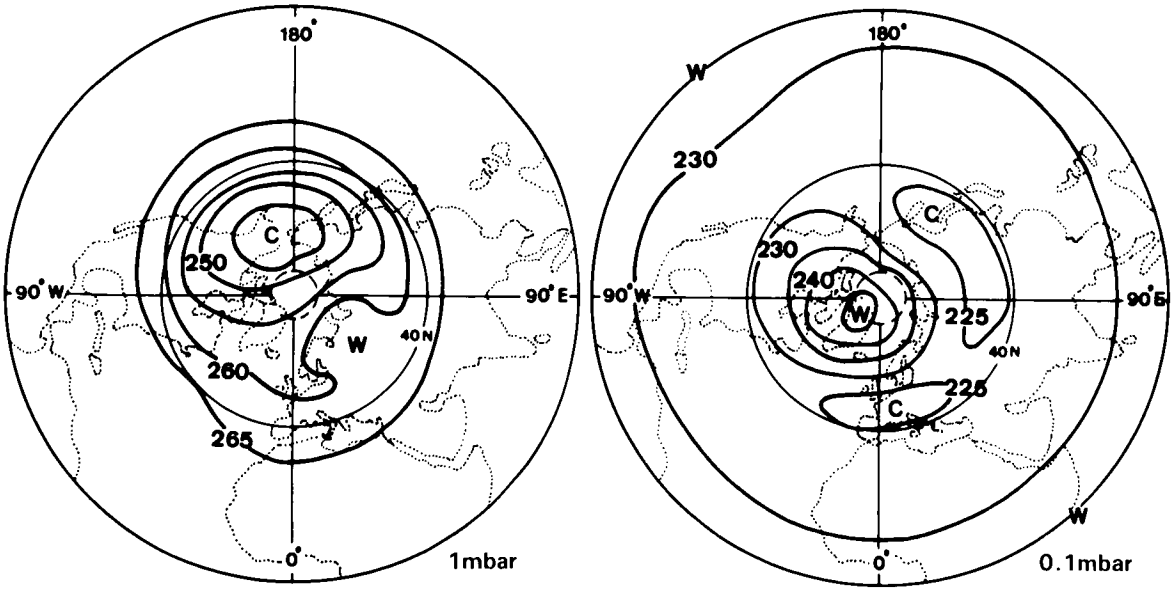

Figure D-27.2. Monthly mean temperature charts for January, Northern Hemisphere. (Data: 30-mbar: F.U. Berlin; otherwise: New Reference Atmosphere, MAP-Handbook, 16.)

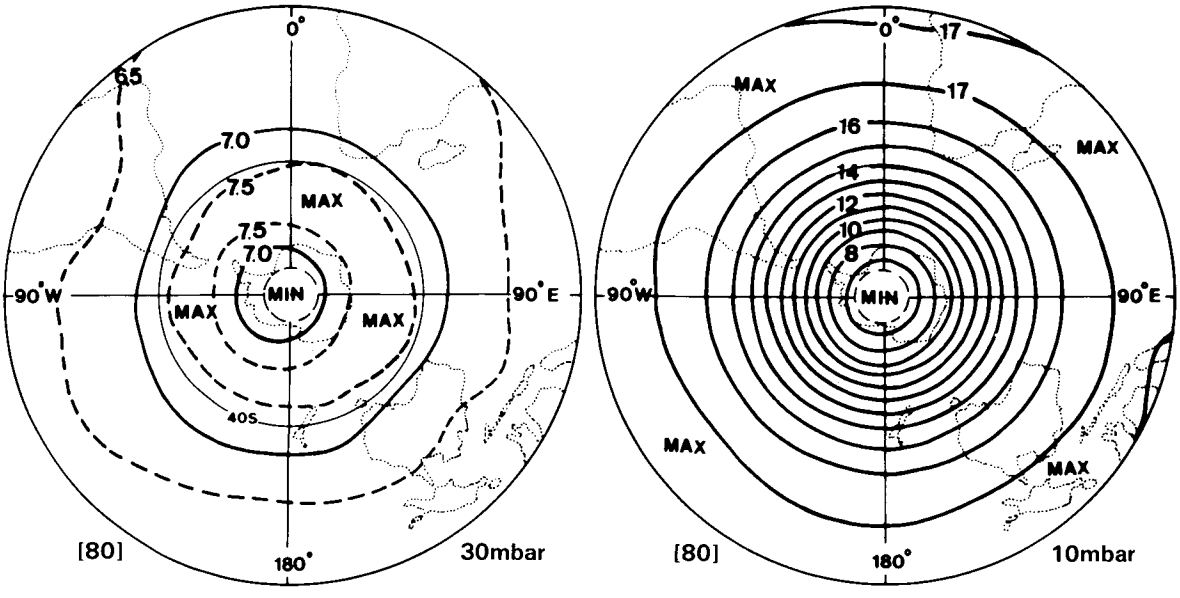

OZONE MASS MIXING RATIO (ppm)
JANUARY S.H.

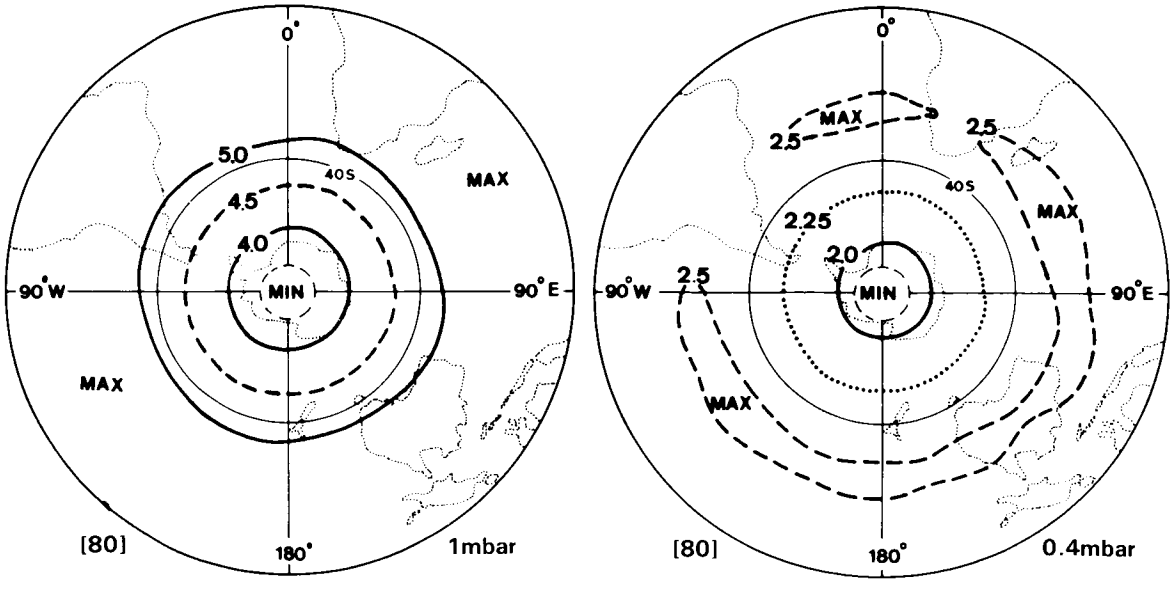

Figure D-27.3. Monthly average ozone mass mixing ratio (ppm) for the Southern Hemisphere from 1978–1982, for January. (R.M. Nagatani and A.J. Miller, personal communication.)

C-5

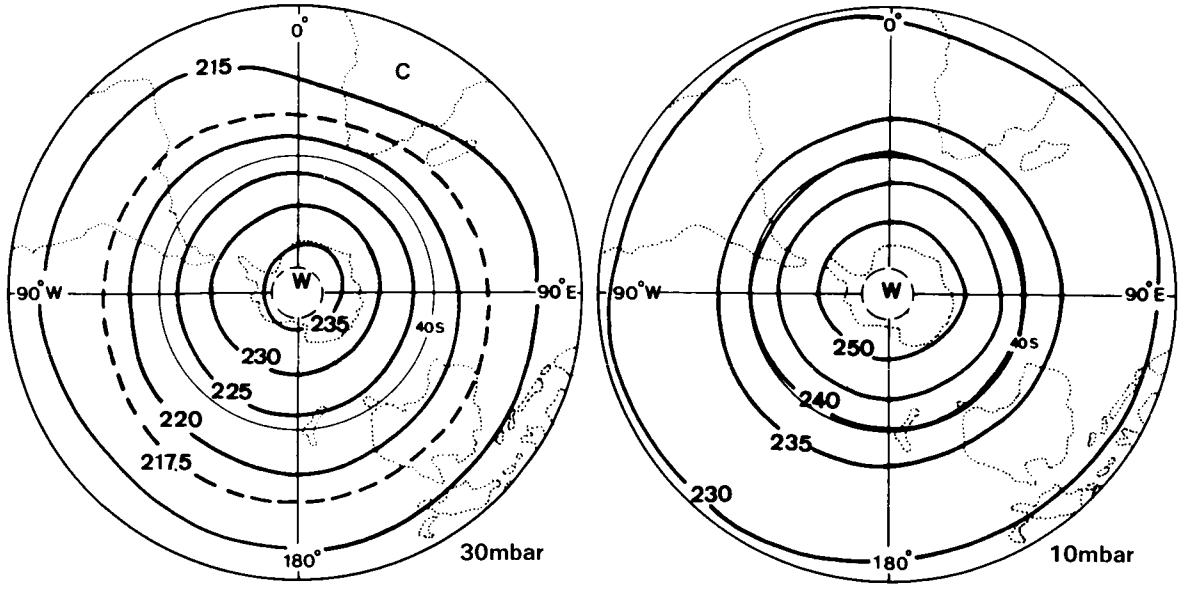

TEMPERATURE (K)
JANUARY S.H.

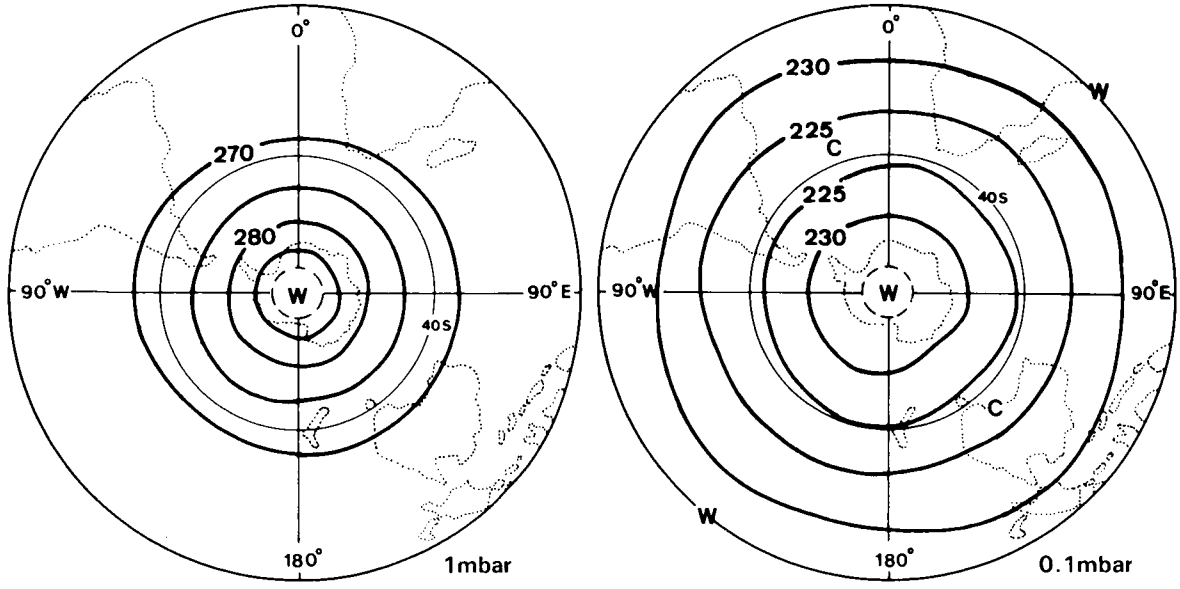

Figure D-27.4. Monthly mean temperature charts for January, Southern Hemisphere. (Data: 30-mbar: Knittel, 1976; otherwise: New Reference Atmosphere, MAP-Handbook, 16.)

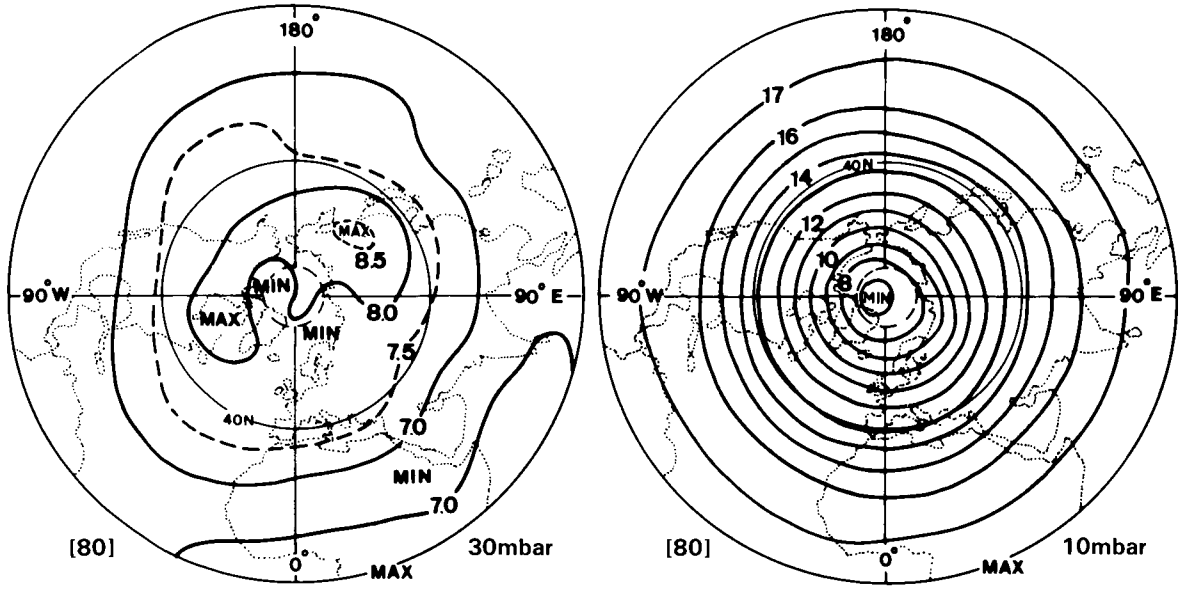

OZONE MASS MIXING RATIO (ppm)
APRIL N.H.

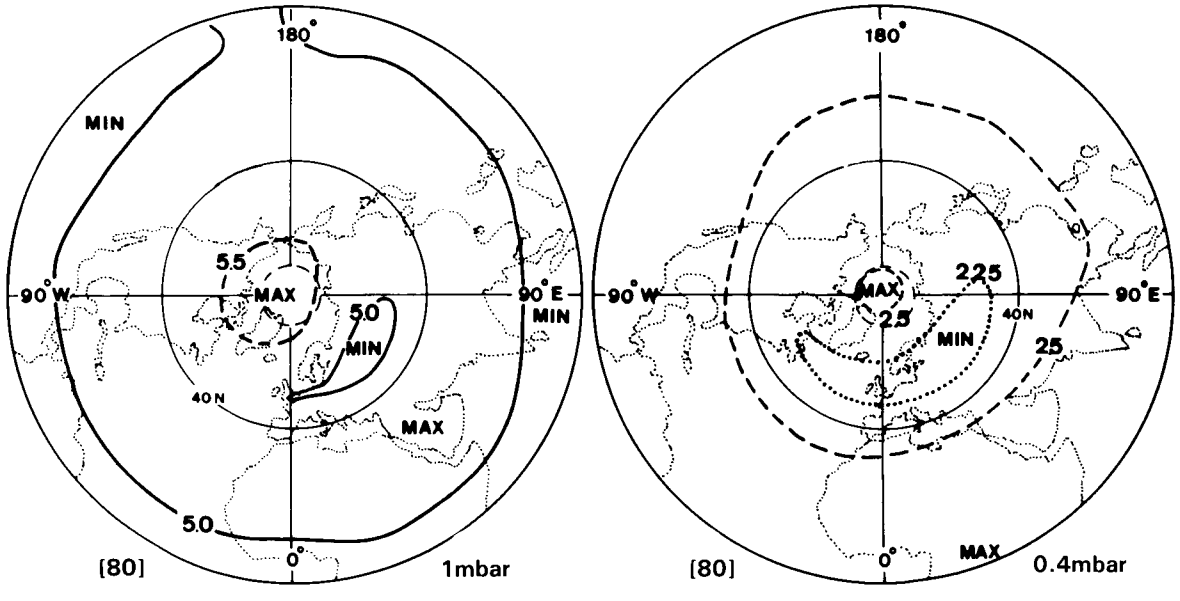

Figure D-28.1. Monthly average ozone mass mixing ratio (ppm) for the Northern Hemisphere from 1978–1982, for April. (R.M. Nagatani and A.J. Miller, personal communication.)

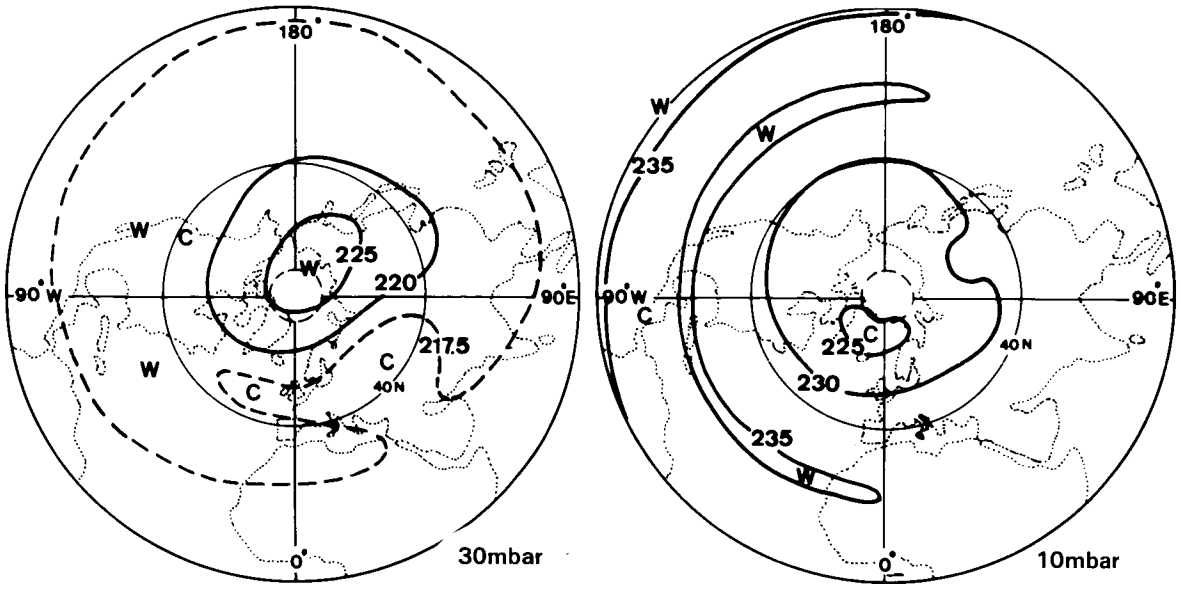

TEMPERATURE (K)
APRIL N.H.

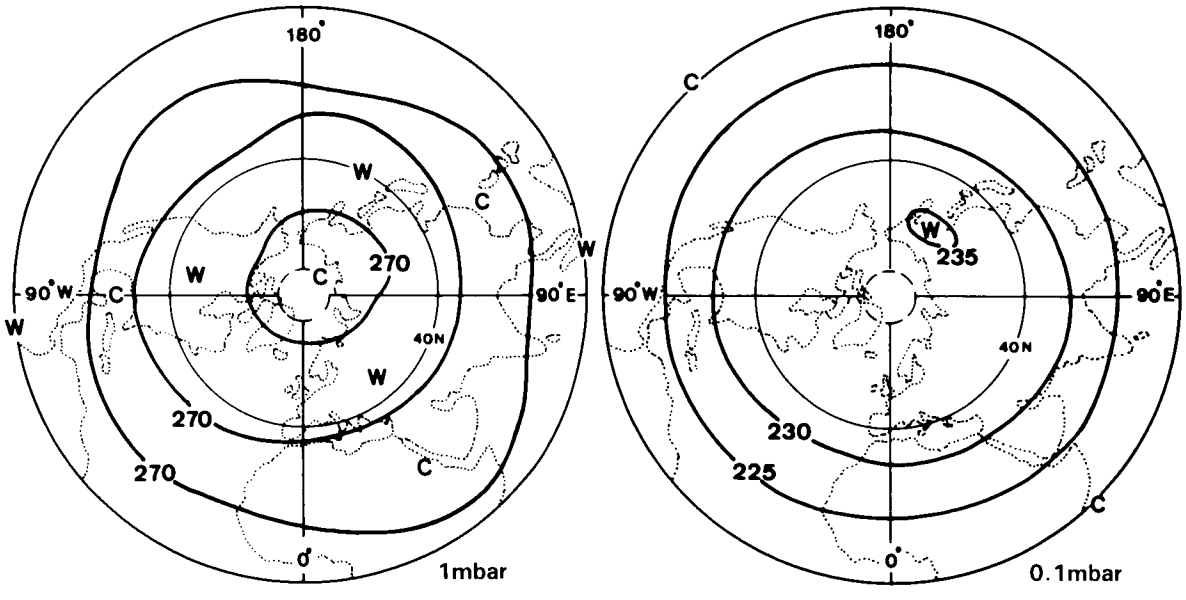

Figure D-28.2. Monthly mean temperature charts for April, Northern Hemisphere. (Data: 30-mbar: F.U. Berlin; otherwise: New Reference Atmosphere, MAP-Handbook, 16.)

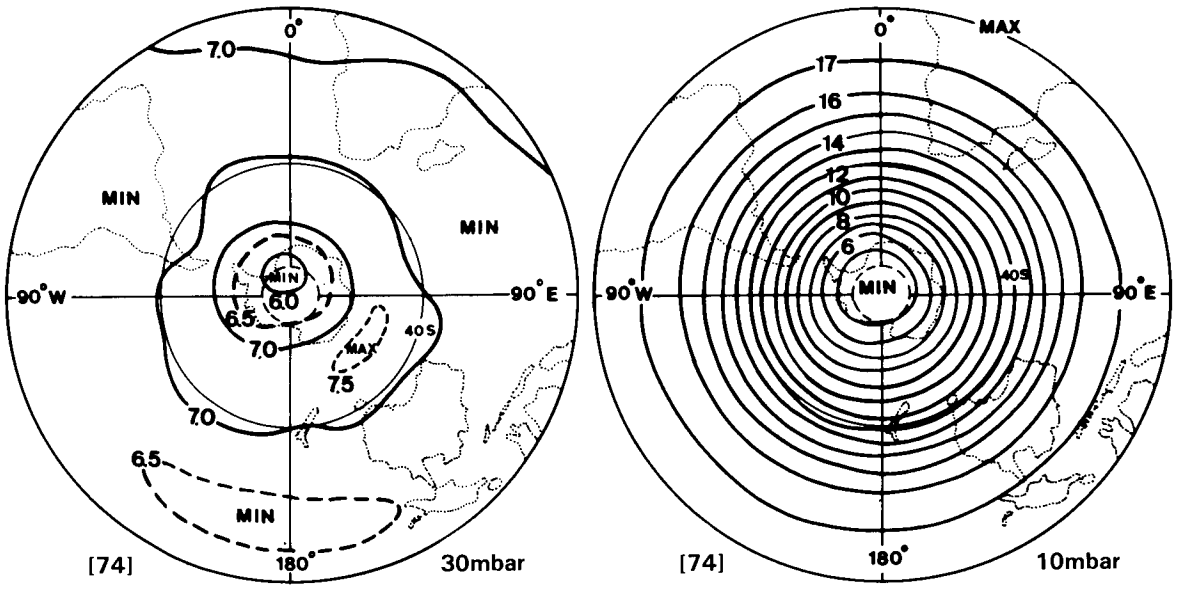

OZONE MASS MIXING RATIO (ppm)
APRIL S.H.

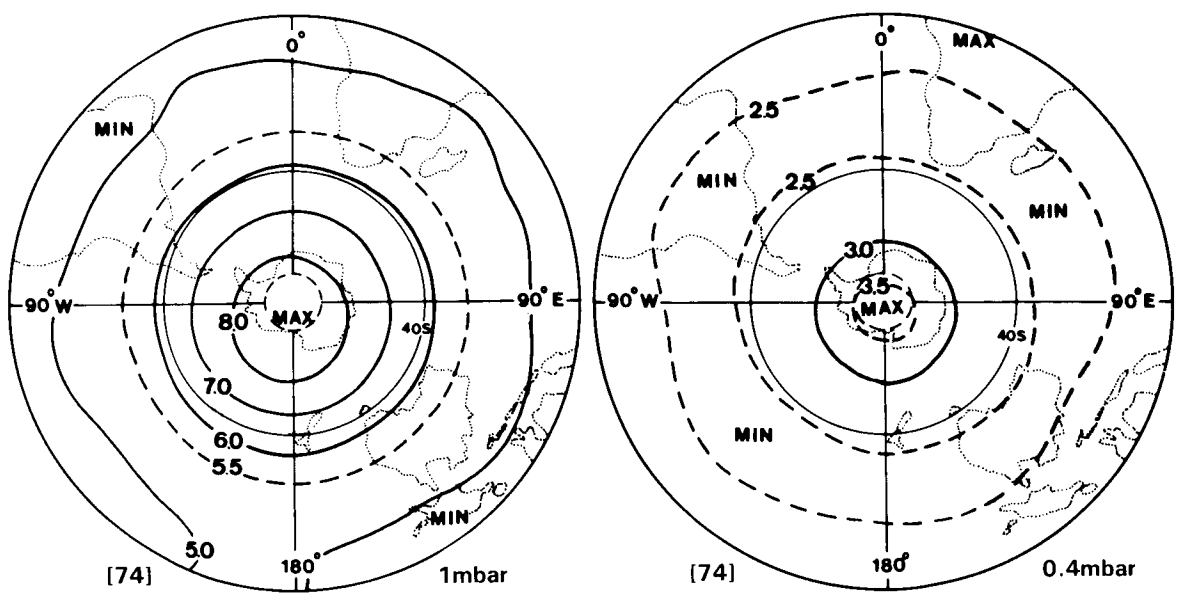

Figure D-28.3. Monthly average ozone mass mixing ratio (ppm) for the Southern Hemisphere from 1978–1982, for April. (R.M. Nagatani and A.J. Miller, personal communication.)

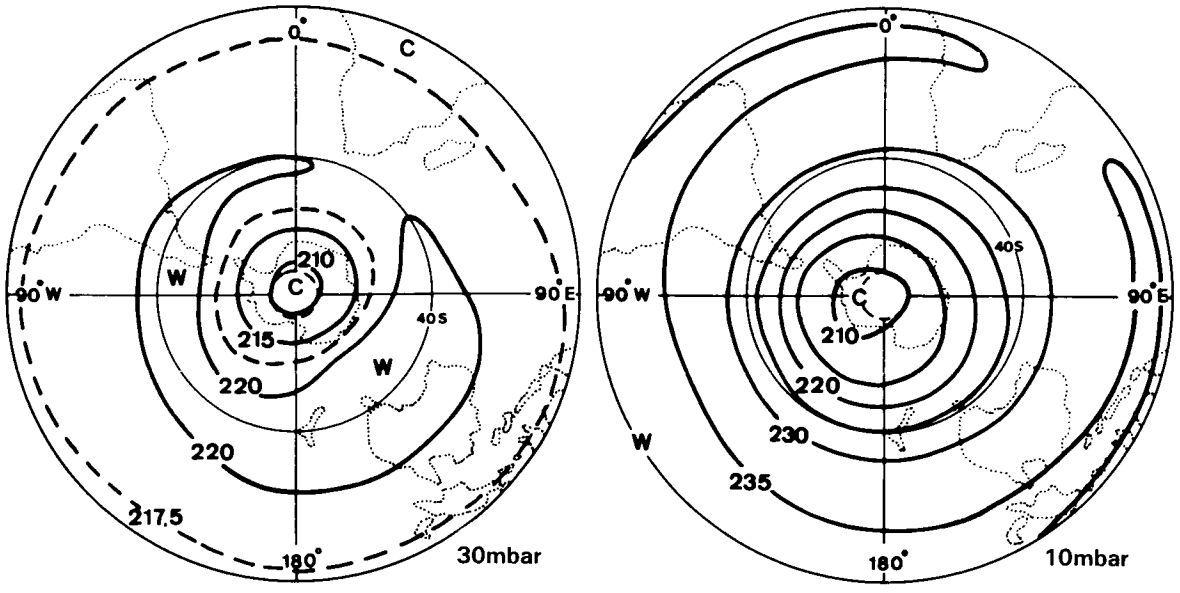

TEMPERATURE (K)
APRIL S.H.

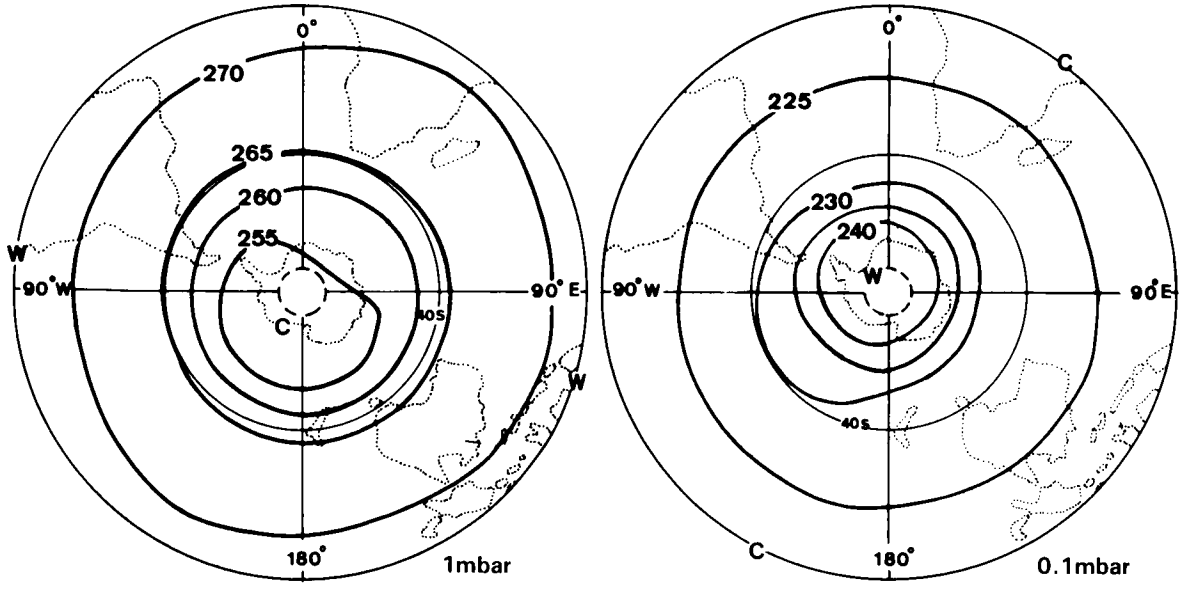

Figure D-28.4. Monthly mean temperature charts for April, Southern Hemisphere. (Data: 30-mbar: Knittel, 1976; otherwise: New Reference Atmosphere, MAP-Handbook, 16.)

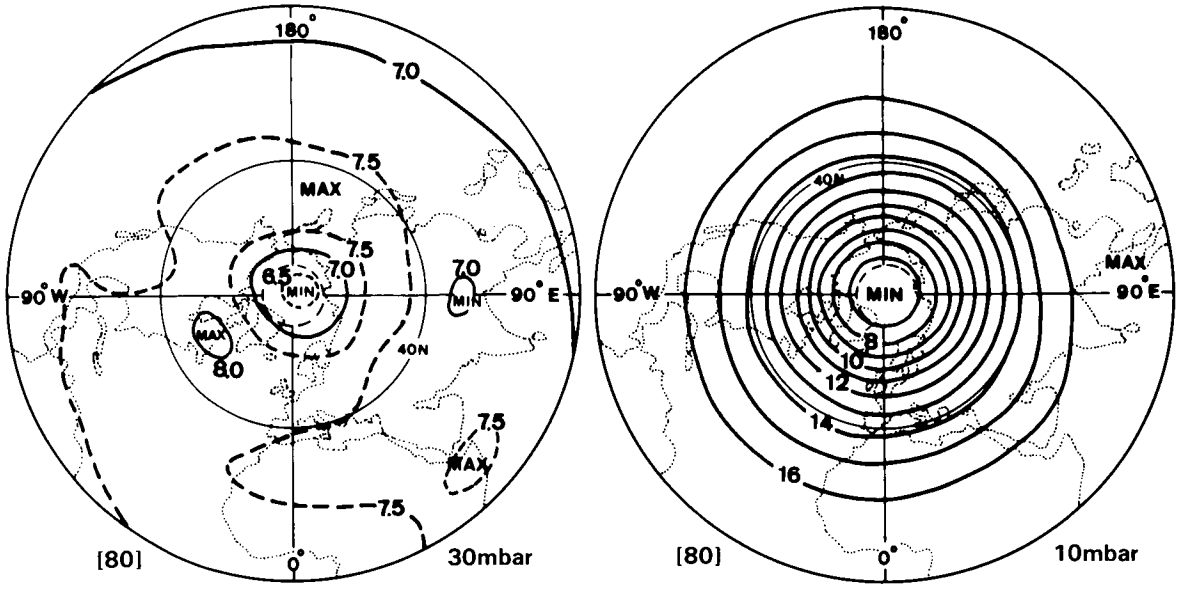

OZONE MASS MIXING RATIO (ppm)
JULY N.H.

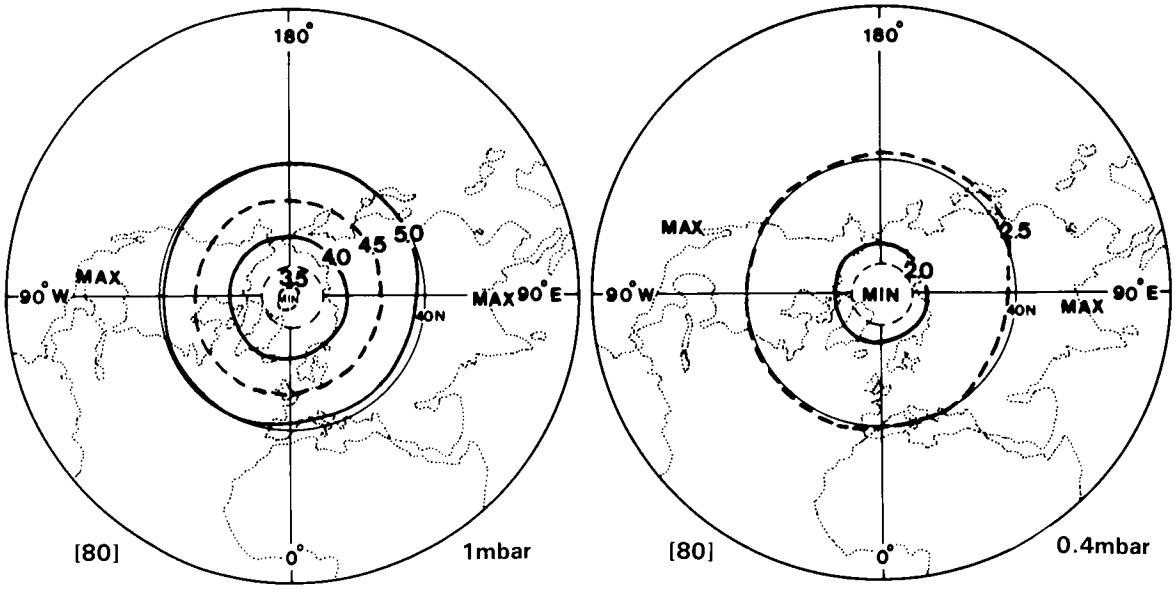

Figure D-29.1. Monthly average ozone mass mixing ratio (ppm) for the Northern Hemisphere from 1978–1982, for July. (R.M. Nagatani and A.J. Miller, personal communication.)

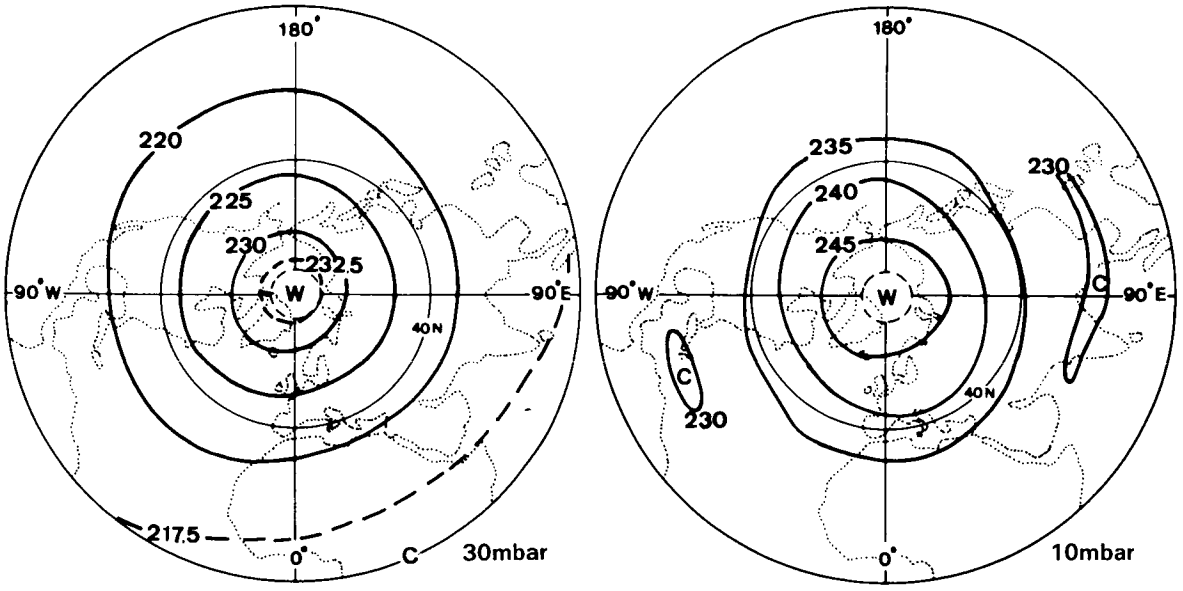

TEMPERATURE (K)
JULY N.H.

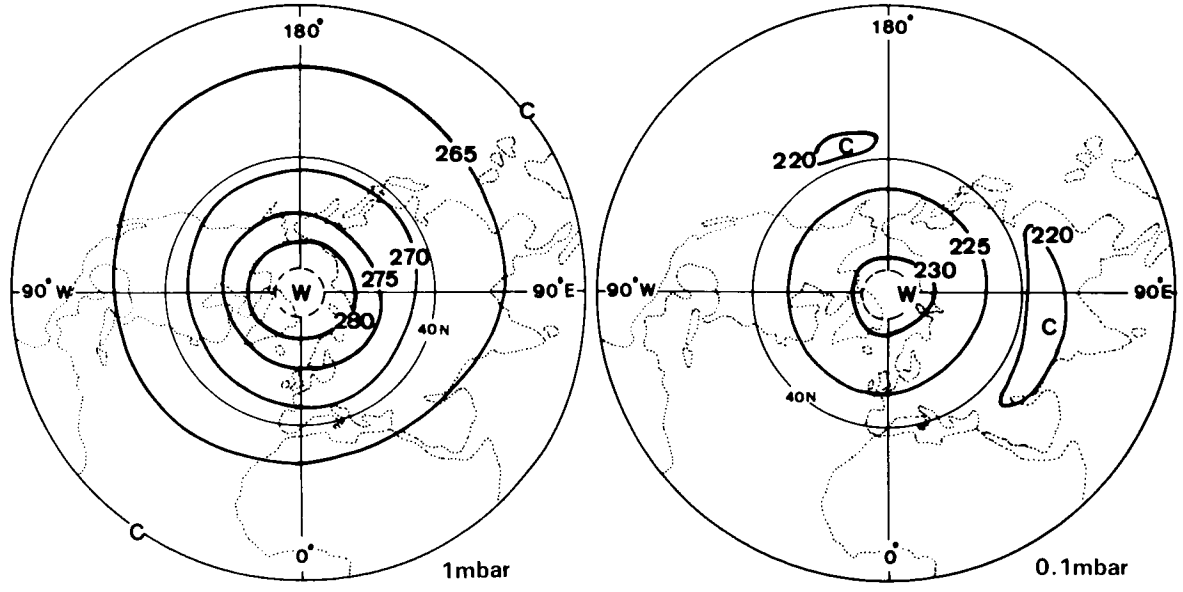

Figure D-29.2. Monthly mean temperature charts for July, Northern Hemisphere. (Data: 30-mbar: F.U. Berlin; otherwise: New Reference Atmosphere, MAP-Handbook, 16.)

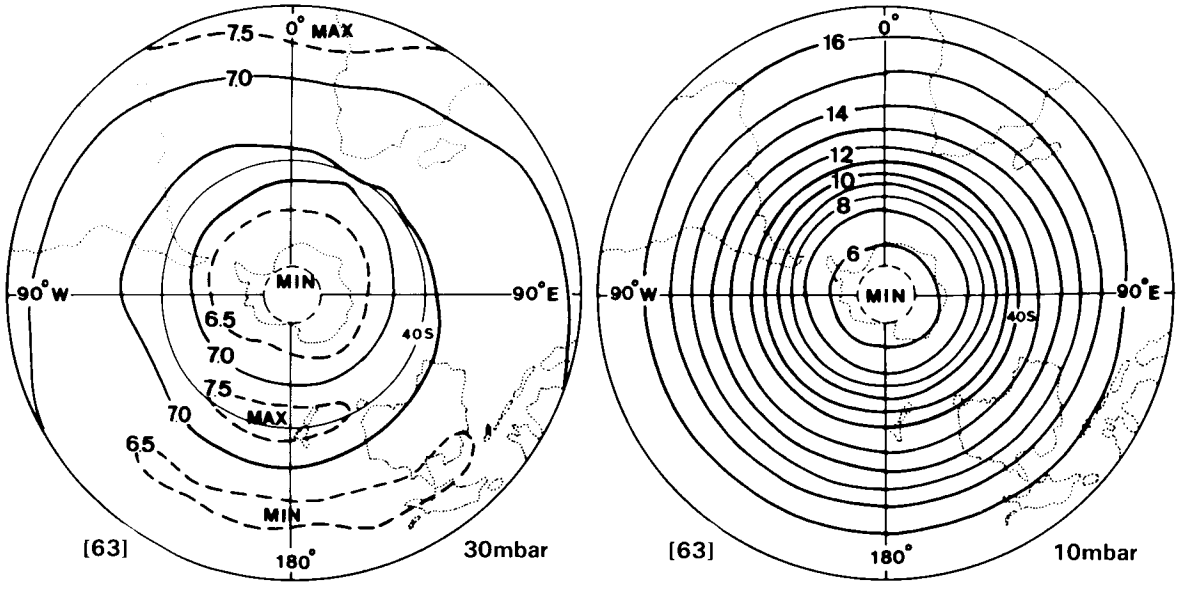

OZONE MASS MIXING RATIO (ppm)
JULY S.H.

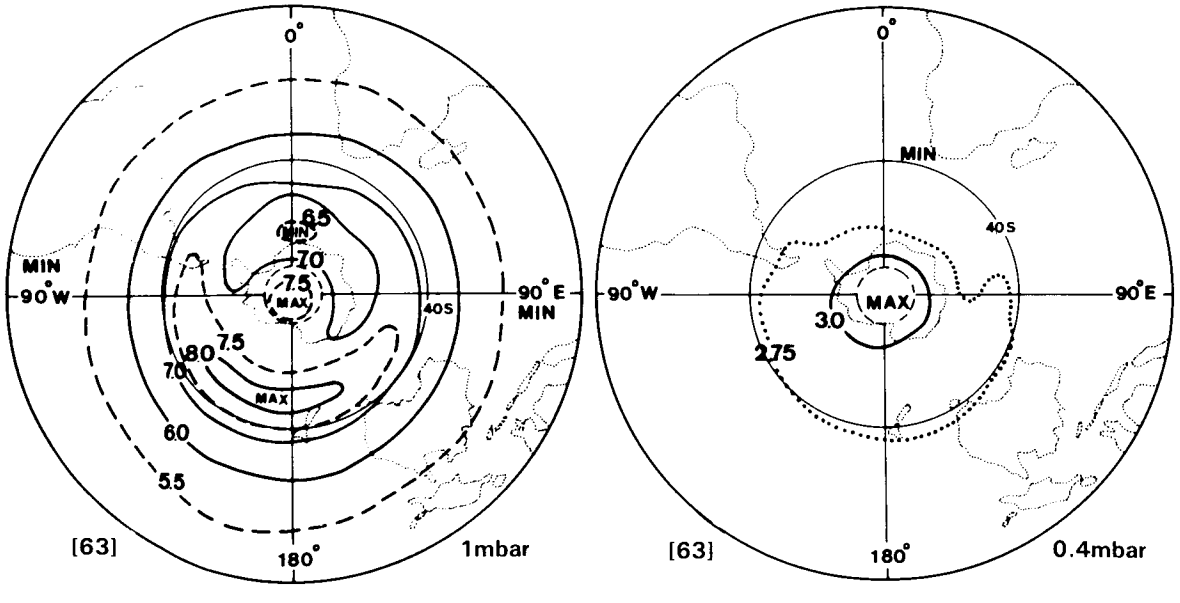

Figure D-29.3. Monthly average ozone mass mixing ration (ppm) for the Southern Hemisphere from 1978–1982, for July. (R.M. Nagatani and A.J. Miller, personal communication.)

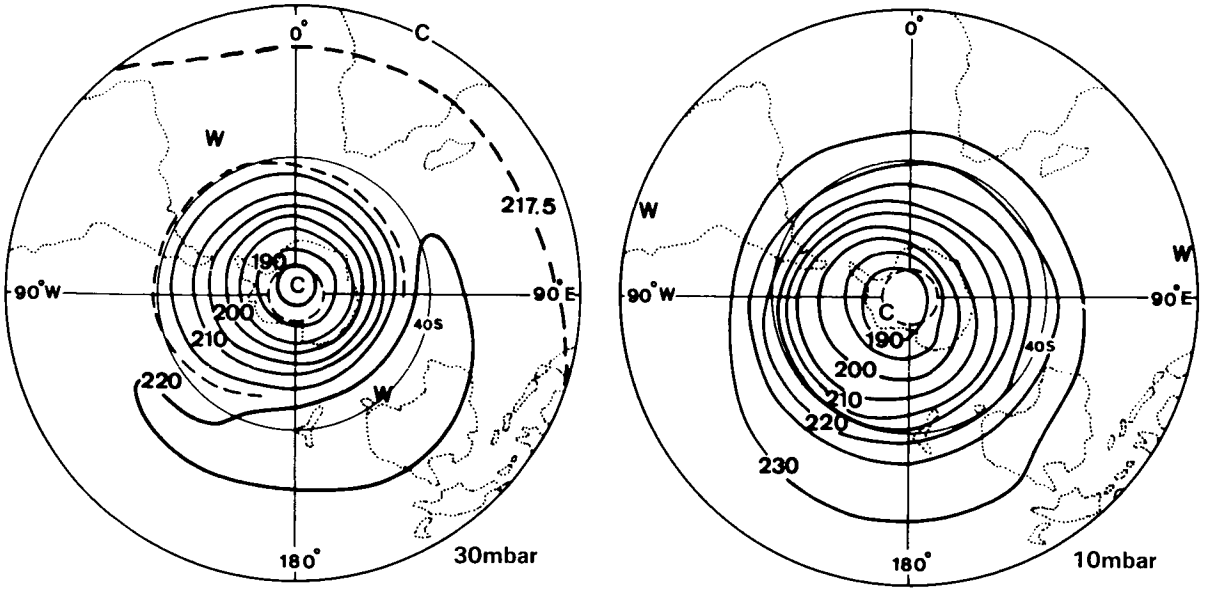

TEMPERATURE (K)
JULY S.H.

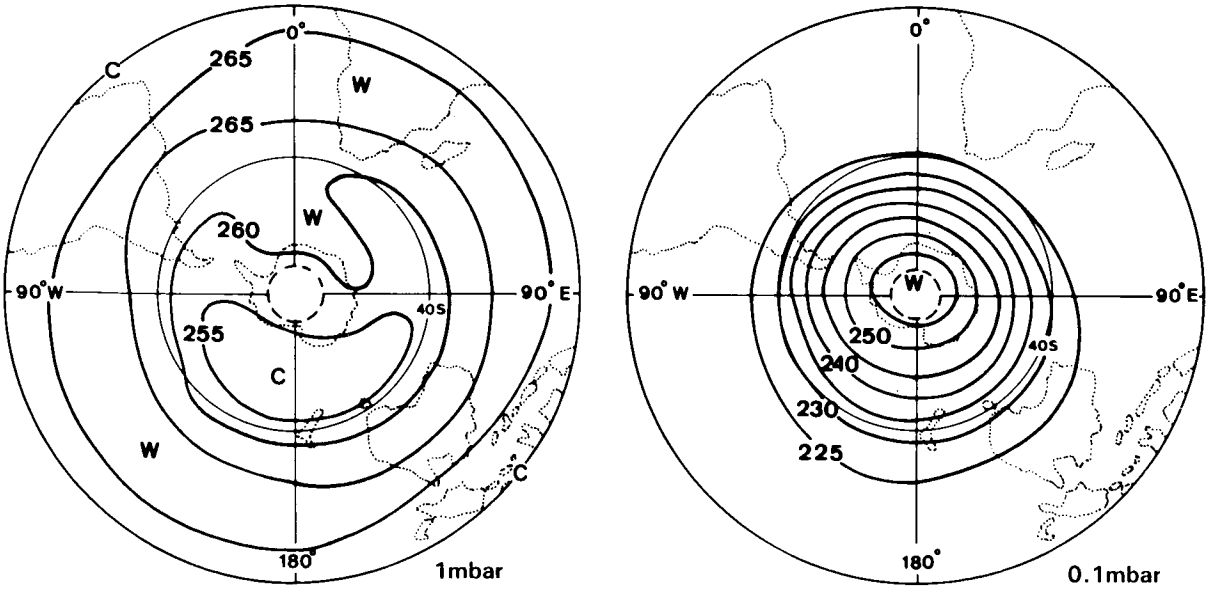

Figure D-29.4. Monthly mean temperature charts for July, Southern Hemisphere. (Data: 30-mbar: Knittel, 1976; otherwise: New Reference Atmosphere, MAP-Handbook, 16.)

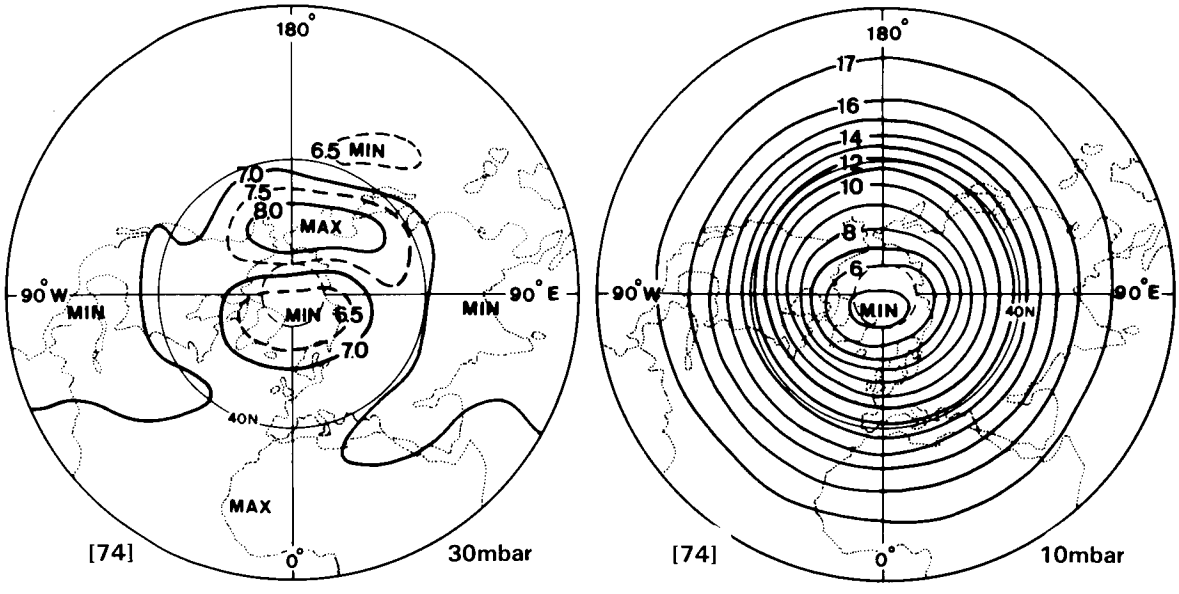

OZONE MASS MIXING RATIO (ppm)
OCTOBER N.H.

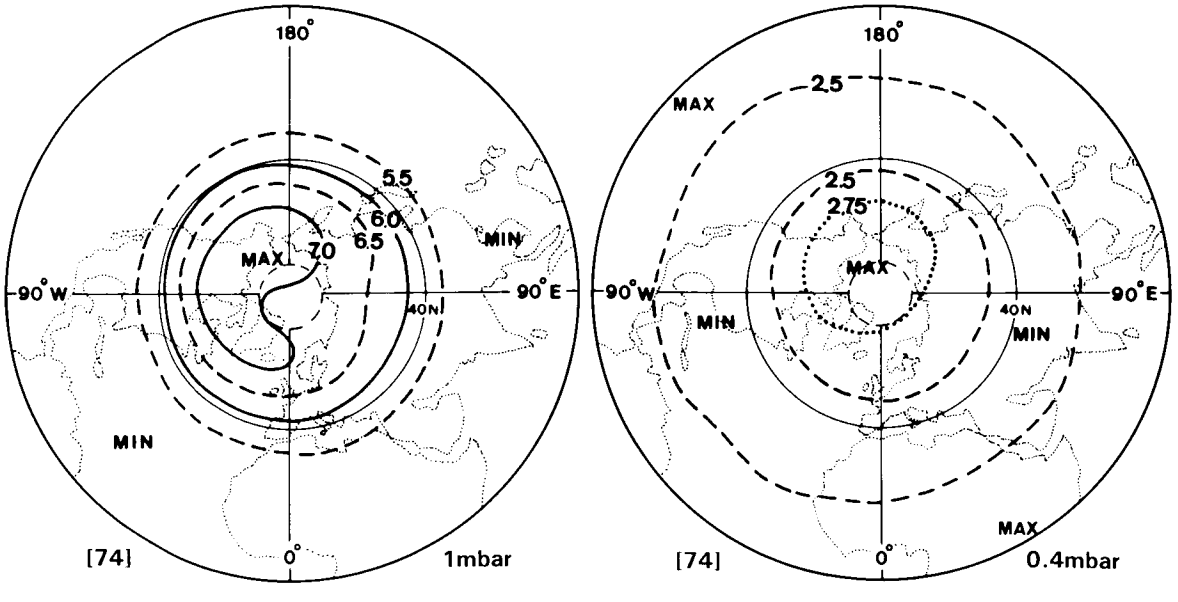

Figure D-30.1. Monthly average ozone mass mixing ratio (ppm) for the Northern Hemisphere from 1978–1982, for October. (R.M. Nagatani and A.J. Miller, personal communication.)

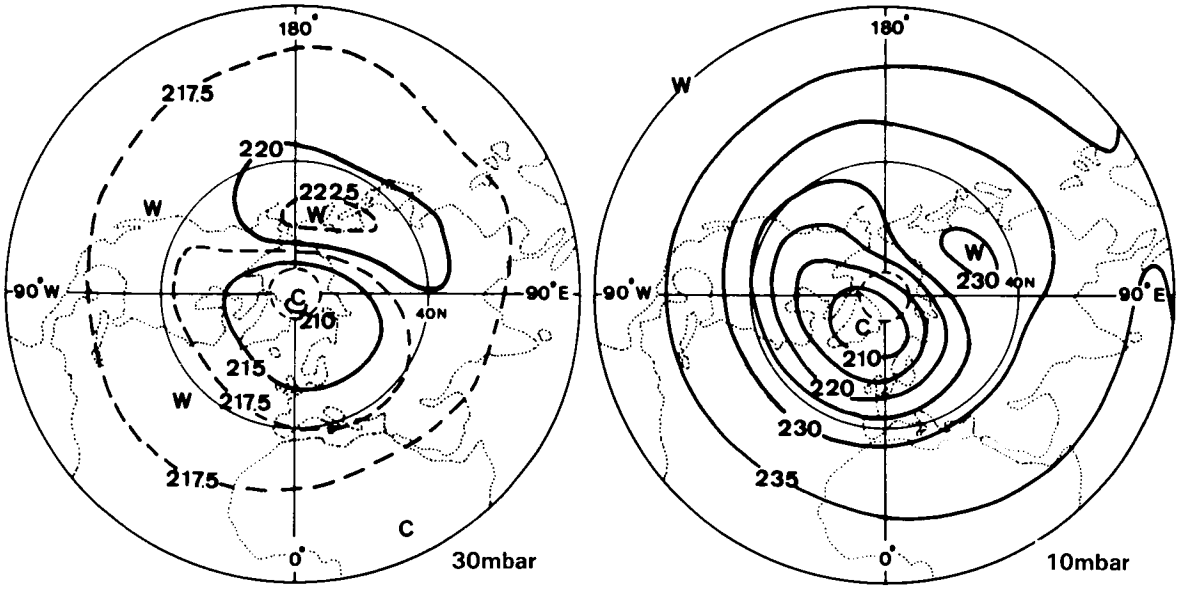

TEMPERATURE (K)
OCTOBER N.H.

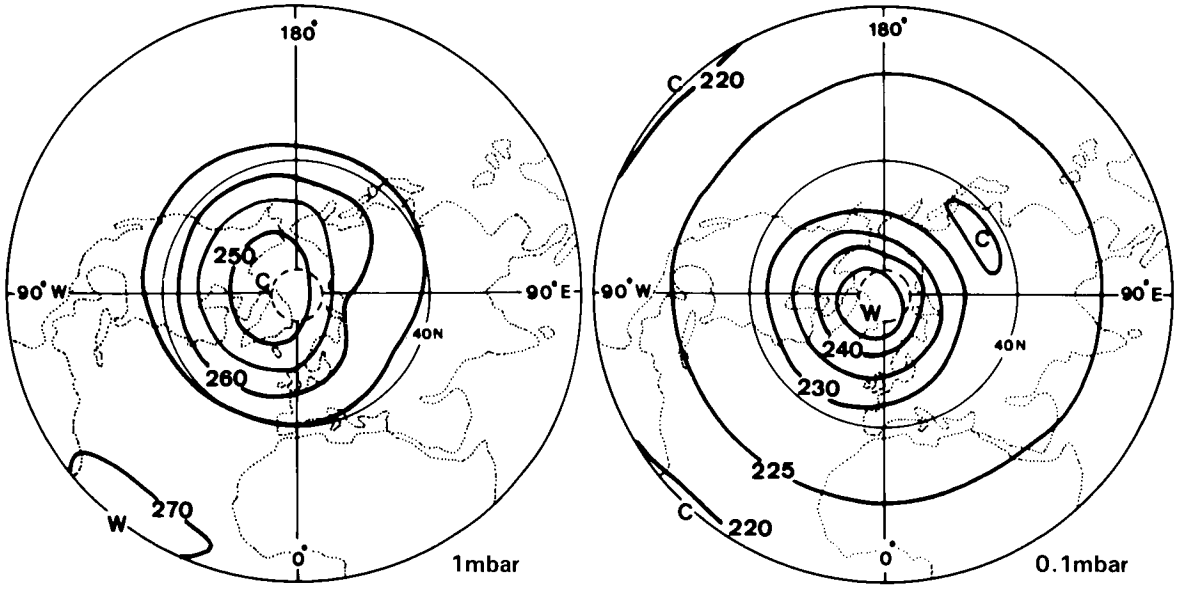

Figure D-30.2. Monthly mean temperature charts for October, Northern Hemisphere. (Data: 30-mbar: F.U. Berlin; otherwise: New Reference Atmosphere, MAP-Handbook, 16.)

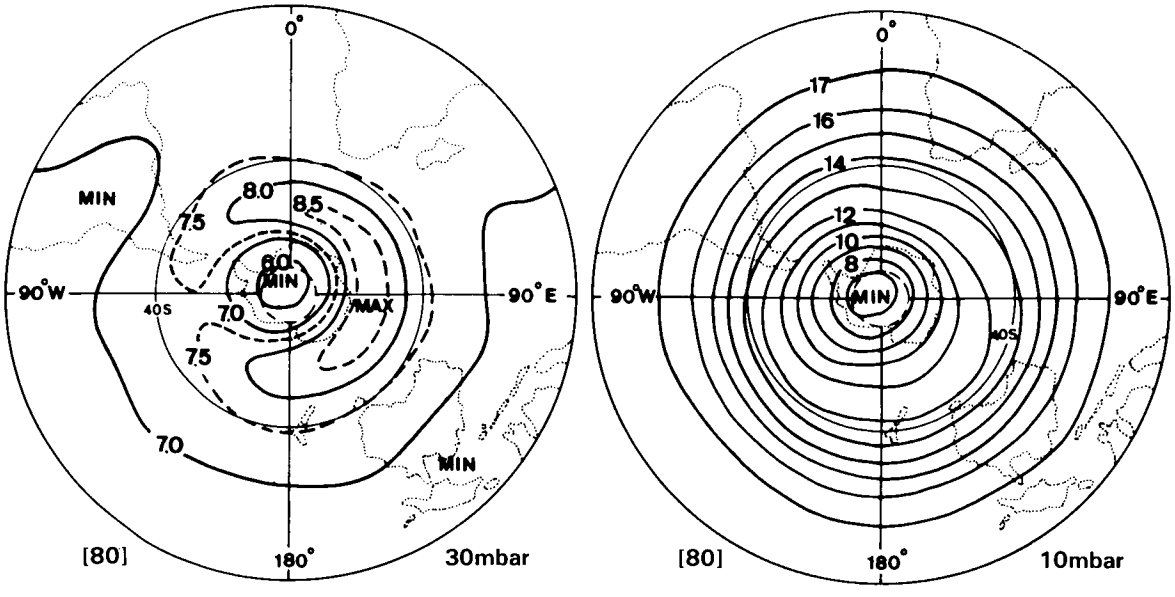

OZONE MASS MIXING RATIO (ppm)
OCTOBER S.H.

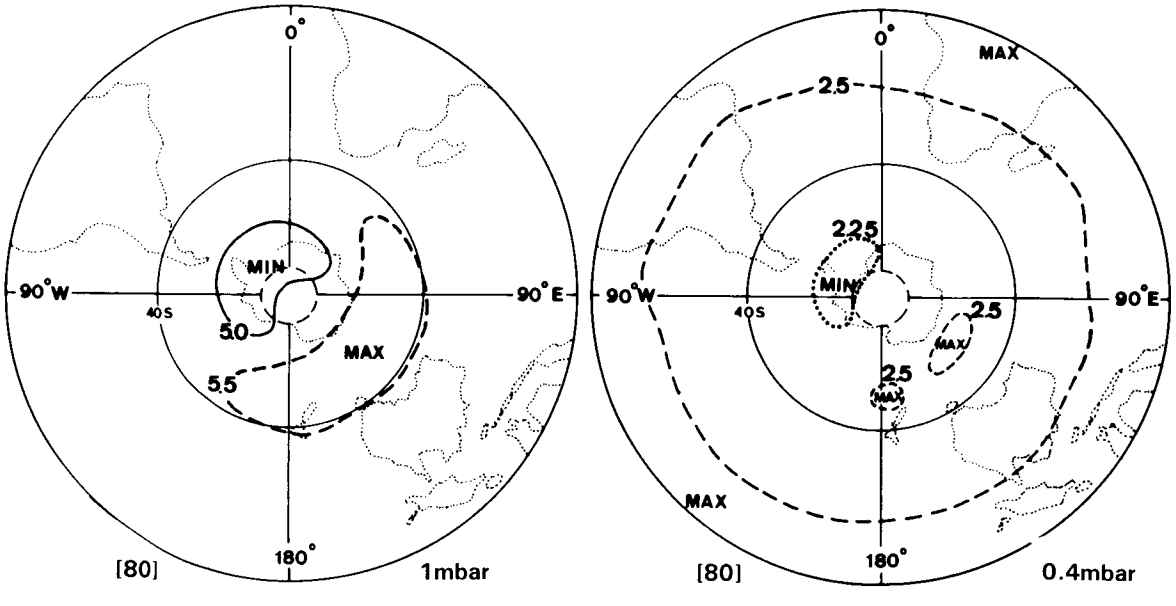

Figure D-30.3. Monthly average ozone mass mixing ratio (ppm) for the Southern Hemisphere from 1978–1982, for October. (R.M.Nagatani and A.J.Miller, personal communication.)

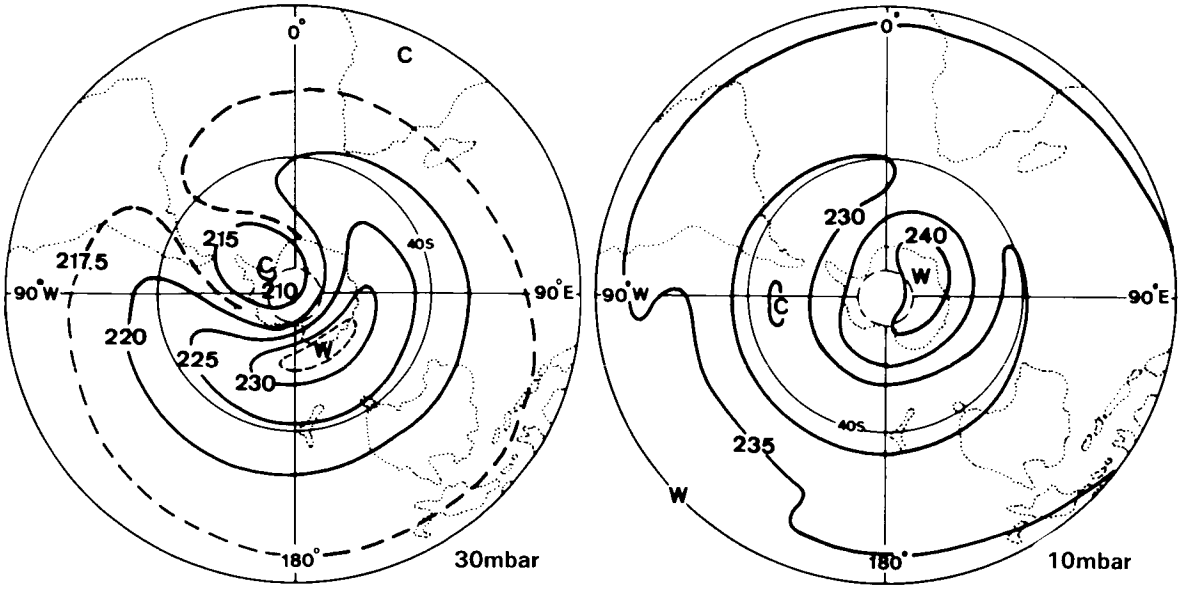

TEMPERATURE (K)
OCTOBER S.H.

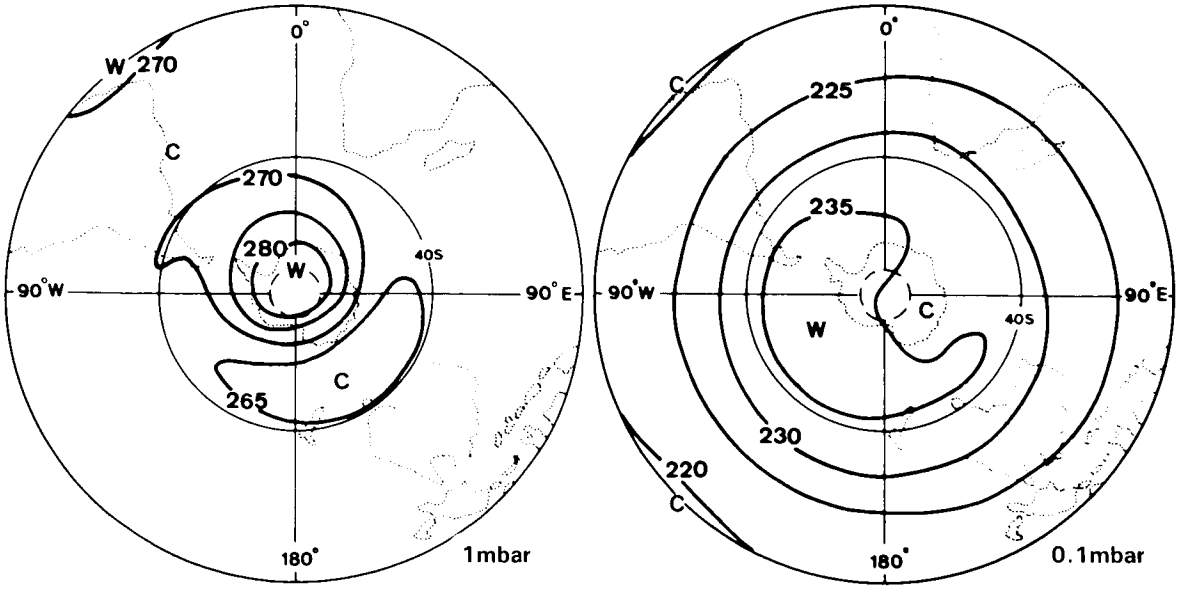

Figure D-30.4. Monthly mean temperature charts for October, Southern Hemisphere. (Data: 30-mbar: Knittel, 1976; otherwise: New Reference Atmosphere, MAP-Handbook, 16.)

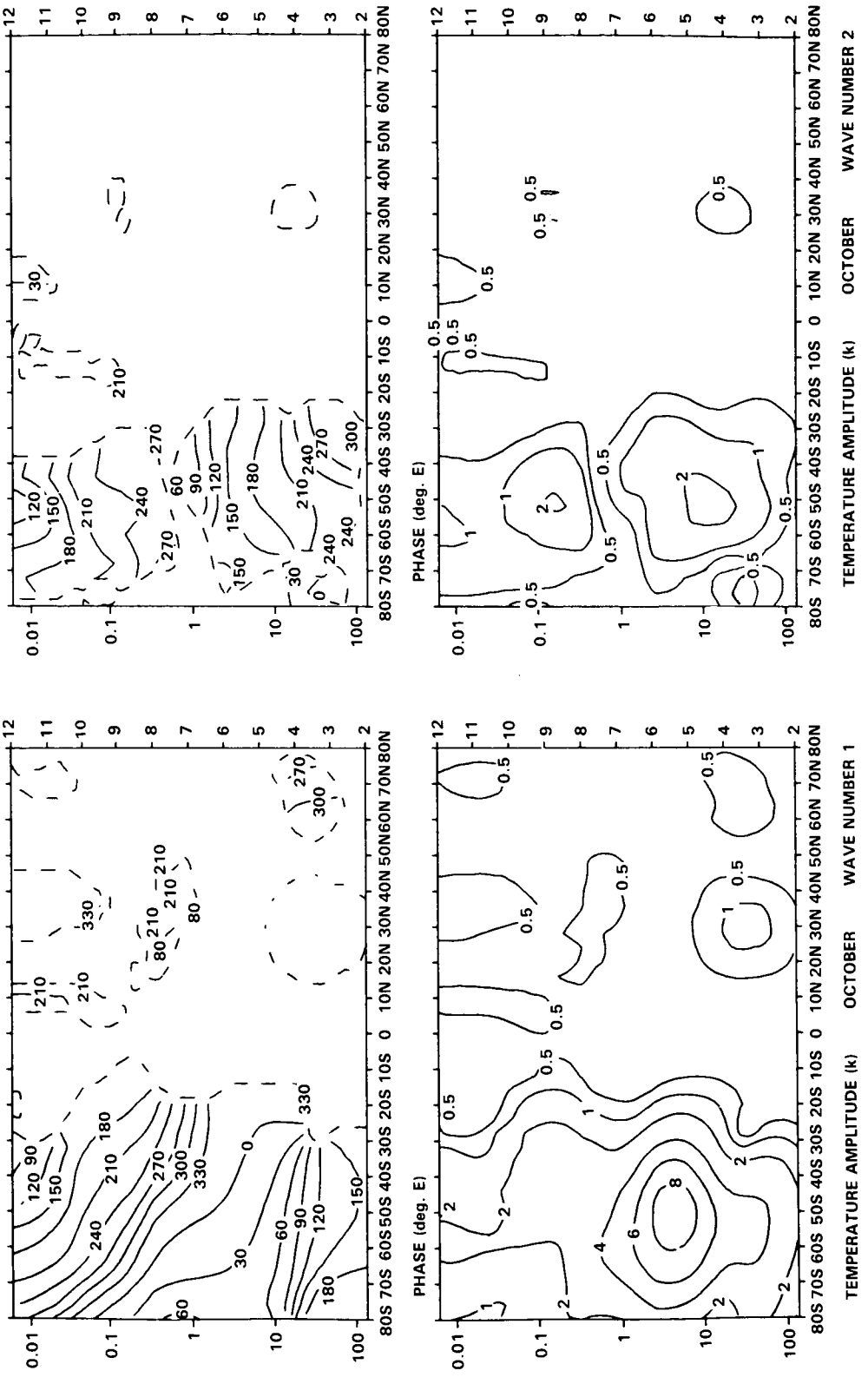

Figure D-31.1. Meridional height sections of temperature waves 1 and 2, January. (Data: New Reference Atmosphere, MAP-Handbook, 16.)

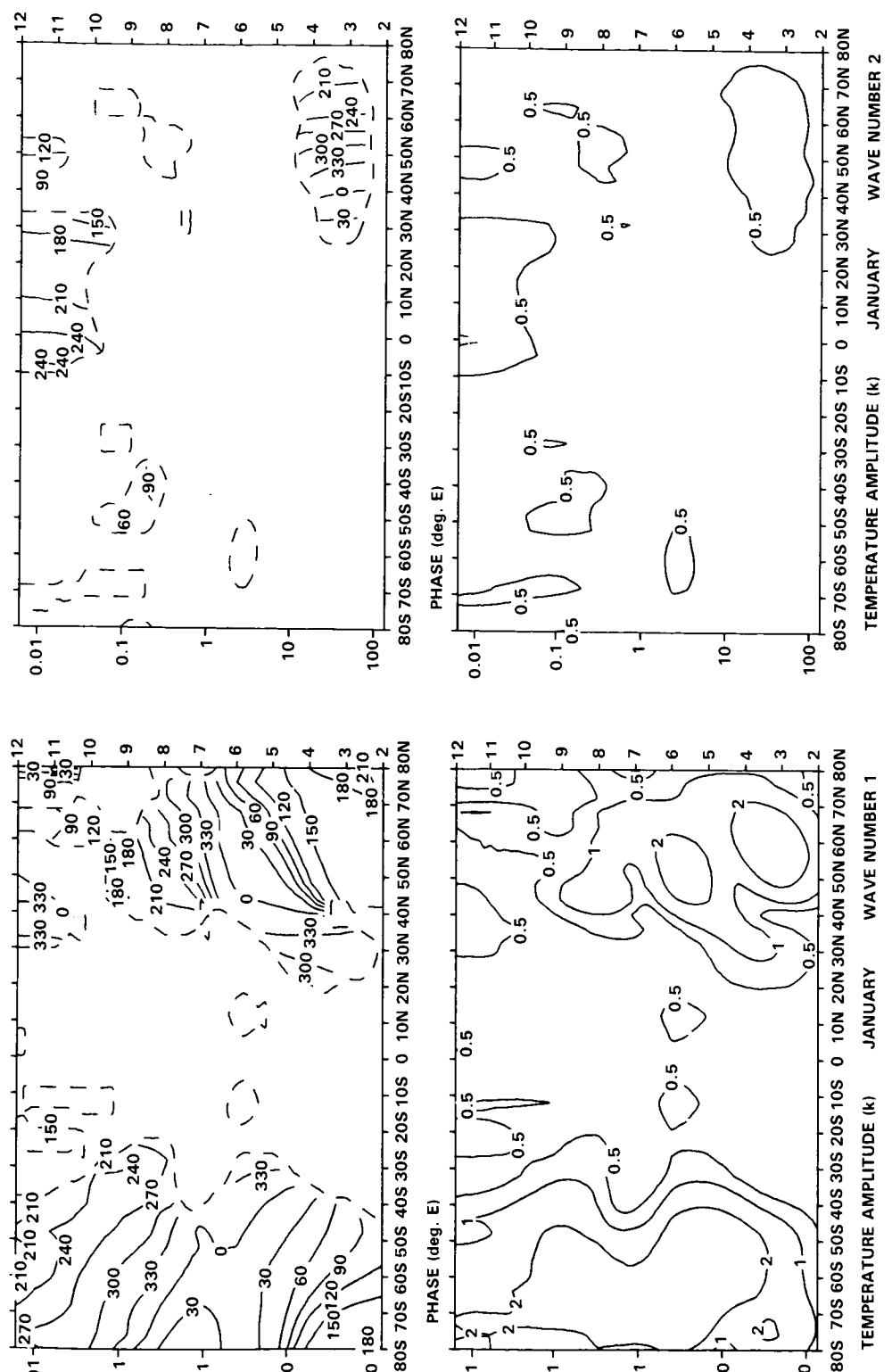

Figure D-31.2. Meridional height sections of temperature waves 1 and 2, April. (Data: New Reference Atmosphere, MAP-Handbook, 16.)

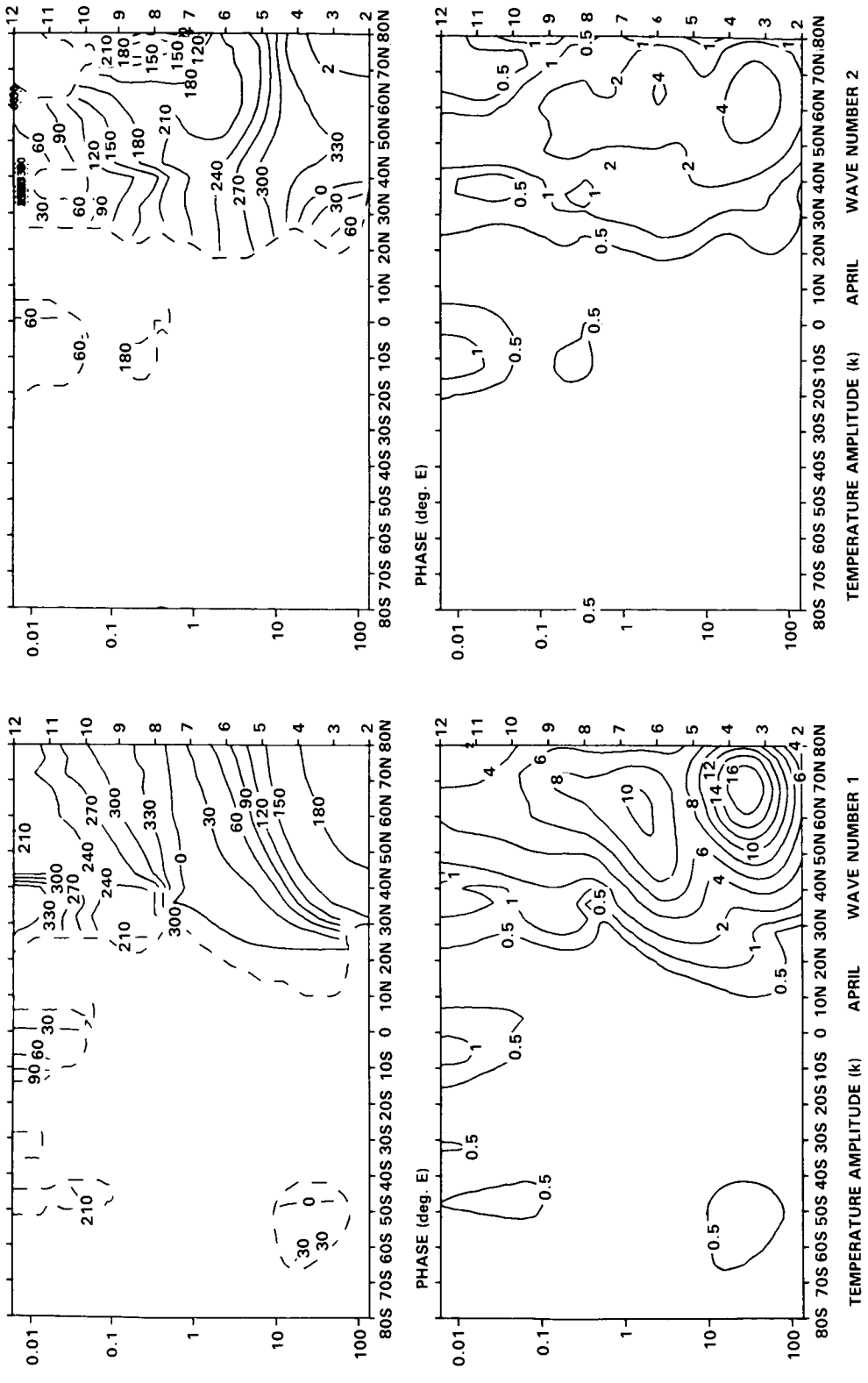

Figure D-31.3. Meridional height sections of temperature waves 1 and 2, July. (Data: New Reference Atmosphere, MAP-Handbook, 16.)

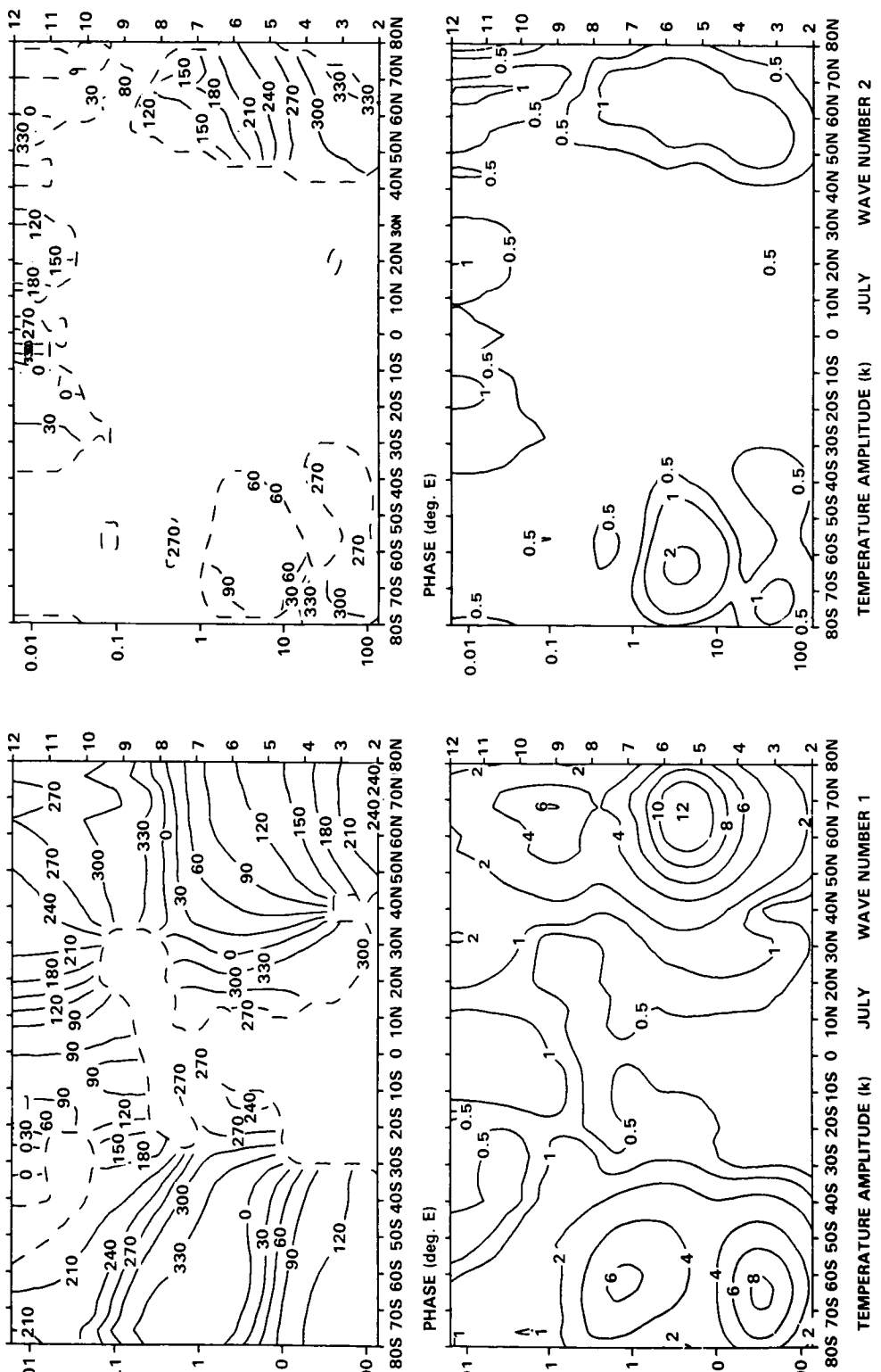

Figure D-31.4. Meridional height sections of temperature waves 1 and 2, October. (Data: New Reference Atmosphere, MAP-Handbook, 16.)

As pointed out before, wave 1 is approximately four times stronger than wave 2, both waves have their maximum in the lower and middle stratosphere over high northern latitudes, but extend into the upper mesosphere, and both waves are sloping westwards with height.

D-4.2.b April

Northern Hemisphere

Over the polar region the warming of the stratosphere and the cooling of the mesosphere is very large from midwinter to spring. But in April, during the spring transition time of the Northern Hemisphere, the remnants of the cold stratospheric polar vortex still dominate the temperature pattern, Figure D-28.2, longitudinal asymmetries still exist and the transition into summer is not completed. This is true also for the lower mesosphere and in strong contrast to the conditions during the spring reversal in the Southern Hemisphere, cf. Section D-3.1.b.

The charts of ozone mixing ratio show the same feature: the transition into summer is not yet completed, and the respective positive and negative correlations between ozone and temperature are remarkably large, considering the different types and times of the observations.

Southern Hemisphere

The radiational cooling of the stratosphere is extremely strong during the southern fall, resulting in an early establishment of the cold polar vortex and a concurrent warming of the mesosphere, Figure D-28.4. Typically, longitudinal variations are small over the Southern Hemisphere. But it is of interest to note the development of a weak warm area south of Australia at the 30-mbar level, Figure D-28.4, together with an ozone maximum at this level, Figure D-28.3.

Vertical Structure of Temperature Waves 1 and 2

During this time of the year both waves are approximately of the same size over both hemispheres, Figure D-31.2. This means that the waves during the northern spring are as weak as during the southern fall. And it is of interest to compare this with the respective Figure for October, cf. Figure D-31.4.

D-4.2.c July

Northern Hemisphere

During the northern summer the stratosphere is warmest over the polar region, Figure D-29.2, but not as warm as over the southern Arctic, cf. Figure D-27.4. This has been noted before (e.g., Barnett, 1974) and is due to the difference in solar heating of ozone, because of the ellipticity of the Earth's orbit, which produces a 6% modulation of the solar input. This temperature difference appears to exist throughout the mesosphere.

The ozone distribution is very regular during this time of the year.

Southern Hemisphere

During the southern winter the stratospheric polar vortex is extremely cold in the middle stratosphere, Figure D-29.4, and much colder than during the northern winter. In contrast, due to a more intense meri-

dional circulation the upper stratosphere and the lower mesosphere are less cold than during the northern winter, cf. Figure D-27.2. This explains why the height of the maximum of the annual temperature waves is lower over the Antarctic than over the Arctic, cf. Section D-2.1.a.

Note the very similar asymmetry of the temperature and ozone patterns at the 1-mbar level.

Vertical Structure of Temperature Waves 1 and 2

The vertical structure of the waves is given in Figure D-31.3. Compared with the respective Figure for January, Figure D-31.1, it is obvious that the amplitudes of the temperature waves 1 and 2 are only half of the values observed during the northern winters.

D-4.2.d October

Northern Hemisphere

During the northern fall the radiational cooling leads to the establishment of the cold stratospheric polar vortex together with the development of the "Aleutian High", i.e., the development of the planetary wave 1, Figures D-30.2 and D-31.4. This is one of the most important differences between the two hemispheres.

The build up of the ozone maximum in the lower stratosphere in conjunction with the build up of the Aleutian High is well in progress, Figure D-30.1.

Southern Hemisphere

In contrast to the Northern Hemisphere the transition into summer is already well advanced in the *upper* stratosphere, Figure D-30.4, (cf. Figure D-22). This characteristic difference has been described before, (Labitzke, 1974). One has to keep in mind, however, that this is not true for the *lower* stratosphere where the transition into summer is finished much later, cf. Section D-2.1.a.

Vertical Structure of Temperature Waves 1 and 2

The vertical structure of the temperature waves 1 and 2 is given in Figure D-31.4. As mentioned before the comparison with the respective Figure for April (Figure D-31.2) shows clearly the very different intensity of the planetary waves 1 and 2 over both hemispheres during spring and fall, respectively. In the lower stratosphere most of the wave activity of the Southern Hemisphere takes place during spring when the very intense "Final Warmings" bring the transition into summer. In contrast the largest wave activity in the Northern Hemisphere is observed during winter.

During the northern fall the planetary waves develop to much larger amplitudes than during the southern fall, Figs. D-31.4 and D-31.2.

A Fourier analysis along high latitudes results in large values of the amplitudes of wave 1, but also in relatively large values of wave 2, Figure D-31.1. For the quasi-stationary pattern which the monthly mean charts are presenting, these two waves account for 98% of the total variance, van Loon *et al.*, 1972.

Wave 1 is sloping westwards with height, Figure D-31.1, and is still well pronounced at the 1-mbar level (48km) which represents the upper stratosphere, Figure D-27.2.

The temperature gradient is reversed in the mesosphere, but wave 1 is still noticeable at the 0.1-mbar level (65km) which represents the lower mesosphere.

The charts showing the ozone mixing ratios, Figure D-27.1, reflect the strong positive correlation of ozone with temperature in the lower stratosphere as well as the strong negative correlation in the upper stratosphere and lower mesosphere. As regards the relatively regular pattern of ozone mixing ratio at the 10-mbar level, the reader is referred to Section D-1.2, Figure D-1. The weakest influence of dynamics must be expected in this region around the maximum of the ozone mixing ratio where the vertical advection term will be the smallest.

It should be noted that these maps represent an averaged state of the middle atmosphere and that the short-term variability during the northern winters is very large in connection with high-latitude stratospheric warmings-mesospheric coolings. This has been subject of many studies of which only a few are given here for reference: Labitzke, 1981 and 1982; McInturff,1978; Schoeberl, 1978.

Southern Hemisphere

During summer when the mean zonal winds in the stratosphere are from the east, the tropospheric waves cannot propagate into the stratosphere. Therefore the temperature distribution is very symmetric around the pole, Figure D-27.4.

The summer stratosphere is warmest over the polar region due to the heating of the ozone layer and the highest temperatures of the middle atmosphere are found over the South Pole at the stratopause, i.e., the 1-mbar level, and the lower mesosphere is still warmest over the polar region, although colder than at the stratopause, with a generally very flat temperature gradient.

The ozone distribution is similarly regular, Figure D-27.3. The negative correlation at the 0.1/0.4-mbar level is particularly worth noting, indicating rising motion within the belt of low temperatures/ large values of ozone mixing ratio.

Vertical Structure of Temperature Waves 1 and 2

The vertical structure of the temperature waves 1 and 2 is summarized in meridional height-sections, Figure D-31.1, which show the amplitudes and phases of these waves. For wave 1 the phase is the longitude (deg.E) of the maximum, while for wave 2 the phase is twice that longitude. Wave components are available for both hemispheres but are not given here for the Southern Hemisphere because they are small (about 0.5K) in summer. It should be noted that phases are not given where the amplitude is less than the lowest contour value and that this contour is indicated by a dashed line on the phase diagrams.

APPENDIX

LIST OF CONTRIBUTORS

CONTRIBUTORS

OVERALL CHAIRMAN

R.T. Watson
National Aeronautics and Space Administration—Headquarters
Washington, D.C. 20546

CHAPTER CHAIRMEN

D.L. Albritton—*Appendix C*
NOAA
Aeronomy Lab
R/E/AL6, Room 24-2107
325 Broadway
Boulder, Colorado 80303

G. Brasseur—*Chapter 8*
Institut d'Aeronomie Spatiale de Belgique
3 Avenue Circulaire
Brussels, B-1180 Belgium

R.A. Cox—*Chapter 2*
AERE Harwell
Environmental and Medical Science Div. B364
Oxfordshire OX11 ORA, England

W.B. DeMore—*Appendix A*
Jet Propulsion Laboratory
4800 Oak Grove Drive
Pasadena, California 91103

J.E. Frederick—*Chapter 7*
University of Chicago
Dept. of Geophysical Sciences
5734 South Ellis Avenue
Chicago, Illinois 60637

R. Gammon—*Chapter 3*
NOAA
PMEL/RE/PM
Bin #C25700
Building 3
7600 Sand Point Way, NE
Seattle, Washington 98115-0070

J.E. Harries—*Chapter 10*
Rutherford and Appleton Laboratories
Science Research Council
Chilton Didcot Oxon OQX, England

N. Husson—*Appendix B*
C.N.R.S.
Laboratoire de Meteorologie Dynamique
Ecole Polytechnique Route
Departmental 36
91198 Palaiseau Cedex, France

H.S. Johnston—*Chapter 13*
University of California
Department of Chemistry
Berkeley, California 94720

F. Kaufman, (deceased)—*Chapter 13*
University of Pittsburgh
Department of Chemistry
205 SRCC Building
Pittsburgh, Pennsylvania 15206

K. Labitzke—*Chapter 14* and *Appendix D*
Free University of Berlin
Dietrich-Schafer Weg 6-10
D-1000 Berlin 41, FRG

C.B. Leovy—*Chapter 7*
University of Washington
Department of Atmospheric Sciences
Seattle, Washington 98150

CONTRIBUTORS

A.J. Miller—*Chapters 8 and 14*
NOAA
National Meteorological Center
W333, Room 210
5200 Auth Road
Washington, D.C. 20233

V.A. Mohnen—*Chapter 4*
State University of New York
Atmospheric Science Research Center
400 Washington Avenue
Albany, New York 12222

M.J. Molina—*Chapter 11*
Jet Propulsion Laboratory
Mail Code: 183-601
4800 Oak Grove Drive
Pasadena, California 91109

R.A. Plumb—*Chapter 6*
CSIRO
Division of Atmospheric Research
Aspendale 3195 Victoria, Australia

J. Pyle—*Chapter 12*
University of Cambridge
Department of Physical Chemistry
Lensfield Rd.
Cambridge CB2 1EP England

V. Ramanathan—*Chapter 15*
National Center for Atmospheric Research
Climate Section
P.O. Box 3000
Boulder, Colorado 80307

H.I. Schiff—*Chapter 9*
York University
Department of Chemistry
4700 Keele Street
Downsview, Ontario M3J 1P3, Canada

A.F. Tuck—*Chapter 5*
Met.015
Meteorological Office
London Road
Bracknell Berkshire RG12 2SZ, England

S.C. Wofsy—*Chapter 3*
Harvard University
Pierce Hall
29 Oxford Street
Cambridge, Massachusetts 02138

R.J. Zander—*Appendix C*
University of Liege
Institute of Astrophysics
5 Avenue de Cointe
B-4200 Liege-Ougree, Belgium

OVERVIEW EDITORIAL COMMITTEE

Chapter Chairmen were responsible for editing their own chapters. The role of the editorial committee was to work with the chairmen to coordinate a wide range of activities associated with producing the chapters and to present a consistent style for the report.

F.M. Ormond
ORI, Inc.
Rockville, Maryland

R.S. Stolarski
NASA Goddard Space Flight Center
Greenbelt, Maryland

R.T. Watson
NASA Headquarters

PEER REVIEW PANEL AND AGENCY LIAISONS

Co-Chairmen

M. Geller
NASA Goddard

R.T. Watson
NASA Headquarters

D.L. Albritton—*Appendix C**
NOAA Aeronomy Laboratory

H. Bauer
Gesellschaft fur Strahlen und
Umweltforschung MBH Munchen
Bereich Projekttragerschaften
Josephspitalstr. 15
8000 Munchen 2, FRG

G. Brasseur—*Chapter 8*
Institut d'Aeronomie Spatiale de Belgique

R.A. Cox—*Chapter 2*
AERE Harwell

P. Crutzen
Max-Planck Institute for Atmospheric
Chemistry
SAARSTR 23, Postbox 3060
D-6500 Mainz, FRG

W.B. DeMore—*Appendix A*
Jet Propulsion Laboratory

D.H. Ehhalt
Institut fur Chemie
3 Atmosphaerische Chemie der
Kernforschung Sanlage
Julich GMBH Postfach 1913, FRG

J.E. Frederick—*Chapter 7*
University of Chicago

R. Gammon—*Chapter 3*
NOAA/PMEL

M.A. Geller
NASA
Goddard Space Flight Center
Code: 610
Greenbelt, Maryland 20771

A. Ghazi
Commission of the European Communities
Directorate-General for Science
Research and Development
Rue de la Loi 200
1049 Brussels, Belgium

R.F. Hampson
NASA Headquarters
Code: EE
Washington, D.C. 20546

J.E. Harries—*Chapter 10*
Rutherford and Appleton Laboratories

N. Husson—*Appendix B*
C.N.R.S.

H.S. Johnston—*Chapter 13*
University of California

N.P. Krull
Federal Aviation Administration
Office of Environment and Energy, AEE-30
800 Independence Avenue, S.W.
Washington, D.C. 20591

K. Labitzke—*Chapter 14 and Appendix D*
Free University of Berlin

*Full addresses for Chapter Chairmen are in first listing.

J. Mahlman
NOAA
Princeton University
Geophysical Fluid Dynamics Laboratory
P.O. Box 308
Princeton, New Jersey 08542

M.B. McElroy
Harvard University
Division of Applied Sciences
1350 Massachusetts Avenue
Cambridge, Massachusetts 02138

A.J. Miller—*Chapters 8 and 14*
NOAA

V. Mohnen—*Chapter 4*
State University of New York

M. Molina—*Chapter 11*
Jet Propulsion Laboratory

R.A. Plumb—*Chapter 6*
CSIRO

J. Pyle—*Chapter 12*
University of Cambridge

V. Ramanathan—*Chapter 15*
National Center for Atmospheric Research

F.S. Rowland
University of California
Department of Chemistry
Irvine, California 92717

H. I. Schiff—*Chapter 9*
York University

R.S. Stolarski
NASA
Goddard Space Flight Center
Code: 616
Greenbelt, Maryland 20771

N. Sundararaman
World Meteorological Organization
Case Postal 5
CH 1211 Geneva 20, Switzerland

N.D. Sze
Atmospheric and Environmental Research Inc.
840 Memorial Drive
Cambridge, Massachusetts 02139

A.F. Tuck—*Chapter 5*
Met. Office

P. Usher
United Nations Environment Program
P.O. Box 30552
Nairobi, Kenya

R.T. Watson
NASA Headquarters
Code: EE
Washington, D.C. 20546

PANEL MEMBERS

Alphabetical listing of all panel members. Some served on more than one panel. See the chapter title pages to identify membership of each panel.

D.E. Anderson, Jr.
Naval Research Laboratory

G.P. Anderson
Air Force Geophysical Laboratory

D.G. Andrews
Oxford University, England

J.K. Angell
National Oceanic and Atmospheric Administration

A. Barbe
Laboratoire de Physique Moleculaire
Faculte des Sciences, France

J.J. Barnett
Oxford University, England

P.K. Bhartia
Systems and Applied Sciences Corp.

P. Bowman
National Aeronautics and Space
Administration - Goddard

G. Brasseur
Institut d'Aeronomie Spatiale
de Belgique, Brussels, Belgium

E.V. Browell
National Aeronautics and Space
Administration - Langley

L.R. Brown
Jet Propulsion Laboratory

C. Burnett
National Oceanic and Atmospheric
Administration

D.M. Butler
National Aeronautics and Space
Administration - Headquarters

L.B. Callis, Jr.
National Aeronautics and Space
Administration - Langley

D. Cariolle
EERM/CNRM, France

B. Carli
Instituto de Ricerca
Onde Elettromagnetiche - CNR, Italy

R.D. Cess
State University of New York

W. Chameides
Georgia Institute of Technology

R.J. Cicerone
National Center for Atmospheric Research

M.T. Coffey
National Center for Atmospheric Research

M. Corney
Oxford University, England

E.F. Danielsen
National Aeronautics and Space
Administration - Ames

A.C. Delany
National Center for Atmospheric Research

J. DeLuisi
National Oceanic and Atmospheric
Administration

K.L. Demerjian
Environmental Protection Agency

W.B. DeMore
Jet Propulsion Laboratory

R. deZafra
State University of New York

R.E. Dickinson
National Center for Atmospheric Research

S.R. Drayson
University of Michigan

W.F.J. Evans
Atmospheric Environment Service, Canada

P. Fabian
Max-Planck Institute for
Aeronomie, FRG

C.B. Farmer
Jet Propulsion Laboratory

CONTRIBUTORS

S. Fels
National Oceanic and Atmospheric Administration

E.E. Ferguson
National Oceanic and Atmospheric Administration

H. Fischer
University of Münich, FRG

A.J. Fleig
National Aeronautics and Space Administration - Goddard

J.E. Frederick
University of Chicago

L. Froidevaux
Jet Propulsion Laboratory

R.R. Garcia
National Center for Atmospheric Research

M.A. Geller
National Aeronautics and Space Administration - Goddard

J. Gille
National Center for Atmospheric Research

D.M. Golden
Stanford Research Institute

A. Goldman
University of Denver

W.L. Grose
National Aeronautics and Space Administration - Langley

P.D. Guthrie
National Aeronautics and Space Administration - Goddard

L.A. Hall
Air Force Geophysical Laboratory

R.F. Hampson
National Aeronautics and Space Administration - Headquarters

J.E. Hansen
Goddard Institute for Space Studies

R.T. Harriss
National Aeronautics and Space Administration - Langley

W. Heaps
National Aeronautics and Space Administration - Goddard

D. Heath
National Aeronautics and Space Administration - Goddard

E. Hilsenrath
National Aeronautics and Space Administration - Goddard

J. Holton
University of Washington

B. Hoskins
University of Reading, England

C.J. Howard
National Oceanic and Atmospheric Administration

I.S.A. Isaksen
National Center for Atmospheric Research

D.R. Johnson
University of Wisconsin

R. Jones
Meteorological Office, England

G.M. Keating
National Aeronautics and Space Administration - Langley

M.A.K. Khalil
Oregon Graduate Center

J. Kiehl
National Center for Atmospheric Research

D. Kley
Institut für Chemie, Julich, FRG

M. Ko
Atmospheric and Environmental
Research, Inc.

C.E. Kolb
Aerodyne Research, Inc.

A.J. Krueger
National Aeronautics and Space
Administration - Goddard

W.R. Kuhn
University of Michigan

M.J. Kurylo
National Bureau of Standards

A. Lacis
Goddard Institute of Space Studies

D. Lenschow
National Center for Atmospheric Research

R. Lesclaux
Universite de Bordeaux I, France

J.A. Logan
Harvard University

N. Louisnard
ONERA, France

F.M. Luther
Lawrence Livermore National Laboratory

J.D. Mahlman
NOAA Geophysical Fluid
Dynamics Laboratory

W.G. Mankin
National Center for Atmospheric Research

J.J. Margitan
Jet Propulsion Laboratory

C. Mateer
Atmospheric and Environment
Service, Canada

M.P. McCormick
National Aeronautics and Space
Administration - Langley

R.J. McNeal
National Aeronautics and Space
Administration - Headquarters

G. Megie
Service d'Aeronomie, CNRS, France

J.E. Mentall
National Aeronautics and Space
Administration - Goddard

P. Midgley
ICI Americas, Inc.

A.J. Miller
National Oceanic and Atmospheric
Administration

M.J. Molina
Jet Propulsion Laboratory

G.H. Mount
National Research Laboratory, England

D.G. Murcray
University of Denver

R.M. Nagatani
National Oceanic and Atmospheric
Administration

T.B. Narijokat
Free University of Berlin, FRG

R. Newell
Massachusetts Institute of Technology

CONTRIBUTORS

M. Nicolet
Aeronomy Laboratory, Brussels, Belgium

J. Noxon
National Oceanic and Atmospheric Administration

A. O'Neill
Meteorological Office, England

A.J. Owens
DuPont Company

S.A. Penkett
AERE Harwell, England

H.M. Pickett
Jet Propulsion Laboratory

U. Platt
Institut für Chemie - KFA, FRG

R.A. Plumb
CSIRO, Australia

S. Pollitt
National Physical Laboratory, England

M. Prather
Goddard Institute for Space Studies

J. Pyle
University of Cambridge, England

A.R. Ravishankara
National Oceanic and Atmospheric Administration

R.A. Reck
General Motors Research Laboratories

G. Reinsel
University of Wisconsin

B.A. Ridley
National Center for Atmospheric Research

D.E. Robbins
National Aeronautics and Space Administration - Johnson

A.E. Roche
Lockheed Palo Alto Research Laboratories

C.D. Rodgers
Oxford University, England

H. Roscoe
Oxford University, England

L.S. Rothman
Air Force Geophysical Laboratory

G. Rottman
University of Colorado

J.M. Russell, III
National Aeronautics and Space Administration - Langley

M.L. Salby
University of Colorado

S.P. Sander
Jet Propulsion Laboratory

M.E. Schlesinger
Oregon State University

U. Schmailzl
Max-Planck Institut für Chemie, FRG

A.L. Schmeltekopf
National Oceanic and Atmospheric Administration

U. Schmidt
Institut für Chemie, FRG

M.R. Schoeberl
National Aeronautics and Space Administration - Goddard

U. Schurath
University of Bonn, FRG

P. da Silva Dias
University of Sao Paulo, Brazil

P.C. Simon
Institut d'Aeronomie Spatiale
de Belgique, Brussels, Belgium

M.A.H. Smith
National Aeronautics and Space
Administration - Langley

S. Solomon
National Oceanic and Atmospheric
Administration

F. Stordal
National Center for Atmospheric Research

N.D. Sze
Atmospheric and Environmental
Research, Inc.

G. Tiao
University of Chicago

R.J. Thomas
University of Colorado

W.A. Traub
Smithsonian Astrophysical Observatory

K.K. Tung
Massachusetts Institute of Technology

G. Vaughan
University College of Wales, UK

R.A. Vincent
University of Adelaide, Australia

G. Visconti
University of Aquila, Italy

J.W. Waters
Jet Propulsion Laboratory

R.T. Watson
National Aeronautics and Space
Administration - Headquarters

D.J. Wuebbles
Lawrence Livermore National
Laboratory

R.J. Zander
University of Liege, Belgium

R. Zellner
Universitat Goettingen, FRG

ACKNOWLEDGEMENTS

(exclusive of those already listed above)

Reviewers

A. Aikin
NASA/Goddard

J.G. Anderson
Harvard University

A.M. Bass
National Bureau of Standards

C. Bruehl
Max Planck Institut für Chem.

A. Chedin
C.N.R.S.

P. Connell
Lawrence Livermore National Laboratory

A. Douglass
Applied Research Corporation

D.E. Freeman
Harvard University

R. Greenstone
ORI, Inc.

J. Herman
NASA/Goddard

C. Jackman
NASA/Goddard

J. Kaye
NASA/Goddard

S. Liu
NOAA Aeronomy Lab.

S. Manabe
Geophysical Fluid Dynamics Lab.

D.S. McKenna
U.K. Met. Office

R. McPeters
NASA/Goddard

R.G. Prinn
MIT

R. Rood
Applied Research Corporation

R. Selkirk
MIT Met. Dept.

R. Stewart
NASA/Goddard

Editorial

M.A. Baldauf
RMS, Inc.

R. Duffy
NASA/Goddard

G. Escobar
NCAR

B. Kibling
ORI, Inc.

C.A. Meetre
SAR, Inc.

K. Taylor
ORI, Inc.

Design, Art, Typesetting and Production
Jands, Inc.
Silver Spring, Maryland

Jerry Mendelson, President

David Callahan, Studio Director

Dorothy Jenkins, Publications Manager

Jodine Bloom, Production Supervisor

Chris Miller, Senior Proofreader

and a dedicated group of 27 art,
typesetting and production personnel

APPENDIX F

LIST OF FIGURES

APPENDIX F
INDEX OF FIGURES

FIGURES

FIGURES

FIGURES

Page

FIGURES

FIGURES

Page

FIGURES

FIGURES

FIGURES

FIGURES

FIGURES

FIGURES

Page

Page

FIGURES

FIGURES

FIGURES

FIGURES

FIGURES

APPENDIX

LIST OF TABLES

APPENDIX G
INDEX OF TABLES

TABLES

TABLES

TABLES

APPENDIX H

MAJOR ACRONYMS

APPENDIX H
ACRONYMS

Units, Instruments, Satellites, and Programs

AE	Atmospheric Explorer
AEM	Applications Explorer Mission
ATMOS	Atmospheric Trace Molecule Spectroscopy Experiment
AVHRR	Advanced Very High Resolution Radiometer
BMLS	Balloon-borne Microwave Limb Sounder
BSU	Basic Sounding Unit
BUV	Backscattered Ultraviolet Spectrometer
BIC	Balloon Intercomparison Campaign
BOIC	Balloon Ozone Intercomparison Campaign
CIAP	Climatic Impact Assessment Program
DMSP	Defense Meteorological Satellite Program
DU	Dobson Unit = milliatm-cm = 2.687×10^{16} molecules cm^{-2}
ECC	Electrochemical cell (ozonesonde)
ECD	Electron Capture Detection
ERBS	Earth Radiation Budget Satellite
FTS	Fourier Transform Spectrometer
GARP	Global Atmospheric Research Program
GATE	GARP Atlantic Tropical Experiment
GC	Gas Chromatography
GCM	General Circulation Model
GMCC	Geophysical Monitoring for Climatic Change
GOES	Geosynchronous Operational Environment Satellite
GLOBUS	Global Budget of Stratospheric Trace Constituents
HALOE	Halogen Occultation Experiment
HAPP	High Altitude Pollution Program
HIRS	High Resolution Infrared Radiation Sounder
IORI	International Ozone Rocketsonde Intercomparison
IRIS	Infrared Interferometer Spectrometer
ITCZ	Intertropical Convergence Zone
ITOS	Improved TIROS Operational Satellite
ITPR	Infrared Temperature Profile Radiometer

ACRONYMS

LHR	Laser Heterodyne Radiometer
LIMS	Limb Infrared Monitor of the Stratosphere
LRIR	Limb Radiance Inversion Radiometer
MAP	Middle Atmosphere Program
MFR	Multichannel Filter Radiometer
MM	Mechanistic Model
MS	Mass Spectrometry
MST	Mesosphere, Stratosphere, Troposphere (radar)
MSU	Microwave Sounding Unit
MUSE	Monitor of Ultraviolet Solar Energy
NOPS	Nimbus Operational Processing System
OAO	Orbiting Astronomical Observatory
OGO	Orbiting Geophysical Observatory
OSO	Orbiting Solar Observatory
PEPSIOS	Poly-Etalon Pressure Scanned Interferometer
PMR	Pressure Modulated Radiometer
SAGE	Stratospheric Aerosol and Gas Experiment
SAMS	Stratospheric and Mesospheric Sounder
SAM II	Stratospheric Aerosol Measurement II
SBUV	Solar and Backscatter Ultraviolet Spectrometer
SCR	Selective Chopper Radiometer
SIRS	Satellite Infrared Spectrometer
SME	Solar Mesosphere Explorer
SPE	Solar Proton Event
SSH	Special Sensor H (also called MFR)
SST	Supersonic Transport
SSU	Stratospheric Sounding Unit
TIROS	Television and Infrared Observation Satellite
TOMS	Total Ozone Mapping System/Spectrometer
TOVS	TIROS Operational Vertical Sounder
UARS	Upper Atmosphere Research Satellite
VTPR	Vertical Temperature Profile Radiometer

Institutions

AER, Inc.	Atmospheric and Environmental Research, Incorporated 872 Massachusetts Avenue Cambridge, Massachusetts 02139 USA
AERE Harwell	Atomic Energy Research Establishment Harwell Oxfordshire OX11 ORA, United Kingdom
AES	Atmospheric Environment Service 4905 Dufferin Street Downsview, Ontario M3H 5T4, Canada
AFGL	Air Force Geophysics Laboratory Bedford, Massachusetts USA
AIAA	American Institute of Aeronautics and Astronautics, Inc. Technical Information Center 555 West 57th Street New York, New York 10019 USA
ARC	Ames Research Center Moffett Field, California 94035 USA
ASL	Atmospheric Sciences Laboratory White Sands Missile Range New Mexico 88002 USA
BMFT	Bundesministerium für Forschung und Technologie Federal Republic of Germany
BMO	British Meteorological Office London Road Bracknell, Berkshire RG12 2SZ, United Kingdom
CEC	Commission of the European Communities Rue de la Loi 200 Brussels, Belgium
CMA	Chemical Manufacturers Association 2501 M Street, N.W. Washington, DC 20037 USA
CNRS	Center National de la Recherche Scientifique 91370 Verrieres le Buisson, France

ACRONYMS

CNRS-FRS	CNRS - Faculte des Sciences de Reims
CNRS-SA	CNRS - Service d'Aeronomie CNRS - Laboratoire de Meteorologie Dynamique
CODATA	Committee on Data for Science and Technology 51 Boulevard de Montmorency Paris, France
COMESA	Committee on Meteorological Effects of Stratospheric Aircraft Meteorological Office Bracknell, United Kingdom
CSIRO	Commonwealth Scientific and Industrial Research Organization Australia
DOD	Department of Defense (USA)
DOT	Department of Transportation (USA)
DU	Denver University
Du Pont	E.I. du Pont de Nemours & Co. Experimental Station Wilmington, Delaware 19898 USA
EERM	Meteorologie Nationale EERM Boulogne-Billancourt France
EPA	Environmental Protection Agency Washington, D.C. 20460 USA
FAA	Federal Aviation Administration Washington, D.C. 20591 USA
FPP	Fluorocarbon Program Panel (of the CMA)
GFDL	Geophysical Fluid Dynamics Laboratory P.O. Box 308, Princeton University Princeton, New Jersey 08540 USA
GISS	Goddard Institute of Space Studies New York, New York 10025 USA

GIT	Georgia Institute of Technology Atlanta, Georgia 30332 USA
GSFC	Goddard Space Flight Center Greenbelt, Maryland 20771 USA
HU	Harvard University Cambridge, Massachusetts USA
IASB	Institut d'Aeronomie Spatiale de Belgique Brussels, Belgium
IROE	Instituto diRicherca sulle Onde Electromagnetiche (Italy)
JPL	Jet Propulsion Laboratory 4800 Oak Grove Drive Pasadena, California 91103 USA
JSC	Johnson Space Center Houston, Texas USA
KFA	Institut für Chemie der Kernforschungsanlage Julich Postfach 1913, D-5170 Julich Federal Republic of Germany
KPNO	Kitt Peak National Observatory Tucson, Arizona USA
LaRC	Langley Research Center Hampton, Virginia 23665 USA
LLNL	Lawrence Livermore National Laboratory P.O. Box 808 Livermore, California 94550 USA
MET. O.	Meteorological Office London Road Bracknell, Berkshire RG12 2S2 United Kingdom
MIM	Met. Institut Munich, Federal Republic of Germany
MIT	Massachusetts Institute of Technology Cambridge, Massachusetts 02139 USA

ACRONYMS

MOH	Meteorologisches Observatorium Hohenpeissenberg, Federal Republic of Germany
MPAE	Max Planck Institut für Aeronomie Postfach 20, D-3411 Katlenburg, Lindau 3 Federal Republic of Germany
MPN	Meteorologie Nationale (France)
MPIC, MPI-Mainz	Max Planck Institut für Chemie Saarstrasse 23, D-65 Mainz Federal Republic of Germany
NAS	National Academy of Sciences 2101 Constitution Avenue, N.W. Washington, D.C. 20418 USA
NASA	National Aeronautics and Space Administration Headquarters Washington, D.C. 20546 USA
NBS	National Bureau of Standards Gaithersburg, Maryland 20899 USA
NCAR	National Center for Atmospheric Research P.O. Box 3000 Boulder, Colorado 80307 USA
NCC	National Climatic Center Asheville, North Carolina 28801 USA
NESS	National Earth Satellite Service Suitland, Maryland 20233 USA
NOAA	National Oceanic and Atmospheric Administration Headquarters Rockville, Maryland 20852 USA
NOAA-AL	NOAA Aeronomy Laboratory, Boulder, Colorado 80303 USA
NOAA-ERL	NOAA Environmental Research Lab., Boulder, Colorado 80303 USA
NOAA-GMCC	NOAA Geophysical Monitoring for Climate Change USA
NPL	National Physics Laboratory Teddington, Middlesex, United Kingdom
NRC	National Research Council (of the NAS) Washington, D.C. USA

NSF	National Science Foundation Washington, D.C. USA
NSSDC	National Space Science Data Center Goddard Space Flight Center Greenbelt, Maryland 20771 USA
NTIS	National Technical Information Service Springfield, Virginia 22151 USA
OECD	Organization for Economic Cooperation and Development Paris, France
OHP	Observatoire de Haute Provence Chiran, France
ONERA	Office National d'Etudes et de Recherches Aerospatiales Chatillion, Bagneux, France
ONR	Office of Naval Research, Washington, D.C. USA
NWS	National Weather Service Silver Spring, Maryland 20910 USA
RAL	Rutherford and Appleton Laboratories Chilton, Didcot OXON OQX, United Kingdom
SAO	Smithsonian Astrophysical Observatory Cambridge, Massachusetts USA
SUNY	State University of New York
UK DOE	United Kingdom Department of the Environment
UL	Universite de Liege Liege-Ougree, Belgium
UM	University of Minnesota
UNEP	United Nations Environment Program Nairobi, Kenya
UO	University of Oxford Oxford, United Kingdom

ACRONYMS

UT	University of Tokyo, Japan
WMO	World Meteorological Organization Case Postal No. 5 Geneva 20, Switzerland

APPENDIX

CHEMICAL FORMULAE AND NOMENCLATURE

APPENDIX I

Chemical Formulae and Nomenclature

Symbol	Name
O	atomic oxygen
O_2	molecular oxygen
O_3	ozone
O_x	odd oxygen (O,$O(^1D)$,O_3)
N_2	molecular nitrogen
N_2O	nitrous oxide
NO	nitric oxide
NO_2	nitrogen dioxide
NO_3	nitrogen trioxide, nitrate radical
NO_y	odd nitrogen (NO, NO_2, NO_3, N_2O_5, $ClONO_2$, HNO_4, HNO_3)
NO_x	oxides of nitrogen (NO, NO_2, NO_3)
N_2O_5	dinitrogen pentoxide
HNO_2, HONO	nitrous acid
HNO_3, $HONO_2$	nitric acid
HNO_4, HO_2NO_2	peroxynitric acid
NH_3	ammonia
H_2O	water vapor
H_2O_2	hydrogen peroxide
OH, HO	hydroxyl radical
HO_2	hydroperoxyl radical
HO_x	odd hydrogen (OH, HO_2, H_2O_2)

Symbol	Name
CO	carbon monoxide
CO_2	carbon dioxide
CS_2	carbon disulfide
COS, OCS	carbonyl sulfide
SO_2	sulfur dioxide
SF_6	sulfur hexafluoride
H_2SO_4	sulfuric acid
HF	hydrogen fluoride
HCl	hydrogen chloride
HCN	hydrogen cyanide
HOCl	hypochlorous acid
Cl	chlorine atom
ClO	chlorine monoxide
$ClONO_2$, $ClNO_3$	chlorine nitrate
Cl_x	odd chlorine, inorganic chlorine
CH_4	methane
C_2H_6	ethane
C_3H_8	propane
C_2H_4	ethylene
C_2H_2	acetylene
CH_2O	formaldehyde
CH_3CHO	acetaldehyde
$(CH_3)_2CO$	acetone

Symbol	Name
CH_3O_2H	methyl hydroperoxide
CH_2CHCHO	acrolein
C_2Cl_4	tetrachloroethylene
CH_3Cl	methyl chloride
CH_2Cl_2	methylene chloride, dichloromethane
$CHCl_3$	chloroform, trichloromethane
CFC	chlorofluorocarbon
HC	hydrocarbon
NMHC	non-methane hydrocarbons
PAN	peroxyacetylnitrate
CH_3CCl_3	methyl chloroform
C_2F_6	hexafluoroethane
CCl_4	carbon tetrachloride (FC-10)
CCl_3F	trichlorofluoromethane (FC-11)
CCl_2F_2	dichlorodifluoromethane (FC-12)
$CClF_3$	chlorotrifluoromethane (FC-13)
CF_4	tetrafluoromethane (FC-14)
$CHCl_2F$	dichlorofluoromethane (FC-21)
$CHClF_2$	chlorodifluoromethane (FC-22)
CCl_2FCClF_2	trichlorotrifluoroethane (FC-113)
$CClF_2CClF_2$	dichlorotetrafluoroethane (FC-114)
$CClF_2CF_3$	chloropentafluoroethane (FC-115)
CF_3CF_3	hexafluoroethane (FC-116)

FORMULAE

Symbol	Name
CH_3CN	methyl cyanide
CH_3I	methyl iodide
Br	bromine atom
BrO	bromine monoxide
BrO_x	odd bromine, inorganic bromine
$CBrF_3$	trifluorobromomethane
$CHBr_3$	bromoform, tribromomethane
CH_3Br	methyl bromide
CH_2Br_2	dibromomethane
$CHBr_2Cl$	dibromochloromethane
CH_2BrCl	bromochloromethane
$C_2H_4Br_2$	dibromoethane
$CBrClF_2$	Halon 1211 (BCF) FC-12B1
CF_3Br	Halon 1301 FC-13B1

APPENDIX J

PRESSURE—ALTITUDE CONVERSION CHART

APPENDIX J

PRESSURE-ALTITUDE CONVERSION CHART

PRESSURE-ALTITUDE

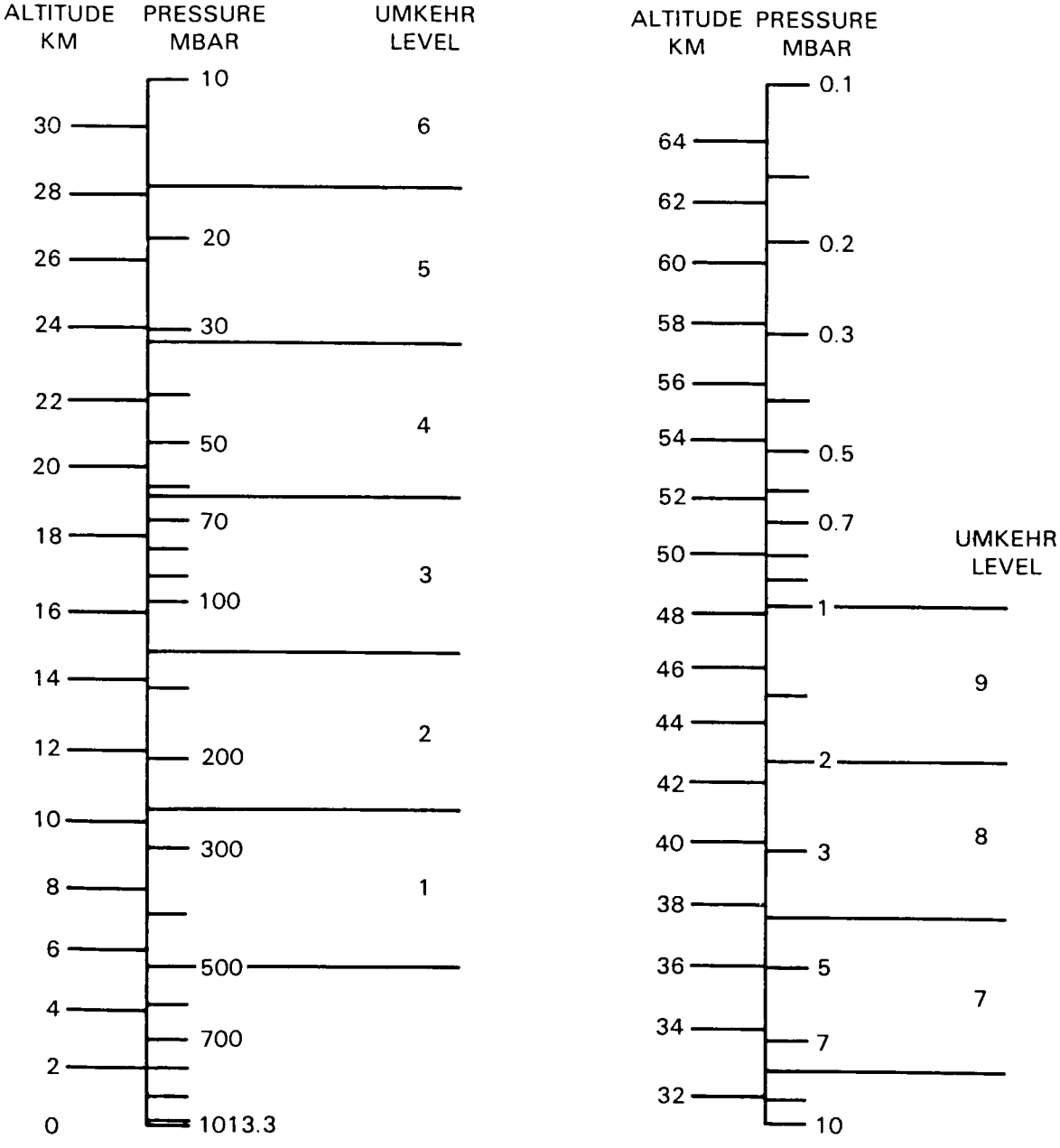

ALTITUDES ARE BASED ON U.S. STANDARD ATMOSPHERE, 1976. THE ACTUAL ALTITUDE FOR A GIVEN PRESSURE MAY DIFFER BY AS MUCH AS 2 KM, DEPENDING ON SEASON, LATITUDE, AND SHORT TERM VARIATIONS.